Effective Numerical Schemes to Investigate the Price and Greeks of Financial Options

THESIS

Submitted in partial fulfillment of the requirements

for the degree of

DOCTOR OF PHILOSOPHY

by

Komal Deswal

ID No. 2018PHXF0027P

Under the Supervision of

Dr. Devendra Kumar

Department of Mathematics

BITS Pilani, Pilani Campus

Rajasthan, India

[2022]

BIRLA INSTITUTE OF TECHNOLOGY AND SCIENCE, PILANI

PILANI CAMPUS, RAJASTHAN, INDIA

CERTIFICATE

This is to certify that the thesis entitled, **"Effective Numerical Schemes to Investigate the Price and Greeks of Financial Options"** and submitted by **Ms. Komal Deswal** ID No. **2018PHXF0027P** for the award of Ph.D. degree of the institute embodies original work done by her under my supervision.

Signature of the Supervisor

Name : **Dr. Devendra Kumar**

Designation : **Associate Professor, Department of Mathematics, BITS Pilani, Pilani Campus**

Date: 29/08/2022

Dedicated to
My Beloved Family

ACKNOWLEDGEMENTS

A journey is certainly easier when you travel together. Throughout my Ph.D. I have been accompanied and supported by many people. It's a great perk with the grace of God that I now have the opportunity to thank them all.

First, I want to express my deep appreciation and sincere gratitude to my thesis supervisor Dr. Devendra Kumar, for his valuable guidance and continuous encouragement throughout my Ph.D. duration. Under his motivating mentorship, my cognitive process and creative thinking got matured. His knowledge and endless pursuit of excellence inspired me to work harder. His simplicity and kindness, attention to detail, hard work, and patience have set an example for me, which possibly, I hope to match someday.

I am also thankful to all the professors of the Department of Mathematics of BITS Pilani, Pilani Campus for their guidance and valuable suggestions in my research work. I feel fortunate to have my Doctoral Advisory Committee (DAC) members as Dr. Ashish Tiwari and Dr. Rajesh Kumar whose constant encouragement and support made my work focused. Their comments and suggestions have helped improve my work at various stages.

I would also like to extend my sincere gratitude to my parents (Mr. Suresh Kumar Deswal and Mrs. Kavita Deswal) for believing in me more than myself. Their constant support and tremendous understanding kept me motivated throughout my Ph.D. and my life in general. I would also like to thank my brother Mr. Sumit Kumar Deswal and my sister-in-law Mrs. Ritu Deswal for being a sympathetic ear and encouraging me. I would also like to give my affection to my little master Naman Deswal for being a delightful diversion from monotony and frustration. I am deeply indebted to my entire family for their trust in me which made me confident enough to accomplish this journey. Not to forget, I could not have completed this thesis without my friends who provided stimulating discussions and happy distractions to rest my mind outside my research. I am also thankful to the office staff members who helped me with all the formalities. Finally, I am extremely grateful to CSIR, New Delhi, India for their financial support.

Komal Deswal

Place: BITS Pilani, Pilani Campus
Date: 29/08/2022

(Komal Deswal)

ABSTRACT

The pricing of options is a fairly complicated aspect of applied finance that has been getting a lot of attention. Investigating the sensitivities of the price of an option with various parameters known as Greeks are as important as pricing an option. Knowing how option prices fluctuate allows a trader to mitigate the risks of holding an option. For trading an option various analytical and numerical approaches have been developed to compute its price. Yet the pricing of options is not trivial and has many complexities thus it still remains a topic open to research. In this thesis, we develop more simple and efficient numerical approaches to compute the price and Greeks of various option pricing problems. It comprises of eight chapters.

The fundamental components of option pricing will be covered in the first chapter. It all starts with the idea of a financial derivative, option, its classification, and its features. Then, to set the groundwork for estimating the fair price of an option, we introduce the well-known scientific option pricing model known as the Black–Scholes option model. The chapter will then move on to some basic concepts in numerical analysis, as well as the numerical complexities in solving the Black-Scholes PDE.

An approach based on the wavelet approximation is developed in Chapter 2 for European vanilla options. In it, the Haar basis functions constructed by simple block pulse functions are used to generate the solution of the Black-Scholes PDE. As the payoff function (terminal condition) for the European option problem is discontinuous in nature thus its Greeks result in spiked functions. To this end, the Haar wavelet method is appropriate to compute the Greeks since the discontinuous nature of the Haar wavelets gives a better approximation of the spiked functions. Also, the present method explicitly provides the values of all derivatives of the solution function, making the option Greeks easy to approximate. Also, we will prove the convergence of the proposed scheme and implement the algorithm with a variety of examples.

In Chapter 2, we investigate the Greeks of American options. Even though tractable solutions can be obtained for European option pricing in most for most of the methods,

this is not possible for American options. Since the American options result in a free boundary value problem with a discontinuous payoff and non smooth Greeks. Therefore to investigate this problem we have constructed the novel Haar wavelet based method for various such option pricing problems Also in this chapter on the American call and put options, the wavelets' multi-resolution approach and the proposed wavelet scheme's convergence are thoroughly examined. Later in this chapter to demonstrate the competency and resilience of the current method, the wavelet analysis is accompanied by informative examples and graphical representations.

To explore the exotic options, and to deal with the discontinuity of payoff and Greeks a wavelet based approximation technique is developed. The proof of the consistency and stability of the proposed method are given and it has been shown that the proposed method is the first and second-order accurate in the temporal and spatial directions, respectively. Several numerical examples of distinct binary options have been taken into account, confirming the theoretical findings (consistency and stability).

Extending the work to higher dimensions, we have considered the multi-asset option pricing model. The two dimensional Haar wavelet method is constructed to study the solution to this problem and to investigate various hedging parameters. To explore these financially relevant problems systematically, the final value problem is reformulated into a less cluttered dimensionless initial value problem. Also, it has been shown that irrespective of the problem's geometry, the proposed method is highly accurate and the time taken to get this level of accuracy is significantly less.

The accuracy in numerical analysis plays an important role thus in Chapter 6 a highly accurate orthogonal spline collocation approach is provided to improve the precision of the approximation in space. Furthermore, because the suggested problem includes non-smooth underlying data, we have examined the Rannacher time-marching scheme instead of the BE and CN methods to increase time accuracy. unlike wavelet methods, the present approach has a higher order of convergence also as in wavelet methods to handle spiked payoff and Greeks we have used a non-classical time marching scheme. To validate the performance and accuracy of the current strategy, numerical experiments are

conducted for call and put American option pricing situations.

It's worth noting that the time derivatives as fractional are catching more attention these days because integer-order derivative base models would miss some important historical details. Due to their nonlocal nature, fractional derivatives, on the other hand, are highly versatile for defining the behavior of differential equations and adding historical information. Therefore in Chapter 7, we will move on to the fractional order option pricing problems. In this chapter a time fractional constant elasticity of variance model is considered. Its importance over the standard Black-Scholes model will also be explained. To solve this model the Atangana-Baleanu Caputo operator is used in time and a finite difference scheme is considered in space. The stability analysis of the proposed scheme will be provided. Two test problems will be considered to validate the theoretical results.

Contents

List of Tables

List of Figures

Chapter 1

Introduction

1.1 Background

Finance is the management of wealth and includes topics like investing, borrowing, lending, budgeting, saving, and forecasting [1–3]. The financial industry is usually one of the most important parts of a country's economy. The wave of globalisation and liberalisation has seen multiple increases in the amount of international trade and business during the last decade. As a result, global demand for international money and financial instruments has risen dramatically.

1.1.1 Financial derivatives

A derivative is a financial instrument whose value is determined by the value of the underlying assets or group of assets which means a derivative has no independent value, its value is entirely derived from the value of the underlying asset. Thus, the security of a derivative contract is the underlying asset. This could be a derivative value stock, bond, currencies or other hybrid securities [4–6]. Most financial derivatives are just mixtures of older generation derivatives and/or regular cash market instruments, rather than innovative new products. Derivatives markets are vast and rapidly expanding around the world, and

Figure 1.1: Representing different types of derivatives

their expansion in developing countries is likely to be even faster. Derivative trading, which was first introduced in India in the mid-2000s, has become an inextricable feature of the stock markets. The derivatives market operates in the same way as any other financial market, with three main types of participants:

1. **Hedgers.** Hedgers are traders who want to secure themselves against the danger of price fluctuations. They are always searching for new ways to pass this risk on to those who are ready to take it.

2. **Speculators.** These are those who have an opinion on the market's future trajectory. They predict whether prices will rise or fall in the future, and then buy or sell futures and options to profit from the underlying asset's future price changes.

3. **Arbitragers.** These are the derivatives market's third most prominent players. They invest in financial markets in order to obtain lower-risk profits. Arbitragers are always looking for a position with minimum risk.

Note. The key distinction between derivatives and shares is that, although shares are assets, derivatives are typically contracts (with the exception of warrants and convertible bonds, which are assets).

Basically, there are four types of derivatives: options, futures, forwards, swaps [7]. Each of these derivatives allows investors to lodge their money in a variety of ways,

ensuring both the preservation of their initial investment and the development of further returns. It's the finest instrument for investors who want to forecast their cash flows in the future, but it can also have a market impact. In the long run, derivatives assist investors in increasing their savings and investments. It aids in the transfer of risks from risk averse to risk takers. Modern derivative contracts are made up of many different combinations of these four fundamental categories, resulting in incredibly complicated contracts.

1.1.2 Options

An option is a type financial derivative that gives its owner the right but not the duty to sell or acquire an underlying asset at a defined price (strike price) on or before a certain date (expiration date) [8, 9]. Because of this, options typically require you to pay a premium representing a fraction of the agreement's value known as the option premium. Options are of two types - calls and puts. Calls give the buyer the right but not the obligation (compulsion) to buy a given quantity of the underlying asset, at a given price on or before a given future date. Puts give the buyer the right, but not the obligation to sell a given quantity of the underlying asset at a given price on or before a given date.

Option terminologies

- **Premium.** The price that traders pay for a put or call option contract is known as the option premium.
- **Intrinsic value.** Intrinsic value refers to the value of an option that the buyer derives from the right to exercise that option on a specific day.
- **Option buyer/holder.** The buyer of an option pays a premium and acquires the right to exercise that option, but not obligated to do so.
- **Option seller/writer.** A premium is paid to an option seller in exchange for losing his right to asset until it expires.
- **Strike price/Exercise price.** The pre-agreed price at which you can buy or sell the stock if you choose to exercise the option.

- **Asset price.** It is the current price of the underlying asset in the market.
- **Interest rate.** Interest rates determine the amount paid by borrowers (debtors) for holding money from lenders (creditors).
- **Dividend.** It is the amount of money paid by the company to its shareholders out of its profits.
- **Volatility.** It is the degree to which the price of the underlying asset fluctuates on a regular basis.
- **Expiration date/Maturity.** The last day that derivative contracts, such as options or futures, remain valid is known as an expiration date.
- **Exercise date.** The date on which actually the underlying asset is purchased (in the case of a call) or sold (in the case of a put) by the option holder.
- **Payoff.** It is the net profit or we say the gross of the premium paid by the buyer and received by the seller.

Moneyness of options

Moneyness refers to the market's intrinsic worth of an option's premium. It is a criteria that assesses whether an option contract will profit if it is exercised promptly.

- **In the money.** The word "in the money" refers to an option that has intrinsic value.
- **Out of the money.** The word "out of the money" refers to an option that does not have intrinsic value.
- **At the money.** If the options contract strike price is the same as the stock price then it is said to be "at the money".

Over the course of an option contract, the degree of moneyness can fluctuate.

There are numerous regulations that govern how and when the option may be exercised. The most basic type is the "European" option, which can be exercised at a set price on a

future date. An "American" option can be exercised at any time prior to a future date. The aforementioned alternatives are sometimes referred to as "vanilla" options because they are more standardised and less intriguing than "exotic" options [10].

During the last several decades the trade of options has experienced an increasing interest in both scientific work and everyday life. Therefore, there is a great need of different price calculation models to forecast the fair value of options. To better comprehend and examine the creation of financial options and their prices, we will look at some financial models.

1.2 Financial modelling and option pricing

We must first introduce the foundations upon which financial models [11] are built in order to examine and understand such natural phenomenon.

1.2.1 Stochastic differential equation

We see differential equations everywhere, almost any phenomenon, whether physical, chemical, biological, or financial, can be represented using differential equations. We deal with deterministic differential equations in most of these phenomena, but we also get stochastic differential equations (SDEs) in some of them. A SDE is a differential equation which involves one or more stochastic terms, resulting in a stochastic solution [12]. The differential equation which is resultant of the modelling of unstable asset prices S is a SDE defined as

$$dS = (r - \delta)S\,dt + \sigma S\,dW_t,$$

where r is the rate of interest, δ is the dividend yield and σ is the volatility, whereas W_t denotes the Wiener process which is a random process.

Wiener process. A Wiener process is a time-continuous process for $t \geqslant 0$ with the following properties

1. W_t is a stochastic process.

2. $W_0 = 0$.

3. $W_t \sim \mathcal{N}(0, t)$ for all $t \geqslant 0$. That is, for each t the random variable W_t is distributed normally, with mean 0 and variance t.

4. All increments $\triangle W_t = W_{t+\triangle t} - W_t$ ($\triangle t$ is an increment in time) on non overlapping time intervals are independent.

The key role in financial modelling belongs to a concept of the fair price of options. Nonetheless, the buyer and seller might utilise a theoretical fair price as a reference point in their negotiations by obtaining one. The most influential mathematical model in modern finance for option pricing is the Black-Scholes (B-S) model given by Fisher Black and Meron Scholes [13] in 1973. The B-S equations derive their essence from the stochastic dynamic of options and other financial derivatives.

1.2.2 The Black-Scholes model for option pricing

The B-S equation is a partial differential equation (PDE) that was developed in the 1970's as a tool to value the price of a call or put option over time. In the situation where the underlying assets prices follow specific stochastic processes, it describes the relationship between the prices of the options and the underlying assets under the following assumptions:

- Stock prices follow a lognormal distribution, which is based on the idea that asset prices can't go negative and are bounded by zero.

- There are no arbitrage opportunities (that is, there is no way to make a risk-free gain at no expense).

- Buying or selling the underlying asset has no transaction fees.

- Stock returns are normally distributed therefore volatility remains constant throughout time.

- The rate of return is a constant function.

Let $V(S,t)$ be the value or price of an option, assuming r be the interest rate, δ be the dividend, and σ be the volatility then the call or put option price V satisfies the parabolic PDE [14],

$$\frac{\partial V}{\partial t} + \frac{1}{2}\sigma^2 S^2 \frac{\partial^2 V}{\partial S^2} + (r-\delta)S\frac{\partial V}{\partial S} - rV = 0.$$

This is a parabolic PDE and is titled the B-S equation. To ensure a unique solution to a specific type of option, final conditions at $t = T$ and boundary conditions are required (we always consider the option holders case).

1.2.3 European option

The option which gives buyer or seller a chance to exercise the contract only at the maturity date is known as European option [14, 15]. The price of this option satisfies the B-S equation with the the terminal and boundary conditions are defined as follows:

Call Option. The payoff function (final condition) and boundary conditions for the call option are as follows:

$$V(S,T) = \max\{S-K, 0\}.$$

In the case of the call option, the contract becomes out of the money when the price of the stock decreases to zero *i.e.,* the contract becomes meaningless when $S \to 0$, so

$$\lim_{S\to 0} V(S,t) = 0,$$

and the other boundary condition is given by

$$\lim_{S\to +\infty} V(S,t) = Se^{-\delta(T-t)} - Ke^{-r(T-t)}.$$

Put Option. The payoff function and boundary conditions for the put option are as follows:

$$V(S,T) = \max\{K-S, 0\}.$$

The boundary condition as $S \to 0$ is

$$\lim_{S \to 0} V(S,t) = Ke^{r(T-t)} - Se^{-\delta(T-t)}.$$

In the case of a put option, the contract becomes out of the money when the price of the stock increases boundlessly *i.e.,* the contract becomes meaningless when $S \to +\infty$, so

$$\lim_{S \to +\infty} V(S,t) = 0.$$

1.2.4 American option

In contrast to European options, which have set maturities, American options can be exercised at any moment before they expire [16–18]. The value of American option can never be less than the value of European option i.e,

$$V^{Am}(S,t) \geqslant V^{Eur}(S,t),$$

where V^{Am} is the value of American option and V^{Eur} is the value of European option. At any moment, the American option cannot be less than the pay-off. Otherwise, the option provides a possibility for arbitrage *i.e.,* for put and call options, we have

$$V(S,t) \geqslant (K-S)^+,$$

and

$$V(S,t) \geqslant (S-K)^+,$$

respectively, for all (S,t). Here $(K-S)^+$ represents the $\max\{K-S, 0\}$ and similar holds for the other equation. We present the formulation of the American option problem as a linear complementarity problem (LCP). The associated differential operator to the

LCP is of the form

$$\mathcal{L} \equiv \frac{\partial}{\partial t} + \frac{1}{2}\sigma^2 S^2 \frac{\partial^2}{\partial S^2} + (r-\delta)S\frac{\partial}{\partial S} - rI,$$

where $S \in (0, \infty)$ is the price of the underlying asset at any time $t \in [0, T)$, and the rest of the parameters $r \geq 0$, $\delta \geq 0$, and $\sigma > 0$ are same as defined the in previous section.

The American option under the B-S framework defined on an unbounded domain is a free BVP, with no closed-form solution. In the case of American style call option with strike price K, for $V(S,t) >$ payoff, the B-S equation holds, *i.e.,* $\mathcal{L}V(S,t) = 0$, and for $V(S,t) =$ payoff, it is optimal to exercise the option. Through the combined effect of both the relations, we can derive the following LCP:

$$(\mathcal{L}V(S,t)).(V - \mathcal{F}) = 0, \quad S \in (0,\infty),\ t \in [0,T),$$

with the constraints

$$\mathcal{L}V(S,t) \geq 0, \text{ and } (V - \mathcal{F}) \geq 0,$$

where $\mathcal{F} = (S-K)^+$ is the terminal condition, also known as the payoff function. In a similar manner, we get this inequality for the American style put option with $\mathcal{F} = (K-S)^+$. In pricing the option, the following boundary condition is imposed at the left end of the underlying interval

$$\lim_{S\to 0} V(S,t) = \begin{cases} 0, & \text{for call,} \\ (K-S)^+, & \text{for put,} \end{cases}$$

that means in the case of a call option, the contract becomes worthless and for a put option, it is deep in the money for $S \to 0$. The right boundary condition is given by

$$\lim_{S\to \infty} V(S,t) = \begin{cases} (S-K)^+, & \text{for call,} \\ 0, & \text{for put,} \end{cases}$$

that means in the case of a call, the option is in the money and for a put option, it is meaningless for $S \to \infty$.

1.2.5 Binary option

A binary option is a form of option in which the payout is either fixed or nothing if the underlying stock passes a certain threshold (or striking price) [19]. In the option life, the option value depends upon whether the underlying price staying inside the barriers or cross it. If the underlying price ends up above the striking price, a binary call pays a specified amount, whereas a binary put pays a fixed amount if the underlying price ends up below the strike price at option maturity. They are classified as high investments. After all, trading binary options necessitates a thorough examination of the relevant market.

A binary option is also known as a digital or fixed return option, there are several binary options such as: high/low binary option *i.e.,* if a high/low option is employed, a specified profit is encashed if the price of the underlying asset rises/falls respectively, by one or more ticks before expiration. When dealing with boundary type binary options, the profit is realised if the price of the underlying asset is within predefined boundaries at the time of expiry. Another type is above/below binary option. In this case, we estimate that the price at expiry is above or below a certain price level. This price level is usually different than the current price, which in the previous case is known as the strike price. Some of the examples of binary options are cash-or-nothing call, asset-or-nothing call, gap call, etc. Under the B-S framework the payoff function and final boundary condition for the cash-or-nothing call option are

$$V(S,T) = \begin{cases} A, & \text{if } S \geqslant K, \\ 0, & \text{if } S < K, \end{cases}$$

and

$$\lim_{S \to +\infty} V(S,t) = Ae^{-r(T-t)},$$

respectively [20]. It means that the value of the option is determined by a predetermined

fixed amount and time in conjunction with an increase in the asset price. Unlike a cash-or-nothing option, the payoff of the more complex binary call "asset-or-nothing" option is not predetermined; it is subject to the underlying asset price. It pays off nothing if the underlying asset price S finishes below the strike price K, or pays out the asset price S itself if the underlying asset finishes above the strike price. The payoff function for the asset-or-nothing call option satisfies

$$V(S,T) = \begin{cases} S, & \text{if } S \geqslant K, \\ 0, & \text{if } S < K, \end{cases}$$

and the right boundary condition is given by

$$\lim_{S \to +\infty} V(S,t) = Se^{-\delta(T-t)}.$$

In the case of call options, the contract becomes out of the money when the price of the stock decreases to zero, *i.e.,* the contract becomes meaningless when the price of the stock drops, so in all the binary calls $\lim_{S \to 0} V(S,t) = 0$.

1.2.6 Multi-asset option pricing model

Multi-asset, multivariate or correlation options are instruments whose payment depends on at least two underlying assets not necessarily belonging to the same class. These include stock prices, exchange rates, index values or prices of commodities.

Multi-asset options have payoffs that are based on N separate assets, and the option's price is based on these assets. The pricing of these options is a higher dimensional version of the standard B-S model. In option contract trading many options involve trading of more than one asset, and the payoff of these multi-asset options is some function of ranked vanilla payoffs. The multi-asset option price $V(S,t)$ of European-style with N underlying assets satisfies a parabolic PDE under the B-S framework [21, 22], $S = (S_1, S_2, \ldots, S_N) \in \mathbb{R}^{+^N}$, $N \in \mathbb{N}$, and $S_n > 0$, $1 \leq n \leq N$, at the time $t \in [0,T)$, is

diagnosed by the following PDE:

$$\frac{\partial V(S,t)}{\partial t} + \mathcal{L}V(S,t) = 0, \quad (S,t) \in \mathbb{R}^{+N} \times [0,T).$$

In the above equation the operator $\mathcal{L}$ is defined as

$$\mathcal{L} \equiv \frac{1}{2}\sum_{n=1}^{N}\sum_{n'=1}^{N}\sigma_n\sigma_{n'}\rho_{nn'}S_nS_{n'}\frac{\partial^2 V}{\partial S_n \partial S_{n'}} + \sum_{n=1}^{N}(r-\delta_n)S_n\frac{\partial V}{\partial S_n} - rI,$$

where $r \geq 0$ is the risk-free interest rate, $\sigma_n > 0$ indicates the volatility of the nth underlying asset, $\delta_n \geq 0$ is the corresponding dividend yield and $\rho_{nn'}$ symbolizes the correlation between the n-th and n'-th underlying assets. It represents the relationship between different underlying assets. The price of the option is affected by the increase and decrease in the value of this correlation coefficient.

In options linked with multiple assets, there are distinct ways of defining the payoff function as in the case of a European-style multi-asset option. Different assets can behave differently at the time of maturity T, and based upon their performance, the boundary conditions change. Some of the examples are max/min options, index option, spread option, multi-strike option, etc.

Options on the minimum or maximum of the underlying assets are known as max/min option. The payoff functions of these options are determined by

$$V(S,T) = \begin{cases} \left(\max(S_1, S_2, \ldots, S_N) - K\right)^+, & \text{Max call option,} \\ \left(\min(S_1, S_2, \ldots, S_N) - K\right)^+, & \text{Min call option,} \end{cases}$$

where K is the strike price and $a^+ = \max\{a, 0\}$. The corresponding boundary conditions (for $(S,t) \in \partial\mathbb{R}^{+N} \times [0,T)$) are

$$V(S,t) = \begin{cases} \left(\max(S_1e^{-\delta_1(T-t)}, \ldots, S_Ne^{-\delta_N(T-t)}) - Ke^{-r(T-t)}\right)^+, & \text{Max call option,} \\ \left(\min(S_1e^{-\delta_1(T-t)}, \ldots, S_Ne^{-\delta_N(T-t)}) - Ke^{-r(T-t)}\right)^+, & \text{Min call option.} \end{cases}$$

Another most common example of multi asset option is the basket or index option. These options are traded with the payoff function

$$V(S,T) = \left(\sum_{n=1}^{N} w_n S_n - K \right)^+ ,$$

and the boundary conditions

$$V(S,t) = \left(\sum_{n=1}^{N} w_n S_n e^{-\delta_n (T-t)} - K e^{-r(T-t)} \right)^+ , \quad (S,t) \in \partial \mathbb{R}^{+N} \times [0,T),$$

where w_n are the portfolio weights.

Such options provide a more realistic view of the financial markets since most of the assets are related to each other. Thus, the change in any of the assets, using correlation parameter will show a combined affect on the price of an option.

1.2.7 Fractional Black-Scholes model

In this part, we introduce the time-fractional option pricing model under the B-S framework, where the order of the temporal derivative is taken to be a fraction rather than an integer. Fractional derivatives are quite flexible for characterizing the behavior of differential equations and adding historical information due to their nonlocal nature [23]. Therefore, in this section we derive the time fractional B-S PDE. Therefore, if the path of the stock price S is modelled by the following fractional stochastic differential equation

$$dS = (r-\delta)Sdt + \sigma S W_t (dt)^{\frac{\alpha(S,t)}{2}}, \ 0 < \alpha \leq 1.$$

Now, using the fractional Taylor series expansion and the fractional Ito's lemma, we obtain the time-fractional B-S equation [24, 25]

$$\frac{\partial^{\alpha(S,t)} V}{\partial t^{\alpha(S,t)}} + \sigma^2 S^2 \frac{\Gamma(1+\alpha(S,t))}{2} \frac{\partial^2 V}{\partial S^2} + (r-\delta) S \frac{t^{1-\alpha(S,t)}}{\Gamma(2-\alpha(S,t))} \frac{\partial V}{\partial S} - r \frac{t^{1-\alpha(S,t)}}{\Gamma(2-\alpha(S,t))} V = 0,$$

subject to the following terminal and boundary conditions for a European call option

$$V(S,T) = \max\{S-K,0\},$$
$$\lim_{S\to 0} V(S,t) = 0,$$
$$\lim_{S\to +\infty} V(S,t) = Se^{-\delta(T-t)} - Ke^{-r(T-t)},$$

and for European put the boundary condition as $S \to 0$ is $V(S,t) \to Ke^{r(T-t)} - Se^{-\delta(T-t)}$, and for $\to +\infty$, $V(S,t) \to 0$. Also, the payoff function is defined as

$$V(S,T) = \max\{K-S,0\}.$$

1.3 Greeks

The B-S model depends upon various parameters. This section will consider the various measures of how the price of an option changes by varying these parameters. These measures are known as the Greeks as each of them is symbolized by a Greek letter. Greeks are important for determining how sensitive a portfolio of options is to market conditions [26–28]. In an option position, the Greeks can be useful tools for assessing and managing risk. Different and unique Greeks are used to measure different aspects of the risk associated with an option position. As the price of an option fluctuates, so does the risk of the option. As a result, knowing how the option price varies allows the trader to mitigate the risk of the option. Here, we explain some of these Greeks and how they are used.

Delta (Δ). The simplest Greek "Delta" is the rate at which the option price changes with respect to the price of the underlying asset. In the B-S model, the generic option price V depends on the parameters, S, t, K, r, σ, then the Greek Δ is given by $\Delta = \frac{\partial V}{\partial S}$, where S is an underlying asset price.

Gamma (Γ). "Gamma" measures the delta's sensitivity to a small change in the underlying assets. It is also the second derivative of the option price with respect to the

underlier. In the B-S model, the Greek Γ is given by $\Gamma = \frac{\partial \Delta}{\partial S} = \frac{\partial^2 V}{\partial S^2}$. As the put and call prices differ by a linear function, their Gamma's are the same. It measures the convexity of the value function, which makes options interesting for many investors.

Theta (Θ). The Greek "Theta" is the derivative of the value of a given option expiring on a given day with respect to time. As it measures the change in the option price to the movement of time to maturity, it is negative of the derivative with respect to the parameter t and is given by $\Theta = -\frac{\partial V}{\partial t}$, where t is the passage of time. It represents that with the passage of time, the value of an option contract will change. In most cases, the option will experience a decrease in value with the passage of time. This is known as time decay.

Charm. "Charm", also known as delta decay or delta bleed, measures the delta's sensitivity to a small movement in time to maturity *i.e.,* it is the rate at which the delta of an option or warrant changes with respect to time to the maturity. Thus it refers to the negative of the second-order derivative (one with respect to both time and asset) of an option's value. It is also the derivative of theta with respect to the underlying asset price. Mathematically, it is given by

$$\text{Charm} = -\frac{\partial \Delta}{\partial t} = -\frac{\partial^2 V}{\partial S \partial t}.$$

Color. "Color", also known as the gamma decay, measures gamma's sensitivity to a small movement in time to maturity *i.e.,* it is the rate at which the gamma of an option changes with respect to time towards maturity. It is a negative of the third-order derivative (one and two with respect to time and asset, respectively) of the option's value. Mathematically, it is given by

$$\text{Color} = -\frac{\partial \Gamma}{\partial t} = -\frac{\partial^3 V}{\partial S^2 \partial t}.$$

Now we'll go over some fundamental risk concepts that involve the use of Greeks.

1.3.1 Delta hedging

Delta hedging is an investment strategy that combines the purchase or sale of an option with an offsetting transaction in the underlying asset to minimize the risk of the option's price moving in one direction [29]. It makes the portfolio less sensitive to small price changes in the securities invested in.

For example if the price of a call option does not change at all, the call option loses its time value, and the investor makes money on call options while losing money on the underlying stock by selling the call option. Using the delta derived from the B-S option pricing model, the option holder can find out the delta-hedged portfolio with lower risk than the non-hedged portfolio.

Figure 1.2: Managing risk

How other Greeks help in risk management: Gamma and other Greeks' (which are derived from delta) hedging are trading strategies in which the option holder tries to maintain a constant delta in an options position, often one that is delta-neutral, with the change in respective parameters.

Formally, theta is the negative of the first derivative of the option pricing model with respect to changes in the time until expiration. To reduce the risk one has to construct a portfolio with a positive theta, *i.e.,* with the passage of time there is an increase in the

value of the portfolio. In the similar manner, we analyse rest of the Greeks to study the market impact on the option's price.

1.4 Numerical techniques

Many important and challenging problems in computational science and engineering involve PDEs which are tedious to solve analytically. Therefore, mathematicians have developed numerical techniques (methods) to solve such differential equations [30]. These methods require development, analysis and use of algorithms. Numerical algorithms invariably involve a large number of arithmetic calculations and, therefore, require fast and efficient computing devices

Numerical methods are explicit or implicit computed in one step or multiple steps. An explicit method computes the numerical solution at the next time point using the previous numerical solution at the previous time point. While an implicit method evaluates a function using the numerical solution at the next time point which is solved for.

1.4.1 Characteristics of computational numerical methods

The following are some properties that can be used to validate and prove the efficacy of a numerical method:

- **Accuracy.** Every method of numerical computation contains flaws. It is possible that they are caused by the computer's inexact representation and manipulation of numbers. The accuracy of the results is harmed as a result of these inaccuracies.
- **Efficiency.** It refers to the amount of human and computer effort required to put the method into practise.
- **Consistency.** A discretization scheme is said to be consistent if the discretized equations for decreasing mesh size should approach to the original differential equations.
- **Stability.** The general idea behind stability is to investigate how small perturbations (e.g., caused by round-off errors) influence the subsequent time steps.

- **Convergence.** When the spatial and temporal grids are refined, one of the most important requirements for a discretization method is that the approximate solution approaches the actual solution.

1.4.2 Challenges in the Black-Scholes option pricing model

The following are the difficulties that must be overcome while numerically investigating an option:

- **Discontinuous payoff.** In the B-S model, the payout function (final condition) is discontinuous. Standard numerical techniques struggle with discontinuous final conditions. In particular, expected convergence rates are not observed, and oscillations are more likely to occur in the solution.

- **Non dimensionalization.** The actual B-S model is not dimension free, so it is tough to assess the relation between different parameters. As a result, before solving the problem, it is preferable to make it dimensionless.

- **Infinite domain.** The B-S model has a unbounded domain. Thus, to avoid the large truncation error, finite boundaries should be employed for numerical implementation [31].

- **Non-smooth Greeks.** Approximating Greeks in option pricing is a challenging task since they are non-smooth functions. This non-smoothness creates quantization error, which can lead to a significant reduction in numerical scheme convergence rates.

- **Final value problem.** The B-S model results in a final value problem. But for the numerical implementation it is necessary to convert the final value problem to an initial value problem.

- **Free boundary.** American style vanilla options result in free-boundary value problems since such options can be exercised at any time on or before expiration

date. Thus, one has to use special techniques to such moving boundary value option pricing models.

Options are like miraculous pills but must be handled with care and caution, as they may be detrimental to your financial health if wrongly used (calculated). Thus the goal is to develop an appropriate numerical technique with suitable transformation to correctly predict the price of an option. Also, the technique should be efficient to compute the derivatives of the option price function to replicate the portfolio periodically to offset any risk associated with the movements in different parameters present the model.

1.5 Motivation

An applied mathematics research thesis covers the area that makes a remarkable change to the world. In financial markets a significant number of prices must be calculated in a short period of time, hence an accurate and quick calculation of option pricing is critical. Thus, there is always a need for fast, accurate and efficient numerical methods for the valuation of various contracts. Every research project must, in some way, address a gap which covers the topic that has not yet been explored or is under-explored. Therefore the numerical schemes presented here are not yet applied to option pricing problems.

Moreover, a research always starts with new developments and creations. In this context, we have developed various computational methods to study a variety of problems and conquer the challenges present in solving the option pricing models and finding the hedging parameters, useful for managing financial risks. Also, there is always a scope of extension and improvement in a research topic therefore, we have taken it to a new platform of fractional option pricing models.

1.6 Thesis contribution

In this thesis we develop, analyse, and implement a number of numerical approaches for simulating the price and Greeks of various options involving higher dimensional models, free boundary value problems, fractional differential equations and other problems. More-

over, since numerical approaches are more for application purposes, we are investigating the Hedging parameters (risk management parameters in finance, specifically the change in the option price with various factors) that are difficult to determine with usual methods. Therefore, option pricing principles and techniques are both reflected in this thesis.

The present work fills the applicability gaps of various computing schemes on financial models. Wavelet schemes are applied to an option pricing model on which no light has yet been shed. We are also filling in the blanks in methodologies that provide high accuracy for financial models in space. The combination of Rannacher time marching scheme with the highly accurate orthogonal spline collocation method to tackle the non smoothness of the payoff function is an example. Also, we have extended our work to fractional option pricing models. Since fractional derivatives are quite flexible for characterizing the behavior of differential equations and adding historical information due to their non-local nature. A novel fractional operator known as Atangana-Baleanu Caputo derivative is operated and analysed to study the solution of the fractional financial differential equations.

This work concentrates on the creation of various numerical schemes such as wavelet approaches, spline based approximations, difference schemes etc, for PDEs with discontinuous initial and final conditions. It also provide the readers the idea to solve free boundary value problems using wavelets and spline based approaches. We have also discussed the convergence, stability, and consistency of various techniques. The pros and cons of the described option pricing techniques are discussed.

1.7 Thesis organisation

This thesis is a result of my true interest in option pricing. It consists of eight chapters. The fundamental components of the financial derivatives and B-S pricing model have been covered in Chapter 1. It all starts with the idea of an option, its classification, and its features. The stochastic differential equation depicting the movement of the asset price is next introduced to build the groundwork for our ultimate deduction of the famous B-S Equation. Finally, we look at how different styles of exercising, payoff functions and boundary conditions generate distinct options. Following that, we have introduced a section

involving the discussion on numerical approaches and their various characteristics with the challenges one faces to solve the B-S PDEs. Finally, in this section, we have introduced the motivation behind the present work and the thesis contribution. Chapter 2 covers the theoretical and numerical aspects of the simple and widely used European options. The chapter comprises the literature survey on the European option pricing problem and the methods developed to solve them. A new method known as the Haar wavelet method is constructed to solve these options and their Greeks. Details of the method including the introduction, formation, implementation, convergence, and application are presented.

Chapter 3 deals with the pricing of American options with applications to the hedging parameters. The chapter discusses the challenges related to solving free boundary problems. It included an overview of the American option in context to the the European option. The chapter focuses on solving the Greeks of American option having vast applications in financial markets using the Haar wavelet scheme. The explanation of the method and its properties are discussed comprehensively. Chapter 4 presents the wavelet based numerical approaches for solving the various path-independent binary options with spiked solution functions and Greeks. The present wavelet based approach is proved to be a good option to solve such spiked functions. The consistency and stability analysis of the Haar wavelet scheme is discussed in detail.

Chapter 5 extends the B-S PDE to higher dimensions and covers the effectiveness of the two-dimensional Haar wavelet scheme to solve it. The effectiveness of the method to solve multi-dimensional problems is shown theoretically and numerically. Moreover, various hedging parameters are computed and their applications have been discussed to find notifiable facts in various subsets. Chapter 6 discusses the challenges related to solving the PDEs with non-smooth initial data with classical time marching schemes. To address the challenges, the standard finite difference schemes are studied and compared to their conjunctive Rannacher scheme. Moreover to improve the accuracy of the method in space in this chapter we consider a new scheme known as the spline collocation at Gauss points. Following that, in the core of the chapter, the convergence of the numerical method is presented. Finally, numerical results in the form of tables and graphs are provided to

prove the effectiveness of the scheme.

In Chapter 7, we extend the integer order option pricing problems to fractional PDEs, which is a challenging target problem with a lot of applications. In this chapter, we discuss a modified B-S model of option pricing with variable order time-fractional derivative. The model's formulation is briefly described, and then the approach and operator used to solve the model are thoroughly explored. Furthermore, through rigorous analysis, the stability of the numerical scheme is described. Finally to support the theoretical findings numerical results are discussed. Subsequently, Chapter 8 provides some closing observations and discuss potential future extensions of the work.

Chapter 2

A wavelet based numerical scheme to explore Greeks' of European options

---

In financial markets, investors use options to speculate or hedge against investment risk. As a result, one of the major difficulties in both theoretical study and practical implementations is to find the fair price of the option, and to determining the Greeks of an option. As discussed earlier, options are a great investment instrument because they provide you more freedom, lower your risks, and improve your earnings in the stock market. You will utilise options in your financial portfolio for the rest of your life if you understand how to use them effectively. In this chapter, we develop an efficient numerical scheme to investigate the price and sensitivities of European vanilla option. European option is the simplest of vanilla style options, therefore it gives the reader a detailed look at how option prices and Greeks react to changes in input prices as well as graphical representations of these changes.

2.1 Literature survey

Many studies have made a significant contribution in investigating the price of European options and their Greeks. The pioneering work done by Fischer Black and Merton Scholes

provided one of the effective and widely used models for option pricing problem that is the well-known Black-Scholes model [13]. Several analytical and numerical methods have been developed for European options, for instance, Achdou and Tchou [32] proposed a variational analysis and provide FEM and FDM based numerical simulations for the Black-Scholes equation for the price of a European option. Later, using discontinuous functions in time and continuous functions in space Ern *et al.* [33] investigated FEMs for European options. They have used adaptive mesh refinement technique which is computationally better compared to the usual mesh. For a detailed literature survey of valuation models to the option pricing problems from its origin to 2004 the readers are referred to [34]. To solve the PDE associated with the European option pricing, Matache *et al.* [35] suggested θ-scheme in temporal direction and a wavelet Galerkin method in the spatial direction. Gracia and Oosterlee [36] have developed a novel method for pricing European options based on the wavelet approximation method and the characteristic function. They have focused on the discounted expected payoff pricing formula and computed it by means of wavelets.

Černá and Finěk [37] used quadratic and cubic spline wavelet functions to solve the Black-Scholes model for calculating the price of European put and call options on a basket of assets. Rad *et al.* [38] suggested the meshfree radial basis point interpolation (RBPI) method for the Black–Scholes model for the European and American options. The RBPI is combined with a number of numerical techniques, including an exponential change of variables, which allows the option prices to be approximated over their entire spatial domain. A mesh refinement algorithm, which has proven to be very useful in dealing with non-smooth options' payoff, and an implicit Euler Richardson extrapolated scheme, which provides a satisfactory level of time accuracy was used.

In another work, Rad *et al.* [39] proposed and analyzed the local weak form meshfree methods for option pricing. In this study, they have considered the local boundary integral equation approach, which is based on moving least squares approximation, and the local radial point interpolation, which is based on Wu's compactly supported radial basis functions. They [40] have also proposed a meshfree local Petrov–Galerkin method for the

American option problems. Recently, Maree *et al.* [41] extended the theory of Shannon Wavelet Inverse Fourier Technique (SWIFT) for European options. They have shown that the method converges exponentially to the wavelet approximation scale. They have also shown that under specific parameter choices the SWIFT can be reduced to the COS method which is based on Fourier-cosine series [42]. Most of the researches listed above have not concentrated on computing the Greeks of the European options since the Greek functions are non-smooth in nature and hard to evaluate.

To this end, there is always a need for more effective and simple numerical algorithms to explore such problems. In this chapter, a two-dimensional Haar wavelet method is developed to study the sensitivities of the price of an option. The method is appropriate to analyze these sensitivities as it explicitly gives the values of all the derivatives of the solution, so it easily approximates the option Greeks. The Black-Scholes model for European style options has been considered to analyze the physical and numerical aspects of the put and the call option Greeks. We have used the concept of coordinate transformation to make the Black-Scholes equation dimensionless and to resolve the obstacle in approximating the Greeks having discontinuities at the strike price. Also, the infinite spatial domain has been truncated into the finite domain to avoid large truncation errors. Through rigorous analysis, the method is shown to be first-order accurate in the L^2-norm. The numerical computations performed to approximate the option price and various Greeks, like delta, theta, gamma, etc, confirm the theoretical results in the L^2-norm. The relative errors and the maximum absolute errors are also presented. The motivational work of option Greeks analysis may leave a significant impact on financial institutes; it helps them to manage the risk by setting the portfolio's new value and to estimate the probability of losing money.

2.2 Model description

We can determine the price of European call and put options with the help of the Black-Scholes PDE with specified initial and boundary conditions. We denote by $V(S, \tau)$, the value of option before the expiry time T, where S is the current price of the underlying

asset in the market at the time τ. The value of the option also depends upon the risk-free interest rate r, the strike price K, the volatility σ, and the dividend yield δ. The equation governing the price of different options is given as

$$\frac{\partial V}{\partial \tau} + \frac{1}{2}\sigma^2 S^2 \frac{\partial^2 V}{\partial S^2} + (r-\delta)S\frac{\partial V}{\partial S} - rV = 0, \quad 0 < S < \infty,\ 0 \leqslant \tau < T. \tag{2.2.1}$$

For call option in which the option holder has the right but not the obligation to buy the option, the payoff function is defined as

$$V(S,T) = \max\{S-K, 0\},$$

and the boundary conditions for the call option are as follows

$$\lim_{S\to 0} V(S,\tau) = 0,$$
$$\lim_{S\to +\infty} V(S,\tau) = Se^{-\delta(T-\tau)} - Ke^{-r(T-\tau)}.$$

In case of put option, when the option holder has the right not the compulsion to sell the option, therefore the payoff function and boundary conditions for the put option are as follows:

$$V(S,T) = \max\{K-S, 0\}.$$

The boundary conditions are

$$\lim_{S\to 0} V(S,\tau) = Ke^{r(T-\tau)} - Se^{-\delta(T-\tau)}, \text{ and } \lim_{S\to +\infty} V(S,\tau) = 0.$$

Using a log-transformation, we transform the equation (2.2.1) from final value problem to a non-dimensional initial value problem by introducing the new variables $x = \ln(S/K)$ and $\tau = T - \frac{2t}{\sigma^2}$, which reduces the Black-Scholes equation (2.2.1) into

$$\frac{\partial u}{\partial t} = \frac{\partial^2 u}{\partial x^2}, \tag{2.2.2}$$

where $V(S,\tau) = Ke^{-\left[2\left(\frac{r-\delta}{\sigma^2}\right)-1\right]\frac{x}{2}-\left[\frac{1}{4}\left(2\left(\frac{r-\delta}{\sigma^2}\right)-1\right)^2+\frac{2r}{\sigma^2}\right]t}u(x,t)$. After transformation, the initial and boundary conditions for the call and put options are as follows:

Call option. The initial condition for the call option is given by

$$u(x,0) = \max\left\{e^{\frac{x}{2}\left(\frac{2(r-\delta)}{\sigma^2}+1\right)} - e^{\frac{x}{2}\left(\frac{2(r-\delta)}{\sigma^2}-1\right)},\, 0\right\},$$

and the boundary conditions become

$$\lim_{x\to-\infty} u(x,t) = 0,$$

and

$$\lim_{x\to+\infty} u(x,t) = e^{\frac{x}{2}\left(\frac{2(r-\delta)}{\sigma^2}+1\right)+\frac{t}{4}\left(\frac{2(r-\delta)}{\sigma^2}+1\right)^2} - e^{\frac{x}{2}\left(\frac{2(r-\delta)}{\sigma^2}-1\right)+\frac{t}{4}\left(\frac{2(r-\delta)}{\sigma^2}-1\right)^2}.$$

Put option. The initial condition for the put option is given by

$$u(x,0) = \max\left\{e^{\frac{x}{2}\left(\frac{2(r-\delta)}{\sigma^2}-1\right)} - e^{\frac{x}{2}\left(\frac{2(r-\delta)}{\sigma^2}+1\right)},\, 0\right\},$$

and the boundary conditions become

$$\lim_{x\to-\infty} u(x,t) = e^{\frac{x}{2}\left(\frac{2(r-\delta)}{\sigma^2}-1\right)+\frac{t}{4}\left(\frac{2(r-\delta)}{\sigma^2}-1\right)^2} - e^{\frac{x}{2}\left(\frac{2(r-\delta)}{\sigma^2}+1\right)+\frac{t}{4}\left(\frac{2(r-\delta)}{\sigma^2}+1\right)^2},\quad \lim_{x\to+\infty} u(x,t) = 0.$$

For the numerical implementation, we truncate the infinite domain into a finite domain to avoid the unacceptable large truncation error, by taking the relatively large value of x to get the high accuracy of asymptotic results such that $(x,t) \in [x_{\min}, x_{\max}] \times \left[0, \frac{\sigma^2 T}{2}\right]$.

2.3 Methodology

Wavelets are mathematical functions that satisfy specific properties. These used to localize data sets and functions according to space and scale. To approximate the required function, wavelet analysis uses the precise technique of scaling and shifting of two prototype functions known as the scaling function and the mother wavelet. This technique is also

known as the windowing technique in which we analyze the function by changing the size of the window *i.e.,* we split the domain into sub-domains of different sizes and study each sub-domain separately with a resolution matched to its scale. The "mother wavelet" is defined as follows:

$$\psi_{d_1,d_2}(x) = \frac{1}{\sqrt{|d_1|}}\psi\left(\frac{x-d_2}{d_1}\right),\ d_1, d_2 \in \mathbb{R},\ d_1 \neq 0,$$

where d_1 measures the degree of compression and known as the scaling parameter, whereas d_2 determines the location of the wavelet and known as the shifting parameter *i.e.,* change in the value of d_2 moves the localization center: each function $\psi_{d_1,d_2}(x)$ localized around $x = d_2$. Based on the nature of the mother wavelet, there are two types of wavelet transformations: continuous wavelet transformation (CWT) and discrete wavelet transformation (DWT). Any function belonging to the Hilbert space of $L^2(\mathbb{R})$, is determined by the DWT using the formula $f(x) = \sum_{d_1,d_2=-\infty}^{\infty} \langle f, \psi_{d_1,d_2} \rangle\ \psi_{d_1,d_2}(x)$, where the wavelets ψ_{d_1,d_2} form an orthonormal basis.

Table 2.1: Examples of different families of orthogonal wavelets and their abbreviations.

Wavelet families	Abbreviations
Haar wavelet	haar
Symlets	sym
Coiflets	coif
Daubechies wavelet	db
Meyer wavelet	meyr

2.3.1 Haar wavelet function approximation

Haar wavelet transform is the discrete type of wavelet transform introduced by Alfred Haar in 1909. Haar wavelet is a family of square-shaped functions generated by translation and dilation of a discrete function (mother wavelet), which collectively form the Haar basis [43, 44]. In Haar analysis, the father wavelet (scaling function) and the mother wavelet

are defined as

$$h_1(x) = \begin{cases} 1, & x \in [a, b), \\ 0, & \text{elsewhere}, \end{cases}$$

and

$$h_2(x) = \begin{cases} 1, & x \in [a, \frac{a+b}{2}), \\ -1, & x \in [\frac{a+b}{2}, b), \\ 0, & \text{elsewhere}, \end{cases}$$

respectively, and the rest of the Haar wavelet family generated by the above two basic wavelets for $x \in [a, b]$ is defined as follows:

$$h_i(x) = \begin{cases} 1, & x \in [\alpha_i, \beta_i), \\ -1, & x \in [\beta_i, \gamma_i), \\ 0, & \text{elsewhere}, \end{cases}$$

where $\alpha_i = a + \frac{k(b-a)}{m}$, $\beta_i = a + \frac{(k+0.5)(b-a)}{m}$, and $\gamma_i = a + \frac{(k+1)(b-a)}{m}$. In these formulae $m = 2^j$, $j = 1, 2, \ldots, J$, and $k = 0, 1, \ldots, m-1$, where j indicates the level of resolution, k indicates the translation parameter, and J indicates the maximum level of resolution. The index i is determined by the formula $i = m + k + 1$.

Moreover, the minimal values of k and m are 0 and 2, respectively, and the maximal value of i is 2^{J+1}. The given interval $[a, b]$ is partitioned into $2M$ sub-intervals of equal length using the collocation points $x_l = a + \frac{(l-0.5)(b-a)}{2M}$, $l = 1, 2, \ldots, 2M$.

The integrals of the wavelets are defined as $p_i(x) = \int_a^x h_i(x)\ dx$ and $q_i(x) = \int_a^x p_i(x)\ dx$, these integrals can be calculated using the values of $h_i(x)$ and are given

by

$$p_i(x) = \begin{cases} x - \alpha_i, & x \in [\alpha_i, \beta_i), \\ \gamma_i - x, & x \in [\beta_i, \gamma_i), \\ 0, & \text{elsewhere}, \end{cases} \text{ and } q_i(x) = \begin{cases} \frac{(x-\alpha_i)^2}{2}, & x \in [\alpha_i, \beta_i), \\ \frac{(x-\alpha_i)^2 - 2(x-\beta_i)^2}{2}, & x \in [\beta_i, \gamma_i), \\ \frac{(x-\alpha_i)^2 - 2(x-\beta_i)^2 + (x-\gamma_i)^2}{2}, & x \in [\gamma_i, b), \\ 0, & \text{elsewhere}. \end{cases}$$

Remark In Haar analysis, the mother wavelet is dilated by a power of two and translated by an integer.

2.3.2 Implementation of 2D Haar wavelets

Consider the transformed equation (2.2.2) of the Black-Scholes PDE, where $(x, t) \in [a, b] \times \left[0, \frac{\sigma^2 T}{2}\right]$, where $a = x_{\min}$ and $b = x_{\max}$. To find the solution of the original equation (2.2.1) and its derivatives, we have to determine the unknown functions $u(x, t)$, $u_t(x, t), u_x(x, t)$ and $u_{xx}(x, t)$ satisfying given initial and boundary conditions. Let U and u are the approximate and exact solutions of (2.2.2), respectively. Discretize the spatial domain $[a, b]$ and the temporal domain $\left[0, \frac{\sigma^2 T}{2}\right]$ into $2M_1$ and $2M_2$ parts of equal length with J and J_1 as maximal level of resolution, respectively. Now, consider the wavelet approximation

$$\frac{\partial^3 U(x,t)}{\partial t \partial x^2} = \sum_{i=1}^{2M_1} \sum_{i_1=1}^{2M_2} c_{i,i_1} h_i(x) h_{i_1}(t),$$

where c_{i,i_1} are the unknown coefficients and i, i_1 denotes the indices of Haar functions on spatial and temporal domains, respectively. After integrating the above expression twice with respect to x from a to x, we get

$$\frac{\partial U(x,t)}{\partial t} = \sum_{i=1}^{2M_1} \sum_{i_1=1}^{2M_2} c_{i,i_1} q_i(x) h_{i_1}(t) + \sum_{N_1=0}^{1} \frac{(x-a)^{N_1}}{N_1!} \frac{\partial^{1+N_1} U(a,t)}{\partial t \partial x^{N_1}}.$$

Now, by integrating it with respect to t from 0 to t, we get

$$U(x,t) = \sum_{i=1}^{2M_1}\sum_{i_1=1}^{2M_2} c_{i,i_1} q_i(x) p_{i_1}(t) + U(x,0) + \sum_{N_1=0}^{1} \frac{(x-a)^{N_1}}{N_1!}\frac{\partial^{N_1} U(a,t)}{\partial x^{N_1}} - \sum_{N_1=0}^{1} \frac{(x-a)^{N_1}}{N_1!}\frac{\partial^{N_1} U(a,0)}{\partial x^{N_1}}.$$

After expanding it, we get

$$U(x,t) = \sum_{i=1}^{2M_1}\sum_{i_1=1}^{2M_2} c_{i,i_1} q_i(x) p_{i_1}(t) + U(x,0) + U(a,t) + (x-a)\frac{\partial U(a,t)}{\partial x} - U(a,0) - (x-a)\frac{\partial U(a,0)}{\partial x}.$$

Now, by taking $x = b$ and considering the boundary conditions, we get

$$\frac{\partial U(a,t)}{\partial x} = \frac{1}{b-a}\Bigg\{U(b,t) - \sum_{i=1}^{2M_1}\sum_{i_1=1}^{2M_2} c_{i,i_1} q_i(b) p_{i_1}(t) - U(b,0) - U(a,t) + U(a,0) + (b-a)\frac{\partial U(a,0)}{\partial x}\Bigg\}.$$

On replacing the value of $\frac{\partial U(a,t)}{\partial x}$ back into $U(x,t)$, we get

$$U(x,t) = \sum_{i=1}^{2M_1}\sum_{i_1=1}^{2M_2} c_{i,i_1} q_i(x) p_{i_1}(t) + U(x,0) + U(a,t) - U(a,0) + \frac{x-a}{b-a}\Bigg\{U(b,t) - \sum_{i=1}^{2M_1}\sum_{i_1=1}^{2M_2} c_{i,i_1} q_i(b) p_{i_1}(t) - U(b,0) - U(a,t) + U(a,0)\Bigg\}. \tag{2.3.1}$$

Now by differentiating U once with respect to x, we get

$$\frac{\partial U(x,t)}{\partial x} = \sum_{i=1}^{2M_1}\sum_{i_1=1}^{2M_2} c_{i,i_1} p_i(x) p_{i_1}(t) + \frac{\partial U(x,0)}{\partial x}$$

$$+\frac{1}{b-a}\left\{U(b,t)-\sum_{i=1}^{2M_1}\sum_{i_1=1}^{2M_2}c_{i,i_1}q_i(b)p_{i_1}(t)-U(b,0)-U(a,t)+U(a,0)\right\}. \quad (2.3.2)$$

Again, differentiating it with respect to x, we get

$$\frac{\partial^2 U(x,t)}{\partial x^2}=\sum_{i=1}^{2M_1}\sum_{i_1=1}^{2M_2}c_{i,i_1}h_i(x)p_{i_1}(t)+\frac{\partial^2 U(x,0)}{\partial x^2}. \quad (2.3.3)$$

Similarly, by differentiating (2.3.1) once with respect to t, we get

$$\begin{aligned}\frac{\partial U(x,t)}{\partial t}=&\sum_{i=1}^{2M_1}\sum_{i_1=1}^{2M_2}c_{i,i_1}q_i(x)h_{i_1}(t)+\frac{\partial U(a,t)}{\partial t}+\frac{x-a}{b-a}\left\{\frac{\partial U(b,t)}{\partial t}\right.\\&\left.-\sum_{i=1}^{2M_1}\sum_{i_1=1}^{2M_2}c_{i,i_1}q_i(b)h_{i_1}(t)-\frac{\partial U(a,t)}{\partial t}\right\}. \quad (2.3.4)\end{aligned}$$

Now, by putting the approximated values of $\frac{\partial u(x,t)}{\partial t}$ and $\frac{\partial^2 u(x,t)}{\partial x^2}$ in equation (2.2.2), and by considering the initial and boundary conditions, we get a system of linear equations in unknown coefficients c_{i,i_1}. By substituting the values of the coefficients c_{i,i_1} into the equations (2.3.1)-(2.3.4), we get the solution and derivatives of the transformed equation. Finally, for applying back substitution of the coordinate transformation we use $S=Ke^x$ and $\tau=T-\frac{2t}{\sigma^2}$ to get the solution of the Black-Scholes equation and the values of the option Greeks.

2.4 Convergence analysis

In this section, we will show that the two-dimensional Haar wavelet method is the first-order convergent in the L^2-norm.

Theorem 2.4.1. *The upper bounds for the Haar wavelets and their derivatives are as follows:*

$$h_i(x)\leqslant 1,\ \forall\, i \textit{ and } p_i(x)\leqslant\frac{1}{2^{j+1}},\quad q_i(x)<B\left(\frac{1}{2^{j+1}}\right)^2,\ \textit{for } i>1,$$

where j is the level of resolution and $B = \dfrac{8}{3(\lfloor (3/2) \rfloor !)^2}$.

Proof. Refer [45]. □

Theorem 2.4.2. *Let $g(x,t) = \frac{\partial^3 u(x,t)}{\partial x^2 \partial t} \in L^2(\mathbb{R}^2)$ be a continuous function on the domain $[a,b] \times \left[0, \frac{\sigma^2 T}{2}\right]$ and g, $\frac{\partial g}{\partial x}$, $\frac{\partial g}{\partial t}$, $\frac{\partial^2 g}{\partial x \partial t}$ are bounded by η, for some η. Then, the proposed 2D Haar wavelet method converges linearly to the exact solution* i.e.,

$$\|Error_{J,J_1}(x,t)\|_2 = O\left(\frac{1}{2^{\overline{J}+1}}\right), \text{ where } \overline{J} = \min\{J, J_1\}.$$

Proof. The exact solution of the transformed second-order PDE of the Black-Scholes equation can be written as

$$\begin{aligned} u(x,t) =& \sum_{i=0}^{\infty}\sum_{i_1=0}^{\infty} c_{i,i_1} q_i(x) p_{i_1}(t) + \Psi(x,t) \\ =& c_{1,1} q_1(x) p_1(t) + \sum_{j=0}^{\infty}\sum_{k=0}^{2^j-1} c_{2^j+k+1,1} q_{2^j+k+1}(x) p_1(t) + \sum_{j_1=0}^{\infty}\sum_{k_1=0}^{2^{j_1}-1} c_{1,2^{j_1}+k_1+1} q_1(x) \\ & \times p_{2^{j_1}+k_1+1}(t) + \sum_{j=0}^{\infty}\sum_{k=0}^{2^j-1}\sum_{j_1=0}^{\infty}\sum_{k_1=0}^{2^{j_1}-1} c_{2^j+k+1,2^{j_1}+k_1+1} q_{2^j+k+1}(x) p_{2^{j_1}+k_1+1}(t) \\ & + \Psi(x,t), \end{aligned}$$

where j, j_1, and k, k_1 indicate the levels of resolution and translation parameters in spatial and temporal domains, respectively. The function $\Psi(x,t)$ is determined by the given initial and boundary conditions. Moreover, $i = 2^j + k + 1$, and $i_1 = 2^{j_1} + k_1 + 1$ are the respective indices. Now, the approximate solution at the maximum level of resolution is

$$\begin{aligned} U(x,t) =& c_{1,1} q_1(x) p_1(t) + \sum_{j=0}^{J}\sum_{k=0}^{2^j-1} c_{2^j+k+1,1} q_{2^j+k+1}(x) p_1(t) + \sum_{j_1=0}^{J_1}\sum_{k_1=0}^{2^{j_1}-1} c_{1,2^{j_1}+k_1+1} q_1(x) \\ & \times p_{2^{j_1}+k_1+1}(t) + \sum_{j=0}^{J}\sum_{k=0}^{2^j-1}\sum_{j_1=0}^{J_1}\sum_{k_1=0}^{2^{j_1}-1} c_{2^j+k+1,2^{j_1}+k_1+1} q_{2^j+k+1}(x) p_{2^{j_1}+k_1+1}(t) + \Psi(x,t). \end{aligned}$$

Then, the error at the maximum level of resolution is

$$
\begin{aligned}
Error_{J,J_1}(x,t) &= u(x,t) - U(x,t) \\
&= \sum_{j=J+1}^{\infty} \sum_{k=0}^{2^j-1} c_{2^j+k+1,1} q_{2^j+k+1}(x) p_1(t) + \sum_{j_1=J_1+1}^{\infty} \sum_{k_1=0}^{2^{j_1}-1} c_{1,2^{j_1}+k_1+1} q_1(x) \\
&\times p_{2^{j_1}+k_1+1}(t) + \sum_{j=J+1}^{\infty} \sum_{k=0}^{2^j-1} \sum_{j_1=J_1+1}^{\infty} \sum_{k_1=0}^{2^{j_1}-1} c_{2^j+k+1,2^{j_1}+k_1+1} q_{2^j+k+1}(x) p_{2^{j_1}+k_1+1}(t).
\end{aligned}
$$

By taking L^2-norm of the error function, we get

$$
\|Error_{J,J_1}(x,t)\|_2^2 = S_1 + S_2 + S_3 + S_4 + S_5 + S_6,
$$

where

$$
\begin{aligned}
S_1 &= \sum_{j,k} \sum_{r,s} c_{2^j+k+1,1} c_{2^r+s+1,1} \int_a^b q_{2^j+k+1}(x) q_{2^r+s+1}(x)\, dx \int_0^{\frac{\sigma^2 T}{2}} p_1(t) p_1(t)\, dt, \\
S_2 &= \sum_{j_1,k_1} \sum_{r_1,s_1} c_{1,2^{j_1}+k_1+1} c_{1,2^{r_1}+s_1+1} \int_a^b q_1(x) q_1(x)\, dx \int_0^{\frac{\sigma^2 T}{2}} p_{2^{j_1}+k_1+1}(t) p_{2^{r_1}+s_1+1}(t)\, dt, \\
S_3 &= \sum_{j,k} \sum_{r,s} \sum_{j_1,k_1} \sum_{r_1,s_1} c_{2^j+k+1,2^{j_1}+k_1+1} c_{2^r+s+1,2^{r_1}+s_1+1} \int_a^b q_{2^j+k+1}(x) q_{2^r+s+1}(x)\, dx \\
&\times \int_0^{\frac{\sigma^2 T}{2}} p_{2^{j_1}+k_1+1}(t) p_{2^{r_1}+s_1+1}(t)\, dt, \\
S_4 &= 2 \sum_{j,k} \sum_{r_1,s_1} c_{2^j+k+1,1} c_{1,2^{r_1}+s_1+1} \int_a^b q_{2^j+k+1}(x) q_1(x)\, dx \int_0^{\frac{\sigma^2 T}{2}} p_1(t) p_{2^{r_1}+s_1+1}(t)\, dt, \\
S_5 &= 2 \sum_{j,k} \sum_{r,s} \sum_{r_1,s_1} c_{2^j+k+1,1} c_{2^r+s+1,2^{r_1}+s_1+1} \int_a^b q_{2^j+k+1}(x) q_{2^r+s+1}(x)\, dx \\
&\times \int_0^{\frac{\sigma^2 T}{2}} p_1(t) p_{2^{r_1}+s_1+1}(t)\, dt, \\
S_6 &= 2 \sum_{r,s} \sum_{j_1,k_1} \sum_{r_1,s_1} c_{1,2^{j_1}+k_1+1} c_{2^r+s+1,2^{r_1}+s_1+1} \int_a^b q_1(x) q_{2^r+s+1}(x)\, dx
\end{aligned}
$$

$$\times \int_0^{\frac{\sigma^2 T}{2}} p_{2^{j_1}+k_1+1}(t) p_{2^{r_1}+s_1+1}(t)\, dt.$$

The coefficients c_{i,i_1} are given as

$$\begin{aligned} c_{i,i_1} &= \int_a^b \left(\int_0^{\frac{\sigma^2 T}{2}} g(x,t) h_{i_1}(t)\, dt \right) h_i(x)\, dx \\ &= \int_a^b \left(\int_{k_1\left(\frac{\sigma^2 T/2}{2^{j_1}}\right)}^{\left(k_1+\frac{1}{2}\right)\left(\frac{\sigma^2 T/2}{2^{j_1}}\right)} g(x,t)\, dt - \int_{\left(k_1+\frac{1}{2}\right)\left(\frac{\sigma^2 T/2}{2^{j_1}}\right)}^{(k_1+1)\left(\frac{\sigma^2 T/2}{2^{j_1}}\right)} g(x,t)\, dt \right) h_i(x)\, dx. \end{aligned}$$

By using mean value theorem, there exists t_1 and t_2 satisfying $k_1(\frac{\sigma^2 T/2}{2^{j_1}}) \leqslant t_1 \leqslant (k_1 + \frac{1}{2})(\frac{\sigma^2 T/2}{2^{j_1}})$ and $(k_1 + \frac{1}{2})(\frac{\sigma^2 T/2}{2^{j_1}}) \leqslant t_2 \leqslant (k_1 + 1)(\frac{\sigma^2 T/2}{2^{j_1}})$ such that

$$c_{i,i_1} = 2^{-j_1-1} \frac{\sigma^2 T}{2} \int_a^b \left(g(x,t_1) - g(x,t_2) \right) h_i(x)\, dx.$$

Again by using Lagrange's mean value theorem, there exists $t^* \in [t_1, t_2]$ so that

$$c_{i,i_1} = 2^{-j_1-1} \frac{\sigma^2 T}{2} \int_a^b (t_1 - t_2) \frac{\partial g(x,t^*)}{\partial t} h_i(x)\, dx.$$

Similarly, by applying mean value theorem of integral calculus and Lagrange's mean value theorem, there exist x_1, x_2 satisfying $a + k(\frac{b-a}{2^j}) \leqslant x_1 \leqslant a + (k + \frac{1}{2})(\frac{b-a}{2^j})$, $a + (k + \frac{1}{2})(\frac{b-a}{2^j}) \leqslant x_2 \leqslant a + (k + 1)(\frac{b-a}{2^j})$, and $x^* \in [x_1, x_2]$ such that

$$c_{i,i_1} = 2^{-j-j_1-2} \frac{\sigma^2 T}{2} (b-a)(x_1 - x_2)(t_1 - t_2) \frac{\partial^2 g(x^*, t^*)}{\partial x \partial t}.$$

Now as $x_1 - x_2 \leqslant b - a$ and $t_1 - t_2 \leqslant \frac{\sigma^2 T}{2}$, so

$$|c_{i,i_1}| \leqslant \frac{\eta (b-a)^2 (\sigma^2 T/2)^2}{2^{j+1} 2^{j_1+1}}.$$

To find the upper bounds for S_1, S_2, S_3, S_4, S_5, and S_6, we use the following result

$$\sum_{j=J+1}^{\infty}\sum_{k=0}^{2^j-1}\left(\frac{1}{2^{j+1}}\right)^3 \leqslant C\left(\frac{1}{2^{J+1}}\right)^2, \text{ for some constant } C.$$

By using bound for c_{i,i_1} and Theorem 2.4.1, we get

$$S_1 < \sum_{j,k}\sum_{r,s}\frac{B^2\eta(b-a)^2(\sigma^2T/2)^2}{(1!)^2(2^{j+1})^3(2^{r+1})^3} < \frac{C_1}{(2^{\bar{J}+1})^4}, \text{ where } C_1 = CB^2\eta(b-a)^2(\sigma^2T/2)^2.$$

Similarly, we can get the following bounds for S_2, S_3, S_4, S_5, and S_6,

$$S_2 < \frac{C_2}{(2^{\bar{J}+1})^2}, \quad S_3 < \frac{C_3}{(2^{\bar{J}+1})^6}, \quad S_4 < \frac{C_4}{(2^{\bar{J}+1})^3}, \quad S_5 < \frac{C_5}{(2^{\bar{J}+1})^5}, \quad S_6 < \frac{C_6}{(2^{\bar{J}+1})^4},$$

for some constants C_2, C_3, C_4, C_5, and C_6. Thus,

$$\begin{aligned}\|Error_{J,J_1}(x,t)\|_2^2 &= S_1 + S_2 + S_3 + S_4 + S_5 + S_6 \\ &< \frac{C_1}{(2^{\bar{J}+1})^4} + \frac{C_2}{(2^{\bar{J}+1})^2} + \frac{C_3}{(2^{\bar{J}+1})^6} + \frac{C_4}{(2^{\bar{J}+1})^3} + \frac{C_5}{(2^{\bar{J}+1})^5} + \frac{C_6}{(2^{\bar{J}+1})^4}.\end{aligned}$$

So,

$$\|Error_{J,J_1}(x,t)\|_2^2 \leq \mathcal{C}\left(\frac{1}{2^{\bar{J}+1}}\right)^2,$$

for some constant $\mathcal{C}$. Hence, the result follows. □

2.5 Simulating greeks

Using the model proposed by Black and Scholes, in this section, we perform the numerical and physical analysis of the sensitivities of the price of the European call and put options through two test examples. The Black-Scholes model for option pricing consists of various parameters that affect the financial institutes directly or indirectly. In our analysis, we fix the parameters r, σ, δ, K and vary the values of T to compute the values of the price and the Greeks of the options in both examples. The effect of change in the price of the stock and time on the price of the option and the values of the Greeks are depicted pictorially.

Although the numerical solutions of option Greeks can be found by using any numerical method, we consider the two-dimensional Haar wavelet method, since this method is designed in such a form that it directly provides all the possible values of derivatives of the solution function, and hence, we get the values of all the option Greeks explicitly. Moreover, this method gives a small error even by using a few points. The infinite spatial computational domain is truncated into a finite domain by taking the sufficiently large value of stock price indicated as $S_{\max}$. For numerical simulations, we consider the transformed equation (2.2.2) and finally use back substitution to get the solution of equation (2.2.1). So, we consider the transformed computational domain $[x_{\min}, x_{\max}]$ and partitioned it into 2^{J+1} equidistant spatial nodes, and similarly, we discretize the temporal domain. For convenience, we take equal maximum levels of resolutions ($J = J_1$) in both directions. The computational errors are given in three different norms. For a function $w(S, \tau)$ the error measures are computed by using the following formulae:

$$E_2 = \left(\sum_{\nu=1}^{N_1} \sum_{\upsilon=1}^{N_2} \left| \frac{w_{2N_1,2N_2}(S_{2\nu-1}, \tau_{2\upsilon-1}) + w_{2N_1,2N_2}(S_{2\nu}, \tau_{2\upsilon})}{2} - w_{N_1,N_2}(S_\nu, \tau_\upsilon) \right|^2 \right)^{1/2},$$

$$E_\infty = \max_{\nu=1,2,\ldots,N_1} \max_{\upsilon=1,2,\ldots,N_2} \left| \frac{w_{2N_1,2N_2}(S_{2\nu-1}, \tau_{2\upsilon-1}) + w_{2N_1,2N_2}(S_{2\nu}, \tau_{2\upsilon})}{2} - w_{N_1,N_2}(S_\nu, \tau_\upsilon) \right|,$$

$$E_{\text{rms}} = \left(\frac{1}{N_1 N_2} \sum_{\nu=1}^{N_1} \sum_{\upsilon=1}^{N_2} \left| \frac{w_{2N_1,2N_2}(S_{2\nu-1}, \tau_{2\upsilon-1}) + w_{2N_1,2N_2}(S_{2\nu}, \tau_{2\upsilon})}{2} - w_{N_1,N_2}(S_\nu, \tau_\upsilon) \right|^2 \right)^{1/2},$$

where $N_1 = 2^{J+1}$ and $N_2 = 2^{J_1+1}$; $w_{2^{J+1},2^{J_1+1}}$ and $w_{2^{J+2},2^{J_1+2}}$ are the approximated values of w obtained by using $(2^{J+1}, 2^{J_1+1})$ and $(2^{J+2}, 2^{J_1+2})$ nodal points, respectively. All the numerical simulations are performed using MATLAB 2019b.

Example 2.5.1. *Consider the Black-Scholes equation (2.2.1) for the European call option with a fixed rate of interest $r = 0.08$, volatility $\sigma = 0.3$, the exercise time $T = 1$ year, and strike price $K = 40$ with no dividend.*

In this example, the computational domains in the spatial and temporal directions are taken $[-1, 1]$ and $[0, \frac{\sigma^2 T}{2}]$, respectively. In Table 2.2 we have presented the different error measures along with the order of convergence and CPU time (in seconds), the time taken by the computer while calculating the price of the option. Here a noteworthy observation is that we obtained a different order of convergence for different error measures. It can be easily examined that the proposed method achieves a quadratic order of convergence in the case of maximum absolute error and relative mean square error while it gives the linear order of convergence in the L^2-norm.

The Haar solution of the Black-Scholes equation for the European call option and the relation between the call option price (V) and time (τ) is depicted in Figure 2.1. It elucidates that for a fixed asset price the value of the European call option decreases and approaches the payoff function value monotonically as the time approaches maturity T. We also observed that the option price decreases to zero for $S < K$ *i.e.,* the option is getting out of the money, and it increases linearly for $S > K$ *i.e.,* the option is in the money in this case. So, an increase in the price of the asset in the case of a European call option leads us to profit.

In Tables 2.3, 2.4, and 2.5, we have tabulated relative mean square errors with distinct values of time to maturity T for different derivatives of the option price. The increase in the levels of resolution of the Haar wavelet leads to a decrease in the error measure reveals that the proposed method gives accurate approximations for the derivatives of option pricing function with respect to different parameters. Figure 2.2 illustrates that the delta of the European call option changes non linearly with change in the asset price. The figure reports that the value of delta for the European call option lies between 0 and 1. We also observed that for $S > K$ the value of delta approaches 1 as τ approaches expiry T. This can be explained by the fact that as the price of the asset is greater than the price of the strike then there are more chances of exercising the option because the option is in the money in this case. Similarly, for the case when S approaches zero the option becomes out of the money and hence delta approaches zero.

The change in the behavior of option delta with a change in the price of an asset (that

is gamma) is plotted in Figure 2.3. From the figure, we observed that the value of gamma for the European call option is always positive because the value of delta increases as the asset price increases. The graphical analysis also reveals that the gamma becomes more and more spiked near the strike price as there is a sudden change in the value of delta near the strike price. From Figure 2.3(b) it can be observed that for $S > K$ gamma approaches zero because in that region the value of delta approaches 1 (a constant). A similar observation has been made for gamma tends to zero for $S < K$ as the option is out of the money so delta approaches zero there.

The change in the price of the option with a decrease in the time to maturity is depicted in Figure 2.4. The figure illustrates that the variation in the option price with the change in time is always negative for the European call option. This observation is in agreement with the results given in [46]. The negative value of theta is due to the decrease in the price of the option as the time approaches expiration date because as the time approaches maturity the chance of expiration of the option in the money is getting low with time.

Example 2.5.2. *Consider the Black-Scholes equation (2.2.1) for the European put option with fixed rate of interest* $r = 0.06$*, volatility* $\sigma = 0.45$*, the exercise time* $T = 0.25$ *year and strike price* $K = 10$ *with no dividend.*

In this example, we have demonstrated the efficiency of the 2D Haar wavelet method to calculate the price of the European put option and its Greeks. Throughout this example we take $x_{\min} = -1$, $x_{\max} = 1$, and $t \in [0, \frac{\sigma^2 T}{2}]$. In Table 2.6 we have shown the convergence trends of the present method via three different types of error measures. The computational orders of convergence in L^2-norm have been validated with the theoretical results proved in the previous section. A significant difference can be noticed in the order of convergence of the proposed numerical method with different error measures.

Figure 2.5(b) represents the value of the European put option for different values of τ along with the payoff function. The surface plot in Figure 2.5(a) reveals that the value of the European put option approaches zero for $S > K$, however, it increases linearly for $S < K$ as the option is in the money here. A noteworthy observation is that the option

price function's behavior change rapidly near the strike price which can be explained by the fact the for $S < K$ the put option is in the money and for $S > K$ the put option becomes out of the money.

In Tables 2.7, 2.8, and 2.9, we have presented the relative mean square errors of the proposed method while computing the Greeks with the increase in the level of resolution of Haar wavelets. The approximated value of delta of the European put option at $T = 0.25$ is drawn in Figure 2.6(a) while Figure 2.6(b) depicts the value of delta of European put option at different values of τ. It is evident from Figure 2.6 that the value of delta for European put option approaches zero as the price of the asset increases, it can be justified from the fact that the increase in the asset price reduces the put option price. A novel observation is that there are fewer chances for the option to expire in the money as we approach maturity.

The value of gamma of European put option at different values of τ and the approximated solution of gamma of the European put option at $T = 0.25$ is being pictorially depicted in Figure 2.7. This figure illustrates that the value of gamma is negative since the value delta is decreasing. It is perceived from the figure that the value gamma is almost equal to zero for $S > K$ which is evident from the fact that the value of delta for the put option approaches zero in the region $S > K$, which means that there is not much change in the value of delta with when the asset price is greater than the strike price.

Figure 2.8 depicted that the value of theta is positive which means that the option is deep in the money. The fall in the graph reports that the value of the option decreases as time increases. A significant observation is that there is a rapid change in theta near the maturity which explained the fact that when we are at a short distance from the maturity, the time decay is at its peak. The present numerical study shows the significant impact of the study of option Greeks in the financial markets and good agreement with the financial theory given in [47].

Table 2.2: E_2, E_∞, E_{rms}, and the CPU time (in seconds) with parameters as given in Example 2.5.1 for calculating the call option price.

	Maximum Level of Resolution J				
	1	2	3	4	5
E_2	$9.9753e-02$	$5.1062e-02$	$2.5806e-02$	$1.3033e-02$	6.5836e-03
	0.9661	0.9845	0.9855	0.9852	
E_∞	$4.9917e-02$	$1.3394e-02$	$3.7811e-03$	$1.0314e-03$	$2.7535e-04$
	1.8979	1.8247	1.8742	1.9053	
E_{rms}	$2.5213e-02$	$6.5089e-03$	$1.6662e-03$	$4.2541e-04$	$1.0855e-04$
	1.9537	1.9659	1.9696	1.9705	
CPU Time	0.077	0.103	0.113	0.171	1.643

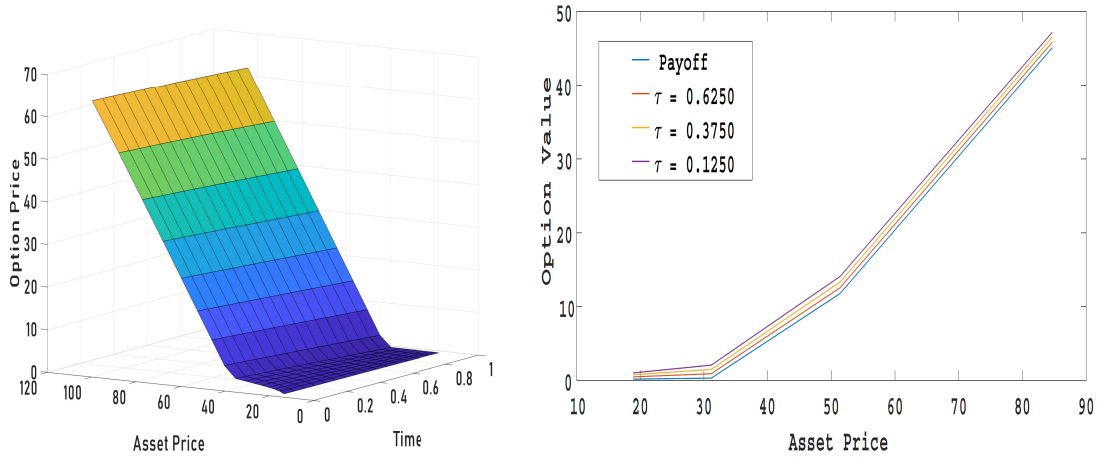

(a) $T = 1$

(b) different values of τ and option's payoff

Figure 2.1: The approximated value of the European call option.

Table 2.3: E_{rms} in delta for European call option at different values of time to expiration T with parameters as given in Example 2.5.1.

	Maximum Level of Resolution J				
Maturity	1	2	3	4	5
$T = 0.25$	$3.8629e-03$	$1.1154e-03$	$2.8874e-04$	$8.0163e-05$	$2.1882e-05$
$T = 0.50$	$3.6960e-03$	$1.0424e-03$	$3.0811e-04$	$8.7528e-05$	$2.4451e-05$
$T = 0.75$	$3.3796e-03$	$1.0744e-03$	$3.2843e-04$	$9.3679e-05$	$2.6212e-05$
$T = 1.00$	$3.1199e-03$	$1.1041e-03$	$3.3867e-04$	$9.6062e-05$	$2.6708e-05$

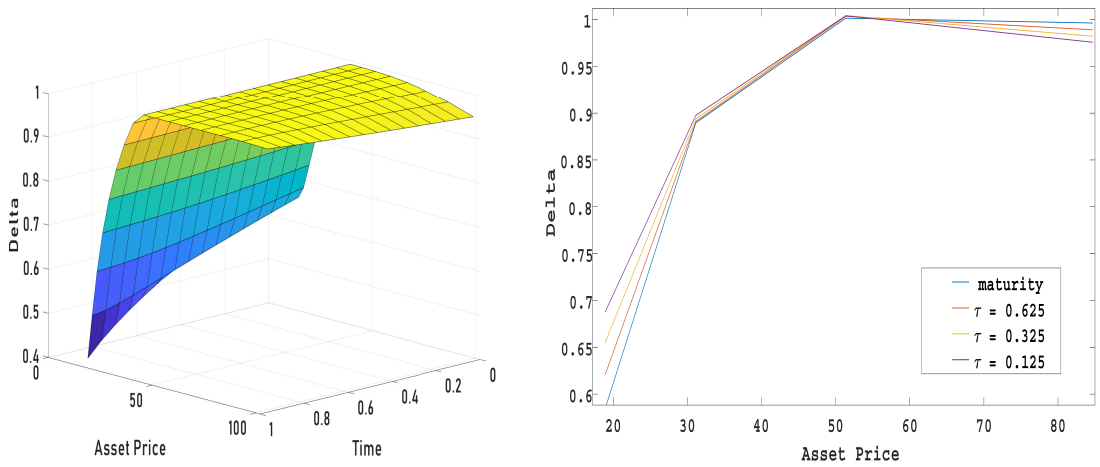

(a) $T = 1$ (b) different values of τ

Figure 2.2: The approximated value of delta for the European call option.

Table 2.4: E_{rms} in gamma for European call option at different values of time to expiration T with parameters as given in Example 2.5.1.

	Maximum Level of Resolution J				
Maturity	1	2	3	4	5
$T = 0.25$	$2.3205e-03$	$2.6828e-03$	$6.1163e-04$	$1.3720e-04$	$3.3630e-05$
$T = 0.50$	$3.5729e-03$	$1.9224e-03$	$4.1024e-04$	$1.0009e-04$	$2.4879e-05$
$T = 0.75$	$3.9969e-03$	$1.5113e-03$	$3.5490e-04$	$8.8514e-05$	$2.2112e-05$
$T = 1.00$	$4.0736e-03$	$1.3229e-03$	$3.3081e-04$	$8.3296e-05$	$2.0857e-05$

Table 2.5: E_{rms} in theta of European call option at different expiration times T with parameters as given in Example 2.5.1.

	Maximum Level of Resolution J				
Maturity	1	2	3	4	5
$T = 0.25$	$2.8736e-02$	$2.4061e-02$	$5.3181e-03$	$1.4441e-03$	$4.1072e-04$
$T = 0.50$	$4.1368e-02$	$1.4242e-02$	$3.1775e-03$	$9.4063e-04$	$2.8735e-04$
$T = 0.75$	$4.6973e-02$	$9.6357e-03$	$2.0895e-03$	$6.1565e-04$	$1.9393e-04$
$T = 1.00$	$5.0589e-02$	$8.1650e-03$	$1.5309e-03$	$3.8782e-04$	$1.1813e-04$

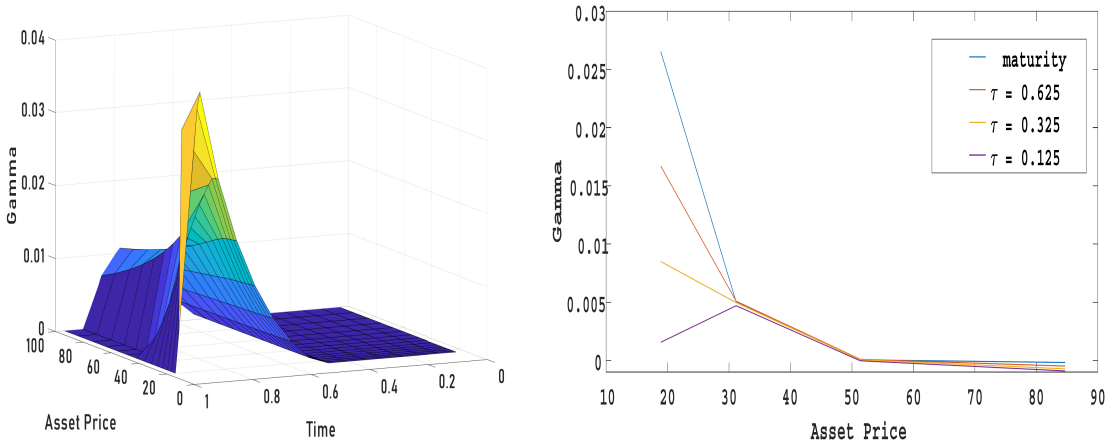

(a) $T = 1$ (b) different values of τ

Figure 2.3: The approximated value of gamma for the European call option.

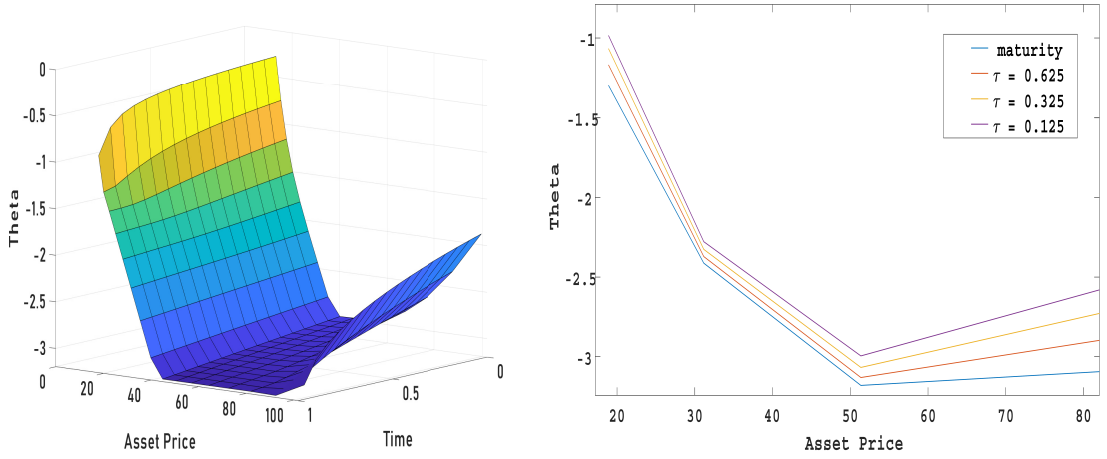

(a) $T = 1$ (b) different values of τ

Figure 2.4: The approximated value of theta for the European call option.

Table 2.6: E_2, E_∞, E_{rms}, and the CPU time (in seconds) with parameters as given in Example 2.5.2 for calculating the put option price.

	Maximum Level of Resolution J				
	1	2	3	4	5
E_2	$1.4014e-01$	$7.2345e-02$	$3.6872e-02$	$1.8556e-02$	$9.2973e-03$
	0.9539	0.9724	0.9906	0.9970	
E_∞	$5.9864e-02$	$1.6949e-02$	$4.5116e-03$	$1.1639e-03$	$2.9560e-04$
	1.8205	1.9095	1.9547	1.9772	
E_{rms}	$3.5259e-02$	$9.2693e-03$	$2.3637e-03$	$5.9422e-04$	$1.4897e-04$
	1.9275	1.9714	1.9920	1.9960	
CPU Time	0.6554	0.6638	0.7145	2.3217	79.0715

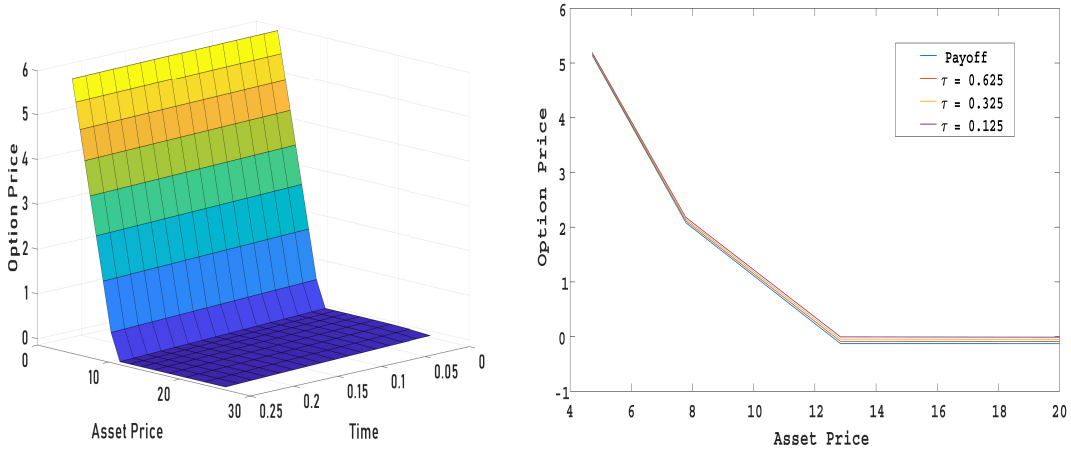

(a) $T = 0.25$

(b) different values of τ and option's payoff

Figure 2.5: The approximated value of the European put option.

Table 2.7: E_{rms} in delta for European put option at different expiration times T with parameters as given in Example 2.5.2.

	Maximum Level of Resolution J				
Maturity	1	2	3	4	5
$T = 0.25$	$2.0652e-03$	$5.5494e-04$	$1.4230e-04$	$3.5991e-05$	$9.0389e-06$
$T = 0.50$	$2.1042e-03$	$5.5317e-04$	$1.4218e-04$	$3.6515e-05$	$9.4341e-06$
$T = 0.75$	$2.2241e-03$	$5.8418e-04$	$1.5398e-04$	$4.1123e-05$	$1.1117e-05$
$T = 1.00$	$2.4416e-03$	$6.4221e-04$	$1.7475e-04$	$4.8628e-05$	$1.3659e-05$

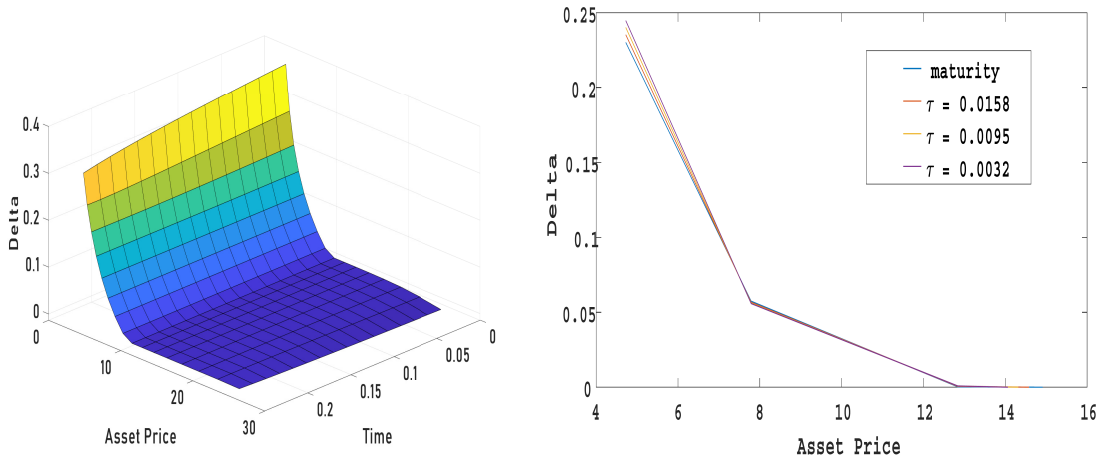

(a) $T = 0.25$ (b) different values of τ

Figure 2.6: The approximated value of delta for the European put option.

Table 2.8: E_{rms} in gamma for European put option at different expiration times T with parameters as given in Example 2.5.2.

	Maximum Level of Resolution J				
Maturity	1	2	3	4	5
$T = 0.25$	$6.8206e-03$	$2.5420e-03$	$5.2746e-04$	$1.2776e-04$	$3.1674e-05$
$T = 0.5$	$6.7964e-03$	$1.6829e-03$	$4.0131e-04$	$9.9477e-05$	$.4799e-05$
$T = 0.75$	$6.0714e-03$	$1.4448e-03$	$3.5848e-04$	$8.9480e-05$	$2.2354e-05$
$T = 1.00$	$5.4687e-03$	$1.3399e-03$	$3.3728e-04$	$8.4478e-05$	$2.1135e-05$

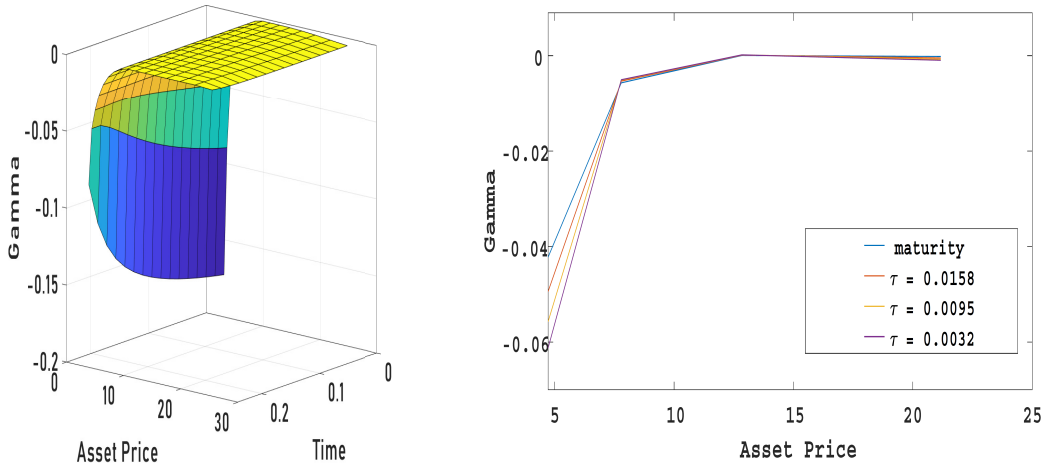

(a) $T = 0.25$ (b) different values of τ

Figure 2.7: The approximated value of gamma for the European put option.

Table 2.9: E_{rms} in theta for European put option at different expiration times T with parameters as given in Example 2.5.2.

	Maximum Level of Resolution J				
Maturity	1	2	3	4	5
$T = 0.25$	$1.6114e-02$	$5.0884e-03$	$1.0800e-03$	$2.7921e-04$	$7.4581e-05$
$T = 0.50$	$1.6696e-02$	$3.7015e-03$	$9.7470e-04$	$2.7738e-04$	$7.9451e-05$
$T = 0.75$	$1.6067e-02$	$3.7863e-03$	$1.0867e-03$	$3.2108e-04$	$9.4038e-05$
$T = 1.00$	$1.5922e-02$	$4.1289e-03$	$1.2291e-03$	$3.6878e-04$	$1.0891e-04$

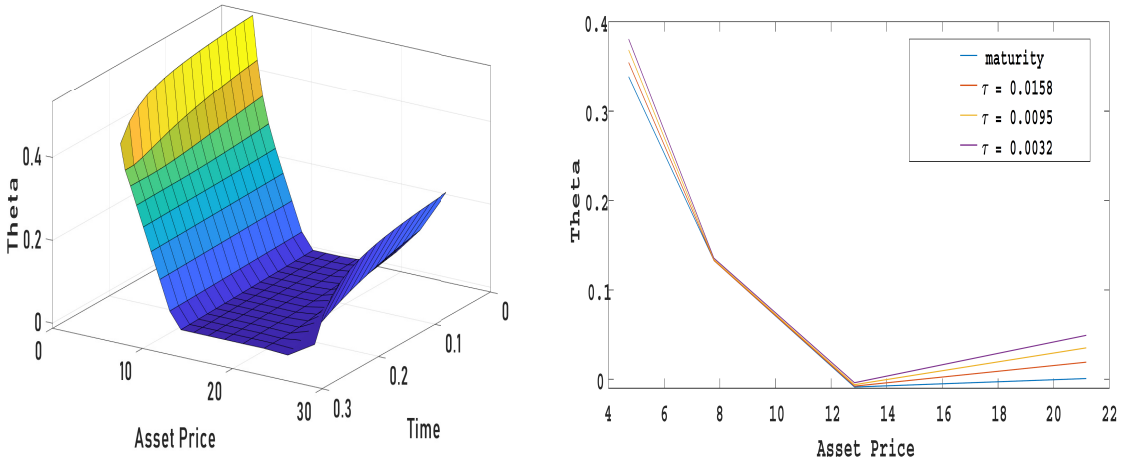

(a) $T = 0.25$ (b) different values of τ

Figure 2.8: The approximated value of theta for the European put option.

2.6 Conclusions

The present study is a novel numerical approach to analyze the sensitivity of the price of an option with respect to the different parameters involved in the Black-Scholes equation. In this chapter, we have used a two-dimensional Haar wavelet method for finding the numerical solution to the Black-Scholes equation and its Greeks. The windowing technique and the multi-resolution analysis of Haar wavelets are used to get a more accurate estimation of the initial functions. This approach of finding the numerical solutions of the option Greeks is novel and effortless as it explicitly gives the approximation of the derivatives of the initial function. For avoiding the truncation error, the infinite domain is truncated into a finite domain. Although, we have proved the convergence of the proposed method in the L^2-norm, the computational errors and the associated orders of convergence of the proposed method are also presented in different error measures. We do emphasize that this method gives better accuracy even when only a few points are used. The effects of various parameters on the price of options such as varying stock price S, time τ, maturity T are depicted numerically and graphically. The observations and outcomes can be used by the money investors or shareholders in small markets as well as in big financial institutes in hedging the risk and managing the portfolios.

Chapter 3

Exploring the Greeks of American options, a free boundary value problem

---

One of the most widely studied topics in quantitative finance is the pricing of American options. In the United States and Canada, a large range of commodities and commodity futures contracts are currently traded. Almost majority of these choices are in the American style. Unlike European option, an American option can be exercised at any time before it expires that leads to an optimization problem, namely, the linear complementarity problem (LCP). As a result, American options are more adaptable, and so more useful in general. The "moneyness" of the option, the interest rate, the remaining time until expiry, and whether the underlying pays dividends are the primary factors that determine the price difference between American and European options. Finding solutions to the American option valuation problem is more challenging than it is in European because of the added feature of early exercise.

The challenge with pricing an American option is that determining the ideal moment to exercise it is tough. The "early exercise premium" is the value of the right to exercise early. The goal of American option pricing is to figure out how much the early exercise premium is worth. Also, due to future uncertainties, underlying assets may increase or

decrease in value. American options as important financial derivatives will generate more diverse financial markets. In general, there is no closed form approach to pricing American options. Therefore, option price simulations can serve as a key input when important financial decisions are made.

This chapter presents a novel and highly accurate wavelet-based approximation technique to explore the sensitivities and value of American options diagnosed by linear complementarity problems. For a detailed analysis of such financially relevant problems, first the actual final value problem under the Black-Scholes framework is transformed into a dimensionless initial value problem. To avoid the unacceptable large truncation error, the unbounded domain is trimmed into a bounded domain [31]. A remarkable observation is that to investigate the various physical and numerical aspects of the options' sensitivities; the proposed scheme is efficient as it explicitly provides the numerical approximation of all the derivatives of the solution function. The multi-resolution technique of the wavelets and the convergence of the proposed wavelet scheme are comprehensively analyzed. The wavelet analysis is accompanied by illustrative examples to demonstrate the proficiency and robustness of the present method coupled with graphical representations. It has been shown that the present method is efficient to solve free boundary problems. It is worthy to note that the highly accurate and promising computational results are enough to confirm the performance of the proposed method. The simulated results of options' Greeks analyzed and discussed have vast applications in different financial institutes and trading markets.

3.1 Literature survey

For the theoretical development of American option pricing problem see [48], while an extensive literature on the resolution of LCPs can be seen in the book by Cottle *et al.* [49]. The discretized linear complementarity approach for a wide range of the options ranging from vanilla American to highly complex multi-asset option can be seen in Wilmott *et al.* [50]. [51], to the best of our knowledge is one of the earliest researches on the LCP for pricing an American put option. There are several numerical methods developed for these problems, such as finite volume methods (FVM) [52–54], finite element methods (FEM)

[55–57], and finite difference methods (FDM) [51, 58–60]. The meshfree algorithms based on the radial basis functions approach can be seen in [61, 62]. For operator splitting methods for American option pricing the readers are referred to [17]. On the other hand, for the analytic solutions for these problems the readers are referred to [63] for the integral equation method, and [64] for the Laplace transform method.

The most common numerical tool for pricing options is the FDM. In particular, a more accurate approach (second-order in time) is the Crank-Nicolson scheme, which is difficult to apply to the LCPs. Huang and Pang [65] presented second-order upwind FDMs for the problem of the form (3.2.1) and derived the fundamental properties of the discretized form. Using a PDE approach Christara and Dang [66] developed adaptive schemes for the solution of the problems of the form (3.2.1). They have used a penalty method for free boundary; the FDMs and FEMs on the adaptive mesh, generated by an error equidistribution technique in spatial direction; and the Crank-Nicolson difference formula with the time step size selector in the temporal direction. Reisinger and Witte [67] demonstrated a policy iteration algorithm for the solution of LCPs obtained by using the FDM and FEM approximation of American options. To formulate the LCP from the parabolic variational inequality, Memon [68] used the penalty function approach. The unbounded domain is truncated into a bounded domain and the FEM is applied to the penalized problem on the truncated domain. To formulate an LCP of American options under the Bates model, Salmi *et al.* [69] used FDM and quadrature rule. The resulting LCP is then solved by using a projected algebraic multigrid (PAMG) method. They have observed that for small stepsize the PAMG method leads to better scalability than the PSOR method when the discretization is refined.

Later, to solve the Black–Scholes model for European and American options, Rad *et al.* [39] proposed meshfree radial basis point interpolation (RBPI) combined with an exponential change of variables, a mesh refinement algorithm, and an implicit Euler Richardson extrapolated scheme. In the case of American options, they have used PSOR, the Bermudan approximation, and the penalty approach for the solution of free boundary problems. Rad *et al.* [40] proposed the local weak form meshless methods for the

American option. They have used the Richardson extrapolation technique to covert the free boundary problem into LCP. The infinite domain is truncated into a finite domain by using the change of variables proposed by Clarke and Parrott [70]. The matrix method is used to show the unconditional stability of the θ-weighted scheme for the implicit Euler ($\theta = 0$) and Crank-Nicolson ($\theta = 1/2$) schemes. The power penalty methods for LCP arising from American option pricing can be seen in [71] where the authors have applied the nonlinear Jacobian method to solve the penalized equations obtained by discretizing the LCP in space and time. For more development of the penalty methods, the readers are referred to [72, 73]. For reduced basis methods for pricing options with the Black-Scholes model readers can go through [16]

To solve the LCP resulting by using a log-transformation for the Black-Scholes-Merton model of American option pricing, Shi *et al.* [74] used θ method. A fixed point iterative method via the splitting technique of the matrix, which is more accurate than the PSOR, is used to solve the resulting system of equations. Recently, for the solution of LCP, Cen and Chen [75] introduced a first-order in time and second-order in spatial directions, differential identity expansion FDM comprising an implicit Euler method to discretize the time variable and FDM on a piecewise-uniform mesh in the spatial variable which results in an M-matrix.

How the value of an option price changes if one (or more) of the parameter changes is equally important as pricing an option. So, we also explore the sensitivities such as Delta (Δ), Gamma (Γ), and Theta (Θ). The sensitivity of a portfolio of options to change in market conditions is diagnosed by using Greeks. As the price of an option changes the risk of the option changes too. Therefore, knowing how the option price changes enable the trader to hedge the risks of holding the option.

3.2 American option pricing model

The early exercise feature of an American option results in a moving boundary value problem (BVP). The value $P(S, \tau)$ of such an option is diagnosed by one of the pricing methods that includes the linear complementarity formulation introduced in [50]. The

associated differential operator $\mathcal{L}$ to the LCP is of the form

$$\mathcal{L} \equiv \frac{\partial}{\partial \tau} + \frac{1}{2}\sigma^2 S^2 \frac{\partial^2}{\partial S^2} + (r-\delta)S\frac{\partial}{\partial S} - rI,$$

where $S \in (0, \infty)$ is the price of the underlying asset at any time $\tau \in [0, T)$, $r \geq 0$ is the risk-free rate of return, $\delta \geq 0$ is the dividend yield and $\sigma > 0$ is the volatility, which is the fickleness of the underlying asset in the market.

The American option under the Black-Scholes framework defined on an unbounded domain is a free BVP, with no closed-form solution. In the case of American style call option with strike price K, for $P(S, \tau) >$ payoff, the Black-Scholes equation holds, *i.e.,* $\mathcal{L}P(S, \tau) = 0$, and for $P(S, \tau) =$ payoff it is optimal to exercise the option. Through the combined effect of both the relations we can derive the following LCP:

$$(\mathcal{L}P(S, \tau)).(P - \mathcal{F}) = 0, \quad S \in \Omega_S = (0, \infty),\ \tau \in [0, T), \tag{3.2.1a}$$

with the constraints

$$\mathcal{L}P(S, \tau) \geq 0, \text{ and } (P - \mathcal{F}) \geq 0, \tag{3.2.1b}$$

where $\mathcal{F} = (S - K)^+$ is the terminal condition, also known as the payoff function, and for a function a the superscripted a is defined as $a^+ = \max\{a, 0\}$.

In a similar manner, we get this inequality for the American style put option with $\mathcal{F} = (K - S)^+$. In pricing the option, the following boundary condition is imposed at the left end of the underlying interval

$$\lim_{S \to 0} P(S, \tau) = \begin{cases} 0, & \text{for call,} \\ (K - S)^+, & \text{for put,} \end{cases} \tag{3.2.1c}$$

that means in the case of a call option, the contract becomes worthless and for a put option,

it is deep in the money for $S \to 0$. The right boundary condition is given by

$$\lim_{S\to\infty} P(S,\tau) = \begin{cases} (S-K)^+, & \text{for call,} \\ 0, & \text{for put,} \end{cases} \tag{3.2.1d}$$

that means in the case of a call, the option is in the money and for a put option, it is meaningless for $S \to \infty$.

Since the problem (3.2.1) is defined over an infinite domain Ω_S and in practice from the numerical point of view it is difficult to consider the problem over the infinite domain. So, for numerical implementation by introducing a log-transformation $y = \ln(S/K)$, we truncate the infinite domain Ω_S into the finite domain $\Omega_y = (\alpha, \beta)$, where α and β are chosen to be sufficiently large negative and large positive number respectively, to avoid the large computational error which occurs due to the truncation of the domain. Furthermore, for detailed analysis of such financially relevant problem and to make it convenient for numerical implementation, the terminal value problem is transformed into a dimensionless initial value problem by taking $\tau = T - \frac{2t}{\sigma^2}$. As pointed out in [76], the truncation of the domain from Ω_S to Ω_y only bring inconsequential error in the solution of (3.2.1). It is expected that if the desired error estimate of (3.2.1) is finally derived through that of (3.2.2), the value of α will not affect the former, as a result of the domain of (3.2.1) being a subset of containing α. Moreover, for symmetric purposes, we set $\alpha = -\beta$ as adopted by some published works.

Also, under the above transformation, the Black-Scholes equality (3.2.1a) reduces into

$$\left(\frac{\partial v}{\partial t} - \frac{\partial^2 v}{\partial y^2}\right)(v - \tilde{g}) = 0, \quad y \in (-\infty, \infty),\ t \in \left(0, \frac{\sigma^2 T}{2}\right], \tag{3.2.2a}$$

and the constraints expressed in (3.2.1b) get transformed into

$$\frac{\partial v}{\partial t} - \frac{\partial^2 v}{\partial y^2} \geq 0, \text{ and } (v - \tilde{g}) \geq 0, \tag{3.2.2b}$$

where $\tilde{g}(y,t)$ is expressed as

$$\tilde{g}(y,t) = \begin{cases} e^{\left(\frac{t}{4}\left(\frac{2(r-\delta)}{\sigma^2}-1\right)^2+\left(\frac{2r}{\sigma^2}\right)t\right)}\left(e^{\frac{y}{2}\left(\frac{2(r-\delta)}{\sigma^2}+1\right)}-e^{\frac{y}{2}\left(\frac{2(r-\delta)}{\sigma^2}-1\right)}\right)^+, & \text{for call,} \\ e^{\left(\frac{t}{4}\left(\frac{2(r-\delta)}{\sigma^2}-1\right)^2+\left(\frac{2r}{\sigma^2}\right)t\right)}\left(e^{\frac{y}{2}\left(\frac{2(r-\delta)}{\sigma^2}-1\right)}-e^{\frac{y}{2}\left(\frac{2(r-\delta)}{\sigma^2}+1\right)}\right)^+, & \text{for put.} \end{cases}$$

Furthermore, the transformed initial condition for call and put options is given by

$$v(y,0) = \tilde{g}(y,0),$$

and the reformulated boundary conditions are obtained as

$$\lim_{y\to-\infty} v(y,t) = \lim_{y\to-\infty} \tilde{g}(y,t), \tag{3.2.2c}$$

and

$$\lim_{y\to\infty} v(y,t) = \lim_{y\to\infty} \tilde{g}(y,t). \tag{3.2.2d}$$

The new variable $v(y,t)$ is related to $P(S,\tau)$ as

$$P(S,\tau) = Ke^{-\left[2\left(\frac{r-\delta}{\sigma^2}\right)-1\right]\frac{y}{2}-\left[\frac{1}{4}\left(2\left(\frac{r-\delta}{\sigma^2}\right)-1\right)^2+\frac{2r}{\sigma^2}\right]t}v(y,t).$$

3.3 Wavelet based approximation technique

Wavelets are wave-like oscillations of limited duration that are used to approximate a function through the compression and reconstruction techniques.

3.3.1 Properties of Haar wavelets and their integrals

Haar wavelets are the rectangular-shaped wave-forms consist of piecewise constant function. Haar wavelet transform does not permit the overlapping of the window while approximating a function. Haar wavelets are a discrete type of wave-forms that is generated by operating translation and dilation on a single prototype function. The Haar wavelet

family of orthogonal functions for $y \in [\alpha, \beta]$ is defined as follows:

$$h_i(y) = \begin{cases} 1, & y \in [\nu_1(i), \nu_2(i)), \\ -1, & y \in [\nu_2(i), \nu_3(i)), \\ 0, & \text{elsewhere}, \end{cases}$$

where

$$\begin{aligned} \nu_1(i) &= \alpha + \frac{\kappa(\beta - \alpha)}{m}, \\ \nu_2(i) &= \alpha + \frac{(\kappa + 0.5)(\beta - \alpha)}{m}, \\ \nu_3(i) &= \alpha + \frac{(\kappa + 1)(\beta - \alpha)}{m}. \end{aligned}$$

We indicate the different levels of resolution by j and the maximum level of resolution by J so that $j = 0, 1, \ldots, J$. We also consider $m = 2^j$ with $\kappa = 0, 1, \ldots, m-1$, as the translation parameter. The Haar index i is computed by the formulaic expression $i = m + \kappa + 1$. From the choices of j, the minimal value of κ and m are 0 and 1, respectively. $2M = 2^{J+1}$ is the maximal value of i which signifies the total number of Haar wavelets. The grid points are determined by $y_s = \alpha + \frac{(s-0.5)(\beta-\alpha)}{2M}$, where $s = 1, 2, \ldots, 2M$, which splits the given interval $[\alpha, \beta]$ into $2M$ uniformly distributed sub-intervals.

Orthonormality. The collection of Haar functions generated by the mother wavelet

$$\xi(y) = h_2(y) = \begin{cases} 1, & y \in \left[\alpha, \frac{\alpha+\beta}{2}\right), \\ -1, & y \in \left[\frac{\alpha+\beta}{2}, \beta\right), \\ 0, & \text{elsewhere}, \end{cases}$$

form an orthonormal basis in the interval $[\alpha, \beta]$, ***i.e.,***

$$\int_\alpha^\beta h_i(y) h_{\tilde{i}}(y)\, dy = \delta_{i\tilde{i}}, \; i, \tilde{i} = 1, 2, \ldots, 2M,$$

where $\delta_{i\tilde{i}}$ is the Kronecker delta.

Function approximation. An arbitrary function $u \in L^2(\mathbb{R})$ can be expanded as the linear combination of functions of Haar basis as

$$u(y) = \sum_{i=1}^{\infty} c_i h_i(y), \tag{3.3.1}$$

where the Haar coefficients c_i are determined by

$$c_i = \int_{\alpha}^{\beta} u(y) h_i(y)\, dy,\ i = 1, 2, \ldots, 2M.$$

If $u(y)$ can be approximated as a piecewise constant function in each sub-interval then RHS of Equation (3.3.1) is terminated after $2M$ finite terms and thus we deduce

$$u(y) = \sum_{i=1}^{2M} c_i h_i(y).$$

In matrix form, we can write it as

$$U = C^T H(y),$$

where the row vector U is the discrete form of the function $u(y)$; C^T is a transpose of a $2M \times 1$ column vector of constant coefficients, and

$$H = \begin{bmatrix} h_1(y_1) & h_2(y_1) & \ldots & h_{2M}(y_1) \\ h_1(y_2) & h_2(y_2) & \ldots & h_{2M}(y_2) \\ \vdots & \vdots & \ddots & \vdots \\ h_1(y_{2M}) & h_2(y_{2M}) & \ldots & h_{2M}(y_{2M}) \end{bmatrix},$$

is a square matrix of order $2M \times 2M$. In the following analysis, the first and second

integrals of the Haar wavelets are defined as

$$p_i(y) = \int_\alpha^y h_i(y)\,dy, \quad \text{and,} \quad q_i(y) = \int_\alpha^y p_i(y)\,dy.$$

In general, the k-th integral of $h_i(y)$ is given by

$$I_k h_i(y) = \begin{cases} \frac{1}{k!}(y-\nu_1(i))^k, & y \in [\nu_1(i), \nu_2(i)), \\ \frac{1}{k!}[(y-\nu_1(i))^k - 2(y-\nu_2(i))^k], & y \in [\nu_2(i), \nu_3(i)), \\ \frac{1}{k!}[(y-\nu_1(i))^k - 2(y-\nu_2(i))^k + (y-\nu_3(i))^k], & y \in [\nu_3(i), \beta), \\ 0, & \text{elsewhere.} \end{cases}$$

An important advantage of Haar functions is the possibility to integrate these wave-forms arbitrary times.

3.3.2 Multi-resolution analysis

In this section, we discuss the technique used by Haar wavelet to approximate an arbitrary function. Multi-resolution analysis (MRA) is an approach that refers to the sequence of functions approximated at different levels of resolution. At each level, the approximation gets more accurate and finer than the preceding version. Such an analysis provides the existence of shifting and scaling filters. In order to prove the MRA of $L^2(\mathbb{R})$, the following theorems and lemmas are useful.

Theorem 3.3.1. *Assume that Y_j, $j \in \mathbb{Z}$ be a space of constant functions defined on the intervals of the form $\left(\frac{\kappa}{2^j}, \frac{\kappa+1}{2^j}\right)$, where $\kappa \in \mathbb{Z}$. Then*

$$\ldots Y_{-2} \subset Y_{-1} \subset Y_0 \subset Y_1 \subset Y_2 \ldots.$$

Moreover, $\bigcap_{j\in\mathbb{Z}} Y_j = \{0\}$ and $\bigcup_{j\in\mathbb{Z}} Y_j$ is dense in $L^2(\mathbb{R})$.

Proof. Any function $g \in Y_j$ implies $g \in Y_{j+1}$, so far every interval $\left(\frac{\kappa}{2^{j+1}}, \frac{\kappa+1}{2^{j+1}}\right)$ is contained in $\left(\frac{\kappa}{2^j}, \frac{\kappa+1}{2^j}\right)$, thus $\ldots Y_{-2} \subset Y_{-1} \subset Y_0 \subset Y_1 \subset Y_2 \ldots$. Also, if $g \in \bigcap_{j\in\mathbb{Z}} Y_j$ then for

all j; g is constant function on the interval $(0, 2^j)$. If $g = c$ on $(0, 2^j)$, then for all j

$$\|g\|^2 \geq \int_0^{2^j} |c|^2 \, dy = 2^j |c|^2,$$

and if $\|g\| < \infty$ *i.e.,* $c = 0$ and hence $g = 0$ a.e. on $(0, \infty)$. In similar manner, $g = 0$ a.e. for $(-\infty, 0)$. Furthermore, to show $\bigcup_{j \in \mathbb{Z}} Y_j$ is dense in $L^2(\mathbb{R})$, let $g \in L^2(\mathbb{R})$ and $\epsilon > 0$. Now from standard results on functions belong to L^2, we say there exist $N \in \mathbb{N}$ and g_1, a continuous function, such that $g_1(y) = 0$ for $|y| \geq N$ and $\|g - g_1\|_2 < \frac{\epsilon}{2}$.

Now g_1 is uniformly continuous on the interval $[-N, N]$, so there exist $j > 0$ such that g_1 does not differ more than $\frac{\epsilon}{\sqrt{8N}}$ for all $\left(\frac{\kappa}{2^j}, \frac{\kappa+1}{2^j}\right)$, implies there exist a step function g_2 such that

$$\|g_1 - g_2\|_2 \leqslant \left(\int_{-N}^{N} \frac{\epsilon^2}{8N} \, dy \right)^{1/2} = \frac{\epsilon}{2},$$

hence by using triangle inequality, we deduce $\|g - g_2\|_2 < \epsilon$, so $\bigcup_{j \in \mathbb{Z}} Y_j$ is dense in $L^2(\mathbb{R})$. □

Lemma 3.3.1. *A function g belongs to Y_j iff the function $y \to g(2^{-j}y)$ belongs to Y_0. Also, Y_j has an orthonormal basis consisting of functions that are represented as $\psi(y) = 2^{j/2}\psi(2^j y - \kappa)$.*

Proof. Refer [77]. □

Lemma 3.3.2. *$Y_{j+1} = Y_j \oplus X_j$ for all $j \in \mathbb{Z}$, where X_j has the orthonormal basis $2^{\frac{j}{2}}\xi(2^j y - \kappa)$, $\kappa \in \mathbb{Z}$, where ξ represents the Haar wavelet given by $\xi(y) = \psi(2y) - \psi(2y - 1)$.*

Proof. Refer [77]. □

Theorem 3.3.2. *$L^2(\mathbb{R})$ can be written as an orthogonal direct sum of $\ldots, X_{-1}, X_0, X_1 \ldots$,* i.e.,

$$L^2(\mathbb{R}) = \ldots \oplus X_{-2} \oplus X_{-1} \oplus X_0 \oplus X_1 \oplus X_2 \oplus \ldots.$$

Hence, the wavelets $\xi(y) = 2^{\frac{j}{2}}\xi(2^j y - \kappa),\ j, \kappa \in \mathbb{Z}$ form an orthonormal basis of $L^2(\mathbb{R})$.

Proof. If $g \in X_i$ and $g_1 \in X_j$, for $i < j$, then $g \in Y_{i+1} \subset Y_j$, hence $\langle g, g_1 \rangle = 0$, as $Y_j \perp X_j$, thus all combined orthonormal bases from all X_j gives a sequence which is still orthonormal. Now particularly we show that it also give a basis for $L^2(\mathbb{R})$. Clearly, any closed subspace Y of $L^2(\mathbb{R})$ has an orthogonal complement $Y^\perp$, such that, $L^2(\mathbb{R}) = Y \oplus Y^\perp$, where $Y^\perp = \{g \in L^2(\mathbb{R}) : \langle g, g_1 \rangle = 0, \, \forall g_1 \in Y\}$. Let $\mathfrak{P}_Y : L^2(\mathbb{R}) \to Y$ be an orthogonal projection, such that $\mathfrak{P}_Y(r+s) = r$, where $r \in Y$ and $s \in Y^\perp$. It is a closed point in Y to $r+s$.

Now using Lemma 3.3.2

$$L^2(\mathbb{R}) = Y_{n+1} \oplus Y_{n+1}^\perp = Y_n \oplus X_n \oplus Y_{n+1}^\perp, \; n \in \mathbb{N}.$$

Thus

$$I = \mathfrak{P}_{Y_n} + \mathfrak{P}_{X_n} + \mathfrak{P}_{Y_{n+1}^\perp},$$

where I is the identity operator yields

$$I = \mathfrak{P}_{Y_n} + \mathfrak{P}_{X_n} + (I - \mathfrak{P}_{Y_{n+1}}).$$

So,

$$\mathfrak{P}_{X_n} = \mathfrak{P}_{Y_{n+1}} - \mathfrak{P}_{Y_n}. \tag{3.3.2}$$

Now $\mathfrak{P}_{Y_n}(g) \to g$, for $n \to \infty$, as $\bigcup_{n \in \mathbb{Z}} Y_n$ is dense in $L^2(\mathbb{R})$. Also, $\mathfrak{P}_{Y_n}(g) \to 0$ for $n \to -\infty$, as $\bigcap_{n \in \mathbb{Z}} Y_n = \{0\}$. This implies

$$\mathfrak{P}_{X_{-2M} \oplus \ldots \oplus X_{-1} \oplus X_0 \oplus X_1 \oplus \ldots \oplus X_{2M}}(g) = \sum_{n=-2M}^{2M} \mathfrak{P}_{X_n}(g),$$

using (3.3.2), we deduce

$$\mathfrak{P}_{X_{-2M} \oplus \ldots \oplus X_{-1} \oplus X_0 \oplus X_1 \oplus \ldots \oplus X_{2M}}(g) = \sum_{n=-2M}^{2M} (\mathfrak{P}_{Y_{n+1}} - \mathfrak{P}_{Y_n})(g)$$

$$= (\mathfrak{P}_{Y_{2M+1}} - \mathfrak{P}_{Y_{2M}})(g)$$
$$\to g, \text{ as } M \to \infty.$$

Hence $L^2(\mathbb{R}) = \ldots \oplus X_{-2} \oplus X_{-1} \oplus X_0 \oplus X_1 \oplus X_2 \oplus \ldots$. □

MRA of $L^2(\mathbb{R})$ is illustrated by the existence of a cluster of subspaces $Y_j,\ j \in \mathbb{Z}$, generated by the direct sum of orthogonal or semi-orthogonal wavelets as

$$Y_j = \ldots \oplus X_{j-2} \oplus X_{j-1}.$$

The subspaces Y_j possess the following properties [78, 79]:

- Nested: $Y_j \subset Y_{j+1},\ \forall\, j \in \mathbb{Z}$.
- Dense: $\overline{\bigcup\limits_{j\in\mathbb{Z}} Y_j} = L^2(\mathbb{R})$.
- Separation: $\bigcap\limits_{j\in\mathbb{Z}} Y_j = \{0\}$.
- $Y_{j+1} = Y_j \oplus X_j,\ \forall\, j \in \mathbb{Z}$.
- Scaling: For any function g; $g(y) \in Y_j \iff g(2y) \in Y_{j+1},\ \forall\, j \in \mathbb{Z}$.
- Orthonormal basis: There exists a scaling function $\phi \in Y_0$ such that $\{\phi_{0,l'}(y) = \phi(y - l') : l' \in \mathbb{Z}\}$ is an orthonormal basis for Y_0.

Here Y_j denotes the approximation spaces and different choices of X_j yield distinct resolution analysis. From the above properties, it is clear that the nested subsequence of subspaces $\{Y_j\}_{j\in\mathbb{Z}}$ covers $L^2(\mathbb{R})$. Here X_j are the orthogonal wavelet subspaces generated by the single prototype function.

Similarly, let $\{Y_j^2\}_{j\in\mathbb{Z}}$ be the multi-scaling approximation of $L^2(\mathbb{R}^2)$. One can show that there exists a unique mother wavelet whose translation and dilation provide an orthonormal basis of each space Y_j^2. To solve the PDEs numerically, the multi-scaling approximation technique includes the representation of unknown function or signals into

wavelets of different resolutions. The key attribute of wavelets is their propensity to reorganize the given differential equation into a system of linear or non-linear equations, which can be solved by different numerical methods.

3.4 Implementation of the proposed wavelet scheme

In this section, we provide the numerical procedure to approximate the solution and the derivatives of the reformulated LCP for the American option. Let V and v are the approximate and exact solutions for the problem (3.2.2), respectively. First, we discretize the spatial domain $[\alpha, \beta]$ and the temporal domain $[0, \sigma^2 T/2]$ into $2M_1$ and $2M_2$ uniformly distributed points (as defined in section 3), respectively. To construct the Haar wavelet method, first, we expand the approximation $\frac{\partial^3 V(y,t)}{\partial t \partial y^2}$ in a linear combination of Haar functions as

$$\frac{\partial^3 V(y,t)}{\partial t \partial y^2} = \sum_{i=1}^{2M_1} a_{i,l} h_i(y),$$

here, i symbolizes the index of Haar functions in the spatial direction, l represents the present time level in the temporal direction, and $a_{i,l}$ are the unknown coefficients. On integrating this expression with respect to t from t_l to t, yields

$$\frac{\partial^2 V(y,t)}{\partial y^2} = (t - t_l) \sum_{i=1}^{2M_1} a_{i,l} h_i(y) + \frac{\partial^2 V(y,t_l)}{\partial y^2}.$$

Similarly, on integrating it with respect to y from α to y, we deduce

$$\frac{\partial V(y,t)}{\partial y} = (t - t_l) \sum_{i=1}^{2M_1} a_{i,l} p_i(y) + \frac{\partial V(y,t_l)}{\partial y} - \frac{\partial V(\alpha,t_l)}{\partial y} + \frac{\partial V(\alpha,t)}{\partial y}.$$

Again, by integrating the above expression with respect to y from α to y, we obtain

$$\begin{aligned} V(y,t) =& (t - t_l) \sum_{i=1}^{2M_1} a_{i,l} q_i(y) + V(y,t_l) - V(\alpha,t_l) - (y - \alpha) \frac{\partial V(\alpha,t_l)}{\partial y} \\ &+ (y - \alpha) \frac{\partial V(\alpha,t)}{\partial y} + V(\alpha,t). \end{aligned} \tag{3.4.1}$$

To find the unknown terms $\frac{\partial V(\alpha,t_l)}{\partial y}$ and $\frac{\partial V(\alpha,t)}{\partial y}$ we use the final boundary condition *i.e.,* by taking $y = \beta$, in (3.4.1) yields

$$\frac{\partial V(\alpha,t)}{\partial y} - \frac{\partial V(\alpha,t_l)}{\partial y} = \frac{1}{\beta-\alpha}\Bigg[V(\beta,t) - (t-t_l)\sum_{i=1}^{2M_1} a_{i,l}q_i(\beta) - V(\beta,t_l) + V(\alpha,t_l) - V(\alpha,t)\Bigg].$$

Replacing the value of $\frac{\partial V(\alpha,t)}{\partial y} - \frac{\partial V(\alpha,t_l)}{\partial y}$ back into (3.4.1), we obtain

$$V(y,t) = (t-t_l)\sum_{i=1}^{2M_1} a_{i,l}q_i(y) + V(y,t_l) - V(\alpha,t_l) + \frac{y-\alpha}{\beta-\alpha}\Bigg[V(\beta,t) - (t-t_l)\sum_{i=1}^{2M_1} a_{i,l}q_i(\beta) - V(\beta,t_l) + V(\alpha,t_l) - V(\alpha,t)\Bigg] + V(\alpha,t). \quad (3.4.2)$$

To find the derivatives of the solution function, first, we differentiate (3.4.2) with respect to t, to obtain

$$\frac{\partial V(y,t)}{\partial t} = \sum_{i=1}^{2M_1} a_{i,l}q_i(y) + \frac{y-\alpha}{\beta-\alpha}\left[\frac{\partial V(\beta,t)}{\partial t} - \sum_{i=1}^{2M_1} a_{i,l}q_i(\beta) - \frac{\partial V(\alpha,t)}{\partial t}\right] + \frac{\partial V(\alpha,t)}{\partial t}. \quad (3.4.3)$$

Similarly, the differentiation of (3.4.2) with respect to y gives

$$\frac{\partial V(y,t)}{\partial y} = (t-t_l)\sum_{i=1}^{2M_1} a_{i,l}p_i(y) + \frac{\partial V(y,t_l)}{\partial y} + \frac{1}{\beta-\alpha}\Bigg[V(\beta,t) - (t-t_l)\sum_{i=1}^{2M_1} a_{i,l}q_i(\beta) - V(\beta,t_l) + V(\alpha,t_l) - V(\alpha,t)\Bigg]. \quad (3.4.4)$$

Again, differentiating the above expression with respect to y, yields

$$\frac{\partial^2 V(y,t)}{\partial y^2} = (t-t_l)\sum_{i=1}^{2M_1} a_{i,l}h_i(y) + \frac{\partial^2 V(y,t_l)}{\partial y^2}. \quad (3.4.5)$$

Finally, by substituting the values of $\frac{\partial V(y,t)}{\partial t}$ and $\frac{\partial^2 V(y,t)}{\partial y^2}$ (from (3.4.3) and (3.4.4)) into the transformed diffusion Equation (3.2.2a) and assuming $t \to t_{l+1}$ and $y \to y_s$, we get

$$\sum_{i=1}^{2M_1} a_{i,l} q_i(y_s) + \frac{y_s - \alpha}{\beta - \alpha}\left[\frac{\partial V(\beta, t_{l+1})}{\partial t} - \sum_{i=1}^{2M_1} a_{i,l} q_i(\beta) - \frac{\partial V(\alpha, t_{l+1})}{\partial t}\right] + \frac{\partial V(\alpha, t_{l+1})}{\partial t}$$
$$= (t_{l+1} - t_l) \sum_{i=1}^{2M_1} a_{i,l} h_i(y_s) + \frac{\partial^2 V(y_s, t_l)}{\partial y^2}. \tag{3.4.6}$$

To calculate the Haar coefficients $a_{i,l}$, first we impose the given constraints, initial condition, and boundary conditions and then solve the system of equations given by (3.4.6) by using a suitable numerical method. Then by successively substituting the value of these wavelet coefficients into (3.4.2)-(3.4.5), we get the approximated solution of the reformulated PDE for American option (3.2.2) and its derivatives. Finally, for applying back substitution of the coordinate transformation we use $y = \ln(S/K)$ and $\tau = T - \frac{2t}{\sigma^2}$, to get the solution of the original problem (3.2.1) for different American options and options' sensitivities.

3.5 Convergence analysis

In the present section, we prove the convergence of the proposed Haar wavelet method. Initially, we introduce some lemmas needed to prove the convergence.

Lemma 3.5.1. *The Haar waveforms and their integral functions are bounded above and their upper bounds are as follows :*

$$h_i(y) \leqslant 1, \ \forall\, i \text{ and } p_i(y) \leqslant \frac{1}{2^{j+1}}, \quad q_i(y) < \mathfrak{C}\left(\frac{1}{2^{j+1}}\right)^2, \text{ for } i > 1,$$

with $\mathfrak{C} = \dfrac{8}{3(\lfloor (3/2) \rfloor !)^2}$.

Proof. Refer [45]. □

Lemma 3.5.2. *Assume that* $\mathfrak{f}(y, t_{l+1}) = \frac{\partial^2 v(y,t_{l+1})}{\partial y^2} \in L^2(\mathbb{R})$ *be a function defined on* $[\alpha, \beta]$ *at* $(l+1)$*-th time level and* $\mathfrak{f}(y, t_{l+1}) \approx \sum_{i=1}^{2M_1} a_{i,l} h_i(y)$. *If for all* $y \in [\alpha, \beta]$ *there exist* ω

such that $|\mathfrak{f}|$ *and* $\left|\frac{\partial \mathfrak{f}}{\partial y}\right|$ *are bounded by* ω*. Then for all* $l = 1, 2, 3, \ldots, 2M_2 - 1$*, the wavelet coefficients* $a_{i,l}$ *are bounded.*

Proof. The wavelet coefficients $a_{i,l}$ can be written as

$$\begin{aligned} a_{i,l} &= \int_{\alpha}^{\beta} \mathfrak{f}(y, t_{l+1}) h_i(y)\, dy \\ &= \int_{\kappa\left(\frac{\beta-\alpha}{2^j}\right)}^{\left(\kappa+\frac{1}{2}\right)\left(\frac{\beta-\alpha}{2^j}\right)} \mathfrak{f}(y, t_{l+1})\, dy - \int_{\left(\kappa+\frac{1}{2}\right)\left(\frac{\beta-\alpha}{2^j}\right)}^{(\kappa+1)\left(\frac{\beta-\alpha}{2^j}\right)} \mathfrak{f}(y, t_{l+1})\, dy. \end{aligned}$$

By applying mean value theorem, there exist y^* and y^{**} satisfying $\kappa\left(\frac{\beta-\alpha}{2^j}\right) \leqslant y^* \leqslant \left(\kappa+\frac{1}{2}\right)\left(\frac{\beta-\alpha}{2^j}\right)$ and $\left(\kappa+\frac{1}{2}\right)\left(\frac{\beta-\alpha}{2^j}\right) \leqslant y^{**} \leqslant (\kappa+1)\left(\frac{\beta-\alpha}{2^j}\right)$, such that

$$a_{i,l} = 2^{-j-1}(\beta - \alpha)\left[\mathfrak{f}(y^*, t_{l+1}) - \mathfrak{f}(y^{**}, t_{l+1})\right].$$

Again by using Lagrange's mean value theorem there exists $\bar{y} \in [y^*, y^{**}]$ such that

$$a_{i,l} = 2^{-j-1}(\beta - \alpha)(y^* - y^{**})\frac{\partial \mathfrak{f}(\bar{y}, t_{l+1})}{\partial y}.$$

Now as $|y^* - y^{**}| \leqslant \beta - \alpha$ and $\left|\frac{\partial \mathfrak{f}(\bar{y}, t_{l+1})}{\partial y}\right| \leqslant \omega$, so for all l

$$|a_{i,l}| \leqslant \frac{\omega(\beta - \alpha)^2}{2^{j+1}}.$$ □

In this theorem, we perform the convergence analysis for the present wavelet-based approximation scheme

Theorem 3.5.1. *Let* $\frac{\partial^2 v(y,t_{l+1})}{\partial y^2} \in L^2(\mathbb{R})$ *be a continuous and bounded function, defined on* $[\alpha, \beta]$*. Then the approximated solution obtained by the present wavelet scheme converges to the actual solution* i.e., $\forall k\ \|Error_J(y, t_{l+1})\|_2 \to 0$ *as* $J \to \infty$*.*

Proof. Suppose $v(y, t_{l+1})$ be the exact solution of the transformed LCP for American option (3.2.2) and $V(y, t_{l+1})$ be its approximate solution obtained by the proposed Haar

wavelet method at $(l+1)$-th time level. Then, we can write

$$\begin{aligned} v(y,t_{l+1}) &= \eta \sum_{i=0}^{\infty} a_{i,l} q_i(y) + \phi \\ &= \eta a_{1,l} q_1(y) + \eta \sum_{j=0}^{\infty} \sum_{\kappa=0}^{2^j-1} a_{2^j+\kappa+1,l} q_{2^j+\kappa+1}(y) + \phi, \end{aligned}$$

where $\eta = T/(2M_2 - 1)$, ϕ is the function determined by imposing the given initial and boundary conditions, i, j and κ are the earlier defined parameters. Now, the Haar solution at the maximum level of resolution can be determined by

$$V(y,t_{l+1}) = \eta a_{1,l} q_1(y) + \eta \sum_{j=0}^{J} \sum_{\kappa=0}^{2^j-1} a_{2^j+\kappa+1,l} q_{2^j+\kappa+1}(y) + \phi.$$

The error function at the maximum level of resolution is computed by

$$\begin{aligned} Error_J(y,t_{l+1}) &= v(y,t_{l+1}) - V(y,t_{l+1}) \\ &= \eta \sum_{j=J+1}^{\infty} \sum_{\kappa=0}^{2^j-1} a_{2^j+\kappa+1,l} q_{2^j+\kappa+1}(y). \end{aligned}$$

Taking L^2-norm to deduce

$$\|Error_J(y,t_{l+1})\|_2^2 = \eta^2 \sum_{j,\kappa} \sum_{r,s} a_{2^j+\kappa+1,l} a_{2^r+s+1,l} \int_{\alpha}^{\beta} q_{2^j+k+1}(y) q_{2^r+s+1}(y)\, dy.$$

To get the upper bounds for $\|Error_J(y,t_{l+1})\|_2^2$, we use the following result [45]

$$\sum_{j=J+1}^{\infty} \sum_{\kappa=0}^{2^j-1} \left(\frac{1}{2^{j+1}}\right)^3 \leqslant C \left(\frac{1}{2^{J+1}}\right)^2, \text{ for some constant } C.$$

By using upper bound for wavelet coefficients $a_{i,l}$ from Lemma 3.5.2 and upper bounds

for Haar wavelets and their integral functions from Lemma 3.5.1, we obtain

$$\|Error_J(y, t_{l+1})\|_2^2 < \eta^2 \sum_{j,\kappa} \sum_{r,s} \frac{\mathfrak{C}^2 \omega^2 (\beta - \alpha)^4}{(2!)^2 (2^{j+1})^3 (2^{r+1})^3} < \frac{C_1}{(2^{J+1})^4},$$

for some constant C_1. Thus, the Haar wavelet approximation method is convergent. □

3.6 Numerical experiments

In this section, some numerical experiments are performed to demonstrate the proficiency and robustness of the proposed scheme to price the American options and to explore the options' Greeks under the Black-Scholes framework. Since the Black-Scholes model involves various parameters and the change in those parameters affect the price of the option, these effects are depicted graphically and discussed in detail. Although the value of an American option can be calculated by using other methods, to calculate the numerical solution of the option's Greeks Haar wavelet method is explicit and straightforward. Also, the multi-resolution technique of the Haar wavelet method to approximate the spiked function plays a primary role in confining the non-smooth payoff function and the Greeks of American options. For numerical simulations, first, we consider the transformed LCP for an American option, and then we use the back-substitution to the price of the option and compute the Greeks. The computed numerical results are analyzed to rationalize the procedure and to justify the performance of the proposed scheme. Also, it has been shown that the present method is effective for solving moving boundary problems with different constraints conditions. It is worthy to note from the results (Tables 3.1 and 3.2) that the proposed wavelet scheme requires fewer computational nodes than standard numerical methods to achieve a high level of accuracy. We can see that to hit the error level 10^{-15}, the Haar wavelet requires a hundred times fewer points than traditional methods. In all the experiments without the loss of generality, we take $M_1 = M_2$. As the exact solutions are not known, the errors are computed in the form of residual. Thus if $P(S, \tau)$ is the actual solution of (3.2.1), then its approximate solution $C(S, \tau)$ introduces an error $E(S, \tau) = (\mathcal{L}C(S, \tau)).(C - \mathcal{F})$ (known as the residual). The formulaic expressions for

different residual error measures are

$$E_2 = \left(\sum_{\mu_1=1}^{2M_1} \sum_{\mu_2=1}^{2M_2} \left| [(\mathcal{L}C(S,\tau)).(C-\mathcal{F})]_{(\mu_1,\mu_2)} \right|^2 \right)^{1/2},$$

$$E_\infty = \max_{1\leqslant\mu_1\leqslant 2M_1} \max_{1\leqslant\mu_2\leqslant 2M_2} \left| [(\mathcal{L}C(S,\tau)).(C-\mathcal{F})]_{(\mu_1,\mu_2)} \right|.$$

The simulations are performed in MATLAB 2019b, and the computation time needed to solve the present LCP to get the American option price is denoted as CPU Time in seconds.

3.6.1 Simulations and discussion for an American call option

To demonstrate the efficiency of the proposed scheme, we perform an experiment by considering the American call option pricing problem. For the numerical implementation, we fix the option's parameters as in Example 3.6.1.

Example 3.6.1. *Let the value of the risk-free rate of return and volatility are* $r = 0.05$ *and* $\sigma = 0.2$*, respectively with maturity* $T = 0.5$*, considering* $K = 30$ *as the strike price, and the dividend yield* $\delta = 0$*.*

In this example, for numerical simulation, the computational domain is considered as $\alpha = -2$ and $\beta = 2$. The numerical errors while computing the solution of the American call option pricing problem in the form of residual is presented in Table 3.1. From the table, it is perceived that the proposed scheme is highly accurate in computing both the price and the Greeks of the American call option. Also, it is easily observed that even at a fewer number of grid points, the present scheme is hundred times accurate than the standard numerical methods. It is significant to note that there is an increase in the error measures in both L^2 and L^∞ norms. It is justified from the fact that with the increase in the value of the maximum level of resolution J, we have to perform more complex calculations, hence the roundoff error accumulate (see [80] for more details). Moreover, we can observe that after many steps, the accumulated error is still quite small.

Table 3.1: E_2, E_∞, and the CPU time (in seconds) with parameters as given in Example 3.6.1 for calculating the American call option price.

	Maximum Level of Resolution J				
	2	3	4	5	6
E_2	$1.208e-15$	$2.757e-15$	$8.471e-15$	$2.393e-14$	$6.845e-14$
E_∞	$8.219e-16$	$1.182e-15$	$2.623e-15$	$2.910e-15$	$5.819e-15$
CPU Time	0.0806	0.0846	0.0862	0.1252	0.3197

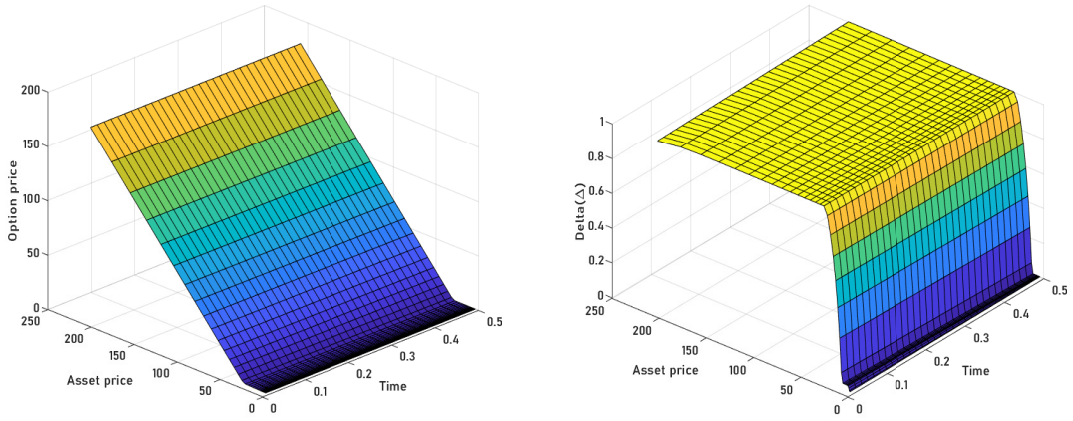

(a) Option price (b) Delta

Figure 3.1: Approximated values of option price and delta for Example 3.6.1.

Figure 3.1(a) depicted the price of the American call option, which is non-linear, it also reveals that the option is deep out of the money for $S \leq K$, and it goes deep in the money for $S > K$ with a high probability that the option will be exercised. The effect of moneyness and the time to maturity on the delta is depicted in Figure 3.1(b). It is significant to note that the value of delta lies between 0 and 1. Also, for extremely high and low values of the underlying asset the option's delta approaches the limits of its range. For S approaching its maximum the intrinsic value of the option is very high, so the delta of the call option approaches 1, and for S approaching towards 0 the option is deep out of the money, thus the value of delta tends to 0. The value of delta helps the investor in

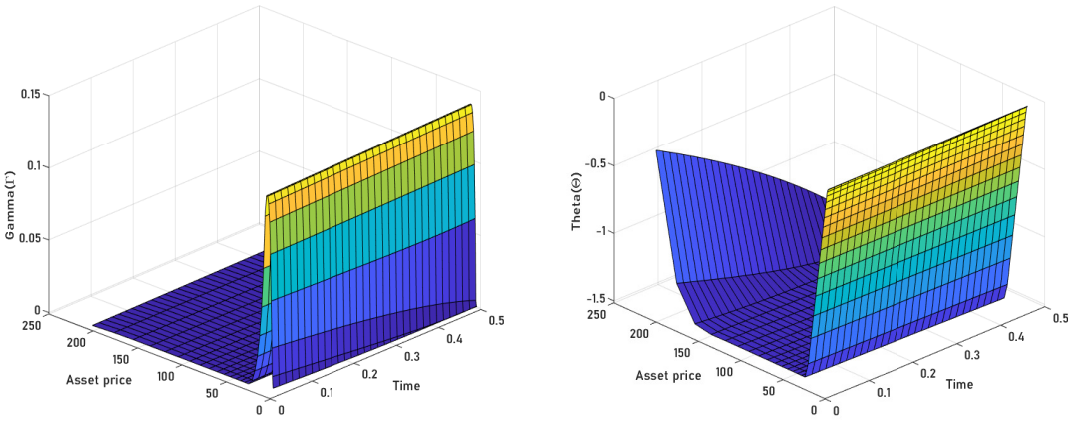

(a) Gamma (b) Theta

Figure 3.2: Approximated values of gamma and theta for Example 3.6.1.

hedging the option by keeping the net delta exposure at zero.

The surface plot of the second derivative of the option price to the underlying asset is illustrated in Figure 3.2(a), which represents the convexity of the option price. The figure reports that close to maturity the value of gamma is negligible. It is justified from the fact that the value of delta is almost constant and equals to 1 near maturity $T = 1$. It is also clear from the figure that the option seller faces higher profit or lower loss arising for S tending to $S_{\max}$. It is worthy to note that the value of gamma is always positive because of the value of delta increases as the asset price increases. The sudden change in the gamma value near the strike price is due to the non-smoothness of the solution function governing the American call option price.

The change in the value of the call option with decay in the time to maturity is depicted in Figure 3.2(b). It is noteworthy that the value of the option is negative as with the passing of time the value of the option will decrease because less time is left for the option to expire.

Table 3.2: E_2, E_∞, and the CPU time (in seconds) with parameters as given in Example 3.6.2 for calculating the American put option price.

	Maximum Level of Resolution J				
	2	3	4	5	6
E_2	$2.362e-18$	$1.064e-17$	$3.102e-17$	$7.006e-17$	$1.827e-16$
E_∞	$1.705e-18$	$6.002e-18$	$1.178e-17$	$1.970e-17$	$4.147e-17$
CPU Time	0.0806	0.0846	0.0862	0.1252	0.3197

3.6.2 Simulations and discussion for an American put option

We consider the following example to illustrate the performance of the present method for computing the price of the American put option and its Greeks with zero dividend yield.

Example 3.6.2. *Consider the LCP with a fixed rate of interest* $r = 0.08$ *and volatility* $\sigma = 0.3$. *Assume the expiry* $T = 1$ *year with strike price* $K = 100$.

The truncated and artificial computational domain for numerical simulations is taken to be $[-1, 1]$. Different error measures presented in Table 3.2 confirm the proficiency and effectiveness of the proposed method. It is worthy to note from the table that the present method is highly accurate and robust, and the CPU time taken by the method to deliver the option price is not so high. Similar to the case of the call option, the numerical error increases with the increase in the number of collocation points are due to the accumulation of the round off error, which is because of the increase in the complexity and non-sparsity of the operational matrix.

In Figure 3.3(a), we have plotted the price of the American put option, which is non-linear in nature. We can observe that the option is out of the money for $S \geq K$ and it goes deep in the money for $S < K$, in this case, the option will most likely be exercised. The amount of change in the price of the option due to the change in the price of the underlying asset is represented in Figure 3.3(b). It is noteworthy that if we are sufficiently close to

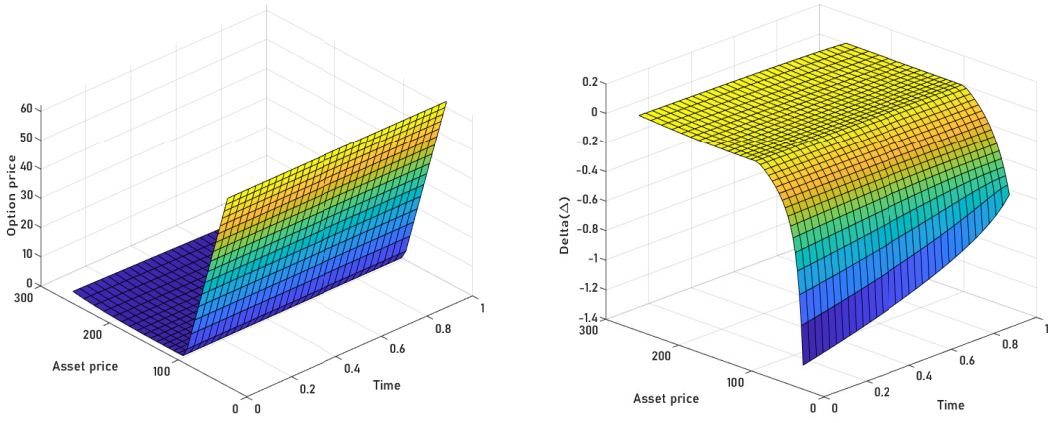

(a) Option price (b) Delta

Figure 3.3: Approximated values of option price and delta for Example 3.6.2.

$S_{\max}$, the option delta is negligible. Exploring the behavior of the American put option's delta helps to manage the portfolio to maintain the delta neutrality.

The value of gamma which represents the second-order sensitivity of the option with the change in the asset's price is depicted in Figure 3.4(a). The figure reveals gamma fades away as the underlying moves closer to its upper bound since delta is close to 0, *i.e.,* the trader faces more loss and lesser profit in case of the put option for $S \geq K$. Probing the gamma behavior affects the gamma-hedging strategies of the trader, which increases the probability of getting more profit. It is noteworthy that the value of gamma is highest and faces a rapid change near the strike price hence at these points, there is a need for frequent Greeks hedging to manage the risk.

Figure 3.4(b) depicted that the value of theta is positive which means that the option is deep in the money. The fall in the graph reveals that the value of the option decreases as the asset price increases. A noteworthy observation is that there is a rise in the value of theta near the expiry, which can be justified from the fact that when we are close to maturity, the time decay is at its peak. The present numerical simulations and discussion reveal the significant impact of the study of options' Greeks in trade markets and in nice agreement with the financial theory given in [47].

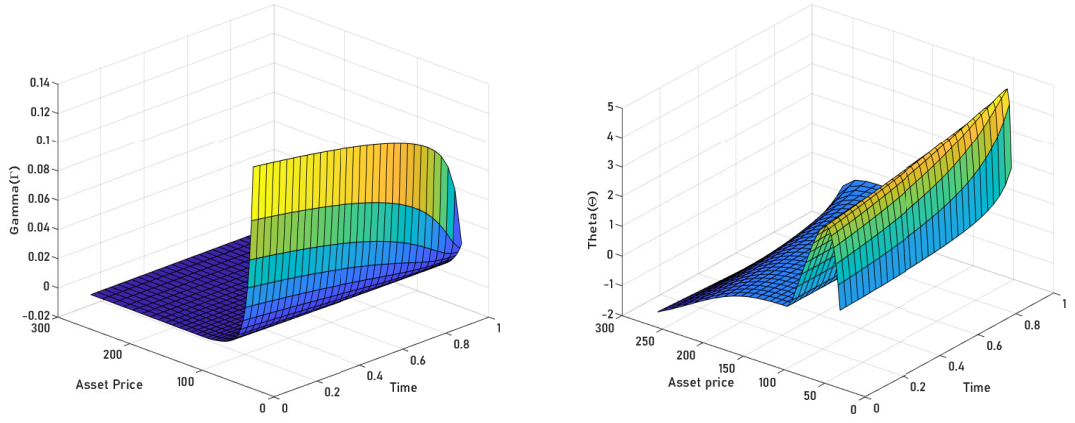

(a) Gamma (b) Theta

Figure 3.4: Approximated values of gamma and theta for Example 3.6.2.

3.7 Conclusion, motivation and extension

In this chapter, we have presented a novel and highly accurate wavelet-based approximation technique for the valuation of the American options and their Greeks. The multi-resolution technique of wavelet approximation is used to get better approximation at each successive level. For numerical implementation, the final value problem is converted into a less cluttered initial value problem, and the unbounded domain is transformed into a bounded domain using log-transformation. We utilize the excellent approximation technique of the Haar wavelet method for spiked functions to approximate the non-smooth solution functions and to estimate the Greeks. Through the study of the convergence behavior of the proposed Haar scheme, it can be concluded that the present method is stable and consistent. Moreover, two test examples are presented to demonstrate the efficiency and to validate the theoretical results of the contributed approach. Computational results, coupled with graphical representations confirm the proficiency and robustness of the proposed method. It is worthy to note that the present method is efficient to solve the free boundary problems. The inspirational and motivational work of the simulated results of options' Greeks analyzed and discussed has a significant impact on various hedging strategies,

which leads to vast applications in different financial institutes and trading markets. This method can be used as an alternative to obtaining highly accurate results of different types of PDEs that arise in mathematical finance. Furthermore, it can also be used to solve moving boundary problems arising in the various areas different from finance.

Chapter 4

Investigating the sensitivities of various path-independent binary options

---

A European option can only be exercised at the expiry date, while an American option can be exercised at any time on or before its expiry. On the other hand, the exotic options differ from the vanilla options in several ways [81]. A binary option is a financial exotic option in which the reward is either a predetermined financial value or nothing at all. Due to the all-or-nothing character of its payoffs, binary options are generally referred to as "digital options." These options are ideal for short-term trading since they provide a potentially significant short-term profit with minimal risk. Here comes the question that what is the significance of binary options? There are different motivations for this such as these options give traders the opportunity to succeed on numerous levels beyond just making a profit. Also, the binary options are an excellent way for novice traders to put their talents to the test because binary option trading begins with predicting direction.

The binary option deal is indeed exciting, but it is based on an emotional wave. It is also not a passive experience; it necessitates attention because the chances of winning are not based on numbers. Instead, and in direct contrast to a gambling situation, the trader's ability to recognize market conditions and manage risk determines the probabilities of

winning. In order to evolve and improve your binary options trading performance, you must be willing to review your own performance on a regular basis. There is no such thing as a free lunch, as we all know. Binary option investments come with hazards in addition to great gains. The purpose of a competent binary option risk management program is not to remove risks, in order to keep up with it you need the Greeks. Pricing a binary options and computing its Greeks with a discontinuous payoff is a challenging task.

This chapter proposes a novel idea of a wavelet-based approximation technique using a multi-resolution analysis to investigate the sensitivities of various path-independent binary options under the Black-Scholes environment. The final value problem is transformed into a dimensionless initial value problem; also, to avoid the large truncation error, the infinite domain is truncated into a finite domain. The suggested Haar wavelet scheme is effective and simple to implement for assessing the different physical and numerical aspects of the options' Greeks since it explicitly offers the numerical approximation of all the derivatives of the solution function. Also, the non-smooth payoff functions are approximated well with the Haar wavelet approximation technique of estimating the spiked functions, so there is no need to deal with the discontinuity separately. The proofs of the consistency and stability of the proposed method are given and it has been shown that the proposed method is the first and second-order accurate in the temporal and spatial directions, respectively. Several numerical examples of distinct binary options have been taken into account, confirming the theoretical findings (consistency and stability). Different attributes of the Greeks are analyzed graphically.

4.1 Literature survey

As an over-the-counter instrument, binary options have been used for decades. Still, it is relatively new for the traders, as the first time, they used it in the United States in 2008 after the approval by the Commodity Futures Trading Commission (CFTC) and regulation through the Nadex [19]. However, Jaworsky [82] reported that the first binary options were presented by the Chicago Board Options Exchange (CBOE) in 2006.

To solve the European and American option pricing models, numerous analytical

and numerical approaches have been proposed. For binary options problems, however, only a few numerical techniques have been proposed [83–89]. The well-known available numerical methods are the finite element method and the finite difference method. These methods use the concept that since the parabolic partial differential equations (PDEs) are the extension of the ordinary differential equations (ODEs) in some sense [90] so, most of the numerical methods first convert the parabolic PDEs into the system of ODEs, called the semi-discretization, and then solve the system of ODEs. It is challenging to price the binary option with a discontinuous payoff as the final payoff is not continuous. Therefore, the classical FDM cannot be used as it gives a significant error in the solutions around the strike, especially for their Greeks [20]. Rannacher [91] presented FEM for the diffusion problems with the irregular initial/boundary data. Heston and Zhou [92] shown that the order of convergence of a method depends on the smoothness of the payoff functions and is much lower than expected in the case of binary option as the payoff functions are discontinuous. However, the accuracy can be improved by modification with some care. They proposed two different methods to enhance the accuracy as we expect for the continuous payoffs: adjusting the discrete-time solution before maturity and smoothing the payoff function. Pooley *et al.* [93] used FEM by using special time-stepping in conjunction with various procedures (averaging the initial data, shifting the grid, and a projection method) for smoothing discontinuities. They have observed that these procedures individually are not sufficient to get the expected solution error, but with the special time-stepping, these are highly efficient. It would also be challenging for the spectral element method to enforce the final condition at the strike price without proper enforcement. Kim and Moon [20] used two types (Type I: at each time it changes adaptively the size of the time step, Type II: it combines two uniform meshes) of hybrid FDMs with variable time-stepping for the solution of the binary option. Recently, Yang *et al.* [94] have suggested a novel local meshfree method based on Hermite radial basis function (RBF) interpolation on set of local nodes for simulating cash-or-nothing and asset-or-nothing options.

Traditional numerical approaches fail to approximate the highly non-smooth behavior

of the payoff function at the strike price. In contrast, as the discontinuous behavior of discrete Haar functions senses the points of discontinuities easily, the estimation technique of the Haar wavelet method for spiked function resolves the obstacle of the discontinuities and jumps. So, the Haar wavelet method effortlessly deals with the numerical sensitivity of computation of discontinuous and spiked functions. Based on the Haar basis functions, in this chapter, we construct an alternative numerical methodology for investigating the sensitivities of the various path-independent binary options. Unlike other methods, such as FDM, it does not require semi-discretization.

4.2 Binary option pricing valuation model

In this chapter, we consider various path-independent binary options with non-smooth payoff functions under the Black-Scholes environment. Consider S as the current price of the underlying asset (referred to stock) in the market at the time τ. The price $V(S,\tau)$ of the derivative with expiry T is diagnosed by the following PDE [10]:

$$\mathcal{L}V(S,\tau) \equiv \frac{\partial V}{\partial \tau} + \frac{1}{2}\sigma^2 S^2 \frac{\partial^2 V}{\partial S^2} + (r-\delta)S\frac{\partial V}{\partial S} - rV = 0, \quad 0 < S < \infty,\ 0 \leqslant \tau < T, \tag{4.2.1}$$

where r is the risk-free interest rate, σ is the volatility, and δ is the dividend yield. For different binary options, the payoff mechanism switches entirely and hence the boundary conditions. In the case of call options, the contract becomes out of the money when the price of the stock decreases to zero, *i.e.,* the contract becomes meaningless when the price of the stock drops, so in all the binary calls

$$\lim_{S\to 0} V(S,\tau) = 0.$$

Binary options intensify the dual role of the strike price: not only it acts as a barrier that decides whether the option finishes in the money, at the money, or out of the money, but it also tells about the size of the payoff. The terminal conditions for different binary calls, also known as the payoff functions and the right boundary conditions, are defined as

follows:

Cash-or-nothing calls. The simplest binary call pays off nothing if the underlying asset price S finishes below the strike price K or pays out a predetermined constant amount A if the underlying asset finishes above the strike price. The payoff function and final boundary condition for the cash-or-nothing call option are

$$V(S,T) = \begin{cases} A, & \text{if } S \geqslant K, \\ 0, & \text{if } S < K, \end{cases}$$

and

$$\lim_{S \to +\infty} V(S,\tau) = Ae^{-r(T-\tau)},$$

respectively. It interprets that the valued option depends upon the predetermined fixed amount and time with an increase in the asset price.

Asset-or-nothing calls. Unlike a cash-or-nothing option, the payoff of the more complex binary call "asset-or-nothing" option is not predetermined; it is subject to the underlying asset price. It pays off nothing if the underlying asset price S finishes below the strike price K, or pays out the asset price S itself if the underlying asset finishes above the strike price. The payoff function for the asset-or-nothing call option satisfies

$$V(S,T) = \begin{cases} S, & \text{if } S \geqslant K, \\ 0, & \text{if } S < K, \end{cases}$$

and the right boundary condition is given by

$$\lim_{S \to +\infty} V(S,\tau) = Se^{-\delta(T-\tau)}.$$

Gap call options. These options are slightly more complex than the standard options. These are paid off nothing if the underlying asset price S finishes below the strike price K, or pays out the difference of asset price S and a predetermined constant amount A if the

underlying asset finishes above the strike price. The payoff function of the gap call option is

$$V(S,T) = \begin{cases} S - A, & \text{if } S \geqslant K, \\ 0, & \text{if } S < K, \end{cases}$$

with the right boundary condition given by

$$\lim_{S \to +\infty} V(S,\tau) = Se^{-\delta(T-\tau)} - Ae^{-r(T-\tau)}.$$

The difference $A - K$ is defined as a gap. The positive gap calls will sell for less than standard calls. It can be derived by taking the difference between the two options (a cash-or-nothing option and an asset-or-nothing option).

Using a log-transformation, we transform the Equation (4.2.1) from the final value problem to a non-dimensional and less cluttered initial value problem by introducing the new variables. We take $x = \ln(S/K)$ and $t = \frac{\sigma^2}{2}(T - \tau)$, which reformulate the Black-Scholes equation into

$$\frac{\partial u}{\partial t} = \frac{\partial^2 u}{\partial x^2}, \tag{4.2.2}$$

where $V(S,\tau)$ and $u(x,t)$ are related by

$$V(S,\tau) = Ke^{-\left[2\left(\frac{r-\delta}{\sigma^2}\right)-1\right]\frac{x}{2} - \left[\frac{1}{4}\left(2\left(\frac{r-\delta}{\sigma^2}\right)-1\right)^2 + \frac{2r}{\sigma^2}\right]t} u(x,t).$$

After the transformation, the left boundary condition for all the three binary options described above is as follows:

$$\lim_{x \to -\infty} u(x,t) = 0.$$

The terminal conditions are now turned into initial conditions, which can be easily extended into boundary conditions for the numerical implementation. The transformed initial

condition and asymptotic right boundary condition for the cash-or-nothing call option are

$$u(x,0) = \begin{cases} \frac{A}{K} e^{\frac{x}{2}\left(\frac{2(r-\delta)}{\sigma^2}-1\right)}, & \text{if } x \geqslant 0, \\ 0, & \text{if } x < 0, \end{cases}$$

and

$$\lim_{x\to+\infty} u(x,t) = \frac{A}{K} e^{\frac{x}{2}\left(\frac{2(r-\delta)}{\sigma^2}-1\right)+\frac{t}{4}\left(\frac{2(r-\delta)}{\sigma^2}-1\right)^2},$$

respectively. After transformation the initial conditions for the asset-or-nothing and gap options become

$$u(x,0) = \begin{cases} e^{\frac{x}{2}\left(\frac{2(r-\delta)}{\sigma^2}+1\right)}, & \text{if } x \geqslant 0, \\ 0, & \text{if } x < 0, \end{cases}$$

and

$$u(x,0) = \begin{cases} e^{\frac{x}{2}\left(\frac{2(r-\delta)}{\sigma^2}+1\right)} - \frac{A}{K} e^{\frac{x}{2}\left(\frac{2(r-\delta)}{\sigma^2}-1\right)}, & \text{if } x \geqslant 0, \\ 0, & \text{if } x < 0, \end{cases}$$

respectively. Moreover, the right boundary condition for the asset-or-nothing option is transformed into

$$\lim_{x\to+\infty} u(x,t) = e^{\frac{x}{2}\left(\frac{2(r-\delta)}{\sigma^2}+1\right)+\frac{t}{4}\left(\frac{2(r-\delta)}{\sigma^2}+1\right)^2},$$

while the right boundary condition for the gap option becomes

$$\lim_{x\to+\infty} u(x,t) = e^{\frac{x}{2}\left(\frac{2(r-\delta)}{\sigma^2}+1\right)+\frac{t}{4}\left(\frac{2(r-\delta)}{\sigma^2}+1\right)^2} - \frac{A}{K} e^{\frac{x}{2}\left(\frac{2(r-\delta)}{\sigma^2}-1\right)+\frac{t}{4}\left(\frac{2(r-\delta)}{\sigma^2}-1\right)^2}.$$

For the numerical implementation, to avoid the unacceptable large truncation error and to get the highly accurate results, we truncate the infinite domain into a finite domain by taking the relatively large value of x *i.e.,* we take $(x,t) \in [x_{\min}, x_{\max}] \times [0, t_{\max}]$, where $t_{\max} = \frac{\sigma^2 T}{2}$; $x_{\min}$ and $x_{\max}$ indicate sufficiently large negative and sufficiently large positive numbers, respectively.

The derivatives of the option price are equally important as the option price, so the question is, how does the option price change if one of the parameters changes? To

answer this question, we introduce the "Greeks". Studying numerous Greeks of various binary options has a big impact on the hedging techniques employed by various financial institutions. The Greeks are the derivatives of option prices with respect to time, the underlying asset, or the parameters used in the formula. The sensitivity of a portfolio of options to change in market conditions is diagnosed using Greeks. As the price of an option varies, the risk of the option changes too. Therefore, knowing how the option price changes enable the trader to hedge the option's risks. All these Greeks have differentiation formulas derived from the Black-Scholes model. In this work, we will study the following Greeks: delta (Δ), gamma (Γ), theta (Θ), charm and color.

4.3 Haar wavelet methodology

The discrete wavelet, in particular the Haar wavelets $(h_i(x))$, can be used to construct a basis of $L^2(\mathbb{R})$ by using the multi-resolution technique. The maximal value of i is $2M_1 = 2^{J+1}$, where J is the maximum level of resolution. The given interval $[x_{\min}, x_{\max}]$ is partitioned into $2M_1$ sub-intervals of equal length using the collocation points $x_s = x_{\min} + \frac{(s-0.5)(x_{\max}-x_{\min})}{2M_1},\ s = 1, 2, \ldots, 2M_1$. We denote by $p_i(x)$ and $q_i(x)$ as the first and second integrals of the Haar wavelet function.

4.4 Implementation of the numerical method

To approximate the solutions and the derivatives of the transformed equations of the path-independent binary options under the Black-Scholes model, first divide the spatial domain $[x_{\min}, x_{\max}]$ and the temporal domain $[0, t_{\max}]$ into $2M_1$ and $2M_2$ parts of equal length, respectively. Let U and u are approximate and exact solutions of (4.2.2), respectively. To derive the Haar wavelet method, the approximation of $\frac{\partial^3 u(x,t)}{\partial t \partial x^2}$ is represented in the form:

$$\frac{\partial^3 U(x,t)}{\partial t \partial x^2} = \sum_{i=1}^{2M_1} c_{i,l} h_i(x),\ t \in [t_l, t_{l+1}],$$

where $c_{i,l}$ are the unknown coefficients, i denotes the index of Haar functions in the spatial direction and l denotes the time level. Integrating the above expression once with respect

to t from t_l to t, we get

$$\frac{\partial^2 U(x,t)}{\partial x^2} = (t-t_l)\sum_{i=1}^{2M_1} c_{i,l} h_i(x) + \frac{\partial^2 U(x,t_l)}{\partial x^2}.$$

Now, by integrating the above expression with respect to x from $x_{\min}$ to x, we obtain

$$\frac{\partial U(x,t)}{\partial x} = (t-t_l)\sum_{i=1}^{2M_1} c_{i,l} p_i(x) + \frac{\partial U(x,t_l)}{\partial x} - \frac{\partial U(x_{\min},t_l)}{\partial x} + \frac{\partial U(x_{\min},t)}{\partial x}.$$

Again, integrating it with respect to x from $x_{\min}$ to x, we obtain

$$\begin{aligned} U(x,t) =& (t-t_l)\sum_{i=1}^{2M_1} c_{i,l} q_i(x) + U(x,t_l) - U(x_{\min},t_l) - (x-x_{\min})\frac{\partial U(x_{\min},t_l)}{\partial x} \\ &+ (x-x_{\min})\frac{\partial U(x_{\min},t)}{\partial x} + U(x_{\min},t). \end{aligned} \tag{4.4.1}$$

To find the unknown terms $\frac{\partial U(x_{\min},t_l)}{\partial x}$ and $\frac{\partial U(x_{\min},t)}{\partial x}$, using the boundary condition for $x = x_{\max}$, we get

$$\begin{aligned} \frac{\partial U(x_{\min},t)}{\partial x} - \frac{\partial U(x_{\min},t_l)}{\partial x} =& \frac{1}{x_{\max}-x_{\min}}\Bigg[U(x_{\max},t) - (t-t_l)\sum_{i=1}^{2M_1} c_{i,l} q_i(x_{\max}) \\ &- U(x_{\max},t_l) + U(x_{\min},t_l) - U(x_{\min},t)\Bigg]. \end{aligned}$$

Replacing it back into (4.4.1) gives

$$\begin{aligned} U(x,t) = (t-t_l)\sum_{i=1}^{2M_1} c_{i,l} q_i(x) + U(x,t_l) - U(x_{\min},t_l) + \frac{x-x_{\min}}{x_{\max}-x_{\min}}\Bigg[U(x_{\max},t) \\ - (t-t_l)\sum_{i=1}^{2M_1} c_{i,l} q_i(x_{\max}) - U(x_{\max},t_l) + U(x_{\min},t_l) - U(x_{\min},t)\Bigg] + U(x_{\min},t). \end{aligned} \tag{4.4.2}$$

Now by differentiating (4.4.2) with respect to t, we obtain

$$\frac{\partial U(x,t)}{\partial t} = \sum_{i=1}^{2M_1} c_{i,l} q_i(x) + \frac{x - x_{\min}}{x_{\max} - x_{\min}} \left[\frac{\partial U(x_{\max}, t)}{\partial t} - \sum_{i=1}^{2M_1} c_{i,l} q_i(x_{\max}) - \frac{\partial U(x_{\min}, t)}{\partial t} \right] + \frac{\partial U(x_{\min}, t)}{\partial t}. \tag{4.4.3}$$

Also, the differentiation of (4.4.2) with respect to x, gives

$$\frac{\partial U(x,t)}{\partial x} = (t - t_l) \sum_{i=1}^{2M_1} c_{i,l} p_i(x) + \frac{\partial U(x,t_l)}{\partial x} + \frac{1}{x_{\max} - x_{\min}} \Big[U(x_{\max}, t) - (t - t_l) \sum_{i=1}^{2M_1} c_{i,l} q_i(x_{\max}) - U(x_{\max}, t_l) + U(x_{\min}, t_l) - U(x_{\min}, t) \Big]. \tag{4.4.4}$$

Differentiate it with respect to x, to obtain

$$\frac{\partial^2 U(x,t)}{\partial x^2} = (t - t_l) \sum_{i=1}^{2M_1} c_{i,l} h_i(x) + \frac{\partial^2 U(x,t_l)}{\partial x^2}. \tag{4.4.5}$$

Substituting the approximated values of

$$\frac{\partial U(x,t)}{\partial t} \quad \text{and} \quad \frac{\partial^2 U(x,t)}{\partial x^2}$$

(given by (4.4.3) and (4.4.5)) into the Equation (4.2.2) and discretizing the results by assuming $t \to t_{l+1}$ and $x \to x_s$, we obtain

$$\sum_{i=1}^{2M_1} c_{i,l} \left[q_i(x_s) - \frac{x_s - x_{\min}}{x_{\max} - x_{\min}} q_i(x_{\max}) - (t_{l+1} - t_l) h_i(x_s) \right] = -\frac{x_s - x_{\min}}{x_{\max} - x_{\min}} \times \left[\frac{\partial U(x_{\max}, t_{l+1})}{\partial t} - \frac{\partial U(x_{\min}, t_{l+1})}{\partial t} \right] - \frac{\partial U(x_{\min}, t_{l+1})}{\partial t} + \frac{\partial^2 U(x_s, t_l)}{\partial x^2}. \tag{4.4.6}$$

Here t_l and t_{l+1} represent the present and next temporal levels, respectively, and x_s denotes the s-th collocation point in the spatial direction. From (4.4.6) we can successively calcu-

late the wavelet coefficients $c_{i,l}$, and then by substituting the values of these coefficients into (4.4.2)-(4.4.5), we get the approximated solution of the transformed Equation (4.2.2) and its derivatives. Finally, for applying back substitution of the coordinate transformation we use $S = Ke^x$ and $\tau = T - \frac{2t}{\sigma^2}$, to get the solution of the original Equation (4.2.1) for different binary options and the values of the options' Greeks.

4.5 Analysis of the numerical method

In this section, we present the consistency and stability analysis of the proposed method by following the technique given in [95]. We also introduce some lemmas, needed to study the consistency and stability. Let the solution of the transformed second-order PDE of the Black-Scholes equation be smooth lying in $C^{2,1}((x_{\min}, x_{\max}) \times [0, t_{\max}])$ and is approximated as

$$U(x,t') = (t'-t_l)\sum_{i=1}^{2M_1} c_{i,l}\left[q_i(x) - \frac{x-x_{\min}}{x_{\max}-x_{\min}}q_i(x_{\max})\right] + \phi(x,t'),$$

where $t' \in [t_l, t_{l+1}]$ and $\phi(x,t')$ is the function determined by the given initial and boundary conditions. We denote $\Lambda = [x_{\min}, x_{\max}]$ and define a projection map $P : L^2(\Lambda) \to \mathbb{V}$, where $\mathbb{V}$ is a subspace in $L^2(\Lambda)$ generated by the direct sum decomposition of orthogonal Haar wavelets defined on Λ (refer section 3.1), such that

$$Pu(x,t_{l+1}) = U(x,t_{l+1}) = \frac{\sigma^2 T}{4M_2}\sum_{i=1}^{2M_1} a_i Q_i(x),$$

where a_i's are the Haar coefficients at l-th time level, and $Q_i(x) = q_i(x) - \frac{x-x_{\min}}{x_{\max}-x_{\min}}q_i(x_{\max})$.

4.5.1 Investigating consistency

We need the following lemma to prove the consistency of the proposed method.

Lemma 4.5.1. *Assume that* $\mathfrak{f}(x,t_l) = \frac{\partial^2 u(x,t_l)}{\partial x^2} \in L^2(\mathbb{R})$ *be a function defined on* Λ *at the* $(l+1)$*-th time level, and* $\mathfrak{f}(x,t_{l+1}) \approx \sum_{i=1}^{2M_1} a_i h_i(x)$. *If for all* $x \in \Lambda$ *there exist* ξ *such that* $\mathfrak{f}$ *and* $\frac{\partial \mathfrak{f}}{\partial x}$ *are bounded by* ξ. *Then, the wavelet coefficients* a_i *are bounded at every*

time level.

Proof. At the l-th time level the wavelet coefficients a_i can be written as

$$\begin{aligned} a_i &= \int_{x_{\min}}^{x_{\max}} \mathfrak{f}(x, t_{l+1}) h_i(x)\, dx, \text{ (using orthonormality)} \\ &= \int_{k\left(\frac{x_{\max}-x_{\min}}{2^j}\right)}^{\left(k+\frac{1}{2}\right)\left(\frac{x_{\max}-x_{\min}}{2^j}\right)} \mathfrak{f}(x, t_{l+1})\, dx - \int_{\left(k+\frac{1}{2}\right)\left(\frac{x_{\max}-x_{\min}}{2^j}\right)}^{(k+1)\left(\frac{x_{\max}-x_{\min}}{2^j}\right)} \mathfrak{f}(x, t_{l+1})\, dx. \end{aligned}$$

Applying mean value theorem, there exist x^* and x^{**} satisfying $k\left(\frac{x_{\max}-x_{\min}}{2^j}\right) \leqslant x^* \leqslant \left(k+\frac{1}{2}\right)\left(\frac{x_{\max}-x_{\min}}{2^j}\right)$ and $\left(k+\frac{1}{2}\right)\left(\frac{x_{\max}-x_{\min}}{2^j}\right) \leqslant x^{**} \leqslant (k+1)\left(\frac{x_{\max}-x_{\min}}{2^j}\right)$, such that

$$a_i = 2^{-j-1}(x_{\max} - x_{\min}) \left[\mathfrak{f}(x^*, t_{l+1}) - \mathfrak{f}(x^{**}, t_{l+1})\right].$$

Again using Lagrange's mean value theorem there exists $\bar{x} \in [x^*, x^{**}]$ such that

$$a_i = 2^{-j-1}(x_{\max} - x_{\min})(x^* - x^{**}) \frac{\partial \mathfrak{f}(\bar{x}, t_{l+1})}{\partial x}.$$

Now as $|x^* - x^{**}| \leqslant x_{\max} - x_{\min}$ and $\left|\frac{\partial \mathfrak{f}(\bar{x}, t_{l+1})}{\partial x}\right| \leqslant \xi$, so for all l

$$|a_i| \leqslant \frac{\xi (x_{\max} - x_{\min})^2}{2^{j+1}}.$$ □

For some $u \in L^2(\Lambda)$, the bound for $\|u - Pu\|$ is given by the following lemma.

Lemma 4.5.2. *Let P be the projection map defined as above and $u(x,t)$ be defined on $L^2(\Lambda)$. Then*

$$\|u - Pu\| \leqslant \frac{C_1}{(2M_1)^2 2M_2},$$

where $2M_1$ and $2M_2$ are the total numbers of collocation points in spatial and temporal directions, respectively, and $C_1 = \max |a_i|$.

Proof. The integration of $U(x,t)$ gives a ramp function $\frac{t_{\max} a_i}{(2M_1)^2 2M_2}\left(\frac{1}{2M_1} + (x - \gamma_i)\right)$ on the interval Λ. It has the average value $\frac{t_{\max} a_i}{2(2M_1)^2 2M_2}\left(\frac{1}{2M_1} + (1 - \gamma_i)\right)$. The difference

between the average and actual ramp values (denoted by $e(x)$) over the interval Λ and given by

$$e(x) = \frac{t_{\max} a_i}{2(2M_1)^2 2M_2}\left(\frac{1}{2M_1} + (1-\gamma_i)\right) - \frac{t_{\max} a_i}{(2M_1)^2 2M_2}\left(\frac{1}{2M_1} + (x-\gamma_i)\right),$$

is known as the error in approximating the ramp. So, the least square of the error on the interval Λ is as follows:

$$\begin{aligned}
(\text{Error}(x))^2 &= \int_\Lambda [e(x)]^2\, dx \\
&= \int_\Lambda \left[\frac{t_{\max} a_i}{2(2M_1)^2 2M_2}\left(\frac{1}{2M_1} + (1-\gamma_i)\right) - \frac{t_{\max} a_i}{(2M_1)^2 2M_2}\left(\frac{1}{2M_1} + (x-\gamma_i)\right)\right]^2 dx \\
&= \left(\frac{t_{\max} a_i}{(2M_1)^2 2M_2}\right)^2 \int_\Lambda \left[\frac{1}{2}\left(\frac{1}{2M_1} + (1-\gamma_i)\right) - \left(\frac{1}{2M_1} + (x-\gamma_i)\right)\right]^2 dx \\
&= \left(\frac{a_i}{(2M_1)^2 2M_2}\right)^2 \int_\Lambda (t_{\max})^2 \left[\frac{1}{2} + \frac{\gamma_i}{2} - \frac{1}{4M_1} - x\right]^2 dx \\
&\leqslant \left(\frac{a_i}{(2M_1)^2 2M_2}\right)^2.
\end{aligned}$$

Thus, we deduce

$$\|u - Pu\| = \max_\Lambda(|\text{Error}(x)|) \leqslant \frac{C_1}{(2M_1)^2 2M_2}. \qquad \square$$

The following theorem shows that the proposed method is consistent.

Theorem 4.5.1. *Suppose $U = Pu$ be the approximate solution obtained by the Haar wavelet collocation method of the equation*

$$\frac{\partial u}{\partial t} = \frac{\partial^2 u}{\partial x^2}, \tag{4.5.1}$$

which is the transformed equation of the Black-Scholes equation. Then we can write

$$\frac{\partial U}{\partial t} = \frac{\partial^2 U}{\partial x^2} + E, \tag{4.5.2}$$

where the error term E satisfies

$$\|E\| \leqslant \frac{C_2}{(2M_1)^2 2M_2},$$

for $C_2 = \max\left|\frac{\partial u}{\partial t}\right| + \max\left|\frac{\partial^2 u}{\partial x^2}\right|$.

Proof. By subtracting Equation (4.5.1) from (4.5.2), we obtain

$$\frac{\partial U}{\partial t} - \frac{\partial^2 U}{\partial x^2} - E - \frac{\partial u}{\partial t} + \frac{\partial^2 u}{\partial x^2} = 0.$$

This implies

$$\begin{aligned} E &= \left(\frac{\partial U}{\partial t} - \frac{\partial u}{\partial t}\right) - \left(\frac{\partial^2 U}{\partial x^2} - \frac{\partial^2 u}{\partial x^2}\right) \\ &= \left(\frac{\partial Pu}{\partial t} - \frac{\partial u}{\partial t}\right) - \left(\frac{\partial^2 Pu}{\partial x^2} - \frac{\partial^2 u}{\partial x^2}\right) \\ &= \frac{\partial (Pu - u)}{\partial t} - \frac{\partial^2 (Pu - u)}{\partial x^2} \\ &= \frac{\partial (P - I)u}{\partial t} - \frac{\partial^2 (P - I)u}{\partial x^2}. \end{aligned}$$

Taking the maximum norm on both sides, we get

$$\begin{aligned} \|E\| &\leqslant \|P - I\| \max\left|\frac{\partial u}{\partial t}\right| + \|P - I\| \max\left|\frac{\partial^2 u}{\partial x^2}\right| \\ &= \|P - I\| \left(\max\left|\frac{\partial u}{\partial t}\right| + \max\left|\frac{\partial^2 u}{\partial x^2}\right|\right). \end{aligned}$$

Now, by applying the result of Lemma 4.5.2, we deduce

$$\|E\| \leqslant \frac{C_2}{(2M_1)^2 2M_2},$$

where $C_2 = \max\left|\frac{\partial u}{\partial t}\right| + \max\left|\frac{\partial^2 u}{\partial x^2}\right|$. □

4.5.2 Stability analysis

The following lemma, which estimates the bounds of the norm of the adjoint of a square matrix will be used to prove the stability.

Lemma 4.5.3. *Let X be a $2M_1 \times 2M_1$ matrix with no zero rows. Then*

$$\|adj(X)\| \leqslant \eta \max_k \prod_{j=1,\, j\neq k}^{2M_1} \|row_j(X)\|, \text{ for some constant } \eta.$$

Here, $adj(X)$ denotes the adjoint of the matrix X, $row_j(X)$ indicates the transpose of the j-th row of X.

Proof. Let Y be any non-singular matrix, then

$$adj(Y^{-1}X)adj(Y) = adj(X).$$

In particular, let Y be a diagonal matrix and the diagonal entries of matrix Y are $\|row_i(X)\|,\ i = 1, 2, \ldots, 2M_1$. Then

$$\|adj(Y)\| = \|b_1 b_2 b_3 \ldots b_{2M_1} diag(b_i^{-1})\| = \max_k \prod_{j=1,\, j\neq k}^{2M_1} \|row_j(X)\|.$$

Note that the rows of $Y^{-1}X$ have norm 1. Now if all the entries X and Y^{-1} are finite then by the definition of norm, $\max \|adj(Y^{-1}X)\|$ exists, and hence we deduce

$$\|adj(X)\| \leqslant \|adj(Y^{-1}X)\|\|adj(Y)\| \leqslant \eta \max_k \prod_{j=1,\, j\neq k}^{2M_1} \|row_j(X)\|,$$

where $\eta = \max \|adj(Y^{-1}X)\|$ is independent of M_1. □

There are many ways to prove the boundedness of the approximate solution of a given PDE. One way to investigate this is to show that the approximate solution U is bounded for all time levels by the initial condition U_0 and some Haar functions. The spatial domain

$[x_{\min}, x_{\max}]$ is divided into $2M_1$ equal parts and l represents the time level. The system of equations (4.4.6) can be written in matrix form as

$$AC = B,$$

where A is $2M_1 \times 2M_1$ matrix; C and B are $2M_1 \times 1$ column vectors. The elements of $A = (a_{\nu\omega})$ are given by

$$a_{\nu\omega} = q_\omega(x_\nu) - \frac{x_\nu - x_{\min}}{x_{\max} - x_{\min}} q_\omega(x_{\max}) - (t_{l+1} - t_l) h_\omega(x_\nu),$$

with $\nu = 1, 2, \ldots, 2M_1$, $\omega = 1, 2, \ldots, 2M_1$, and the column vectors B and C are given by

$$B = \begin{bmatrix} -\frac{x_1 - x_{\min}}{x_{\max} - x_{\min}} \left(\frac{\partial U(x_{\max}, t_{l+1})}{\partial t} - \frac{\partial U(x_{\min}, t_{l+1})}{\partial t} \right) - \frac{\partial U(x_{\min}, t_{l+1})}{\partial t} + \frac{\partial^2 U(x_1, t_l)}{\partial x^2} \\ -\frac{x_2 - x_{\min}}{x_{\max} - x_{\min}} \left(\frac{\partial U(x_{\max}, t_{l+1})}{\partial t} - \frac{\partial U(x_{\min}, t_{l+1})}{\partial t} \right) - \frac{\partial U(x_{\min}, t_{l+1})}{\partial t} + \frac{\partial^2 U(x_2, t_l)}{\partial x^2} \\ \vdots \\ \vdots \\ -\frac{x_{2M_1} - x_{\min}}{x_{\max} - x_{\min}} \left(\frac{\partial U(x_{\max}, t_{l+1})}{\partial t} - \frac{\partial U(x_{\min}, t_{l+1})}{\partial t} \right) - \frac{\partial U(x_{\min}, t_{l+1})}{\partial t} + \frac{\partial^2 U(x_{2M_1}, t_l)}{\partial x^2} \end{bmatrix},$$

and

$$C = \begin{bmatrix} c_{1,l} \\ c_{2,l} \\ \vdots \\ c_{2M_1,l} \end{bmatrix}.$$

Now we confirm the invertibility of the matrix A by showing that all the columns of matrix

A are linearly independent. Assume

$$\begin{aligned}
&\lambda_1\left(q_1(x)-\frac{x-x_{\min}}{x_{\max}-x_{\min}}q_1(x_{\max})-(t_{l+1}-t_l)h_1(x)\right)\\
&+\lambda_2\left(q_2(x)-\frac{x-x_{\min}}{x_{\max}-x_{\min}}q_2(x_{\max})-(t_{l+1}-t_l)h_2(x)\right)\\
&+\lambda_3\left(q_3(x)-\frac{x-x_{\min}}{x_{\max}-x_{\min}}q_3(x_{\max})-(t_{l+1}-t_l)h_3(x)\right)\\
&+\cdots\\
&+\lambda_{2M_1}\left(q_{2M_1}(x)-\frac{x-x_{\min}}{x_{\max}-x_{\min}}q_{2M_1}(x_{\max})-(t_{l+1}-t_l)h_{2M_1}(x)\right)=0,
\end{aligned}$$

for some $\lambda_1,\lambda_2,\ldots,\lambda_{2M_1}$. On replacing the values of $q_i(x)$ and $h_i(x)$ which gives

$$\begin{aligned}
&\lambda_1\left[\begin{cases}\frac{(x-\alpha_1)^2}{2}, & x\in[\alpha_1,\beta_1),\\ \frac{(x-\alpha_1)^2-2(x-\beta_1)^2}{2}, & x\in[\beta_1,\gamma_1),\\ \frac{(x-\alpha_1)^2-2(x-\beta_1)^2+(x-\gamma_1)^2}{2}, & x\in[\gamma_1,x_{\max}),\\ 0, & \text{elsewhere.}\end{cases}-\left(\frac{x-x_{\min}}{x_{\max}-x_{\min}}q_1(x_{\max})\right)-(t_{l+1}-t_l)\begin{cases}1, & x\in[\alpha_1,\beta_1),\\ -1, & x\in[\beta_1,\gamma_1),\\ 0, & \text{elsewhere,}\end{cases}\right]\\
&+\lambda_2\left[\begin{cases}\frac{(x-\alpha_2)^2}{2}, & x\in[\alpha_2,\beta_2),\\ \frac{(x-\alpha_2)^2-2(x-\beta_2)^2}{2}, & x\in[\beta_2,\gamma_2),\\ \frac{(x-\alpha_2)^2-2(x-\beta_2)^2+(x-\gamma_2)^2}{2}, & x\in[\gamma_2,x_{\max}),\\ 0, & \text{elsewhere.}\end{cases}-\left(\frac{x-x_{\min}}{x_{\max}-x_{\min}}q_2(x_{\max})\right)-(t_{l+1}-t_l)\begin{cases}1, & x\in[\alpha_2,\beta_2),\\ -1, & x\in[\beta_2,\gamma_2),\\ 0, & \text{elsewhere,}\end{cases}\right]\\
&+\cdots\\
&+\lambda_{2M_1}\left[\begin{cases}\frac{(x-\alpha_{2M_1})^2}{2}, & x\in[\alpha_{2M_1},\beta_{2M_1}),\\ \frac{(x-\alpha_{2M_1})^2-2(x-\beta_{2M_1})^2}{2}, & x\in[\beta_{2M_1},\gamma_{2M_1}),\\ \frac{(x-\alpha_{2M_1})^2-2(x-\beta_{2M_1})^2+(x-\gamma_{2M_1})^2}{2}, & x\in[\gamma_{2M_1},x_{\max}),\\ 0, & \text{elsewhere.}\end{cases}-\left(\frac{x-x_{\min}}{x_{\max}-x_{\min}}q_{2M_1}(x_{\max})\right)\right.\\
&\left.-(t_{l+1}-t_l)\begin{cases}1, & x\in[\alpha_{2M_1},\beta_{2M_1}),\\ -1, & x\in[\beta_{2M_1},\gamma_{2M_1}),\\ 0, & \text{elsewhere,}\end{cases}\right]=0
\end{aligned}$$

The first row of the above expression gives

$$\begin{aligned}
&\lambda_1\left[\frac{(x-\alpha_1)^2}{2}-\left(\frac{x-x_{\min}}{x_{\max}-x_{\min}}q_1(x_{\max})\right)-(t_{l+1}-t_l)[\alpha_1,\beta_1)\right]\\
&+\lambda_2\left[\frac{(x-\alpha_2)^2}{2}-\left(\frac{x-x_{\min}}{x_{\max}-x_{\min}}q_2(x_{\max})\right)-(t_{l+1}-t_l)\right]\\
&+\cdots\\
&+\lambda_{2M_1}\left[\frac{(x-\alpha_{2M_1})^2}{2}-\left(\frac{x-x_{\min}}{x_{\max}-x_{\min}}q_{2M_1}(x_{\max})\right)-(t_{l+1}-t_l)\right]=0,
\end{aligned}$$

where for the k-th term $x \in [\alpha_k, \beta_k)$. Now as these expressions (the terms including the coefficients $\lambda_1,\ \lambda_2, \ldots, \lambda_{2M_1}$) are in different intervals so for this expression to be zero we must have $\lambda_i = 0$ for $i = 1, 2, \ldots, 2M_1$. Thus, the matrix A is invertible. Now, we claim that $\|A^{-1}\|$ is bounded. As

$$\|A^{-1}\| = \frac{1}{|det(A)|}\|adj(A)\|,$$

from Lemma 4.5.3 and the definitions of Haar functions and their integrals on $[x_{\min}, x_{\max}]$, we deduce that, $\forall\, l$ there exists ζ_l such that

$$\|adj(A)\| \leqslant \eta \max_k \prod_{j=1,\, j\neq k}^{2M_1} \|row_j(A)\| \leqslant \zeta_l,$$

which clearly implies

$$\|A^{-1}\| \leqslant \varsigma_l, \text{ for some } \varsigma_l.$$

Thus, from the initial and boundary conditions, we can say $\|B\|$ is also bounded at every time level on $[x_{\min}, x_{\max}] \times [0, t_{\max}]$, which gives

$$\|C\| \leqslant \rho_l, \text{ for some } \rho_l. \tag{4.5.3}$$

Using the above result and (4.5.3), we can say small changes in initial and boundary conditions bring only a small change in the solution therefore the method is stable.

4.6 Numerical simulations and discussions

This section presents and analyzes the numerical results obtained for the pricing of different binary options acquired by applying the Haar wavelet method. We also explore various Greeks of these options. The attractiveness of binary options trading is a route to profitability, and the study of their Greeks makes this course tranquil. We perform three test problems to study the behavior of the values and Greeks of path-independent binary options. All these solutions and Greek profiles are depicted graphically to explore different

physical and numerical aspects.

For numerical simulations, we consider the transformed equation (4.2.2) and finally use back substitution to get the solution of the original equation (4.2.1). As discussed in Section 2, the spatial is unbounded, and since numerical computation needs finite bounds for x, it is necessary to introduce the artificial value of $x_{\min}$ and $x_{\max}$, so in all test problems we are considering $[x_{\min}, x_{\max}] = [-1, 1]$ and $T = 1$. These values are taken from previous studies for performing the numerical simulations. For numerical computations, we discretize the spatial domain into $N_1 = 2M_1 = 2^{J+1}$ parts of equal length using the collocation points $x_s = x_{\min} + \frac{(s-0.5)(x_{\max}-x_{\min})}{2M_1},\ s = 1, 2, \ldots, 2M_1$, and the temporal domain into $N_2 = 2M_2$ uniformly spaced points so that each partition is of width $t_{\max}/(N_2 - 1)$.

The computational error produced while estimating different expressions by the proposed numerical scheme is measured using maximum error norm and root mean square (RMS) deviation with the following definitions:

$$E_{N_1,N_2} = \max_{\nu=1,2,\ldots,N_1} \left| \frac{w_{2N_1}(S_{2\nu-1}, \tau_{2\upsilon}) + w_{2N_1}(S_{2\nu}, \tau_{2\upsilon})}{2} - w_{N_1}(S_\nu, \tau_\upsilon) \right|, \text{ for some } \upsilon,$$

$$e_{N_1,N_2} = \max_{\nu=1,2,\ldots,N_1} \max_{\upsilon=1,2,\ldots,N_2} \left| \frac{w_{2N_1,2N_2}(S_{2\nu-1}, \tau_{2\upsilon-1}) + w_{2N_1,2N_2}(S_{2\nu}, \tau_{2\upsilon})}{2} - w_{N_1,N_2}(S_\nu, \tau_\upsilon) \right|,$$

$$E_{\text{RMS}} = \sqrt{\frac{1}{N_1 N_2} \sum_{\nu=1}^{N_1} \sum_{\upsilon=1}^{N_2} \left| \frac{w_{2N_1,2N_2}(S_{2\nu-1}, \tau_{2\upsilon-1}) + w_{2N_1,2N_2}(S_{2\nu}, \tau_{2\upsilon})}{2} - w_{N_1,N_2}(S_\nu, \tau_\upsilon) \right|^2},$$

where w_{N_1,N_2} and $w_{2N_1,2N_2}$ are the approximated values of w obtained by using (N_1, N_2) and $(2N_1, 2N_2)$ nodal points, respectively. All the numerical simulations are performed using MATLAB 2019b. Additionally, the numerical rate of convergence is computed by the formula $\log_2(\text{error}_{N_1,N_2}/\text{error}_{2N_1,2N_2})$, where error can be any one of the above three error measures.

4.6.1 Numerical results for cash-or-nothing option

We consider the following example to demonstrate the price and Greeks of the cash-or-nothing call option, which pays a fixed amount at the expiry, but this amount is payable only when at maturity T option ends up in the money.

Example 4.6.1. *Consider the Black-Scholes equation for a cash-or-nothing call option with a fixed rate of interest* $r = 0.1$ *and volatility* $\sigma = 0.6$*. Assume the exercise time* $T = 1$*, strike price* $K = 100$ *with a fixed predetermined amount of payout* $A = 80$*, and the zero dividend yield.*

We have tabulated different error measures with their rates of convergence produced during the computation of the cash-or-nothing option price in Table 4.1 for different maximum levels of resolution J. A worthy observation is that the Haar wavelet method is second-order convergent in the spatial direction, but overall it is first-order convergent. These computational rates of convergence also agree with the theoretical results proved in the previous section. The processing time taken by the computer to calculate the value of the option in seconds denoted by CPU(s) is also presented. These results show that the present scheme is fast and accurate.

The solution of the transformed equation of the cash-or-nothing option under the Black-Scholes model is depicted in Figure 4.1(a). The figure justifies the problem statement as the value of u drops steeply when $x \to x_{\min}$, and there is a sudden shift in the value of u at $x = 0$. In Figure 4.1(b) we have plotted the actual and numerical values of the payoff, which reveals that the proposed scheme provides good approximation even at a few points. A noteworthy observation is that the payoff profile of the cash-or-nothing option looks similar to the delta of a vanilla call option.

Figure 4.2(a) illustrates the behavior of the cash-or-nothing option at different values of S and τ. From this figure, we can observe that if the stock price at any time τ is lesser than the strike price, which acts as a barrier, the option is still active and out of the money *i.e.,* $V = 0$. The more important fact is to check the stock price at T because, based upon that, we can exercise our option.

Table 4.1: Different errors and CPU time (in seconds) for calculating cash-or-nothing call option price with parameters as given in Example 4.6.1.

	Maximum Level of Resolution J					
Error	2	3	4	5	6	7
E_{N_1,N_2}	7.504e-05	1.902e-05	4.789e-06	1.201e-06	3.008e-07	7.528e-08
	1.980	1.990	1.994	1.997	1.998	
e_{N_1,N_2}	7.413e-04	3.690e-04	1.683e-04	7.560e-05	3.448e-05	1.612e-05
	1.006	1.132	1.154	1.132	1.097	
CPU(s)	0.0705	0.0846	0.0919	0.0925	0.1042	0.1844

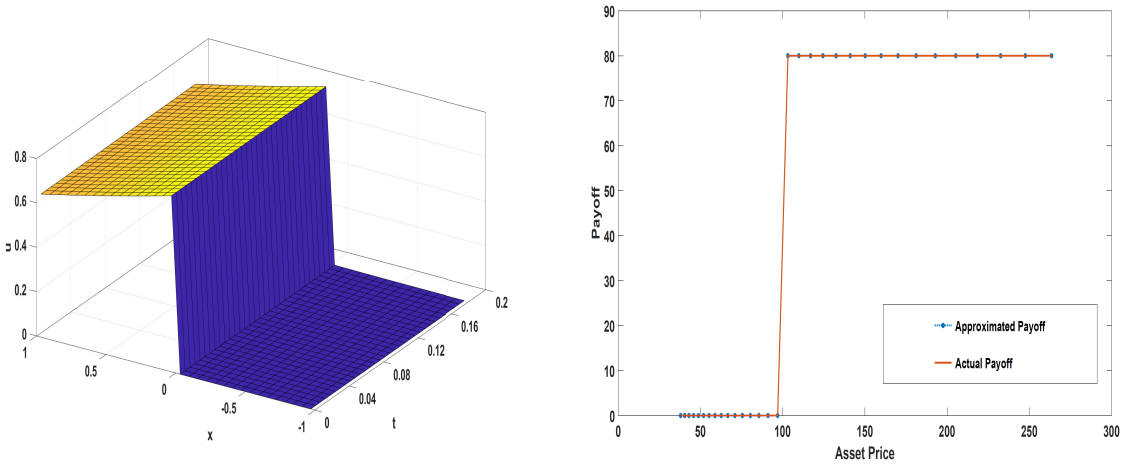

(a) (b)

Figure 4.1: (a) The approximated value of the solution of the transformed equation, and (b) the approximated and actual payoff for the cash-or-nothing call option.

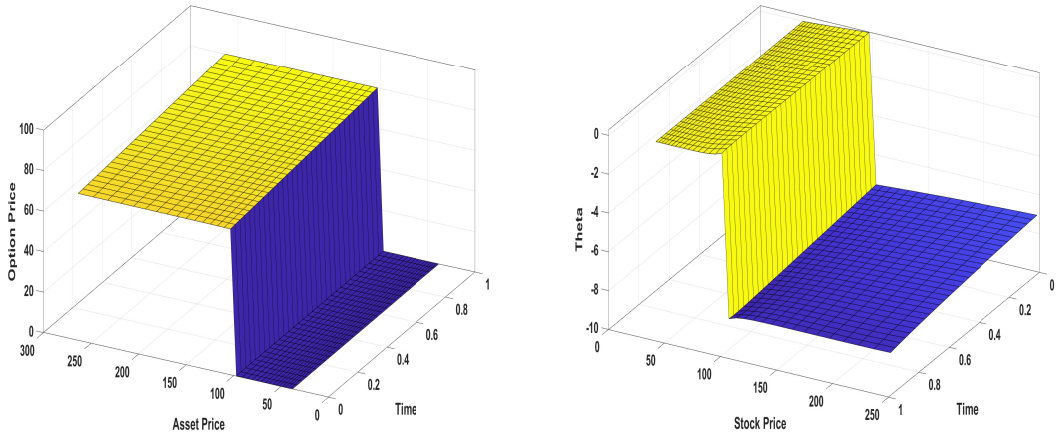

(a) (b)

Figure 4.2: The approximated values of (a) the price, and (b) theta over time to maturity of the cash-or-nothing call option.

Table 4.2: RMS Error for theta of cash-or-nothing call option at different expiries T with parameters as given in Example 4.6.1.

	Maximum Level of Resolution J					
Maturity	2	3	4	5	6	7
$T = 0.25$	2.745e-02	1.124e-02	4.454e-03	1.794e-03	7.536e-04	3.326e-04
$T = 0.50$	3.229e-02	1.400e-02	6.036e-03	2.665e-03	1.217e-03	5.731e-04
$T = 0.75$	3.759e-02	1.701e-02	7.685e-03	3.538e-03	1.668e-03	8.028e-04
$T = 1.00$	4.324e-02	2.005e-02	9.298e-03	4.378e-03	2.098e-03	1.021e-03

The error tables for the Greeks of the binary option prove that this method also has a good level of accuracy for the derivatives of the solution function. From Tables 4.2 and 4.3, it can be noticed that for different maturity times, the RMS error, calculating the value of theta and delta, is decreasing uniformly as we increase the number of grid points (decreasing the mesh size). The behavior of theta of a cash-or-nothing call option is depicted in Figure 4.2(b), an obvious observation is that near the strike price, there is a rapid change in the value of theta, which signifies that the option pricing function is discontinuous at K for all the values of τ.

Table 4.3: RMS Error for the delta of cash-or-nothing call option at different expiries T with parameters as given in Example 4.6.1.

	Maximum Level of Resolution J					
Maturity	2	3	4	5	6	7
$T = 0.25$	1.687e-04	6.822e-05	2.755e-05	1.159e-05	5.155e-06	2.406e-06
$T = 0.50$	2.621e-04	1.103e-04	4.658e-05	2.037e-05	9.298e-06	4.395e-06
$T = 0.75$	3.378e-04	1.463e-04	6.348e-05	2.841e-05	1.318e-05	6.293e-06
$T = 1.00$	4.015e-04	1.772e-04	7.823e-05	3.552e-05	1.664e-05	7.998e-06

The delta profile of the cash-or-nothing option is represented in Figure 4.3(a). It resembles the gamma profile of the vanilla call option as the value of delta for the cash-or-nothing option is highest at K, which is a feature of gamma of a vanilla call option. A significant observation is that the value of delta is positive, which can be explained because the option pricing function is monotonically increasing. This study of the behavior of delta helps to remove the risk in the trading direction. The change in the behavior of delta with the decay in time towards maturity is depicted in Figure 4.3(b). It is perceived that the value of charm is positive near the strike price; its value is slightly increasing just before the strike price and then decreasing slowly, which signifies that at K, the value of the delta function is first increasing steeply and then decreasing suddenly with respect to time.

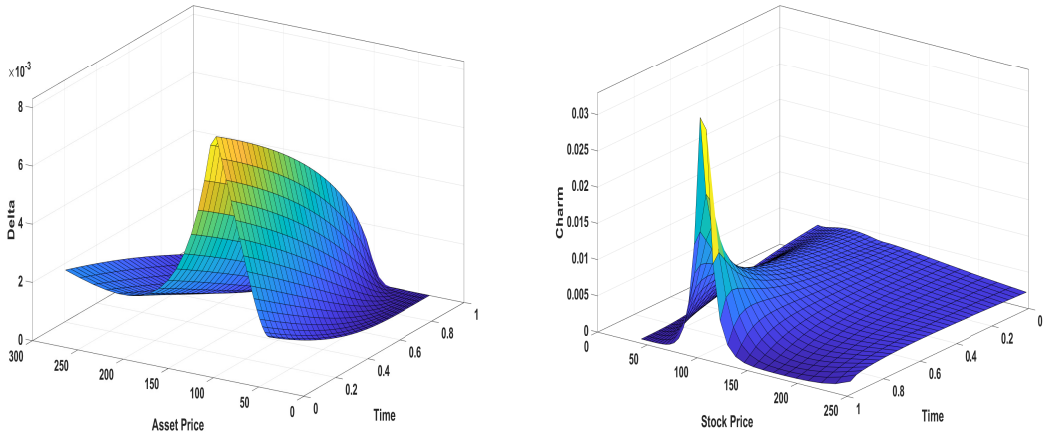

(a) (b)

Figure 4.3: The approximated values of (a) delta, and (b) charm of the cash-or-nothing call option.

Table 4.4: RMS Error for the charm of cash-or-nothing call option at different expiries T with parameters as given in Example 4.6.1.

	Maximum Level of Resolution J					
Maturity	2	3	4	5	6	7
$T = 0.25$	3.349e-04	1.233e-04	4.542e-05	1.737e-05	7.181e-06	3.214e-06
$T = 0.50$	1.718e-04	6.539e-05	2.425e-05	9.980e-06	4.709e-06	2.380e-06
$T = 0.75$	8.775e-05	3.115e-05	1.042e-05	4.913e-06	2.907e-06	1.676e-06
$T = 1.00$	5.452e-05	2.017e-05	9.146e-06	5.594e-06	3.382e-06	1.907e-06

In Tables 4.4, 4.5, and 4.6, we have presented the RMS error produced during the computation of the values of charm, gamma, and color Greeks of the cash-or-nothing option. The surface plot of the gamma of cash-or-nothing binary option, which represents

Table 4.5: RMS Error for the gamma of cash-or-nothing call option at different expiries T with parameters as given in Example 4.6.1.

	Maximum Level of Resolution J					
Maturity	2	3	4	5	6	7
$T = 0.25$	2.759e-06	8.871e-07	3.908e-07	1.974e-07	1.021e-07	5.250e-08
$T = 0.50$	2.671e-06	9.250e-07	3.553e-07	1.555e-07	7.508e-08	3.769e-08
$T = 0.75$	2.523e-06	8.279e-07	2.881e-07	1.205e-07	5.937e-08	3.081e-08
$T = 1.00$	2.469e-06	1.000e-06	4.828e-07	2.528e-07	1.330e-07	6.903e-08

Table 4.6: RMS Error for the color of cash-or-nothing call option at different expiries T with parameters as given in Example 4.6.1.

	Maximum Level of Resolution J					
Maturity	2	3	4	5	6	7
$T = 0.25$	7.542e-05	1.517e-05	6.613e-06	3.597e-06	1.915e-06	9.904e-07
$T = 0.50$	2.222e-05	1.010e-05	6.110e-06	3.427e-06	1.819e-06	9.387e-07
$T = 0.75$	1.455e-05	6.164e-06	3.269e-06	1.760e-06	9.318e-07	4.841e-07
$T = 1.00$	1.287e-05	4.186e-06	1.475e-06	6.634e-07	3.596e-07	1.984e-07

the change in the value of delta with the change in the price of the underlying asset, is depicted in Figure 4.4(a). Measuring gamma helps to monitor the delta-hedging process, we can notice that the value gamma is positive for $S < K$ and negative for S beyond K, this can be interpreted from the increase in the value of delta for $S < K$ and drop in the value of delta for $S \geqslant K$ with respect to the stock price. As we have explained, the value of the delta of the cash-or-nothing option resembles the gamma of a vanilla European option implies that the gamma of the cash-or-nothing option resembles the third derivative with respect to stock price speed (Greek) of the vanilla option. The change in the value of gamma with the decrease in time to maturity is known as color and graphically depicted in Figure 4.4(b). The value of color is highest and lowest near the strike price, which can be justified by looking at the rise and fall of gamma near the strike price corresponding to the time axis in Figure 4.4(a).

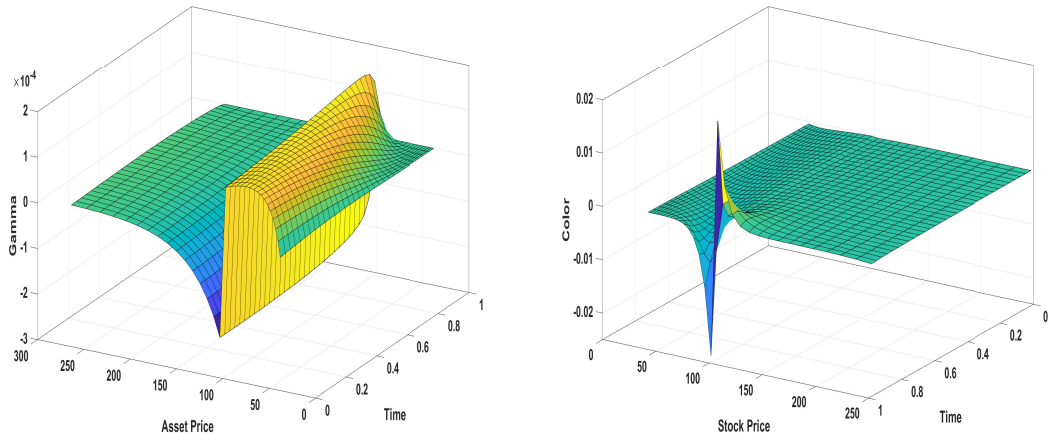

(a) (b)

Figure 4.4: The approximated values of (a) gamma, and (b) color of the cash-or-nothing call option.

4.6.2 Numerical results for asset-or-nothing option

Example 4.6.2. *Consider the Black-Scholes equation for asset-or-nothing call option with fixed rate of interest* $r = 0.02$ *and volatility* $\sigma = 0.6$*. Assume the exercise time* $T = 1$*,*

strike price K is 80 with zero dividend yield.

This example considers a European-style asset-or-nothing binary option where the barrier condition is applied and exercised only at expiry. If the option is out of the money at the expiry date, it is worthless and valueless to the holder. Unlike a cash-or-nothing option, this option has a varying payoff that changes with the change in the underlying asset price. The approximated value of the price (of the transformed equation) of the asset-or-nothing option is represented in Figure 4.5(a). From this figure, we observe that compared to the value of u for the cash-or-nothing option, it is increasing linearly for $x > 0$. A comparative analysis of the actual and approximated payoff function is depicted in Figure 4.5(b), which reveals that the Haar wavelet scheme is efficient for calculating the price of the asset-or-nothing binary option.

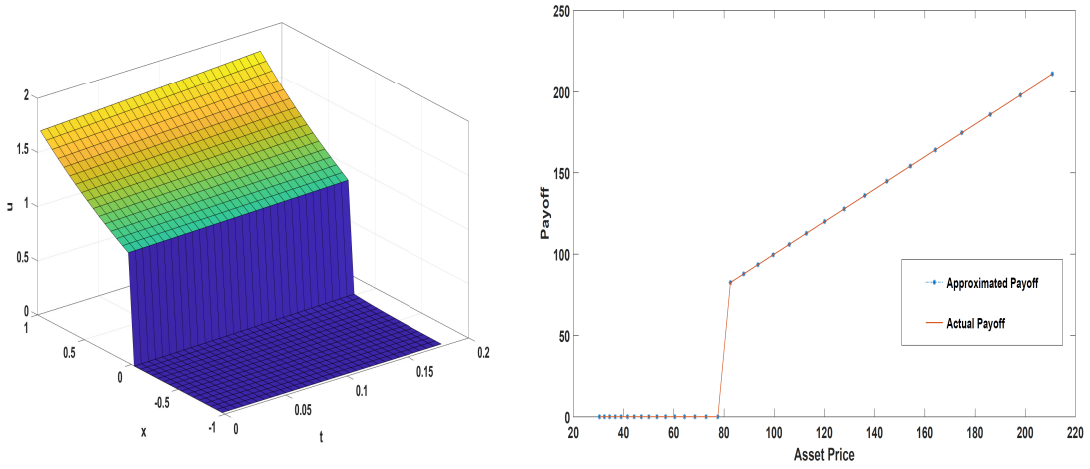

(a) (b)

Figure 4.5: (a) The approximated value of the solution of the transformed equation, and (b) the approximated and actual payoff for the asset-or-nothing call option.

The numerical error generated during the calculation of the asset-or-nothing option price at different levels of resolution is listed in Table 4.7. We can notice that the Haar wavelet approximation scheme gives quadratic and linear convergence rates in the spatial and temporal directions, respectively, for the asset-or-nothing option. The price of the asset-or-nothing option for different values of S and τ is presented in Figure 4.6(a). A

Table 4.7: Different errors and CPU time (in seconds) for calculating asset-or-nothing call option price with parameters as given in Example 4.6.2.

	Maximum Level of Resolution J					
Error	2	3	4	5	6	7
E_{N_1,N_2}	9.802e-04	2.537e-04	6.453e-05	1.627e-05	4.086e-06	1.023e-06
	1.950	1.975	1.987	1.993	1.996	
e_{N_1,N_2}	8.300e-03	4.300e-03	2.100e-03	9.795e-04	4.670e-04	2.256e-04
	0.948	1.033	1.100	1.068	1.049	
CPU(s)	0.0670	0.0707	0.0762	0.1028	0.1865	0.5416

noteworthy observation is that unlike the cash-or-nothing option this option's value is not fixed for $S \geqslant K$, and for $S < K$ it is zero in both the options. It is clear from the figure that the option is in the money for $S \geqslant K$ and it is out of the money for $S < K$. Also, the discontinuous behavior of the option pricing function results in the abrupt changes in its Greeks.

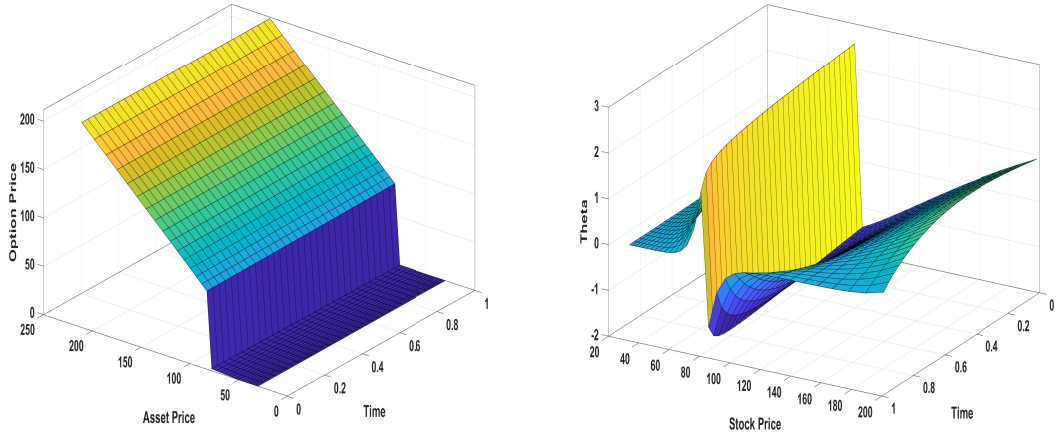

(a) (b)

Figure 4.6: The approximated values of the (a) price, and (b) theta over time to maturity of the European asset-or-nothing call option price.

In Table 4.8, we have listed the RMS error, which we get during the computer process-

ing for calculating the theta of the asset-or-nothing call option for different maturity times. The error decreases as the value of J increases, which is justified by the MRA technique. Change in the price of an option with the decrease in time towards maturity is graphically depicted in Figure 4.6(b). It is observed from the theta profile presented in this figure that the fall in option value with respect to time τ results in the negative value of theta while the rise in the value of the option for $S < K$ results in the positive value of theta.

Table 4.8: RMS Error for theta of asset-or-nothing call option at different expiries T with parameters as given in Example 4.6.2.

	Maximum Level of Resolution J					
Maturity	2	3	4	5	6	7
$T = 0.25$	1.511e-01	5.836e-02	2.032e-02	6.774e-03	2.241e-03	7.688e-04
$T = 0.50$	1.234e-01	4.609e-02	1.530e-02	4.748e-03	1.456e-03	5.007e-04
$T = 0.75$	9.761e-02	3.639e-02	1.186e-02	3.701e-03	1.307e-03	6.017e-04
$T = 1.00$	7.903e-02	2.976e-02	9.732e-03	3.182e-03	1.289e-03	6.575e-04

The dissimilar character of the delta of cash-or-nothing and asset-or-nothing binary options is revealed from Figure 4.3(a) and Figure 4.7(a). In the case of an asset-or-nothing option the value of delta is approaching towards one for $S > K$ because the option is in the money and varying linearly with the underlying asset, but in the case of a cash-or-nothing option the value of delta approaches zero for $S > K$ as the payout is a fixed amount there. The RMS error produced in the numerical calculation of the delta is reported in Table 4.9.

In Tables 4.10, 4.11, and 4.12, we have listed the computational errors for different Greeks, namely, charm, gamma, and color. A remarkable observation is that the error reductions in these tables are uniform, which validates the theoretical results of the proposed scheme. It is easily noticeable from tabulated results that the proposed scheme gives reasonable accuracy in computing the Greeks of European asset-or-nothing options. The value of the charm is depicted in Figure 4.7(b). It is significant to observe that unlike cash-or-nothing charm here, the value of charm is not changing steeply only at maturity.

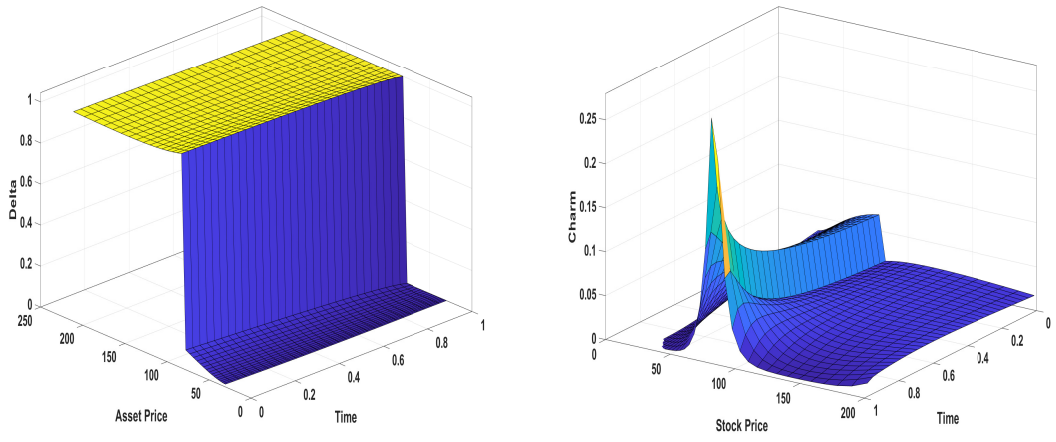

(a) (b)

Figure 4.7: The approximated values of (a) delta, and (b) charm of the asset-or-nothing call option.

Table 4.9: RMS Error for the delta of asset-or-nothing call option at different expiries T with parameters as given in Example 4.6.2.

	Maximum Level of Resolution J					
Maturity	2	3	4	5	6	7
$T = 0.25$	1.583e-03	6.388e-04	2.551e-04	1.058e-04	4.658e-05	2.160e-05
$T = 0.50$	2.502e-03	1.046e-03	4.389e-04	1.913e-04	8.742e-05	4.144e-05
$T = 0.75$	3.299e-03	1.418e-03	6.149e-04	2.766e-04	1.293e-04	6.222e-05
$T = 1.00$	4.073e-03	1.787e-03	7.939e-04	3.649e-04	1.733e-04	8.416e-05

However, at all time levels near the strike price K, there is a rapid change in the value of charm because here the value of the option depends upon the price of the underlying asset which changes with time.

Table 4.10: RMS Error for the charm of asset-or-nothing call option at different expiries T with parameters as given in Example 4.6.2.

	Maximum Level of Resolution J					
Maturity	2	3	4	5	6	7
$T = 0.25$	3.143e-03	1.141e-03	4.057e-04	1.467e-04	5.688e-05	2.423e-05
$T = 0.50$	1.697e-03	6.231e-04	2.168e-04	8.295e-05	3.801e-05	1.935e-05
$T = 0.75$	1.048e-03	3.791e-04	1.324e-04	5.878e-05	3.205e-05	1.779e-05
$T = 1.00$	7.638e-04	2.782e-04	1.061e-04	5.436e-05	3.124e-05	1.745e-05

Table 4.11: RMS Error for the gamma of asset-or-nothing call option at different expiries T with parameters as given in Example 4.6.2.

	Maximum Level of Resolution J					
Maturity	2	3	4	5	6	7
$T = 0.25$	3.300e-05	1.261e-05	5.514e-06	2.630e-06	1.305e-06	6.551e-07
$T = 0.50$	4.010e-05	1.654e-05	7.169e-06	3.299e-06	1.586e-06	7.802e-07
$T = 0.75$	4.368e-05	1.710e-05	6.824e-06	2.889e-06	1.305e-06	6.181e-07
$T = 1.00$	4.349e-05	1.631e-05	6.114e-06	2.404e-06	1.015e-06	4.585e-07

From Figure 4.8 it is clear that the character and behavior of gamma and color of an asset-or-nothing option price are similar to that of the cash-or-nothing option. It explains that the change in delta with the decay in time to maturity and underlying asset behaves similarly but provides different values.

Table 4.12: RMS Error for the color of asset-or-nothing call option at different expiries T with parameters as given in Example 4.6.2.

	Maximum Level of Resolution J					
Maturity	2	3	4	5	6	7
$T = 0.25$	8.236e-04	1.731e-04	6.643e-05	3.366e-05	1.756e-05	9.029e-06
$T = 0.50$	2.558e-04	8.350e-05	4.450e-05	2.498e-05	1.346e-05	7.025e-06
$T = 0.75$	1.800e-04	5.715e-05	2.595e-05	1.425e-05	7.884e-06	4.227e-06
$T = 1.00$	1.649e-04	4.747e-05	1.491e-05	7.317e-06	4.407e-06	2.539e-06

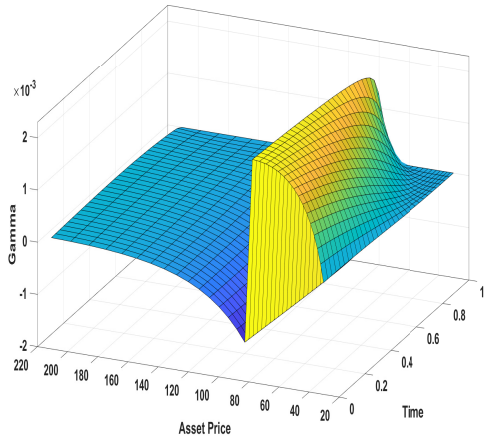

(a)

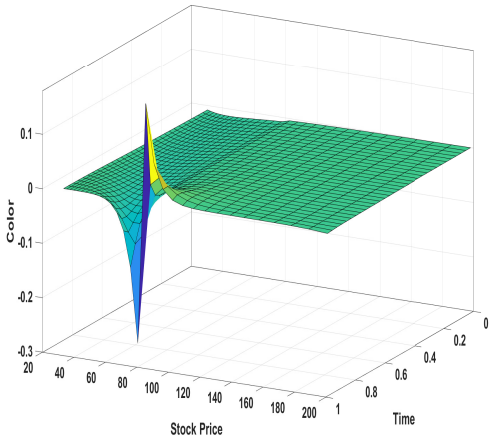

(b)

Figure 4.8: The approximated values of (a) gamma, and (b) color of the asset-or-nothing call option.

4.6.3 Numerical results for gap option

Example 4.6.3. *Consider the Black-Scholes equation for gap call option: with fixed rate of interest* $r = 0.1$ *and volatility* $\sigma = 0.6$*. Assume the exercise time* $T = 1$*, strike price* $K = 100$ *with a fixed predetermined amount* $A = 80$ *and the zero dividend yield.*

This example is considered to demonstrate the efficiency achieved by the Haar wavelet method to calculate the gap option price and its Greeks. In the gap option, the payment depends upon the current price of the stock and the fixed monetary amount. As the name suggests, its payoff precisely indicates the gap or difference between the cash-or-nothing option and the asset-or-nothing option.

Table 4.13: Different errors and CPU time (in seconds) for calculating gap option (call) price with parameters as given in Example 4.6.3.

	Maximum Level of Resolution J					
Error	2	3	4	5	6	7
E_{N_1,N_2}	2.300e-03	5.967e-04	1.529e-04	3.872e-05	9.743e-06	2.443e-06
	1.946	1.963	1.982	1.990	1.995	
e_{N_1,N_2}	1.760e-02	9.200e-03	4.500e-03	2.200e-03	1.100e-03	5.127e-04
	0.935	1.031	1.032	1.000	1.101	
CPU(s)	0.0623	0.0655	0.0728	0.0890	0.1989	0.5654

Different error measures are computed in Table 4.13 to investigate the convergence trends of the proposed scheme for gap options. A novel observation is that the rate of convergence of the Haar wavelet approximation scheme is the same for all the binary options, but the error measures change based upon the complexity of the problem, so the gap option price errors (Table 4.13) are higher than the other two options (cash-or-nothing and asset-or-nothing) given in Tables 4.1 and 4.7. Figure 4.9(a) represents the solution u of the transformed equation of the gap option under the Black-Scholes model. It perceived that the value of u for the gap option resembles the gap between u for the cash-or-nothing and asset-or-nothing options. The effectiveness of the present wavelet

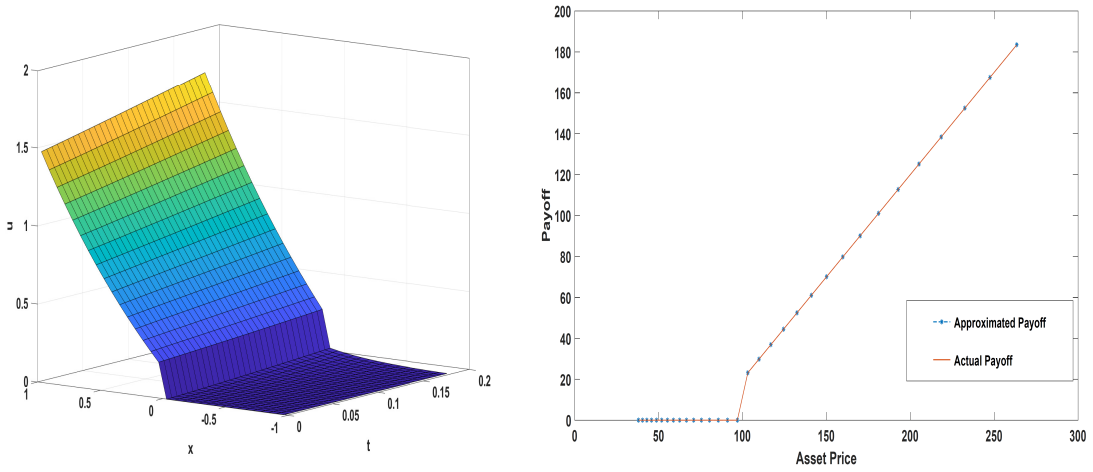

(a) (b)

Figure 4.9: (a) The approximated value of the solution of the transformed equation, and (b) the approximated and actual payoff for the gap call option.

scheme for approximating the option pricing problems is shown in Figure 4.9(b), the perfect overlapping of the actual payoff function and the approximated payoff function reveal its effectiveness.

The value of the gap option is depicted in Figure 4.10(a). It suggests that the price of the gap option is always less than the asset-or-nothing option as the graph of V in the case of the gap option is steeper than that of the asset-or-nothing option. The figure reveals that the gap option is out the money for $S < K$ and in the money for $S > K$. The change in the price of the gap option with respect to the decrease in the time towards maturity is represented in Figure 4.10(b). A novel observation is that the smaller steepness factor in gap option price (see Figure 4.10(a)) as compared to the other two path-independent binary options prices (refer Figures 4.2(a) and 4.6(a)) results in small fluctuations in the value of theta of the gap option near the strike price.

In Tables 4.14 and 4.15, we have tabulated the computational errors for theta and delta of gap option, respectively. The change in the gap option price with the change in the price of the underlying asset is depicted in Figure 4.11(a). It is perceived that the value of delta lies between zero and one, which we justify from the fact that the option is in the money

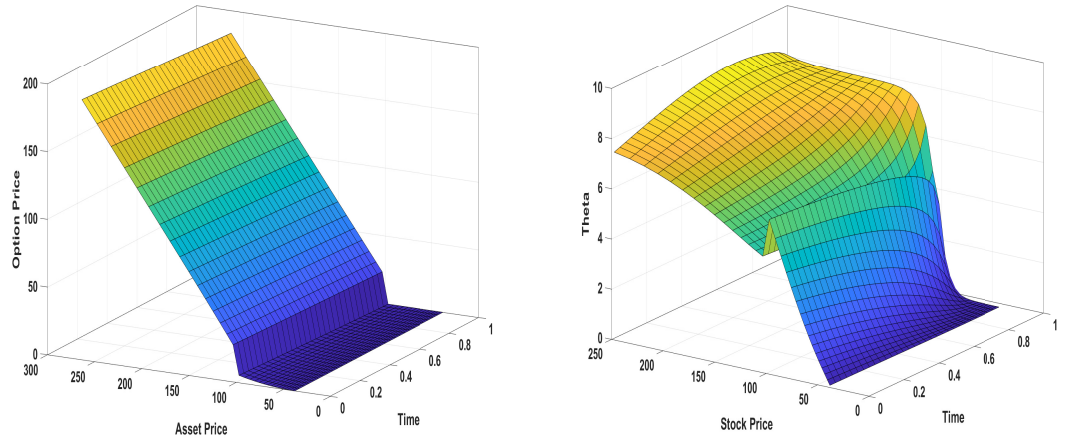

(a) (b)

Figure 4.10: The approximated values of the (a) price, and (b) theta over time to maturity of the European gap call option price.

and its value is increasing linearly for $S \geqslant K$ results in the value of delta approaching towards one and as the option is out of money for $S < K$ implies that the value of delta is approaching towards zero. The character of charm is similar for asset-or-nothing and gap option depicted in Figure 4.11(b) because the delta behavior is the same for both options with the change in the time towards maturity.

Table 4.14: RMS Error for theta of gap option (call) at different expiries T with parameters as given in Example 4.6.3.

	Maximum Level of Resolution J					
Maturity	2	3	4	5	6	7
$T = 0.25$	2.643e-01	9.904e-02	3.344e-02	1.075e-02	3.459e-03	1.215e-03
$T = 0.50$	2.080e-01	7.334e-02	2.256e-02	6.347e-03	2.009e-03	9.840e-04
$T = 0.75$	1.571e-01	5.310e-02	1.513e-02	4.589e-03	2.395e-03	1.483e-03
$T = 1.00$	1.194e-01	3.854e-02	1.049e-02	4.367e-03	2.898e-03	1.789e-03

The error behavior for charm, gamma, and color for gap option is shown in Tables 4.16,

Table 4.15: RMS Error for delta of gap option (call) at different expiries T with parameters as given in Example 4.6.3.

	Maximum Level of Resolution J					
Maturity	2	3	4	5	6	7
$T = 0.25$	2.473e-03	9.898e-04	4.060e-04	1.755e-04	8.028e-05	3.826e-05
$T = 0.50$	3.936e-03	1.649e-03	7.124e-04	3.221e-04	1.517e-04	7.343e-05
$T = 0.75$	5.337e-03	2.306e-03	1.030e-03	4.788e-04	2.296e-04	1.123e-04
$T = 1.00$	6.787e-03	2.994e-03	1.366e-03	6.458e-04	3.130e-04	1.539e-04

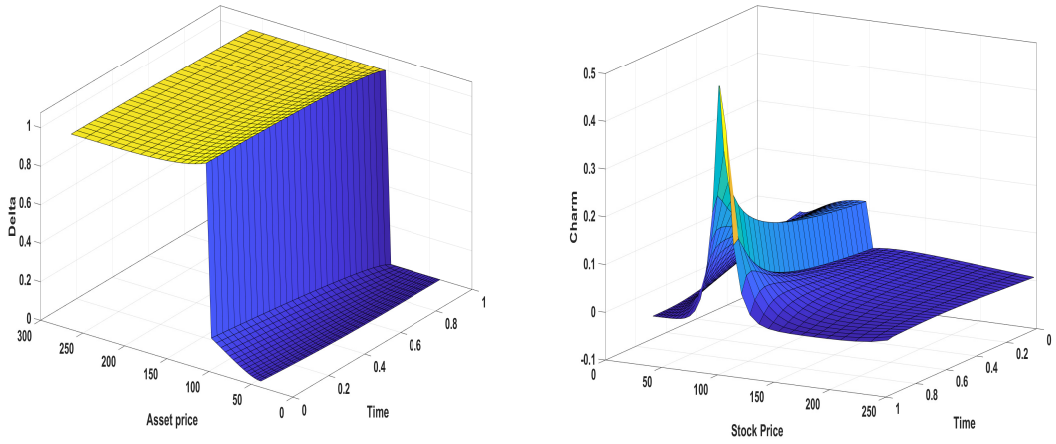

(a) (b)

Figure 4.11: The approximated values of (a) delta, and (b) charm of the gap call option.

Table 4.16: RMS Error for charm of gap option (call) at different expiries T with parameters as given in Example 4.6.3.

	Maximum Level of Resolution J					
Maturity	2	3	4	5	6	7
$T = 0.25$	4.353e-03	1.552e-03	5.641e-04	2.173e-04	9.245e-05	4.290e-05
$T = 0.50$	2.146e-03	8.111e-04	3.276e-04	1.563e-04	8.190e-05	4.328e-05
$T = 0.75$	1.151e-03	4.375e-04	2.109e-04	1.247e-04	7.265e-05	4.007e-05
$T = 1.00$	6.287e-04	2.949e-04	2.017e-04	1.317e-04	7.749e-05	4.256e-05

Table 4.17: RMS Error for gamma of gap option (call) at different expiries T with parameters as given in Example 4.6.3.

	Maximum Level of Resolution J					
Maturity	2	3	4	5	6	7
$T = 0.25$	4.058e-05	1.536e-05	7.426e-06	3.828e-06	1.974e-06	1.008e-06
$T = 0.50$	4.886e-05	2.053e-05	9.337e-06	4.474e-06	2.203e-06	1.097e-06
$T = 0.75$	4.809e-05	1.792e-05	7.006e-06	2.976e-06	1.365e-06	6.564e-07
$T = 1.00$	4.123e-05	1.492e-05	6.131e-06	2.876e-06	1.435e-06	7.273e-07

Table 4.18: RMS Error for color of gap option (call) at different expiries T with parameters as given in Example 4.6.3.

	Maximum Level of Resolution J					
Maturity	2	3	4	5	6	7
$T = 0.25$	1.115e-03	2.120e-04	8.840e-05	5.001e-05	2.732e-05	1.430e-05
$T = 0.50$	2.911e-04	1.112e-04	7.828e-05	4.714e-05	2.583e-05	1.353e-05
$T = 0.75$	1.599e-04	7.974e-05	5.597e-05	3.354e-05	1.847e-05	9.740e-06
$T = 1.00$	1.219e-04	4.323e-05	3.166e-05	2.069e-05	1.204e-05	6.562e-06

4.17, and 4.18. Looking at these tables, we observe that the present scheme is efficient for calculating Greeks. The surface plot of the value of gamma of gap option is depicted in Figure 4.12(a). The study of the gamma function behavior helps to reduce the risk when there are sharp ups and downs in the underlying asset's value, and it is useful in the analysis of delta hedging strategies. Figure 4.12(b) represents the color Greek of the gap option looks similar to other path-independent binary option's color Greeks, which signifies that the character and pictorial behavior of gamma for all of them are the same, but their values are different since their methods of payment are different.

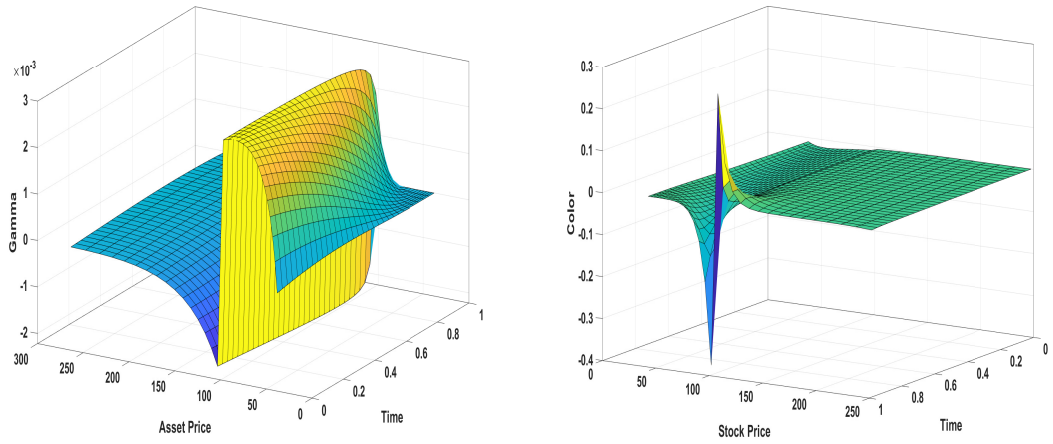

(a) (b)

Figure 4.12: The approximated values of (a) gamma, and (b) color of the gap call option.

4.7 Concluding remarks

In this chapter, we have examined a compactly supported Haar wavelet-based approximation technique to estimate the values of the solution and its Greeks for various binary options, also known as digital or bet options, under the Black-Scholes environment. The windowing technique and multi-resolution analysis are used to get a more accurate solution at each successive level. We utilize the excellent approximation technique of the Haar wavelet method for spiked functions to approximate the discontinuous solution functions

and estimate the Greeks. To avoid the large truncation error, we truncated the infinite domain into a finite domain. This approach of finding the numerical solutions of the options' Greeks is novel and effortless as it explicitly gives the approximation of the derivatives of the solution function. Through the consistency and stability analysis, it has been proved that the proposed scheme is consistent and unconditionally stable with linear and quadratic rates of convergence in the temporal and spatial directions, respectively. Moreover, various computational experiments are presented to demonstrate the efficiency and validate the theoretical results of the contributed approach. The outputs computed and analyzed through numerical simulations can be used in financial institutes to hedge the directional risks associated with the moves of different parameters.

Chapter 5

Wavelet based numerical approximation of the Greeks of multi-asset option pricing models

---

Multi-asset investing is defined as any investment activity in which the composition of an investment product, service, or solution includes more than one asset class. This encompasses everything from the client's needs and product design to the many components of the investing process and portfolio analysis needed to maintain such a product. Multi-asset option is one such investment products. Multi-asset options form a class for which efficient solution methods are not easily obtained.

The initial concept of diversifying a portfolio by investing in several asset classes was founded on the assumption that doing so would provide diversification and that investing in stocks would earn a risk premium. Also, multi-asset option pricing improves in asset allocation, which has long been a cornerstone of good investment management. When the value of an option is determined by the prices of many assets, the linkages between these assets become crucial. Therefore, for successful option trading and risk management the study of multi-asset option Greeks *i.e.,* the change in the option's price with respect to

various assets or other market parameters becomes important.

Trading only one rather than several options involves lower transaction costs, to hedge a risky position consisting of several assets, a cheaper alternative is multi-asset options. Multi-asset options are those whose payoffs depend on N independent stocks and the price of the option depends on these stocks. This chapter presents a numerical method to solve the problems where the payoffs depend on multi underlying assets *i.e.,* the multi-asset problems. In particular, we consider the problems for three different options: Max/Min, Index, and Multi-strike options. These options' pricing are the higher dimensional generalization of the Black-Scholes model initially proposed by Black and Scholes [13]. Since then, several analytical/numerical methods have been developed/improved for option pricing problems by many researchers.

The main contributions of this chapter involve the development of a wavelet-based operational method to study the sensitivities of multi-asset options of diverse forms. To explore these financially relevant problems systematically, the final value problem is reformulated into a less cluttered dimensionless initial value problem. To avoid unacceptable large truncation error the actual infinite domain is trimmed into the finite domain by constructing artificial boundaries. Also, it has been shown that irrespective of the problem's geometry, the proposed method is highly accurate and the time taken to get this level of accuracy is significantly less. The convergence of the present scheme is proved theoretically. The robustness and efficiency of the contributed scheme are conclusively demonstrated with a variety of test examples. The present approach of analyzing the sensitivities of multi-asset options can be used in trading to explore different Greek exposures for hedging.

5.1 Literature survey

Some development of the numerical methods for the multi-asset option pricing problems are introduced here as a review. Fasshauer *et al.* [96] proposed an implicit θ method in temporal discretization and a mesh-free approximation scheme for the assets for the solution of multi-asset American option problems. Kovalov *et al.* [97] suggested a FEM of lines for the problem of pricing multi-asset American-style options in the Black–Scholes–Merton

framework. Persson and Sydow [98] presented an adaptive technique (reduces the number of grid points to a minimum, still keeping the discretization error at a pre-described level) to solve the multi-dimensional European options in the generalized Black-Scholes equation. Jeong *et al.* [99] presented an FDM without transformations of variables for the solution of multi-underlying assets Black-Scholes PDEs. Ruitjer *et al.* [100] extended the COS method for one dimension to higher dimensions to price options on multi-underlying assets. The extension referred to as the 2D-COS method is a highly efficient method. By using Milstein–Taylor explicit and implicit schemes, Hu and Li [101] proposed a forward-path method under general diffusion processes for pricing multi-asset American-style options. Based on the exponential time differencing approach, Yousuf *et al.* [102] investigated an efficient second-order L-stable implicit predictor-corrector method for multi-asset American options. Kadalbajoo *et al.* [103] suggested a θ method in the temporal direction and a local RBF based FDM in the spatial direction for the multi-asset American option problems.

In 2016, Shcherbakov *et al.* [104] proposed a global RBF method as well as RBF partition of unity methods for American multi-asset call options. They have used a penalty approach and designed a penalty term. They have shown that the RBF partition of unity method is reasonably good as compared with FDM and global RBF method. Papiol *et al.* [105] generalized the SWIFT method for one dimension to the multidimensional case (referred to as the 2D-SWIFT method in two-dimensional case). The 2D-SWIFT method is the same advantages over the 2D-COS method as in the one-dimensional case. A numerical method comprising the backward difference formula in time and an RBF generated FDM in space for European and American type multi-asset options was presented by Milovanović and Sydow [106]. In the RBF generated FDM a constant value of the shape parameter always leads to ill-conditioning. To avoid ill-conditioning they have used the shape parameter proportional to the reciprocal of space step-size.

To solve the options prices on several underlying assets Khodayari and Ranjbar [22] used a conventional FDM in temporal direction and the derivatives of linear combinations of multi-quadric RBFs in spatial direction. The method does not require solving a full

matrix at each time step and thus the method is very fast and unlike global RBF the ill-conditioning problem is eliminated. Fazlollah [107] constructed a pseudo-spectral method with a non-uniform mesh (Chebyshev-Gauss-Lobatto points) for solving multi-asset option pricing problems. Recently, Kim *et al.* [108] suggested an operator splitting method for two and three dimensional Black–Scholes equations. Based on the fast Fourier transform, Zhao and Li [109] extended the PROJ method (see [110]) to priced an option in two-dimension. They have shown that the PROJ method for 2D is as good as the one-dimensional approach proposed in [110] for European options. In other methods such as FDM, the correlation term must be treated with special care otherwise it may cause instability in solving the system of linear equations. However, the Haar wavelets based approach does not suffer from such difficulties encountered by cross derivative terms. In this chapter, we propose a Haar wavelet-based numerical method to solve the multi-asset problems for three different options. The proposed method is stable and efficient as it can be seen from the numerical results presented in the tables.

5.2 Multi-dimensional option pricing problems and sensitivities (Greeks)

In option contract trading many options involve trading of more than one asset, and the payoff of these multi-asset options is some function of ranked vanilla payoffs. Under the Black-Scholes framework, the multi-asset option price $V(S,\tau)$ with N underlying assets $S=(S_1,S_2,\ldots,S_N)\in\mathbb{R}^{+N}$, $N\in\mathbb{N}$ and $S_n>0$, $1\leq n\leq N$ at the time $\tau\in[0,T)$ is diagnosed by the following PDE [22]:

$$\frac{\partial V(S,\tau)}{\partial\tau}+\mathcal{L}V(S,\tau)=0,\quad (S,\tau)\in\mathbb{R}^{+N}\times[0,T). \tag{5.2.1}$$

In (5.2.1) the operator $\mathcal{L}$ is defined as

$$\mathcal{L}\equiv\frac{1}{2}\sum_{n=1}^{N}\sum_{n'=1}^{N}\sigma_n\sigma_{n'}\rho_{nn'}S_nS_{n'}\frac{\partial^2}{\partial S_n\partial S_{n'}}+\sum_{n=1}^{N}(r-\delta_n)S_n\frac{\partial}{\partial S_n}-rI,$$

where $r \geq 0$ is the risk-free interest rate, $\sigma_n > 0$ indicates the volatility of the n-th underlying asset, $\delta_n \geq 0$ is the corresponding dividend yield, and $\rho_{nn'}$ symbolizes the correlation between the n-th and n'-th underlying assets.

In options linked with multiple assets, there are distinct ways of defining the payoff function as in the case of a European-style multi-asset option. Different assets can behave differently at the time of maturity, and based upon their performance, the boundary conditions change. In this chapter, we consider the following three different options with distinct payoff functions *i.e.,* in each case, the price of the options behave non-identically at the maturity (T):

- **Max/Min Options:** The payoff functions of these options are determined by

$$V(S,T) = \begin{cases} \left(\max(S_1, S_2, \ldots, S_N) - K\right)^+, & \text{Max call option,} \\ \left(\min(S_1, S_2, \ldots, S_N) - K\right)^+, & \text{Min call option,} \end{cases}$$

  where K is the strike price and $a^+ = \max\{a, 0\}$. The corresponding boundary conditions (for $(S,\tau) \in \partial\mathbb{R}^{+N} \times [0,T)$) are

$$V(S,\tau) = \begin{cases} \left(\max(S_1 e^{-\delta_1(T-\tau)}, \ldots, S_N e^{-\delta_N(T-\tau)}) - K e^{-r(T-\tau)}\right)^+, & \text{Max call,} \\ \left(\min(S_1 e^{-\delta_1(T-\tau)}, \ldots, S_N e^{-\delta_N(T-\tau)}) - K e^{-r(T-\tau)}\right)^+, & \text{Min call.} \end{cases}$$

- **Index Options:** These options are traded with the payoff function

$$V(S,T) = \left(\sum_{n=1}^{N} w_n S_n - K\right)^+,$$

  and the boundary conditions

$$V(S,\tau) = \left(\sum_{n=1}^{N} w_n S_n e^{-\delta_n(T-\tau)} - K e^{-r(T-\tau)}\right)^+, \quad (S,\tau) \in \partial\mathbb{R}^{+N} \times [0,T),$$

  where w_n are the portfolio weights.

- **Multi-Strike Options:** For multi-strike options, the payoff function is given by

$$V(S,T) = (S_1 - K_1, S_2 - K_2, \ldots, S_N - K_N)^+,$$

where $K_1, K_2, \ldots, K_N$ are the strike prices corresponding to the underlying assets $S_1, S_2, \ldots, S_N$, respectively. The boundary conditions (for $(S,\tau) \in \partial\mathbb{R}^{+N} \times [0,T)$) are given by

$$V(S,\tau) = \left(S_1 e^{-\delta_1(T-\tau)} - K_1 e^{-r(T-\tau)}, \ldots, S_N e^{-\delta_N(T-\tau)} - K_N e^{-r(T-\tau)}\right)^+.$$

To study the class of financially relevant problems in a systematic way by introducing the new independent variables $x_n = \ln(S_n/K)$, $t = T - \tau$, we transform the problem (5.2.1) into a non-dimensional and less cluttered problem in which only the free parameters of the problem appears in the coefficients of the equation. For the numerical implementation, we trim the unbounded domain into the bounded domain to avoid the unacceptable large truncation error, *i.e.,* $(x,t) \in \Lambda_N \times (0,T] = (a_1,b_1) \times (a_2,b_2) \times \cdots \times (a_N,b_N) \times (0,T]$, where $x = (x_1, x_2, \ldots, x_N)$. The endpoints of the interval $[a_n, b_n],\ n = 1,2,\ldots,N$ are sufficiently large negative number and sufficiently large positive numbers, respectively. Then, the multi-asset Black-Scholes Equation (5.2.1) is thus reformulated into the following PDE:

$$\frac{\partial u}{\partial t} - \frac{1}{2}\sum_{n=1}^{N}\sum_{n'=1}^{N}\sigma_n\sigma_{n'}\rho_{nn'}\frac{\partial^2 u}{\partial x_n \partial x_{n'}} - \sum_{n=1}^{N}\left(r - \delta_n - \frac{1}{2}\sigma_n^2\right)\frac{\partial u}{\partial x_n} + ru = 0, \quad (5.2.2)$$

where $(x,t) \in \Lambda_N \times (0,T]$. After introducing the transformation, the terminal value problems are now turned into initial value problems.

The reformulated initial and boundary conditions for Equation (5.2.2) are as follows:

- For max/min options the transformed initial and boundary conditions are

$$u(x,0) = \begin{cases} \left(\max(Ke^{x_1}, Ke^{x_2}, \ldots, Ke^{x_N}) - K\right)^+, \ x \in \Lambda_N, & \text{Max call,} \\ \left(\min(Ke^{x_1}, Ke^{x_2}, \ldots, Ke^{x_N}) - K\right)^+, \ x \in \Lambda_N, & \text{Min call,} \end{cases}$$

and

$$u(x,t) = \begin{cases} \left(\max(Ke^{x_1-\delta_1 t}, Ke^{x_2-\delta_2 t}, \ldots, Ke^{x_N-\delta_N t}) - Ke^{-rt}\right)^+, & \text{Max call,} \\ \left(\min(Ke^{x_1-\delta_1 t}, Ke^{x_2-\delta_2 t}, \ldots, Ke^{x_N-\delta_N t}) - Ke^{-rt}\right)^+, & \text{Min call,} \end{cases}$$

with $(x,t) \in \partial\Lambda_N \times (0,T]$.

- The dimensionless initial and boundary conditions for index options are read as

$$u(x,0) = \left(\sum_{n=1}^{N} w_n K e^{x_n} - K\right)^+, \ x \in \Lambda_N,$$

and

$$u(x,t) = \left(\sum_{n=1}^{N} w_n K e^{x_n-\delta_n t} - Ke^{-rt}\right)^+, \ (x,t) \in \partial\Lambda_N \times (0,T],$$

respectively.

- Finally, after the transformation, the initial and boundary condition for multi-strike options get converted into

$$u(x,0) = \left(K_1 e^{x_1} - K_1, K_2 e^{x_2} - K_2, \ldots, K_N e^{x_N} - K_N\right)^+, \ x \in \Lambda_N$$

and

$$u(x,t) = \left(K_1 e^{x_1-\delta_1 t} - K_1 e^{-rt}, K_2 e^{x_2-\delta_2 t} - K_2 e^{-rt}, \ldots, K_N e^{x_N-\delta_N t} - K_N e^{-rt}\right)^+,$$

with $(x,t) \in \partial\Lambda_N \times (0,T]$.

Remark. For multi-strike options the transformation depends on the n-th strike price so we use $x_n = \ln(S_n/K_n),\ n = 1,2,\ldots,N, t = T - \tau$.

5.2.1 Description of sensitivities

When the value of an option is determined by the prices of many parameters and assets, the linkages between these assets become crucial. The analysis of these sensitivities will be discussed in Section 6. The differential formulae for the Greeks can be derived from the Black-Scholes model.

Deltas. We consider the Greek delta for the constant correlation model. Delta is the rate at which the option price changes with respect to the price of the underlying asset. For the multi-dimensional problem (5.2.1), the deltas are the sensitivity of the option price to changes in the price of the n-th underlying. Mathematically, these are defined as $\Delta_{S_n} = \frac{\partial V}{\partial S_n}$, where S_n is the n-th underlying asset price. This gives an N-component delta vector. Furthermore, suppose a (long) call option is deep-in-the-money in S_{n_1}, then $\Delta_{S_{n_1}}$ becomes larger, whereas $\Delta_{S_{n_2}}$ and $\Delta_{S_{n_3}}$ are very close to zero, where S_{n_i} denotes the n_i-th underlying asset for $i = 1,2,3$. These deltas get even more polarized as the volatility of S_{n_1} decreases or as the option approaches maturity.

Gammas. It is the measure of the rate at which the n-th delta changes with respect to the n-th underlying asset. It measures the convexity of the value function, which makes options interesting for many investors. It is also the second derivative of the option price with respect to the underlier. For the multi-dimensional problem (5.2.1), gamma estimates the sensitivity of the delta with respect to the n-th underlying. Mathematically, it is given by $\Gamma_{S_n} = \frac{\partial \Delta}{\partial S_n}$.

Cross-Gammas. It estimates the sensitivity of the delta with respect to the n-th underlying to changes in the price of the n'-th underlying, *i.e.,* the cross-gamma with respect to the n-th and n'-th underlying. Mathematically, it is given by Cross-gamma $= \frac{\partial^2 V}{\partial S_n \partial S_{n'}}$. It is interesting to note that an option may have positive gammas but negative cross-gammas (in the case when S_n increases, Δ_{S_n} increases but $\Delta_{S_{n'}}$ decreases). Thus

cross-gammas may be interpreted as a measure of the stability of $\Delta_{S_{n'}}$ as other underlying prices increase.

Theta. The Greek "Theta" is the derivative, of the value of a given option expiring on a given day with respect to time. As it measures the change in the option price to the movement of time to maturity, it is negative of the derivative with respect to the parameter τ and is given by $\Theta = -\frac{\partial V}{\partial \tau}$, where τ is the time to maturity.

5.3 Implementation of 2D Haar wavelet method

Let $h_{i_1}(x_1)$ and $h_{i_2}(x_2)$ denotes the Haar wavelet basis functions in x_1 and x_2 directions, respectively. $p_{i_1}(x_1)$ and $p_{i_2}(x_2)$ denotes the first integral of $h_{i_1}(x_1)$ and $h_{i_2}(x_2)$, respectively. Furthermore, $q_{i_1}(x_1)$ and $q_{i_2}(x_2)$ represents the second integral of Haar basis functions in their respective directions. For the numerical approximation and simulation purpose, we consider the two-asset option pricing problems ($N = 2$). To adopt the above wavelet approach for the proposed problem, let the numerical solution $U(x_1, x_2, t)$ of the two-asset option pricing problem (5.2.2) can be expressed in the form of wavelets. To proceed, we discretize the spatial domain $[a_1, b_1] \times [a_2, b_2]$ and the temporal domain $[0, T]$ into $2M_1 \times 2M_2$ and $2M_3$ uniformly distributed mesh points respectively. Further, we consider the wavelet approximation of $\frac{\partial^5 u(x_1,x_2,t)}{\partial t \partial x_1^2 \partial x_2^2}$, expressed as

$$\frac{\partial^5 U(x_1, x_2, t)}{\partial t \partial x_1^2 \partial x_2^2} = \sum_{i_1=1}^{2M_1} \sum_{i_2=1}^{2M_2} c_{i_1,i_2,k} h_{i_1}(x_1) h_{i_2}(x_2),$$

where $c_{i_1,i_2,k}$ are the unknown coefficients (note that these are functions of t and are constants at a particular time level); $i_1,\ i_2$ symbolize the indices for Haar wavelets in x_1 and x_2 directions, respectively; and k indicates the time level. Now, on integrating the above expression twice with respect to x_1 from a_1 to x_1, we obtain

$$\frac{\partial^3 U(x_1, x_2, t)}{\partial t \partial x_2^2} = \sum_{i_1=1}^{2M_1} \sum_{i_2=1}^{2M_2} c_{i_1,i_2,k} q_{i_1}(x_1) h_{i_2}(x_2) + \sum_{N_1=0}^{1} \frac{(x_1 - a_1)^{N_1}}{N_1!} \frac{\partial^{1+N_1+2} U(a_1, x_2, t)}{\partial t \partial x_1^{N_1} \partial x_2^2}.$$

Similarly, integrating it twice with respect to x_2 from a_2 to x_2, yields

$$\begin{aligned}\frac{\partial U(x_1,x_2,t)}{\partial t} =& \sum_{i_1=1}^{2M_1}\sum_{i_2=1}^{2M_2} c_{i_1,i_2,k} q_{i_1}(x_1) q_{i_2}(x_2) + \sum_{N_1=0}^{1} \frac{(x_1-a_1)^{N_1}}{N_1!} \frac{\partial^{1+N_1} U(a_1,x_2,t)}{\partial t \partial x_1^{N_1}} \\ &- \sum_{N_1=0}^{1} \frac{(x_1-a_1)^{N_1}}{N_1!} \sum_{N_2=0}^{1} \frac{(x_2-a_2)^{N_2}}{N_2!} \frac{\partial^{1+N_1+N_2} U(a_1,a_2,t)}{\partial t \partial x_1^{N_1} \partial x_2^{N_2}} \\ &+ \sum_{N_2=0}^{1} \frac{(x_2-a_2)^{N_2}}{N_2!} \frac{\partial^{1+N_2} U(x_1,a_2,t)}{\partial t \partial x_2^{N_2}}.\end{aligned}$$

Again, by integrating it once with respect to t from t_k to t, we obtain

$$\begin{aligned}U(x_1,x_2,t) =& (t-t_k) \sum_{i_1=1}^{2M_1}\sum_{i_2=1}^{2M_2} c_{i_1,i_2,k} q_{i_1}(x_1) q_{i_2}(x_2) + U(x_1,x_2,t_k) \\ &+ \sum_{N_1=0}^{1} \frac{(x_1-a_1)^{N_1}}{N_1!} \frac{\partial^{N_1} U(a_1,x_2,t)}{\partial x_1^{N_1}} - \sum_{N_1=0}^{1} \frac{(x_1-a_1)^{N_1}}{N_1!} \frac{\partial^{N_1} U(a_1,x_2,t_k)}{\partial x_1^{N_1}} \\ &+ \sum_{N_2=0}^{1} \frac{(x_2-a_2)^{N_2}}{N_2!} \frac{\partial^{N_2} U(x_1,a_2,t)}{\partial x_2^{N_2}} - \sum_{N_2=0}^{1} \frac{(x_2-a_2)^{N_2}}{N_2!} \frac{\partial^{N_2} U(x_1,a_2,t_k)}{\partial x_2^{N_2}} \\ &- \sum_{N_1=0}^{1} \frac{(x_1-a_1)^{N_1}}{N_1!} \sum_{N_2=0}^{1} \frac{(x_2-a_2)^{N_2}}{N_2!} \frac{\partial^{N_1+N_2} U(a_1,a_2,t)}{\partial x_1^{N_1} \partial x_2^{N_2}} \\ &+ \sum_{N_1=0}^{1} \frac{(x_1-a_1)^{N_1}}{N_1!} \sum_{N_2=0}^{1} \frac{(x_2-a_2)^{N_2}}{N_2!} \frac{\partial^{N_1+N_2} U(a_1,a_2,t_k)}{\partial x_1^{N_1} \partial x_2^{N_2}}. \end{aligned} \tag{5.3.1}$$

In the above expression to deduce the unknown terms $\frac{\partial U(a_1,x_2,t)}{\partial x_1}$, $\frac{\partial U(a_1,x_2,t_k)}{\partial x_1}$, $\frac{\partial^2 U(a_1,a_2,t)}{\partial x_1 \partial x_2}$ and $\frac{\partial^2 U(a_1,a_2,t_k)}{\partial x_1 \partial x_2}$ we use the boundary condition at $x_1 = b_1$, which gives

$$\begin{aligned}&\left[\frac{\partial U(a_1,x_2,t)}{\partial x_1} - \frac{\partial U(a_1,x_2,t_k)}{\partial x_1}\right] - (x_2-a_2)\left[\frac{\partial^2 U(a_1,a_2,t)}{\partial x_1 \partial x_2} - \frac{\partial^2 U(a_1,a_2,t_k)}{\partial x_1 \partial x_2}\right] \\ &= \frac{1}{b_1-a_1}\Bigg[U(b_1,x_2,t) - U(b_1,x_2,t_k) - (t-t_k)\sum_{i_1=1}^{2M_1}\sum_{i_2=1}^{2M_2} c_{i_1,i_2,k} q_{i_1}(b_1) q_{i_2}(x_2) \\ &- U(a_1,x_2,t) + U(a_1,x_2,t_k) - \sum_{N_2=0}^{1} \frac{(x_2-a_2)^{N_2}}{N_2!} \frac{\partial^{N_2} U(b_1,a_2,t)}{\partial x_2^{N_2}}\end{aligned}$$

$$+\sum_{N_2=0}^{1}\frac{(x_2-a_2)^{N_2}}{N_2!}\frac{\partial^{N_2}U(b_1,a_2,t_k)}{\partial x_2^{N_2}}+U(a_1,a_2,t)+(b_1-a_1)\frac{\partial U(a_1,a_2,t)}{\partial x_1}$$
$$+(x_2-a_2)\frac{\partial U(a_1,a_2,t)}{\partial x_2}-U(a_1,a_2,t_k)-(b_1-a_1)\frac{\partial U(a_1,a_2,t_k)}{\partial x_1}$$
$$-(x_2-a_2)\frac{\partial U(a_1,a_2,t_k)}{\partial x_2}\Bigg]. \tag{5.3.2}$$

Substituting the value of $\left[\frac{\partial U(a_1,x_2,t)}{\partial x_1}-\frac{\partial U(a_1,x_2,t_k)}{\partial x_1}\right]-(x_2-a_2)\left[\frac{\partial^2 U(a_1,a_2,t)}{\partial x_1\partial x_2}-\frac{\partial^2 U(a_1,a_2,t_k)}{\partial x_1\partial x_2}\right]$ from (5.3.2) into (5.3.1) yields

$$U(x_1,x_2,t)=(t-t_k)\sum_{i_1=1}^{2M_1}\sum_{i_2=1}^{2M_2}c_{i_1,i_2,k}\left[q_{i_1}(x_1)-\frac{x_1-a_1}{b_1-a_1}q_{i_1}(b_1)\right]q_{i_2}(x_2)+U(x_1,x_2,t_k)$$
$$+U(a_1,x_2,t)-U(a_1,x_2,t_k)+\sum_{N_2=0}^{1}\frac{(x_2-a_2)^{N_2}}{N_2!}\frac{\partial^{N_2}U(x_1,a_2,t)}{\partial x_2^{N_2}}$$
$$-\sum_{N_2=0}^{1}\frac{(x_2-a_2)^{N_2}}{N_2!}\frac{\partial^{N_2}U(x_1,a_2,t_k)}{\partial x_2^{N_2}}-U(a_1,a_2,t)-(x_1-a_1)\frac{\partial U(a_1,a_2,t)}{\partial x_1}$$
$$-(x_2-a_2)\frac{\partial U(a_1,a_2,t)}{\partial x_2}+U(a_1,a_2,t_k)+(x_1-a_1)\frac{\partial U(a_1,a_2,t_k)}{\partial x_1}$$
$$+(x_2-a_2)\frac{\partial U(a_1,a_2,t_k)}{\partial x_2}+\frac{x_1-a_1}{b_1-a_1}\Bigg[U(b_1,x_2,t)-U(b_1,x_2,t_k)-U(a_1,x_2,t)$$
$$+U(a_1,x_2,t_k)-\sum_{N_2=0}^{1}\frac{(x_2-a_2)^{N_2}}{N_2!}\frac{\partial^{N_2}U(b_1,a_2,t)}{\partial x_2^{N_2}}+\sum_{N_2=0}^{1}\frac{(x_2-a_2)^{N_2}}{N_2!}\frac{\partial^{N_2}U(b_1,a_2,t_k)}{\partial x_2^{N_2}}$$
$$+U(a_1,a_2,t)+(b_1-a_1)\frac{\partial U(a_1,a_2,t)}{\partial x_1}+(x_2-a_2)\frac{\partial U(a_1,a_2,t)}{\partial x_2}-U(a_1,a_2,t_k)$$
$$-(b_1-a_1)\frac{\partial U(a_1,a_2,t_k)}{\partial x_1}-(x_2-a_2)\frac{\partial U(a_1,a_2,t_k)}{\partial x_2}\Bigg]. \tag{5.3.3}$$

Similarly, to get the unknown terms $\frac{\partial U(x_1,a_2,t)}{\partial x_2}$ and $\frac{\partial U(x_1,a_2,t_k)}{\partial x_2}$, we use the final boundary condition in x_2 direction *i.e.,* put $x_2=b_2$ in (5.3.3), to get

$$\frac{\partial U(x_1,a_2,t)}{\partial x_2}-\frac{\partial U(x_1,a_2,t_k)}{\partial x_2}=$$
$$\frac{1}{b_2-a_2}\Bigg[U(x_1,b_2,t)-\Bigg\{\sum_{i_1=1}^{2M_1}\sum_{i_2=1}^{2M_2}c_{i_1,i_2,k}\left[q_{i_1}(x_1)-\frac{x_1-a_1}{b_1-a_1}q_{i_1}(b_1)\right]q_{i_2}(b_2)$$

$$+ U(x_1, b_2, t_k) + U(a_1, b_2, t) - U(a_1, b_2, t_k) + U(x_1, a_2, t) - U(x_1, a_2, t_k)$$
$$- U(a_1, a_2, t) - (x_1 - a_1)\frac{\partial U(a_1, a_2, t)}{\partial x_1} - (b_2 - a_2)\frac{\partial U(a_1, a_2, t)}{\partial x_2} + U(a_1, a_2, t_k)$$
$$+ (x_1 - a_1)\frac{\partial U(a_1, a_2, t_k)}{\partial x_1} + (b_2 - a_2)\frac{\partial U(a_1, a_2, t_k)}{\partial x_2} + \frac{x_1 - a_1}{b_1 - a_1}\Bigg(U(b_1, b_2, t)$$
$$- U(b_1, b_2, t_k) - U(a_1, b_2, t) + U(a_1, b_2, t_k) - \sum_{N_2=0}^{1}\frac{(b_2 - a_2)^{N_2}}{N_2!}\frac{\partial^{N_2} U(b_1, a_2, t)}{\partial x_2^{N_2}}$$
$$+ \sum_{N_2=0}^{1}\frac{(b_2 - a_2)^{N_2}}{N_2!}\frac{\partial^{N_2} U(b_1, a_2, t_k)}{\partial x_2^{N_2}} + U(a_1, a_2, t) + (b_1 - a_1)\frac{\partial U(a_2, a_2, t)}{\partial x_1}$$
$$+ (b_2 - a_2)\frac{\partial U(a_1, a_2, t)}{\partial x_2} - U(a_1, a_2, t_k) - (b_1 - a_1)\frac{\partial U(a_1, a_2, t_k)}{\partial x_1}$$
$$- (b_2 - a_2)\frac{\partial U(a_1, a_2, t_k)}{\partial x_2}\Bigg)\Bigg\}\Bigg]. \tag{5.3.4}$$

Substituting the value of $\frac{\partial U(x_1,a_2,t)}{\partial x_2} - \frac{\partial U(x_1,a_2,t_k)}{\partial x_2}$ from (5.3.4) into (5.3.3), we obtain

$$U(x_1, x_2, t) = (t - t_k)\sum_{i_1=1}^{2M_1}\sum_{i_2=1}^{2M_2} c_{i_1,i_2,k}\left[q_{i_1}(x_1) - \frac{x_1 - a_1}{b_1 - a_1}q_{i_1}(b_1)\right]\left[q_{i_2}(x_2) - \frac{x_2 - a_2}{b_2 - a_2}q_{i_2}(b_2)\right]$$
$$+ U(x_1, x_2, t_k) + U(a_1, x_2, t) - U(a_1, x_2, t_k) + U(x_1, a_2, t) - U(x_1, a_2, t_k) - U(a_1, a_2, t)$$
$$- (x_1 - a_1)\frac{\partial U(a_1, a_2, t)}{\partial x_1} - (x_2 - a_2)\frac{\partial U(a_1, a_2, t)}{\partial x_2} + U(a_1, a_2, t_k) + (x_1 - a_1)\frac{\partial U(a_1, a_2, t_k)}{\partial x_1}$$
$$+ (x_2 - a_2)\frac{\partial U(a_1, a_2, t_k)}{\partial x_2} + \frac{x_1 - a_1}{b_1 - a_1}\Bigg[U(b_1, x_2, t) - U(b_1, x_2, t_k) - U(a_1, x_2, t) + U(a_1, x_2, t_k)$$
$$- \sum_{N_2=0}^{1}\frac{(x_2 - a_2)^{N_2}}{N_2!}\frac{\partial^{N_2} U(b_1, a_2, t)}{\partial x_2^{N_2}} + \sum_{N_2=0}^{1}\frac{(x_2 - a_2)^{N_2}}{N_2!}\frac{\partial^{N_2} U(b_1, a_2, t_k)}{\partial x_2^{N_2}} + U(a_1, a_2, t)$$
$$+ (b_1 - a_1)\frac{\partial U(a_1, a_2, t)}{\partial x_1} + (x_2 - a_2)\frac{\partial U(a_1, a_2, t)}{\partial x_2} - U(a_1, a_2, t_k) - (b_1 - a_1)\frac{\partial U(a_1, a_2, t_k)}{\partial x_1}$$
$$- (x_2 - a_2)\frac{\partial U(a_1, a_2, t_k)}{\partial x_2}\Bigg] + \frac{x_2 - a_2}{b_2 - a_2}\Bigg[U(x_1, b_2, t) - \Bigg\{U(x_1, b_2, t_k) + U(a_1, b_2, t)$$
$$- U(a_1, b_2, t_k) + U(x_1, a_2, t) - U(x_1, a_2, t_k) - U(a_1, a_2, t) - (x_1 - a_1)\frac{\partial U(a_1, a_2, t)}{\partial x_1}$$
$$- (b_2 - a_2)\frac{\partial U(a_1, a_2, t)}{\partial x_2} + U(a_1, a_2, t_k) + (x_1 - a_1)\frac{\partial U(a_1, a_2, t_k)}{\partial x_1} + (b_2 - a_2)\frac{\partial U(a_1, a_2, t_k)}{\partial x_2}$$
$$+ \frac{x_1 - a_1}{b_1 - a_1}\Bigg(U(b_1, b_2, t) - U(b_1, b_2, t_k) - U(a_1, b_2, t) + U(a_1, b_2, t_k)$$

$$
\begin{aligned}
&- \sum_{N_2=0}^{1} \frac{(b_2-a_2)^{N_2}}{N_2!} \frac{\partial^{N_2} U(b_1,a_2,t)}{\partial x_2^{N_2}} + \sum_{N_2=0}^{1} \frac{(b_2-a_2)^{N_2}}{N_2!} \frac{\partial^{N_2} U(b_1,a_2,t_k)}{\partial x_2^{N_2}} \\
&+ U(a_1,a_2,t) + (b_1-a_1)\frac{\partial U(a_1,a_2,t)}{\partial x_1} + (b_2-a_2)\frac{\partial U(a_1,a_2,t)}{\partial x_2} \\
&- U(a_1,a_2,t_k) - (b_1-a_1)\frac{\partial U(a_1,a_2,t_k)}{\partial x_1} - (b_2-a_2)\frac{\partial U(a_1,a_2,t_k)}{\partial x_2}\Bigg)\Bigg\}\Bigg]. \qquad (5.3.5)
\end{aligned}
$$

Thus, we obtain the approximated values of all derivatives needed in (5.2.2). Putting the values of these approximations in Equation (5.2.2), we get a $2M_1 \times 2M_2$ system of linear equations with unknown coefficients $c_{i_1,i_2,k}$. Solving this system by using any efficient algorithm such as Gauss elimination gives the values of the coefficients $c_{i_1,i_2,k}$ at each time level. Substituting these values of $c_{i_1,i_2,k}$ into (5.3.5) we get the solution of (5.2.2) at the k-th time level. Finally, the back substitution of the transformation $S_1 = Ke^{x_1}$, $S_2 = Ke^{x_2}$ and $\tau = T - t$ gives the solution of (5.2.1).

Algorithm. To get the numerical approximation of price and sensitivities of two-assets ($N = 2$) option pricing problem governed by Equation (5.2.1) we follow the following algorithm.

- we first compute the wavelet coefficients from the preceding implementation.
- use these coefficients to approximate the value of the solution of Equation (5.2.2) and its derivatives.
- use the coordinate transformations $S_1 = Ke^{x_1}$, $S_2 = Ke^{x_2}$ and $\tau = T - t$ to apply back substitution.
- compute the approximate values of $V(S_1, S_2, \tau)$.
- compute the solution derivatives (Greeks) of the option price with respect to different variables.

5.4 Convergence analysis

In this section, we show that the proposed 2D Haar wavelet scheme is convergent. First, we introduce some lemmas needed to prove the convergence.

Lemma 5.4.1. *The upper bounds for the Haar wavelets and their integrals are as follows:*

$$h_i(x) \leqslant 1,\ \forall\, i \text{ and } p_i(x) \leqslant \frac{1}{2^{j+1}}, \quad q_i(x) < \mathcal{B}\left(\frac{1}{2^{j+1}}\right)^2, \text{ for } i > 1,$$

where $\mathcal{B} = \dfrac{8}{3(\lfloor (3/2) \rfloor !)^2}$.

Proof. Refer [45]. □

Lemma 5.4.2. *Let* $g(x_1, x_2, t_k) = \frac{\partial^4 u(x_1,x_2,t_k)}{\partial x_1^2 \partial x_2^2} \in L^2(\mathbb{R}^2)$ *be a continuous function on the domain* $\Lambda_2 = [a_1, b_1] \times [a_2, b_2]$ *which can also be written as* $g(x_1, x_2, t_{k+1}) = \eta \sum_{i_1=1}^{2M_1} \sum_{i_2=1}^{2M_2} c_{i_1,i_2,k} h_{i_1}(x_1) h_{i_2}(x_2)$, *where* k *represents the* k*-th time level and* $\eta = \frac{T}{2M_3-1}$. *If* g, $\frac{\partial g}{\partial x_1}$, $\frac{\partial g}{\partial x_2}$, *and* $\frac{\partial^2 g}{\partial x_1 \partial x_2}$ *all are bounded by* λ *in* Λ_2. *Then, the Haar coefficients* $c_{i_1,i_2,k}$ *are also bounded for all* k.

Proof. The Haar coefficients $c_{i_1,i_2,k}$ can be written as

$$\begin{aligned} c_{i_1,i_2,k} &= \eta \int_{a_1}^{b_1} \left(\int_{a_2}^{b_2} g(x_1, x_2, t_{k+1}) h_{i_2}(x_2)\, dx_2 \right) h_{i_1}(x_1)\, dx_1 \\ &= \eta \int_{a_1}^{b_1} \left(\int_{\kappa_2\left(\frac{b_2-a_2}{2^{j_2}}\right)}^{\left(\kappa_2+\frac{1}{2}\right)\left(\frac{b_2-a_2}{2^{j_2}}\right)} g(x_1, x_2, t_{k+1})\, dx_2 \right. \\ &\quad \left. - \int_{\left(\kappa_2+\frac{1}{2}\right)\left(\frac{b_2-a_2}{2^{j_2}}\right)}^{(\kappa_2+1)\left(\frac{b_2-a_2}{2^{j_2}}\right)} g(x_1, x_2, t_{k+1})\, dx_2 \right) h_{i_1}(x_1)\, dx_1. \end{aligned}$$

By using mean value theorem, there exists x_2^* and x_2^{**} satisfying $\kappa_2 \left(\frac{b_2-a_2}{2^{j_2}}\right) \leqslant x_2^* \leqslant \left(\kappa_2 + \frac{1}{2}\right)\left(\frac{b_2-a_2}{2^{j_2}}\right)$ and $\left(\kappa_2 + \frac{1}{2}\right)\left(\frac{b_2-a_2}{2^{j_2}}\right) \leqslant x_2^{**} \leqslant (\kappa_2 + 1)\left(\frac{b_2-a_2}{2^{j_2}}\right)$ such that

$$c_{i_1,i_2,k} = 2^{-j_2-1}(b_2 - a_2)\eta \int_{a_1}^{b_1} \left(g(x_1, x_2^*) - g(x_1, x_2^{**})\right) h_{i_1}(x_1)\, dx_1.$$

Again by using Lagrange's mean value theorem there exists $x_2' \in [x_2^*, x_2^{**}]$ such that

$$c_{i_1,i_2,k} = 2^{-j_2-1}(b_2-a_2)\eta \int_{a_1}^{b_1} (x_2^* - x_2^{**}) \frac{\partial g(x_1, x_2')}{\partial x_2} h_{i_1}(x_1)\, dx_1.$$

Similarly, by applying mean value theorem of integral calculus and Lagrange's mean value theorem, there exists x_1^*, x_1^{**} satisfying $\kappa_1 \left(\frac{b_1-a_1}{2^{j_1}}\right) \leqslant x_1^* \leqslant \left(\kappa_1 + \frac{1}{2}\right)\left(\frac{b_1-a_1}{2^{j_1}}\right)$ and $\left(\kappa_1 + \frac{1}{2}\right)\left(\frac{b_1-a_1}{2^{j_1}}\right) \leqslant x_1^{**} \leqslant (\kappa_1+1)\left(\frac{b_1-a_1}{2^{j_1}}\right)$ and $x_1' \in [x_1^*, x_1^{**}]$ such that

$$c_{i_1,i_2,k} = 2^{-j_1-j_2-2}(b_1-a_1)(b_2-a_2)(x_1^* - x_1^{**})(x_2^* - x_2^{**})\eta \frac{\partial^2 g(x_1', x_2')}{\partial x_1 \partial x_2}.$$

Since $x_1^* - x_1^{**} \leqslant b_1 - a_1$, $x_2^* - x_2^{**} \leqslant b_2 - a_2$, and $|\frac{\partial^2 g(x_1', x_2')}{\partial x_1 \partial x_2}| \leq \lambda$, so

$$c_{i_1,i_2,k} \leqslant \frac{\eta\lambda(b_1-a_1)^2(b_2-a_2)^2}{2^{j_1+1}2^{j_2+1}}. \qquad \square$$

The convergence of the present wavelet-based approximation scheme is given by the following theorem.

Theorem 5.4.1. *Let* $\frac{\partial^4 u(x_1,x_2,t_{k+1})}{\partial x_1^2 \partial x_2^2} \in L^2(\mathbb{R}^2)$ *be a continuous function on domain* Λ_2*. Then, the approximate solution obtained by the proposed 2D Haar wavelet method converges to the exact solution in the* L^2-*norm,* i.e., $\forall\, k\ \|Error_{J_1J_2}(x_1, x_2, t_{k+1})\|_2 \to 0$ *as* $J_1, J_2 \to \infty$.

Proof. Suppose $u(x_1, x_2, t_{k+1})$ and $U(x_1, x_2, t_{k+1})$ are the exact and approximate solutions of the transformed Black-Scholes equation (5.2.2) at the $k+1$-th time level, respectively. Then, we can write

$$\begin{aligned} u(x_1, x_2, t_{k+1}) &= \eta \sum_{i_1=0}^{\infty}\sum_{i_2=0}^{\infty} c_{i_1,i_2,k} q_{i_1}(x_1) q_{i_2}(x_2) + \zeta(x_1, x_2, t_{k+1}) \\ &= \eta c_{1,1,k} q_1(x_1) q_1(x_2) + \eta \sum_{j_1=0}^{\infty}\sum_{\kappa_1=0}^{2^{j_1}-1} c_{2^{j_1}+\kappa_1+1,1,k} q_{2^{j_1}+\kappa_1+1}(x_1) q_1(x_2) \\ &\quad + \eta \sum_{j_2=0}^{\infty}\sum_{\kappa_2=0}^{2^{j_2}-1} c_{1,2^{j_2}+\kappa_2+1,k} q_1(x_1) q_{2^{j_2}+\kappa_2+1}(x_2) \end{aligned}$$

$$+\eta\sum_{j_1=0}^{\infty}\sum_{\kappa_1=0}^{2^{j_1}-1}\sum_{j_2=0}^{\infty}\sum_{\kappa_2=0}^{2^{j_2}-1}c_{2^{j_1}+\kappa_1+1,2^{j_2}+\kappa_2+1,k}q_{2^{j_1}+\kappa_1+1}(x_1)q_{2^{j_2}+\kappa_2+1}(x_2)$$
$$+\zeta(x_1,x_2,t_{k+1}),$$

where $\eta=\frac{T}{2M_3-1}$, $\zeta(x_1,x_2,t_{k+1})$ is the function determined by imposing the given initial and boundary conditions; j_1, j_2 and κ_1, κ_2 indicate the levels of resolution and translation parameters in x_1 and x_2 directions, respectively, and $i_1=2^{j_1}+\kappa_1+1$ and $i_2=2^{j_2}+\kappa_2+1$ are the respective Haar indices. Now, the Haar solution at the maximum level of resolution can be determined by

$$\begin{aligned}U(x_1,x_2,t_{k+1})&=\eta c_{1,1,k}q_1(x_1)q_1(x_2)+\eta\sum_{j_1=0}^{J_1}\sum_{\kappa_1=0}^{2^{j_1}-1}c_{2^{j_1}+\kappa_1+1,1,k}q_{2^{j_1}+\kappa_1+1}(x_1)q_1(x_2)\\&+\eta\sum_{j_2=0}^{J_2}\sum_{\kappa_2=0}^{2^{j_2}-1}c_{1,2^{j_2}+\kappa_2+1,k}q_1(x_1)q_{2^{j_2}+\kappa_2+1}(x_2)\\&+\eta\sum_{j_1=0}^{J_1}\sum_{\kappa_1=0}^{2^{j_1}-1}\sum_{j_2=0}^{J_2}\sum_{\kappa_2=0}^{2^{j_2}-1}c_{2^{j_1}+\kappa_1+1,2^{j_2}+\kappa_2+1,k}q_{2^{j_1}+\kappa_1+1}(x_1)q_{2^{j_2}+\kappa_2+1}(x_2)\\&+\zeta(x_1,x_2,t_{k+1}).\end{aligned}$$

The error function at the maximum level of resolution is computed by

$$\begin{aligned}&Error_{J_1,J_2}(x_1,x_2,t_{k+1})=u(x_1,x_2,t_{k+1})-U(x_1,x_2,t_{k+1})\\&=\eta\sum_{j_1=J_1+1}^{\infty}\sum_{\kappa_1=0}^{2^{j_1}-1}c_{2^{j_1}+\kappa_1+1,1,k}q_{2^{j_1}+\kappa_1+1}(x_1)q_1(x_2)\\&+\eta\sum_{j_2=J_2}^{\infty}\sum_{\kappa_2=0}^{2^{j_2}-1}c_{1,2^{j_2}+\kappa_2+1,k}q_1(x_1)q_{2^{j_2}+\kappa_2+1}(x_2)\\&+\eta\sum_{j_1=J_1}^{\infty}\sum_{\kappa_1=0}^{2^{j_1}-1}\sum_{j_2=J_2}^{\infty}\sum_{\kappa_2=0}^{2^{j_2}-1}c_{2^{j_1}+\kappa_1+1,2^{j_2}+\kappa_2+1,k}q_{2^{j_1}+\kappa_1+1}(x_1)q_{2^{j_2}+\kappa_2+1}(x_2).\end{aligned}$$

Taking L^2-norm of the error function $Error_{J_1,J_2}(x_1,x_2,t_{k+1})$, deduce

$$\|Error_{J_1,J_2}(x_1,x_2,t_{k+1})\|_2^2 = \mathcal{V}_1+\mathcal{V}_2+\mathcal{V}_3+\mathcal{V}_4+\mathcal{V}_5+\mathcal{V}_6,$$

where

$$\begin{aligned}
\mathcal{V}_1 =&\eta\sum_{j_1,\kappa_1}\sum_{r_1,s_1} c_{2^{j_1+1}+\kappa_1+1,1,k}c_{2^{r_1}+s_1+1,1,k}\int_{a_1}^{b_1} q_{2^{j_1}+k_1+1}(x_1)q_{2^{r_1}+s_1+1}(x_1)\,dx_1\\
&\times\int_{a_2}^{b_2} q_1(x_2)q_1(x_2)\,dx_2,\\
\mathcal{V}_2 =&\eta\sum_{j_2,\kappa_2}\sum_{r_2,s_2} c_{1,2^{j_2}+\kappa_2+1,k}c_{1,2^{r_2}+s_2+1,k}\int_{a_1}^{b_1} q_1(x_1)q_1(x_1)\,dx_1\\
&\times\int_{a_2}^{b_2} q_{2^{j_2}+\kappa_2+1}(x_2)q_{2^{r_2}+s_2+1}(x_2)\,dx_2,\\
\mathcal{V}_3 =&\eta\sum_{j_1,\kappa_1}\sum_{r_1,s_1}\sum_{j_2,k_2}\sum_{r_2,s_2} c_{2^{j_1}+\kappa_1+1,2^{j_2}+\kappa_2+1,k}c_{2^{r_1}+s_1+1,2^{r_2}+s_2+1,k}\\
&\times\int_{a_1}^{b_1} q_{2^{j_1}+\kappa_1+1}(x_1)q_{2^{r_1}+s_1+1}(x_1)\,dx_1\int_{a_2}^{b_2} q_{2^{j_2}+\kappa_2+1}(x_2)q_{2^{r_2}+s_2+1}(x_2)\,dx_2,\\
\mathcal{V}_4 =&2\eta\sum_{j_1,\kappa_1}\sum_{r_1,s_1} c_{2^{j_1}+\kappa_1+1,1,k}c_{1,2^{r_2}+s_2+1,k}\int_{a_1}^{b_1} q_{2^{j_1}+\kappa_1+1}(x_1)q_1(x_1)\,dx_1\\
&\times\int_{a_2}^{b_2} q_1(x_2)q_{2^{r_2}+s_2+1}(x_2)\,dx_2,\\
\mathcal{V}_5 =&2\eta\sum_{j_1,\kappa_1}\sum_{r_1,s_1}\sum_{r_2,s_2} c_{2^{j_1}+\kappa_1+1,1,k}c_{2^{r_1}+s_1+1,2^{r_2}+s_2+1,k}\int_{a_1}^{b_1} q_{2^{j_1}+\kappa_1+1}(x_1)q_{2^{r_1}+s_1+1}(x_1)\,dx_1\\
&\int_{a_2}^{b_2} q_1(x_2)q_{2^{r_2}+s_2+1}(x_2)\,dx_2,\\
\mathcal{V}_6 =&\,2\eta\sum_{r_1,s_1}\sum_{j_2,\kappa_2}\sum_{r_2,s_2} c_{1,2^{j_2}+\kappa_2+1,k}c_{2^{r_1}+s_1+1,2^{r_2}+s_2+1,k}\int_{a_1}^{b_1} q_1(x_1)q_{2^{r_1}+s_1+1}(x_1)\,dx_1\\
&\int_{a_2}^{b_2} q_{2^{j_2}+\kappa_2+1}(x_2)q_{2^{r_2}+s_2+1}(x_2)\,dx_2.
\end{aligned}$$

To find the bounds for $\mathcal{V}_1$, $\mathcal{V}_2$, $\mathcal{V}_3$, $\mathcal{V}_4$, $\mathcal{V}_5$, and $\mathcal{V}_6$, we use the following result [45]

$$\sum_{j_1=J_1+1}^{\infty}\sum_{\kappa_1=0}^{2^{j_1}-1}\left(\frac{1}{2^{j_1+1}}\right)^3 \leqslant C\left(\frac{1}{2^{J_1+1}}\right)^2.$$

By using the bounds for the Haar functions and their integrals from Lemma 5.4.1 and $c_{i_1,i_2,k}$ from Lemma 5.4.2, we deduce

$$\mathcal{V}_1 < \eta\sum_{j_1,k_1}\sum_{r_1,s_1}\frac{\mathcal{B}^2\lambda^2\eta^2(b_1-a_1)^2(b_2-a_1)^2}{(2!)^2(2^{j_1+1})^3(2^{r_1+1})^3} < \frac{C_1}{(2^{\bar{J}+1})^4}, \text{ for some constant } C_1,$$

where $\bar{J} = \min\{J_1, J_2\}$. Similarly, we compute the following upper bounds for $\mathcal{V}_2$, $\mathcal{V}_3$, $\mathcal{V}_4$, $\mathcal{V}_5$, and $\mathcal{V}_6$

$$\mathcal{V}_2 < \frac{C_2}{(2^{\bar{J}+1})^4}, \quad \mathcal{V}_3 < \frac{C_3}{(2^{\bar{J}+1})^8}, \quad \mathcal{V}_4 < \frac{C_4}{(2^{\bar{J}+1})^4}, \quad \mathcal{V}_5 < \frac{C_5}{(2^{\bar{J}+1})^6}, \quad \mathcal{V}_6 < \frac{C_6}{(2^{\bar{J}+1})^6},$$

where C_2, C_3, C_4, C_5 and C_6 are some constants. Thus,

$$\begin{aligned}\|Error_{J_1,J_2}(x_1,x_2,t_{k+1})\|_2^2 &= \mathcal{V}_1+\mathcal{V}_2+\mathcal{V}_3+\mathcal{V}_4+\mathcal{V}_5+\mathcal{V}_6\\ &< \frac{C_1}{(2^{\bar{J}+1})^4}+\frac{C_2}{(2^{\bar{J}+1})^4}+\frac{C_3}{(2^{\bar{J}+1})^8}+\frac{C_4}{(2^{\bar{J}+1})^4}+\frac{C_5}{(2^{\bar{J}+1})^6}+\frac{C_6}{(2^{\bar{J}+1})^6}\\ &= \mathcal{C}\left(\frac{1}{2^{\bar{J}+1}}\right)^4,\end{aligned}$$

where $\mathcal{C} = C_1+C_2+\frac{C_3}{(2^{\bar{J}+1})^4}+C_4+\frac{C_5}{(2^{\bar{J}+1})^2}+\frac{C_6}{(2^{\bar{J}+1})^2}$. Thus, we obtain $\|Error_{J_1,J_2}(x_1,x_2,t_{k+1})\|_2 \to 0$ as $J_1, J_2 \to \infty$. Hence, the 2D Haar wavelet approximation method is second-order convergent. □

5.5 Numerical simulations and discussions

In this section, we demonstrate the efficiency and robustness of the proposed method through three test examples involving different multi-asset option pricing problems. It is worth noticing that the 2D Haar wavelet method gives high accuracy even when a very

few points are used. To enhance the speed while calculating the operational matrix, we use the MATLAB inbuilt command of Kronecker tensor product (*kron*) instead of the computationally complex loops. The numerical experiments for different two-asset option pricing problems are given. As discussed in the previous section, we confine the actual infinite domain to a finite domain by constructing artificial boundaries. For numerical computations, we discretize the domain $\Lambda_2 \times [0, T]$ into $2M_1$ and $2M_2$ equidistant points using the Haar mesh formulaic expression defined in Section 3 in x_1 and x_2 directions, respectively, and into $2M_3$ equidistant points using the traditional uniform mesh of width $\frac{T}{2M_3-1}$ in the time direction. For convenience, in all numerical experiments we have used equal number of nodal points in all three directions. Initially, the transformed problem (5.2.2) is solved and then by using the back substitution, we get the solution and derivatives to the original problem (5.2.1).

Since the Haar wavelet method does not allow to use the double mesh principle, the error measures are computed in the form of residual. Thus, if $V(S_1, S_2, \tau)$ is the exact solution to (5.2.1) then its approximate solution $P(S_1, S_2, \tau)$ introduces an error $E(S_1, S_2, \tau) = \frac{\partial P(S_1,S_2,\tau)}{\partial \tau} + \mathcal{L}P(S_1, S_2, \tau)$ (known as the residual). In our analysis, we fix the parameters of the rate of return, volatility, dividend, and the correlation between two assets to compute the values of the price and the Greeks of the options in all examples. The effect of change in the price of different underlying assets and time on the price of the options and their sensitivities are depicted graphically.

5.5.1 Max option

Example 5.5.1. *We consider the problem for which the rate of return r has the value 0.06, the volatilizes σ_1 and σ_2 are fixed at 0.2 and 0.25, respectively. The value of correlations are $\rho_{11} = \rho_{22} = 1$ and $\rho_{12} = \rho_{21} = 0.25$, the strike price has given the value $K = 100$, and the maturity T is equal to 1 year.*

This example demonstrates the efficiency of the 2D Haar wavelet method to compute the sensitivities and price of the European style max call option. In this option, associated with every asset the payoff has the same expiry $T = 1$ year, but on the day of expiry, only

Table 5.1: Computational error obtained for solving two-asset max option pricing problem for $J = 3$ with $T = 1$.

	S_2			
S_1	47	58	78	86
47	6.2172e-15	1.7764e-14	1.7764e-14	2.3093e-14
52	6.2172e-15	1.0658e-14	1.5987e-14	2.4869e-14
58	1.1546e-14	1.0658e-14	1.0658e-14	1.9540e-14
64	4.4409e-15	1.4211e-14	1.9540e-14	3.5527e-14
78	6.2172e-15	8.8818e-15	1.4211e-14	2.8422e-14
70	7.1054e-15	8.8818e-15	2.6645e-14	1.4211e-14
86	3.5527e-15	8.8818e-15	1.9540e-14	1.4211e-14
95	4.4409e-15	4.4409e-15	5.3291e-15	2.6645e-15

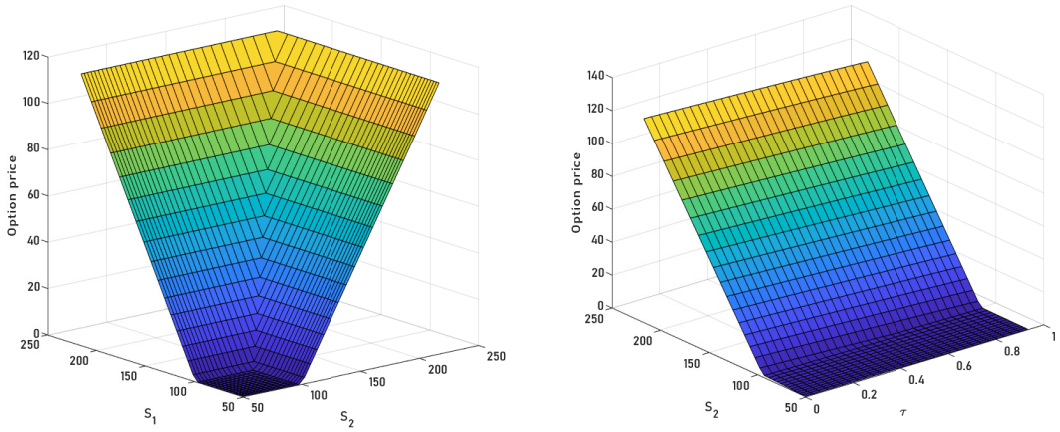

(a) $\tau = 0$ (b) $S_1 = 50$

Figure 5.1: The approximate value of two-asset max option price.

payoff of the best performing asset becomes the final payout. The computational domain for the transformed equation (5.2.2) is taken $[-0.8, 0.8] \times [-0.8, 0.8] \times [0, 1]$. In Table 5.1 the computational errors in the form of residual are tabulated at varying stock prices. The table illustrates that the proposed scheme is highly accurate for solving financially relevant option pricing problems.

The price of the max two-asset option is depicted graphically in Figure 5.1(a). It is worthy to note that the value of the price of the option approaches 0 for $S_1 < K$ and $S_2 < K$, which implies that the option is out of the money below the strike price. For $S_1 \geq K$ and $S_2 \geq K$, the price of the option increases linearly deduce that the option is in the money and the sudden shift and non-smoothness in the layer of linearity is due to the choice of payoff function taken for payout. The solution of equation (5.2.1) for the max option is presented in Figure 5.1(b) by setting $S_1 = 50$. Different sensitivities profiles for the two-asset max option are plotted in Figure 5.2. The surface plot of delta$_{S_1}$ profile depicted in Figure 5.2(a) reveals that the value of delta$_{S_1}$ lies between 0 and 1 which implies that the option is worthless for delta$_{S_1}$ approaches 0 and the option is in the money and will most likely be exercised for delta$_{S_1}$ approaches 1. A similar observation has been made in Figure 5.2(b) depicting the delta$_{S_2}$ *i.e.,* for fix value of S_1 the change in the option price with the change in the second underlying asset. Using these observations we can rebalance the initial hedges and construct the delta neutral position. Figures 5.2(c) and 5.2(d) represent the gamma profile for the max option with respect to S_1 and S_2, respectively. It reveals that the value of delta is almost constant for both $S_1, S_2 \geq K$, hence the gamma approaches 0. The change in the price of the option with the change in both the underlying assets is illustrated in Figure 5.2(e). From this figure it can be observed that there is a sudden rise in the value of cross-gamma near the initial and final boundaries corresponding to both the underlying assets together while there is a sudden drop in the value of cross-gamma near the initial boundary of one underlying asset and final boundary of another underlying asset is due to there different speeds of approaching the initial and terminal condition. Figure 5.2(f) shows the change in the option price with the decay in the time towards maturity T. The graphical analysis discloses that the value of

theta of the max option decreases with the increase in the stock price but there is a sudden rise in the value of theta near final boundaries corresponding to both the underlying assets because time decay is at its peak there.

5.5.2 Index option

This example illustrates the efficiency and accuracy of the proposed scheme to compute the index option and its Greeks. We will also discuss the behavior of its sensitivities in detail.

Example 5.5.2. *For numerical simulation of an index option, let the risk-free rate r of interest is 0.05, the value of σ_1 and σ_2 representing the volatilities are 0.2, and 0.1, respectively. The value of correlations are $\rho_{11} = \rho_{22} = 1$ and $\rho_{12} = \rho_{21} = 0.25$, the strike price is $K = 70$, and the time to maturity T is equal to 1 year.*

Here, the two-asset index option is interpreted over the domain $[-1, 1] \times [-1.5, 1.5] \times [0, 1]$ with portfolio weights $w_1 = 2$ and $w_2 = 1$ under the Black-Scholes framework with zero dividends. The residual errors that occur for different stock prices in solving the index option are presented in Table 5.2. Since the tabulated errors are highly accurate irrespective of the problem's geometry, it shows that the present numerical scheme provides a competitive approach for solving the higher-dimensional option pricing problems. It is perceived that to hit the error level 10^{-15}, Haar wavelet requires a very fewer number of points than other standard numerical methods.

Figure 5.3(a) illustrates the character of the index option price with respect to the two underlying assets of different weights. It is evident from the figure that the value of the option is 0 initially, and then it increases linearly for both the assets, but for S_1, it grows rapidly, which is justified from the fact that the portfolio weight for S_1 is greater than for S_2. The behavior of option price with respect to the single asset S_2 and time τ is graphically depicted in Figure 5.3(b). Figure 5.4 depicts various Greeks of the index option exerted in financial markets to rebalance the dynamic hedges, which is a trading decision. It is evident from the values of delta$_{S_1}$ and delta$_{S_2}$ depicted in Figures 5.4(a)

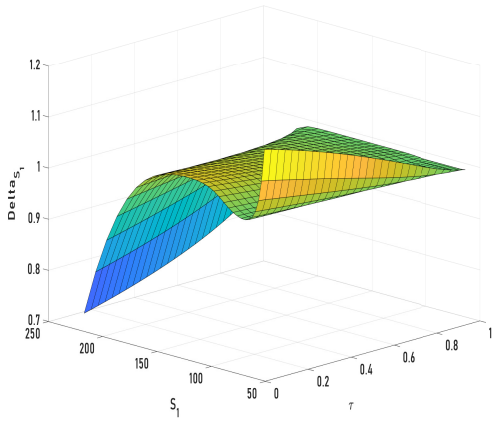

(a) $S_2 = 215$

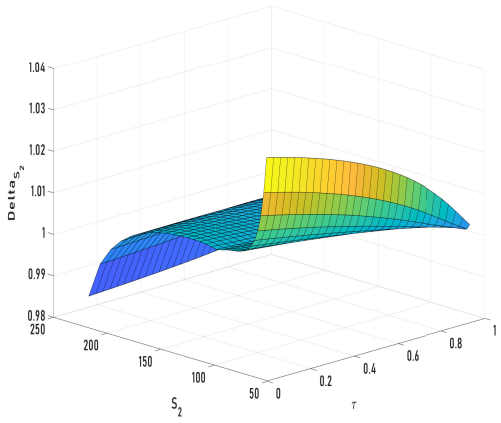

(b) $S_1 = 215$

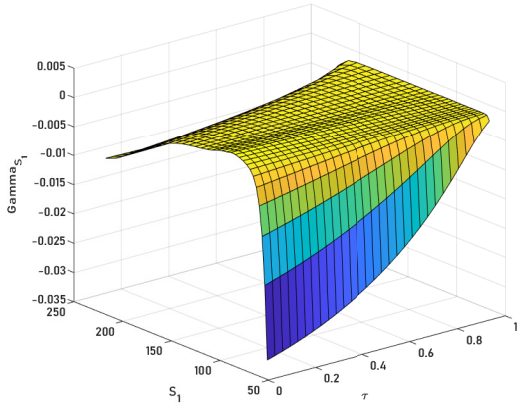

(c) $S_2 = 200$

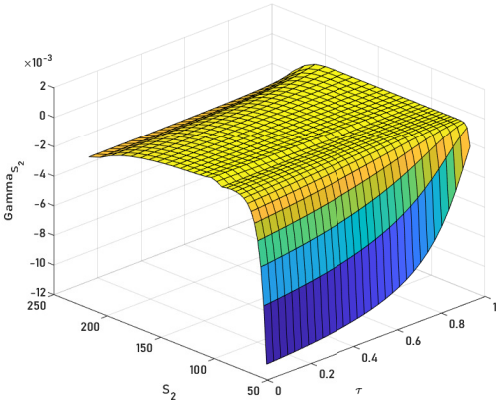

(d) $S_1 = 200$

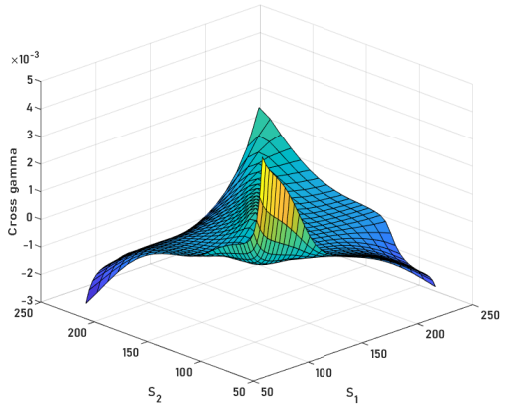

(e) $\tau = 0$

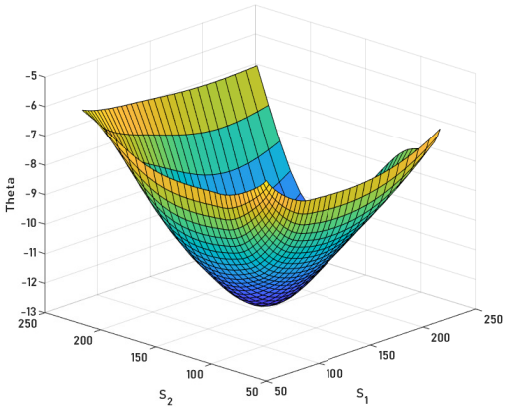

(f) $\tau = 0.013$

Figure 5.2: Sensitivities of max option with maturity $T = 1$.

Table 5.2: Computational error obtained for solving two-asset index option pricing problem for $J = 2$ with $T = 1$.

	S_2			
S_1	18	40	84	178
29	8.8818e-16	1.7764e-15	4.4409e-16	1.3323e-15
37	8.8818e-16	8.8818e-16	1.3323e-15	3.9968e-15
48	1.3323e-15	1.3323e-15	2.2204e-15	2.6645e-15
62	1.7764e-15	1.7764e-15	8.8818e-16	2.2204e-15
79	1.7764e-15	2.2204e-15	2.6645e-15	2.2204e-15
102	1.7764e-15	2.2204e-15	2.2204e-15	4.8850e-15
130	2.2204e-15	2.6645e-15	3.1086e-15	7.9936e-15
168	1.7764e-15	3.9968e-15	3.5527e-15	4.8850e-15

and 5.4(b) that for $S \geq K$ the option price increases linearly for both the assets but it rises with a double rate in case of S_1. Besides this, an abrupt change in the value of deltas (Figures 5.4(a) and 5.4(b)) and gammas (Figures 5.4(c) and 5.4(d)) for both assets near the strike price is due to the non-smoothness of the solution function at $K = 70$. Figure 5.4(e) reported the movement of S_2 on the delta sensitivity of the option to S_1. Moreover, the negative value of theta for a call option is in good agreement with the financial theory [111] and is depicted in Figure 5.4(f).

5.5.3 Multi-strike option

Example 5.5.3. *Consider the two-asset Black-Scholes equation with different strike prices* $K_1 = 100$, $K_2 = 120$ *and the other financial parameters as follows: risk free rate of return* $r = 0.05$, *volatilizes* $\sigma_1 = 0.2$ *and* $\sigma_2 = 0.1$, *correlations* $\rho_{11} = \rho_{22} = 1$ *and* $\rho_{12} = \rho_{21} = 0.25$, *with expiry* $T = 1$ *year.*

We consider this example to show the proficiency of the Haar wavelet method to approximate the non-smooth functions effortlessly by its excellent technique of approximating the spiked functions. Here, the simulations are carried out for the computational domain $[-1, 1] \times [-1, 1] \times [0, 1]$. The residual error that occurs in solving the multi-strike option is presented in Table 5.3. The reported numerical errors show that the present

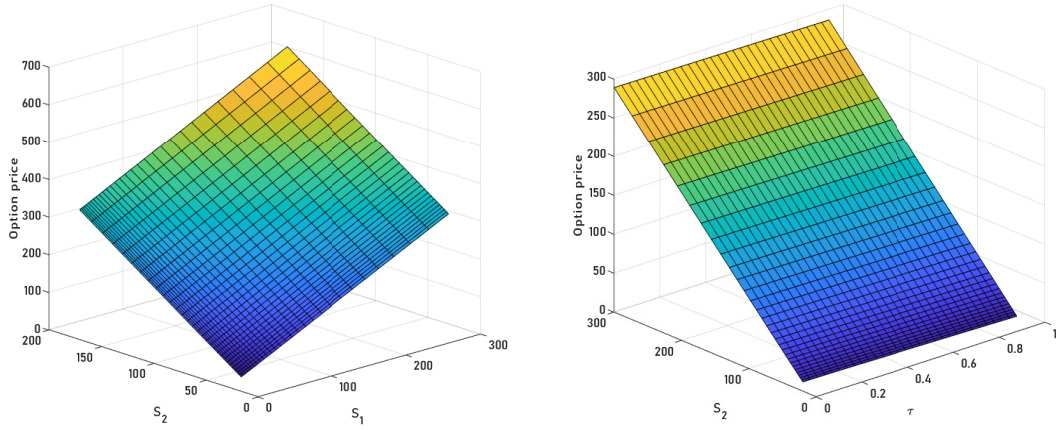

(a) $\tau = 0$ (b) $S_1 = 30$

Figure 5.3: The approximate value of two-asset index option price.

method is a reasonably better approach to solve the multi-asset option pricing problem.

The surface plot of the solution of problem (5.2.1) for the multi-strike option is presented in Figure 5.5(a) at $\tau = 0$. The difference in the peak of the option price function with respect to S_1 and S_2 instead of having the same domain is due to their different strike prices. The option price for a fixed value of S_1 $(= 40)$ is plotted in Figure 5.5(b). To hedge the directional risks associated with the moves of different parameters, we study the behavior of different sensitivities depicted in Figure 5.6. The sensitivity of the option to the price of S_1 and S_2 are presented in Figures 5.6(a) and 5.6(b), respectively. It is perceived from the figure that the value of delta for both the underlying asset approaches its maximum value of 1 as the option goes deep in the money, and it approaches 0 as the option goes deep out of the money. The sensitivity of delta to the movement of the underlying assets S_1 and S_2 are plotted in 5.6(c) and 5.6(d), respectively. It is perceptible that near maturity, the gammas approach 0 since deltas are close to 1. Moreover, the study of cross-gamma depicted in Figure 5.6(e) is important part of risk management and with the increase in the number of asset cross-gamma become more important than gamma. The value of theta depicted in Figure 5.6(f) is negative which is in good agreement with the theoretical fact in finance that the value of theta for a call option is always negative

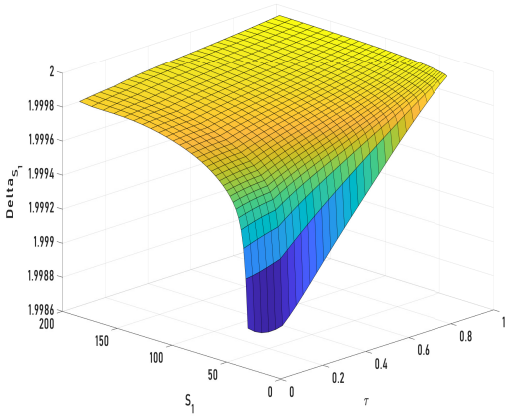

(a) $S_2 = 300$

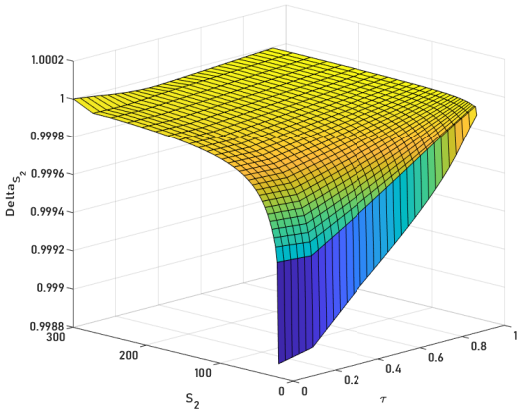

(b) $S_1 = 185$

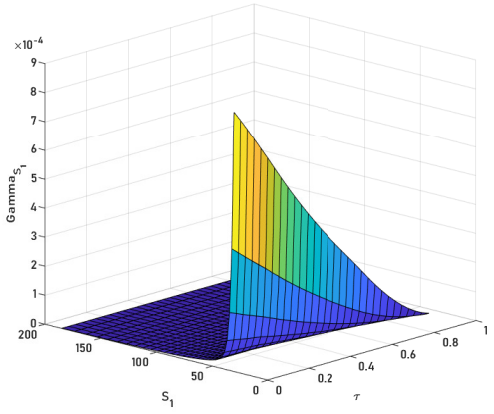

(c) $S_2 = 270$

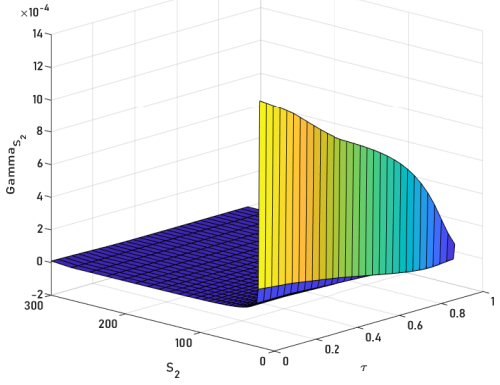

(d) $S_1 = 170$

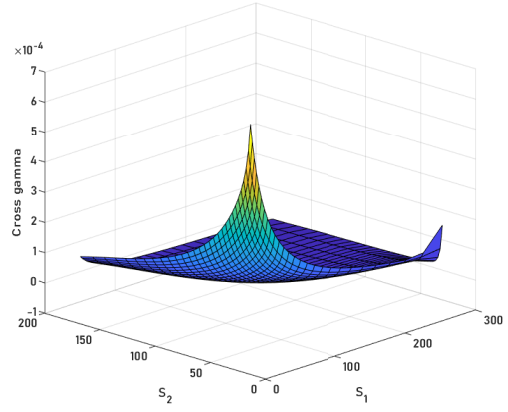

(e) $\tau = 0$

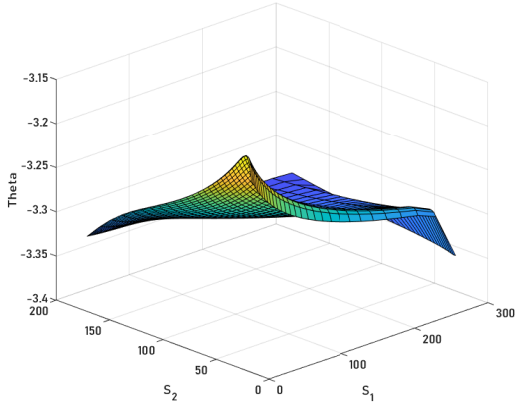

(f) $\tau = 0.013$

Figure 5.4: Sensitivities of index option with maturity $T = 1$.

Table 5.3: Computational error obtained for solving two-asset multi-strike option pricing problem for $J = 3$ with $T = 1$.

	S_2			
S_1	46	77	127	210
39	2.6645e-15	4.4409e-15	4.4409e-15	6.2172e-15
50	3.5527e-15	1.2434e-14	1.2434e-14	1.0658e-14
64	4.4409e-15	1.3323e-14	2.3093e-14	2.4869e-14
82	6.2172e-15	1.7764e-14	1.0658e-14	3.3751e-14
106	2.6645e-15	1.7764e-14	1.4211e-14	2.1316e-14
136	4.4409e-15	1.7764e-14	3.5527e-14	4.2633e-14
175	6.2172e-15	1.5987e-14	8.8818e-15	4.6185e-14
225	5.3291e-15	1.7764e-14	1.0658e-14	1.4211e-14

as the passing of time will lower the value of the option. It is significant to note that the rebalancing of initial hedges is important here since the dynamics of the underlying assets in these options change dramatically.

5.6 Concluding observations and future scope

In this chapter, we have presented a wavelet-based approximation technique to study and analyze the physical and numerical aspects for a variety of option pricing problems with more than one asset and their Greeks under the Black-Scholes framework. The multi-scaling approximation technique of the 2D Haar wavelet is used to estimate the sensitivities and price the different multi-dimensional options. It is difficult to approximate the non-smooth payoff functions and discontinuous Greeks using the standard numerical methods but the Haar wavelet technique of estimating the spiked functions fix this obstruction effortlessly. The present wavelet scheme is convergent and requires fewer computational nodes than traditional methods to achieve a high level of accuracy. We can see that to hit the error level 10^{-15}, Haar wavelet requires a hundred times fewer points than standard numerical methods. Furthermore, it is more economical *i.e.,* the time taken to get this level of accuracy is significantly very less. Numerical simulation shows that the proposed

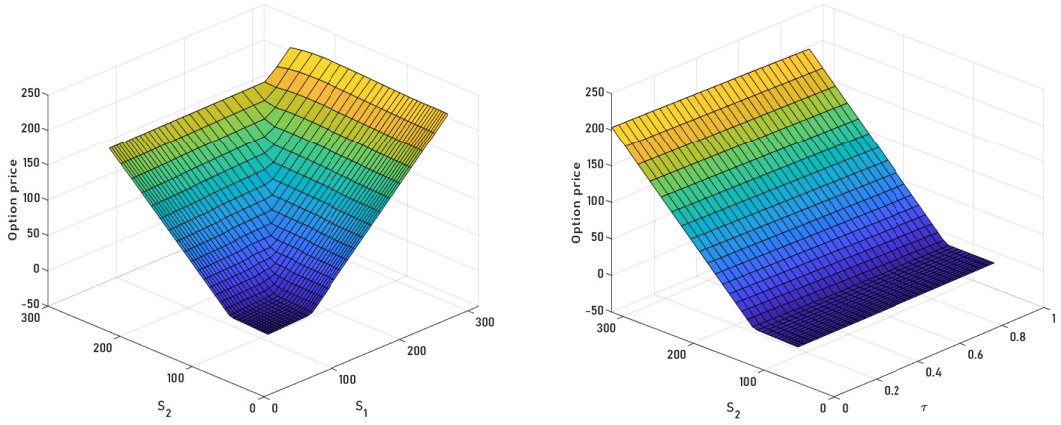

(a) $\tau = 0$ (b) $S_1 = 40$

Figure 5.5: The approximate value of two-asset multi-strike option price.

method is a reasonably better approach to solve the multi-dimensional option pricing problems and their sensitivities. The proof of the convergence of the present scheme signifies that the method is stable, so the rise in the error is not because of the instability issue. The sensitivities of different options are investigated and depicted graphically from which it is observed (already explained in the previous section) that the extracted results and observations are in good agreement with the financial theories. The motivational work of the study of various sensitivities of diverse multi-asset options leads to a significant impact on the hedging strategies used by different trading institutes. The convergence rate of the proposed scheme is independent of the number of underlying assets and so this approach should be increasingly attractive as the dimension of the problem grows. The proposed scheme can be extended to other option pricing problems such as to investigate the sensitivities and explore hedging strategies of various path-independent binary options under the Black-Scholes environment.

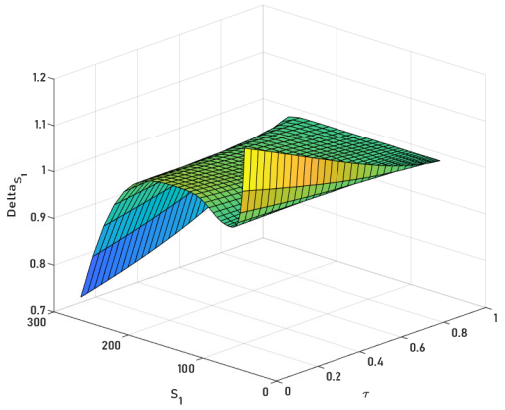

(a) $S_2 = 315$

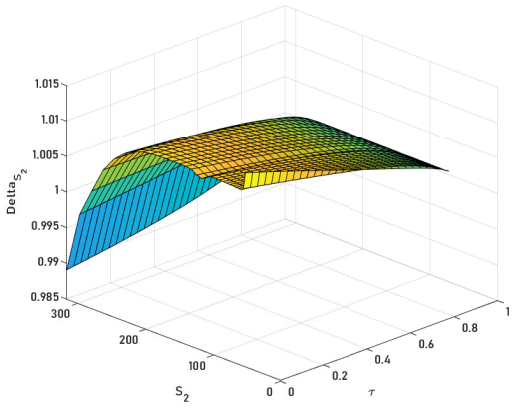

(b) $S_1 = 265$

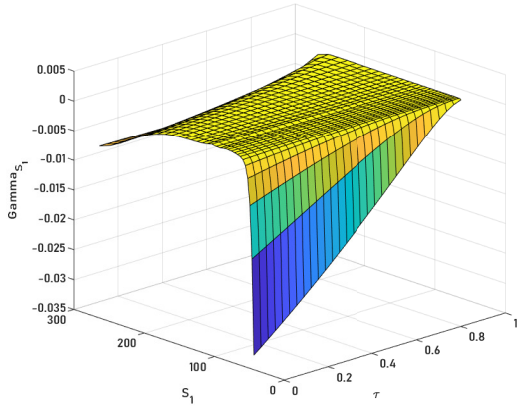

(c) $S_2 = 300$

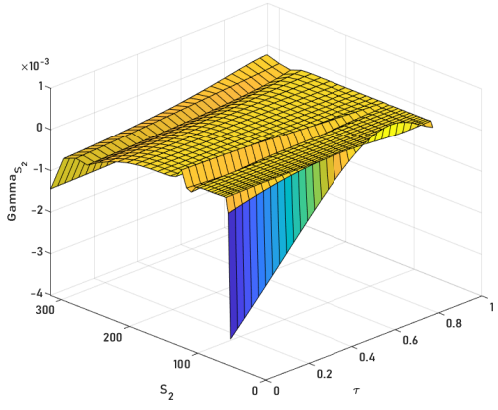

(d) $S_1 = 250$

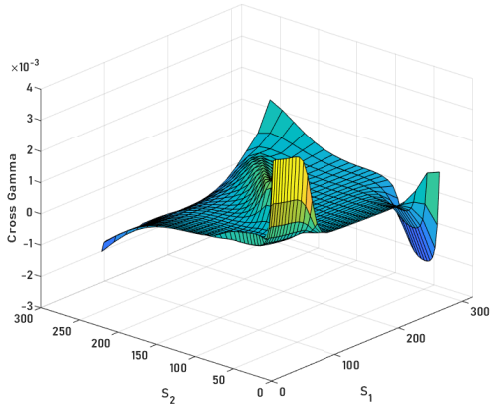

(e) $\tau = 0$

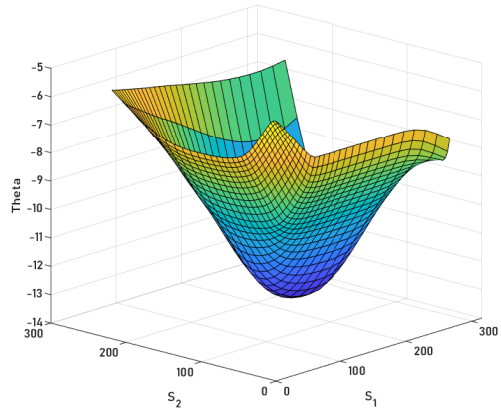

(f) $\tau = 0.013$

Figure 5.6: Sensitivities of multi-strike option with maturity $T = 1$.

Chapter 6

A highly accurate numerical approach for retrieving the discontinuous behavior of the hedging parameters

---

6.1 Introduction

Options are the most common instruments on the trade markets and their valuation is of immense interest to the financial world. In the field of trading, there exists a large variety of options, which can be traded in different styles. The price of an option grounds on different parameters, which limit the behavior of the value of an option. As a resultant, the investigation of the options with respect to the parameters which affect their price is the most interesting topic for researchers. In financial mathematics, such sensitivity of the price of an option with respect to some fundamental parameters is referred to as Greeks (hedging parameters) [29]. Besides this Greeks can also be used in the context of actuarial-specific risk management such as to hedge short and long term risks, profit guarantee from equity linked insurance, pension funding. Thus, these hedging parameters are effective tools for managing the risk in an option position [47]. Any attempt at valuing

and studying the behavior of these Greeks leads the holder towards a smart move. There are several methods for calculating an option's price and Greeks, but there is always a need for a more efficient and accurate method. Also, since the payoff function and Greeks are non-smooth in nature, it is a challenging task to solve them with the classical time marching schemes.

In this chapter, we extensively study the orthogonal spline collocation method with Rannacher time-marching scheme for free boundary value option pricing problems. Such financial problems commonly feature non-smooth payoff functions that cause inaccuracies in approximating the solution and its derivatives. As a result, unlike for the problems with the smooth initial data, the quadratic convergence is not realized by the Crank-Nicolson time-stepping scheme for these problems. Furthermore, the non-smoothness in the initial condition leads to serious degradation in the convergence rates and spurious oscillations near the discontinuity. The rationale is that classical schemes strongly rely on the smoothness of the initial data. To smoothen the data, a rigorous time-marching scheme referred to as Rannacher time-stepping scheme is introduced for the American option's price diagnosed by a linear complementarity problem. Moreover, with careful analysis, second and fourth orders of convergence are established for the present scheme in the temporal and spatial directions, respectively. To validate the theory, the numerical results for two test problems are presented in the form of tables and graphs. These results show that the present scheme achieves higher accuracy and is sufficient to restore the expected behavior.

6.1.1 Overview

In finance, the most effective and widely used model for pricing an option is the famous Black-Scholes model [13], named after the pioneers Fischer Black and Merton Scholes. This model was extended by Merton [112]. We consider here the basic model for the American option and a similar treatment can also be done for other extended models for various options. The payoff function of the option pricing problems is non-smooth *i.e.,* the terminal condition defined in the Black-Scholes partial differential equation is

piecewise smooth, which results in the poor estimation of the Greeks [7]. Spikes in the derivative function (Greeks) lead to decay in the convergence rate of a numerical scheme. A super convergent method that deals with the non-smooth behavior of the American option and its Greeks is proposed in this chapter. A lot of work has been done to compute the price of the option but there is always a need for more accurate methods which tackle their non-smooth behavior with ease and at the economical computational cost. Tavella and Randall [59] presented a finite difference numerical scheme for pricing the options and instigated that the discontinuity in the terminal condition leads to an increase in the discretization error, which affects the rate of convergence. For the last two decades, amazing work has been done to improve the approximation in space for option pricing problems. In [113], Longstaff and Schwartz developed a linear unconditionally stable least square Monte Carlo simulation method. Ikonen and Toivanen [17] suggested an operator splitting method for linear complementarity problem arising for American option and proved that it is more efficient than the projected SOR, while the accuracy of both the methods is linear. Furthermore, the integral method proposed by Kim [114] and the analytical approximations given by Barone-Adesi *et al.* [115, 116] are first-order accurate in space.

Plenteous research has been done by various finite difference approaches to estimate the price of the option but much focus has been paid only to improve the accuracy in space for e.g., in [18], Zhao *et al.* designed a compact finite difference scheme for American option pricing, which is capable to achieve a quadratic rate of convergence in space but at the cost of more computational time. In 2011, Cen and Le [117] presented a numerical scheme for generalized Black-Scholes equation based on central difference spatial discretization on a piecewise uniform mesh and an implicit time-stepping scheme. They proved that the scheme is stable and second-order convergent in space. Kwon and Lee [118] proposed a three time level scheme that results in a linear system with tridiagonal matrices. Furthermore, they have investigated that the scheme is stable and second-order convergent in the discrete L^2-norm. Other numerical schemes based on the finite difference approach can be seen in [60, 75, 119, 120]. All the above schemes

are second-order convergent in space but only first-order accurate in time. In context to the comparison of the spline interpolation with the difference schemes, Caglar *et al.* [121] have analyzed that there is a big difference in the computational errors, although no remarkable difference is noticed in the rates of convergence. Later, Chang *et al.* have also examined that the spline interpolation is more efficient and feasible than the finite difference schemes in order to solve the boundary value problem (BVP) of linear ODEs. For more details the readers are referred to [122] and the references therein. Many authors considered different numerical approaches based on the spline interpolation to approximate the price of an option. Khabir and Patidar [123] presented a classical Euler implicit scheme with B-spline based collocation method to compute the price of the vanilla options. They observed that the B-spline method is efficient than the quasi-radial basis functions based numerical scheme. In 2017, Rashidinia and Jamazadeh [124] developed an algorithm based on a modified cubic B-spline method for American and Barrier options. The order of convergence is found to be approximately two and one in the spatial and temporal directions, respectively. In literature there are many numerical schemes based on spline interpolation to approximate the option price but have a low order of accuracy [125–127] and provide little analysis on the misbehaving temporal convergence rate. All the above investigations are concerned with the accuracy in space but due to the low order of convergence in time the global error decreases with the linear rate. To achieve a higher rate of convergence in both directions a combination of smoothing and modified time-stepping method with a highly accurate numerical scheme in space is required.

In [128], Zlamal has shown that the backward Euler scheme provides unconditionally smoothing results since it is '*strongly A-stable*'. On the other hand, being only *A-stable* the Crank-Nicolson (CN) scheme cannot be expected to have the smoothing property unconditionally since the classical convergence schemes rely on smoothness assumption for the underlying data violated in the case of American option pricing. To resolve the non-smoothness of the initial data, different smoothness techniques are suggested by many authors. In [129], Giles and Carter observed that the accuracy of the CN scheme is inadequate due to the reduced regularity in the initial data. They have also examined

that the CN scheme is unconditionally stable in the L^2-norm (for more detail refer to [130]). They have also investigated a Rannacher time-stepping technique that performs better than the Euler backward and the classical CN schemes. Using this new technique, the non-smoothness of the initial condition can be reduced by using the strongly stable Backward Euler (BE) scheme for the first four time steps and then to improve the accuracy for the rest of the time-steps CN is used. In 2016, Mashayekhi and Hugger [131] analyzed and discussed the conjunction properties of three different time stepping schemes with finite difference method. They have concluded that the Rannacher time stepping scheme removed the high frequency oscillations and provided second order convergence in time. In [132], Mohammadi proposed a quintic spline based collocation scheme to solve the Black-Scholes equation. The author has compared the results using different time-stepping schemes and shown that Rannacher time-marching scheme provides better convergence in time. The method has been proved to be convergent of order $O(h^3 + k^2)$ in the maximum-norm. But due to the use of higher order polynomials, it has a high computational cost.

This chapter also provides an overview of the formulation, analysis, and implementation of the spline collocation method at Gauss points. The chapter's aim is not to touch the deep concepts of finance but to develop an efficient algorithm to solve the problems arising in financial mathematics. So, it does not require any prerequisite knowledge of finance, however, it can be applied to all the financial models. Furthermore, this chapter provides a new insight in improving the order of convergence in both directions, for problems with discontinuities. We outline possible steps explicitly to implement and extend the present scheme towards different non-smooth problems for future computational studies. In particular, in this work we have studied the linear complementarity American option pricing problem with moving boundaries under the Black-Scholes framework to estimate the option's price and the hedging parameters. To improve the accuracy of the approximation in space a highly accurate orthogonal spline collocation method is presented. Moreover, since the proposed problem has non-smooth underlying data, in order to improve the accuracy in time, instead of the BE and CN schemes we have considered the Rannacher time-marching scheme. The computational results show that away from singularity the

conjunction scheme yields good results and does not increase the computational cost. The performance and proficiency of the proposed scheme are validated through two test examples and by comparing with the existing results.

The remainder of the chapter is organized as follows: first, we state the linear complementarity American option pricing problem as a moving boundary value problem in Section 2. Then in Section 3, we comprehensively discuss the orthogonal spline collocation technique together with an overview of the analytical results that require to prove the convergence. The convergence analysis of the present scheme in spatial direction is discussed in Section 4. Then, we shift the focus on the different time-marching schemes that we conjunct with the proposed super-convergent OSC method and prove the overall convergence of the proposed numerical scheme. Moreover, we demonstrate the performance and accuracy of the present method in Section 5. Finally, concluding remarks and future scopes are shared in the last section.

Nomenclature	
$\mathcal{P}$	Price of the option
$\mathcal{S}$	Current stock price
τ	time period
$\mathbb{K}$	Strike price
$\mathbb{T}$	Maturity
ν	Transformed variable $\mathcal{P}$
x	Transformed variable $\mathcal{S}$
t	Transformed variable τ
r	Rate of interest
σ	Volatility
δ	Dividend Yield
$\mathcal{Q}$	Payoff function
α_1	Transformed finite left boundary
α_2	Transformed finite right boundary
A^+	$\max\{A, 0\}$

Remark. Throughout the manuscript C is a generic positive constant, independent of the spatial and temporal discretization parameters. Furthermore, C can take different values at different places.

6.2 Black-Scholes option pricing model

There are many approaches to price American options and evaluate their Greeks but the most effective one is based on the partial differential problem. The linear complementarity problem under the Black-Scholes framework is an proficient way of pricing American-type options. Mathematically, it is a final value problem with free-boundary on an unbounded domain. Define the differential operator

$$\mathcal{L}_{\mathcal{P}} \equiv \frac{\partial}{\partial \tau} + \frac{1}{2}\sigma^2 \mathcal{S}^2 \frac{\partial^2}{\partial \mathcal{S}^2} + (r-\delta)\mathcal{S}\frac{\partial}{\partial \mathcal{S}} - rI, \quad \mathcal{S} \in (0,\infty), \quad \tau \in [0,\mathbb{T}),$$

where $\delta \geq 0$ represents the dividend yield, $r \geq 0$ is the interest rate parameter, and $\sigma > 0$ denotes the volatility which is the unpredictable change in the price of the security (underlying asset) over time. In case of American-style call option, if $\mathcal{Q} = (\mathcal{S} - \mathbb{K})^+$ is the payoff function where $\mathbb{K}$ is the strike price, then for $\mathcal{P}(\mathcal{S},\tau) > \mathcal{Q}$ the Black-Scholes equation holds, *i.e.,* $\mathcal{L}_{\mathcal{P}}\mathcal{P}(\mathcal{S},\tau) = 0$. Although for $\mathcal{P}(\mathcal{S},\tau) = \mathcal{Q}$, it is feasible to exercise the option. Through cumulative impact of both the cases, $\mathcal{P}(\mathcal{S},\tau)$ the price of an American-style option satisfies the partial differential complementarity problem

$$\mathcal{L}_{\mathcal{P}}\mathcal{P}(\mathcal{S},\tau)(\mathcal{P}-\mathcal{Q}) = 0, \tag{6.2.1a}$$

subject to

$$\mathcal{L}_{\mathcal{P}}\mathcal{P}(\mathcal{S},\tau) \leq 0, \quad (\mathcal{P}-\mathcal{Q}) \geq 0. \tag{6.2.1b}$$

By the same token, we get a similar differential equation for put option of American-style with $\mathcal{Q} = (\mathbb{K} - \mathcal{S})^+$. In order to price the option along with the above defined constraints

the left boundary condition is imposed as

$$\lim_{\mathcal{S}\to 0}\mathcal{P}(\mathcal{S},\tau)=\begin{cases}0, & \text{for call,}\\ (\mathbb{K}-\mathcal{S})^{+}, & \text{for put,}\end{cases} \tag{6.2.1c}$$

i.e., for $\mathcal{S}\to 0$, in case of a call, it is valueless to exercise the option besides this, put option is rich in cash. The right boundary condition is given as

$$\lim_{\mathcal{S}\to\infty}\mathcal{P}(\mathcal{S},\tau)=\begin{cases}(\mathcal{S}-\mathbb{K})^{+}, & \text{for call,}\\ 0, & \text{for put,}\end{cases} \tag{6.2.1d}$$

i.e., for $\mathcal{S}\to\infty$, a call option is highly profitable, while a put option is worthless.

Now, by considering $\tau=\mathbb{T}-\frac{2t}{\sigma^2}$, the final value problem is reformulated into a dimension free initial value problem for deep contemplation on a problem that is important in terms of business and to make it more convenient for numerical implementation. Furthermore, in order to obtain a finite domain, the unbounded domain is truncated on introducing a logarithmic change in $\mathcal{S}$ by defining a new variable $x=\ln(\mathcal{S}/\mathbb{K})$. Also, we take $\mathcal{P}(\mathcal{S},\tau)=\mathbb{K}e^{-\left[2\left(\frac{r-\delta}{\sigma^2}\right)-1\right]\frac{x}{2}-\left[\frac{1}{4}\left(2\left(\frac{r-\delta}{\sigma^2}\right)-1\right)^2+\frac{2r}{\sigma^2}\right]t}\nu(x,t)$, hence the equation (6.2.1a) is deduced in

$$\left(\frac{\partial\nu}{\partial t}-\frac{\partial^2\nu}{\partial x^2}\right)(\nu-\tilde{f})=0, \tag{6.2.2a}$$

and the constraints are reduced into

$$\frac{\partial\nu}{\partial t}-\frac{\partial^2\nu}{\partial x^2}\geq 0 \quad \text{and} \quad \nu-\tilde{f}\geq 0, \tag{6.2.2b}$$

where $\tilde{f}(x,t)$ is formulated as

$$\tilde{f}(x,t)=\begin{cases}e^{\frac{t}{4}\left(\frac{2(r-\delta)}{\sigma^2}-1\right)^2+\frac{2r}{\sigma^2}t}\left(e^{\frac{x}{2}\left(\frac{2(r-\delta)}{\sigma^2}+1\right)}-e^{\frac{x}{2}\left(\frac{2(r-\delta)}{\sigma^2}-1\right)}\right)^{+}, & \text{for call,}\\ e^{\frac{t}{4}\left(\frac{2(r-\delta)}{\sigma^2}-1\right)^2+\frac{2r}{\sigma^2}t}\left(e^{\frac{x}{2}\left(\frac{2(r-\delta)}{\sigma^2}-1\right)}-e^{\frac{x}{2}\left(\frac{2(r-\delta)}{\sigma^2}+1\right)}\right)^{+}, & \text{for put,}\end{cases}$$

where $(x,t) \in (-\infty,\infty) \times (0,T_1]$ such that $T_1 = \frac{\sigma^2 \mathbb{T}}{2}$. After transformation the initial condition for call and put options are

$$\nu(x,0) = \tilde{f}(x,0), \tag{6.2.2c}$$

and in terms of new variables the boundary conditions are

$$\lim_{x\to-\infty} \nu(x,t) = \lim_{x\to-\infty} \tilde{f}(x,t), \tag{6.2.2d}$$

and

$$\lim_{x\to\infty} \nu(x,t) = \lim_{x\to\infty} \tilde{f}(x,t). \tag{6.2.2e}$$

In summary, in addition to the boundary conditions, we require $\frac{\partial \nu(x,t)}{\partial t} - \frac{\partial^2 \nu(x,t)}{\partial x^2} = 0$ as well as

$$\nu(x,0) = \tilde{f}(x,0), \quad \text{and} \quad \nu(x,t) \geq \tilde{f}(x,t).$$

For numerical implementation, the interval $(-\infty,\infty)$ is truncated into a bounded interval, $\Omega = (\alpha_1,\alpha_2)$, where in order to nullify the computational error α_1 and α_2 are chosen to be big enough negative and positive numbers, respectively.

6.3 Orthogonal spline collocation method

6.3.1 Preliminaries

Discretize the temporal domain $[0,T_1]$ in to N_t parts of equal length $k = T_1/N_t$, so that the nodal points are $t_n = nk$, $n = 0,1,2,\ldots,N_t$. Now, say $\rho_h = \{x_j\}_{j=0}^{N_x}$ be the partition of $\overline{\Omega}$ such that

$$\alpha_1 = x_0 < x_1 < \ldots < x_{N_x-1} < x_{N_x} = \alpha_2,$$

where N_x be a positive integer with the mesh size $h = x_j - x_{j-1},\ j = 1,2,\ldots,N_x$. Let $\mathbb{P}_r(\Omega_j)$ be the set of all polynomials of degree $\leq r$ defined on $\Omega_j = (x_{j-1},x_j)$ and $C^1(\Omega)$ be the space of functions which are one time continuously differentiable on Ω. Hence, the

subspace of piecewise polynomials of $H^1(\Omega)$ can be defined as

$$M_1^r = \{\mu \mid \mu \in C^1(\Omega),\ \mu|_{\Omega_j} \in \mathbb{P}_r(\Omega_j),\ j = 1, 2, \ldots, N_x\},\ r \geq 3.$$

One can see that M_1^r is a linear space of dimension $N_x(r-1) + r + 1$.

Let δ_k and ω_k are the nodes and weights, respectively, for the $(r-1)$ Gauss-Legendre quadrature rule on Ω. Moreover, let

$$\mathcal{G} = \{\zeta\}_{j=1,k=1}^{N_x,r-1},$$

be the set of Gauss points on Ω, expressed as

$$\zeta_{2(j-1)+k} = x_{j-1} + h\delta_k, \quad j = 1, 2, \ldots, N_x, \quad k = 1, 2, \ldots, r-1.$$

Collection of these Gauss points form a set of collocation points in the OSC scheme. For any $\chi, \psi \in C^0(\overline{\Omega})$, the discrete inner product can be defined as

$$\langle \chi, \psi \rangle = \sum_{j=1}^{N_x} \langle \chi, \psi \rangle_j = \sum_{j=1}^{N_x} \sum_{k=1}^{r-1} \omega_{j,k} \chi(\zeta_{j,k}) \psi(\zeta_{j,k}).$$

This inner product gives rise to the norm

$$|\chi|_{\mathcal{D}} = \left(\sum_{j=1}^{N_x} |\chi|_j^2 \right)^{\frac{1}{2}},$$

where

$$|\chi|_j = \langle \chi, \chi \rangle_j^{\frac{1}{2}} = \left(\sum_{k=1}^{r-1} \omega_{j,k} \chi^2(\zeta_{j,k}) \right)^{\frac{1}{2}}.$$

If $\|.\|_{L^2}$ denotes the usual L^2-norm on the interval Ω, then from ([133], Lemma 3.1),

$$-\langle u, w_{xx} \rangle \geq (u_x, w_x), \quad u, w \in M_1^r,$$

so that

$$-\langle u, u_{xx}\rangle \geq \|u_x\|_{L^2}^2, \quad u \in M_1^r,$$

and

$$|u_x|_{\mathcal{D}} \leq \|u_x\|_{L^2}, \quad u \in M_1^r.$$

We use the remarkable fact that $(r-1)$ point Gauss quadrature is exact for a polynomial g of degree $\leq 2r-3$, so that $\langle g, 1\rangle = \int_0^1 g(x)\,dx,\ g \in \mathbb{P}_{2r-3}$. Hence, $|u_{xx}|_{\mathcal{D}} = \|u_{xx}\|_{L^2},\ u \in M_1^r$.

Let $H^m(\Omega)$, $H_0^m(\Omega)$ represent the regular Sobolev spaces on Ω, and $L^p(Y)$ be the set of vector valued functions from $[0, T_1]$ to Y, so that

$$\|\chi\|_{L^p(Y)}^p = \int_0^{T_1} \|\chi\|_Y^p\,dt, \quad 1 \leq p < \infty,$$

where Y with $\|.\|_Y$ is a normed linear space with prescribed norm, and for $p = \infty$

$$\|\chi\|_{L^\infty(Y)} = \sup_{0\leq t\leq T_1} \|\chi\|_Y.$$

The weighted H^1-norm, that we consider is defined as

$$\|\chi\|_{H^1(\Omega)} = \left(\|\chi_x\|_{L^2}^2 + |\chi|_{\mathcal{D}}^2\right)^{\frac{1}{2}}.$$

6.3.2 Important inequalities

Following inequalities and results will be used to prove the convergence of OSC scheme.

- **Cauchy-Schwartz inequality :** Let Y be a normed linear space and $u_1, u_2 \in Y$, then

$$|\langle u_1, u_2\rangle| \leq \|u_1\|\|u_2\|.$$

- **Poincaré inequality :** For all, $u \in W_0^{1,p}$ (Sobolev space) and $1 \leq p < \infty$

$$\|u\|_{L^p} \leq C\|\nabla u\|_{L^p}.$$

- **Young's inequality :** Let P and Q are non negative real numbers such that $a, b > 0$ and $\frac{1}{a} + \frac{1}{b} = 1$, then

$$PQ \leq \frac{P^a}{a} + \frac{Q^b}{b}.$$

6.3.3 Important lemmas

The following two lemmas will be used in the proof of the main theorem.

Lemma 6.3.1. *Let $\nu \in H^{r+3}(\Omega_j), j = 1, 2, \ldots, N_x$, and $\nu_{\mathcal{H}}$ is the interpolant of ν. If $\phi = \nu - \nu_{\mathcal{H}}$ then, for $s_1 = 0, 1$,*

$$\left| \frac{\partial^{s_1+s_2}\phi}{\partial t^{s_1}\partial x^{s_2}} \right|_j \leq Ch^{r+1-s_2} \left\| \frac{\partial^{s_1}\nu^{(r+1)}}{\partial t^{s_1}} \right\|_{L^2(\Omega_j)}, \quad s_2 = 0, 1,$$

$$\left| \frac{\partial^{s_1}\phi_{xx}}{\partial t^{s_1}} \right|_j \leq Ch^{r} \left\| \frac{\partial^{s_1}\nu^{(r+2)}}{\partial t^{s_1}} \right\|_{L^2(\Omega_j)},$$

$$\left\langle \frac{\partial^{s_1}\phi_{xx}}{\partial t^{s_1}}, 1 \right\rangle \leq Ch^{r+\frac{3}{2}} \left\| \frac{\partial^{s_1}\nu^{(r+3)}}{\partial t^{s_1}} \right\|_{L^2(\Omega_j)}.$$

The proof of this lemma can be seen in [133].

Lemma 6.3.2. *If $\nu \in H^{r+1}(\Omega) \cap H_0^1(\Omega)$ then*

$$\|\phi\|_{H^j} \leq Ch^{r+1-j}\|\phi\|_{H^{r+1}}, \quad j = 0, 1, 2.$$

The proof of this lemma is followed by the Peano Kernel theorem.

Hermite cubic functions

When $r = 3$, the space M_1^3 is known as the space of piecewise Hermite cubic functions with dimension $2N_x + 4$. To define the basis functions of M_1^3, let

$$\mu_1(x) = -2x^3 + 3x^2, \quad \text{and} \quad \mu_2(x) = x^3 - x^2,$$

then the piecewise Hermite cubic functions can be expressed as

$$s_0(x) = \begin{cases} \mu_1(1 - l_0(x)), & x \in \Omega_1, \\ 0, & \text{otherwise}, \end{cases}$$

$$s_{N_x}(x) = \begin{cases} \mu_1(l_{N_x}(x)), & x \in \Omega_{N_x}, \\ 0, & \text{otherwise}, \end{cases}$$

and for $1 \leq i \leq N_x - 1$

$$s_i(x) = \begin{cases} \mu_1(l_{i-1}(x)), & x \in \Omega_i, \\ \mu_1(1 - l_i(x)), & x \in \Omega_{i+1}, \\ 0, & \text{otherwise}. \end{cases}$$

Also,

$$w_0(x) = \begin{cases} -h\mu_2(1 - l_0(x)), & x \in \Omega_1, \\ 0, & \text{otherwise}, \end{cases}$$

$$w_{N_x}(x) = \begin{cases} h\mu_2(l_{N_x}(x)), & x \in \Omega_{N_x}, \\ 0, & \text{otherwise}, \end{cases}$$

and for $1 \leq i \leq N_x - 1$

$$w_i(x) = \begin{cases} h\mu_2(l_{i-1}(x)), & x \in \Omega_i, \\ -h\mu_2(1 - l_i(x)), & x \in \Omega_{i+1}, \\ 0, & \text{otherwise}. \end{cases}$$

Here s_i and w_i are also known as the value function and slope function, respectively, at x_i which collectively form the basis of M_1^3.

6.3.4 Spatial discretization

In this scheme, we seek $V \in M_1^3$ such that

$$\mathcal{L}V(\zeta,t) = 0, \quad \forall \zeta \in \mathcal{G}, \quad t \in (0, T_1], \tag{6.3.1a}$$

where $\mathcal{L}V(\zeta,t)$ is given by $\left(\frac{\partial V(\zeta,t)}{\partial t} - \frac{\partial^2 V(\zeta,t)}{\partial x^2}\right)(V(\zeta,t) - \tilde{f}(\zeta,t))$,

$$\frac{\partial V(\zeta,t)}{\partial t} - \frac{\partial^2 V(\zeta,t)}{\partial x^2} \leq 0, \quad (V(\zeta,t) - \tilde{f}(\zeta,t)) \geq 0, \tag{6.3.1b}$$

$$V(\zeta,0) = \tilde{f}(\zeta,0), \tag{6.3.1c}$$

$$\lim_{\zeta \to -\infty} V(\zeta,t) = \lim_{\zeta \to -\infty} \tilde{f}(\zeta,t), \tag{6.3.1d}$$

$$\lim_{\zeta \to \infty} V(\zeta,t) = \lim_{\zeta \to \infty} \tilde{f}(\zeta,t). \tag{6.3.1e}$$

The solution to the LCP (6.3.1) can be written as

$$V(x,t_n) = \sum_{j=0}^{N_x} \beta_{j,n} s_j(x,t_n) + \gamma_{j,n} w_j(x,t_n),$$

the substitution of this form of the solution function in Equation (6.3.1) yields the collocation equations in addition to the given constraints as well as the boundary conditions. Here s_j and w_j are associated with the collocation points $\zeta_{j,k}$, defined as

$$\zeta_{2(j-1)+1} = x_{j-1} + h\delta_1, \ j = 1, 2, \ldots, N_x,$$
$$\zeta_{2(j-1)+2} = x_{j-1} + h\delta_2, \ j = 1, 2, \ldots, N_x,$$

where $\delta_1 = \frac{1}{2}\left(1 - \frac{1}{\sqrt{3}}\right)$ and $\delta_2 = \frac{1}{2}\left(1 + \frac{1}{\sqrt{3}}\right)$. Finally, calculate the coefficients $\beta_{j,n}$ and $\gamma_{j,n}$ at each time step. Subsequently, use $S_j = \mathbb{K}e^{x_j}$ and $\tau_n = T - \frac{2t_n}{\sigma^2}$, where $j = 1, 2, \ldots, N_x = N_{\mathcal{S}}$ and $n = 1, 2, \ldots, N_t = N_\tau$ to add the coordinate transformation for applying back substitution, to obtain the solution of the original Equation (6.2.1).

6.4 Convergence analysis of proposed method with Rannacher time-marching scheme

This section is devoted to the convergence analysis of the proposed method. Initially, we will prove that the present scheme is third and fourth order accurate in the spatial direction for two different norms. Then, we will show that the method is second-order convergent in time.

6.4.1 The continuous-time orthogonal spline collocation method

The solution to the problem (6.2.2) approximated by orthogonal B-spline collocation method, in particular, using Hermite cubic basis functions is a differentiable map

$$V : (0, T_1] \to M_1^3,$$

that satisfies

$$V_t(\zeta, t) - V_{xx}(\zeta, t) = 0, \quad \zeta \in \mathcal{G}, \quad t \in (0, T_1], \tag{6.4.1}$$

which is equivalent to

$$\langle\, V_t - V_{xx}, \Upsilon \,\rangle = \langle\, 0, \Upsilon \,\rangle, \quad \Upsilon \in M_1^3, \quad t \in (0, T_1]. \tag{6.4.2}$$

Set $e = \nu - V$ and write

$$e = (\nu - \nu_{\mathcal{H}}) - (V - \nu_{\mathcal{H}}) := \phi - \Theta,$$

where $\phi = \nu - \nu_{\mathcal{H}}$ defined as before and $\Theta = V - \nu_{\mathcal{H}}$.

The error bounds in different norms for the spatial coordinate are derived in the following theorem.

Theorem 6.4.1. *Suppose ν and V are the solutions of (6.2.2) and (6.4.2), respectively and*

let $V(0) = \nu_{\mathcal{H}}(0)$. *If* $\nu \in L^\infty(H^6) \cap L^\infty(H_0^1)$ *and* $\nu_t \in L^2(H^6)$ *for* $t \in (0, T_1]$, *then*

$$\|\nu - V\|_{L^\infty(H^1)} \leq Ch^3,$$

and

$$\|\nu - V\|_{L^\infty(\mathcal{D})} \leq Ch^4.$$

Proof. The equivalent form of (6.2.2) coupled with (6.4.2), yields

$$\langle\, \Theta_t, \Upsilon \,\rangle - \langle\, \Theta_{xx}, \Upsilon \,\rangle = \langle\, \phi_t, \Upsilon \,\rangle - \langle\, \phi_{xx}, \Upsilon \rangle, \quad \Upsilon \in M_1^3, \tag{6.4.3}$$

for $\Upsilon = \Theta_t$

$$|\Theta_t|_{\mathcal{D}}^2 - \langle\, \Theta_{xx}, \Theta_t \rangle = \langle\, \phi_t, \Theta_t \rangle - \langle\, \phi_{xx}, \Theta_t \rangle. \tag{6.4.4}$$

From the bounds given in [133] and inequalities provided in subsection 6.3.2, we obtain

$$-\langle\, \Theta_{xx}, \Theta_t \rangle \geq \frac{1}{2}\frac{d}{dt}\|\Theta_x\|_{L^2(\Omega)}^2, \tag{6.4.5}$$

and

$$\langle\, \phi_t, \Theta_t \rangle \leq C|\phi_t|_{\mathcal{D}}^2 + \frac{1}{2}|\Theta_t|_{\mathcal{D}}^2. \tag{6.4.6}$$

Rewriting (6.4.4) as

$$\frac{1}{2}|\Theta_t|_{\mathcal{D}}^2 + \frac{1}{2}\frac{d}{dt}\|\Theta_x\|_{L^2}^2 \leq C|\phi_t|_{\mathcal{D}}^2 - \langle\, \phi_{xx}, \Theta_t \rangle, \tag{6.4.7}$$

which on integrating over the interval $(0, t)$ and using $\Theta(0) = 0$ deduces into

$$\int_0^t |\Theta_t|_{\mathcal{D}}^2 \, d\tau + \|\Theta_x\|_{L^2}^2 \leq C\int_0^t |\phi_t|_{\mathcal{D}}^2 \, d\tau - 2(\langle\, \phi_{xx}, \Theta \rangle - \int_0^t \langle\, \phi_{xxt}, \Theta \rangle \, d\tau). \tag{6.4.8}$$

We now calculate the bounds for $\langle\, \phi_{xx}, \Theta \rangle$ and $\int_0^t \langle\, \phi_{xxt}, \Theta \rangle \, d\tau$ as follows

$$\langle\, \phi_{xx}, \Theta \rangle = \sum_{j=1}^{N_x} \langle\, \phi_{xx}, \Theta \rangle_j = \sum_{j=1}^{N_x} \langle\, \phi_{xx}, \overline{\Theta}_j \rangle_j + \sum_{j=1}^{N_x} \langle\, \phi_{xx}, \Theta - \overline{\Theta}_j \rangle_j, \tag{6.4.9}$$

where

$$\overline{\Theta}_j = \frac{1}{h}\langle\, \Theta, 1\rangle_j.$$

The inequalities from subsection 6.3.2 together with Lemma 6.3.1, yields

$$\begin{aligned}\langle\, \phi_{xx}, \overline{\Theta}_j\rangle_j &\leq \sum_{j=1}^{N_x}\langle\, \phi_{xx}, 1\rangle_j |\overline{\Theta}_j|_j \\ &\leq Ch^4 \|\nu^6\|_{L^2(\Omega_j)} |\Theta|_j \\ &\leq Ch^8 \|\nu^6\|^2_{L^2(\Omega_j)} + \frac{1}{4}|\Theta|^2_j. \end{aligned} \tag{6.4.10}$$

Also, we have

$$\langle\, \phi_{xx}, \Theta - \overline{\Theta}_j\rangle_j \leq Ch^4 \|\nu^{(5)}\|_{L^2(\Omega_j)} \|\Theta_x\|_{L^2(\Omega_j)} \leq Ch^8 \|\nu^{(5)}\|^2_{L^2(\Omega_j)} + \frac{1}{4}\|\Theta_x\|^2_{L^2(\Omega_j)}. \tag{6.4.11}$$

Substitution of (6.4.10) and (6.4.11) in (6.4.9) deduces

$$\langle\, \phi_{xx}, \Theta\rangle \leq \frac{1}{4}(\|\Theta_x\|^2_{L^2} + |\Theta|^2_{\mathcal{D}}) + Ch^8(\|\nu^{(5)}\|^2 + \|\nu^{(6)}\|^2). \tag{6.4.12}$$

Now we integrate (6.4.12) over the interval $(0, t)$ to get the bound for

$$\int_0^t \langle\, \phi_{xxt}, \Theta\rangle\, d\tau \leq \frac{1}{4}\int_0^t (\|\Theta_x\|^2_{L^2} + |\Theta|^2_{\mathcal{D}})\, d\tau + Ch^8 \int_0^t (\|\nu^{(5)}_t\|^2 + \|\nu^{(6)}_t\|^2)\, d\tau. \tag{6.4.13}$$

Substituting (6.4.12) and (6.4.13) in (6.4.8) and using Lemma 6.3.1, we get

$$\begin{aligned}\int_0^t |\Theta_t|^2_{\mathcal{D}}\, d\tau + \|\Theta_x\|^2_{L^2} \leq \int_0^t ((&\|\Theta_x\|^2_{L^2} + |\Theta|^2_{\mathcal{D}})\, d\tau + Ch^8(\|\nu^{(5)}_t\|^2 \\ &+ \|\nu^{(6)}_t\|^2 + \|\nu^{(4)}\|^2 + \|\nu^{(4)}_t\|^2))\, d\tau \\ &+ Ch^8(\|\nu^{(5)}\|^2_{L^\infty(L^2)} + \|\nu^{(6)}\|^2_{L^\infty(L^2)}) + \|\Theta_x\|^2_{L^2} + |\Theta|^2_{\mathcal{D}}. \end{aligned} \tag{6.4.14}$$

Clearly

$$\int_0^t |\Theta|_{\mathcal{D}}^2 \, d\tau \leq C \int_0^t (\|\Theta_x\|_{L^2}^2 + |\Theta|_{\mathcal{D}}^2) \, d\tau. \tag{6.4.15}$$

Now the use of Gronwall's inequality yields

$$\int_0^t |\Theta_t|_{\mathcal{D}}^2 \, d\tau + \|\Theta\|_{L^\infty(H^1)}^2 \leq Ch^8(\|\nu^{(4)}\|_{L^\infty(L^2)}^2 + \|\nu^{(5)}\|_{L^\infty(L^2)}^2 + \|\nu^{(6)}\|_{L^\infty(L^2)}^2 + \|\nu_t^{(4)}\|_{L^2(L^2)}^2 + \|\nu_t^{(5)}\|_{L^2(L^2)}^2 + \|\nu_t^{(6)}\|_{L^2(L^2)}^2). \tag{6.4.16}$$

Also, Lemmas 6.3.1 and 6.3.2 provide

$$\|\phi\|_{L^\infty(H^1)}^2 \leq C(h^6\|\nu^{(4)}\|_{L^\infty(L^2)}^2 + h^8\|\nu^{(4)}\|_{L^\infty(L^2)}^2). \tag{6.4.17}$$

Finally, the inequalities (6.4.16) and (6.4.17) with the bounds for the derivative of ν yield

$$\|\nu - V\|_{L^\infty(H^1)} \leq \|\phi\|_{L^\infty(H^1)} + \|\Theta\|_{L^\infty(H^1)} \leq Ch^3. \tag{6.4.18}$$

Since $\Theta(0) = 0$, an application of

$$|\Theta|_{\mathcal{D}} = \int_0^t |\Theta_t(t)|_{\mathcal{D}} \, d\tau \leq \left(\int_0^t |\Theta_t|_{\mathcal{D}}^2 \, d\tau \right)^{1/2},$$

and

$$\|\nu - V\|_{L^\infty(\mathcal{D})} \leq \|\phi\|_{L^\infty(\mathcal{D})} + \|\Theta\|_{L^\infty(\mathcal{D})} \leq Ch^4,$$

gives $\|\nu - V\|_{L^\infty(\mathcal{D})} \leq Ch^4$. □

6.4.2 The Rannacher time-marching scheme and its convergence analysis

With the notations

$$V^n(\cdot) = V(\cdot, t_n), \quad 0 \leq n \leq N_t,$$

$$\overline{\partial_t} V^n = \frac{V^n - V^{n-1}}{k}, \quad 1 \le n \le N_t,$$
$$V^{n-\frac{1}{2}} = \frac{V^n + V^{n-1}}{2}, \quad 1 \le n \le N_t,$$

the Rannacher scheme with OSCM consists to determine $\{V\}_{n=1}^{N_t} \subset M_1^3$ such that

$$\overline{\partial_t} V^n(\zeta) - V_{xx}^n(\zeta) = 0, \quad \zeta \in \mathcal{G}, \quad n = 1, 2, 3, \tag{6.4.19}$$

and

$$\overline{\partial_t} V^n(\zeta) - V_{xx}^{n-\frac{1}{2}}(\zeta) = 0, \quad \zeta \in \mathcal{G}, \quad n = 4, 5, \ldots, N_t. \tag{6.4.20}$$

Remark. In the above scheme, the first finite steps (there here) are solved using backward Euler method, though exactly how much is sufficient is not known a priori and has to be found experimentally.

As to smoothen the solution, the backward Euler scheme is used only for first few steps, so in the convergence analysis of this method, we use the following equivalent form of (6.4.20)

$$\left\langle \overline{\partial_t} V^n(\zeta) - V_{xx}^{n-\frac{1}{2}}(\zeta), \Upsilon \right\rangle = \left\langle 0, \Upsilon \right\rangle, \quad \Upsilon \in M_1^3. \tag{6.4.21}$$

The error bounds in both directions in distinct norms are given by the following theorem.

Theorem 6.4.2. *Suppose $\nu \in L^\infty(H^6) \cap L^\infty(H_0^1)$ is the solution of (6.2.2) and $\nu_t \in L^2(H^6)$ for $t \in (0, T_1]$. Then, if $\{V^n\}_{n=1}^{N_t}$ with $V^0 = \nu_H^0$ is the solution obtained by the Rannacher scheme (6.4.19)-(6.4.20). Then, for sufficiently small k*

$$\|\nu^n - V^n\|_{l^\infty(H^1)} \le C(k^2 + h^3),$$

and

$$\|\nu^n - V^n\|_{l^\infty(\mathcal{D})} \le C(k^2 + h^4).$$

Proof. Since $\nu^n - V^n = (\nu^n - \nu_{\mathcal{H}}^n) - (V^n - \nu_{\mathcal{H}}^n) \equiv \phi^n - \Theta^n,\ n = 4, \ldots, N_t$, at $t = t_{n-\frac{1}{2}}$,

(6.2.2) and (6.4.21) yield

$$\langle \overline{\partial_t}\Theta^n, \Upsilon\rangle - \big\langle \Theta_{xx}^{n-\frac{1}{2}}, \Upsilon\big\rangle = \langle \overline{\partial_t}\phi^n, \Upsilon\rangle - \big\langle \phi_{xx}^{n-\frac{1}{2}}, \Upsilon\big\rangle + \langle \lambda^{n-\frac{1}{2}}, \Upsilon\rangle, \tag{6.4.22}$$

where $\lambda^{n-\frac{1}{2}} = \lambda_1^{n-\frac{1}{2}} + \lambda_2^{n-\frac{1}{2}}$ with $\lambda_1^{n-\frac{1}{2}} = \partial_t\nu^n - \nu_t(t_{n-\frac{1}{2}}),\ \lambda_2^{n-\frac{1}{2}} = \nu_{xx}^{n-\frac{1}{2}} - \nu_{xx}(t_{n-\frac{1}{2}})$. Substituting $\Upsilon = \overline{\partial_t}\Theta^n$ in (6.4.22), we obtain

$$|\overline{\partial_t}\Theta^n|_{\mathcal{D}}^2 - \big\langle \Theta_{xx}^{n-\frac{1}{2}}, \overline{\partial_t}\Theta^n\big\rangle = \langle \overline{\partial_t}\phi^n, \overline{\partial_t}\Theta^n\rangle + \langle \lambda^{n-\frac{1}{2}}, \overline{\partial_t}\Theta^n\rangle - \big\langle \phi_{xx}^{n-\frac{1}{2}}, \overline{\partial_t}\Theta^n\big\rangle. \tag{6.4.23}$$

The bound for the second term in the L.H.S. of (6.4.23) is given by

$$-\big\langle \Theta_{xx}^{n-\frac{1}{2}}, \overline{\partial_t}\Theta^n\big\rangle \geq \frac{1}{2}\overline{\partial_t}\|\Theta_x^n\|^2. \tag{6.4.24}$$

Also, for the first two terms in the R.H.S. of (6.4.23), we consider the inequality

$$\langle \overline{\partial_t}\phi^n, \overline{\partial_t}\Theta^n\rangle + \langle \lambda^{n-\frac{1}{2}}, \overline{\partial_t}\Theta^n\rangle \leq C(|\overline{\partial_t}\phi^n|_{\mathcal{D}}^2 + |\lambda^{n-\frac{1}{2}}|_{\mathcal{D}}^2) + \frac{3}{4}|\overline{\partial_t}\Theta^n|_{\mathcal{D}}^2. \tag{6.4.25}$$

The inequalities (6.4.24)-(6.4.25) when used in (6.4.23) give

$$\frac{1}{4}|\overline{\partial_t}\Theta^n|_{\mathcal{D}}^2 + \frac{1}{2}\overline{\partial_t}(\|\Theta_x^n\|^2 \leq C(|\overline{\partial_t}\phi^n|_{\mathcal{D}}^2 + |\lambda^{n-\frac{1}{2}}|_{\mathcal{D}}^2) + \frac{1}{2}\langle \overline{\partial_t}\Theta^n, \Theta^{n-1}\rangle - \big\langle \phi_{xx}^{n-\frac{1}{2}}, \overline{\partial_t}\Theta^n\big\rangle.$$

Applying summation from $n = 4$ to m, we obtain

$$\begin{aligned} k\sum_{n=4}^{m}|\overline{\partial_t}\Theta^n|_{\mathcal{D}}^2 + \overline{\partial_t}(\|\Theta_x^m\|^2 \leq C\big[k\sum_{n=4}^{m}|\overline{\partial_t}\phi^n|_{\mathcal{D}}^2 + k\sum_{n=4}^{m}|\lambda^{n-\frac{1}{2}}|_{\mathcal{D}}^2 + k\sum_{n=4}^{m}\langle \overline{\partial_t}\Theta^n, \Theta^{n-1}\rangle \\ - 2k\sum_{n=4}^{m}\big\langle \phi_{xx}^{n-\frac{1}{2}}, \overline{\partial_t}\Theta^n\big\rangle\big]. \end{aligned} \tag{6.4.26}$$

Now, Lemma 6.3.1 yields

$$k\sum_{n=4}^{m}|\phi^n|_{\mathcal{D}}^2 \leq Ch^8\|\nu^{(4)}\|_{L^2(L^2)}^2,$$

$$k\sum_{n=4}^{m}|\overline{\partial_t}\phi^n|^2_{\mathcal{D}} \leq Ch^8\|\nu_t^{(4)}\|^2_{L^2(L^2)},$$
$$k\sum_{n=4}^{m}|\overline{\partial_t}\phi^n_{xx}|^2_{\mathcal{D}} \leq Ch^6\|\nu_t^{(5)}\|^2_{L^2(L^2)}.$$

Moreover, on applying the Young's inequality, the third term of the R.H.S of (6.4.26) gives

$$k\sum_{n=4}^{m}\langle\overline{\partial_t}\Theta^n,\Theta^{n-1}\rangle \leq Ck\sum_{n=4}^{m}|\Theta^n|^2_{\mathcal{D}}. \tag{6.4.27}$$

For any fixed m such that $4 \leq m \leq N_t$, we have

$$\langle\phi^m_{xx},\Theta^m\rangle = \sum_{j=1}^{N_x}\langle\phi^m_{xx},\Theta^m\rangle_j = \sum_{j=1}^{N_x}\langle\phi^m_{xx},\overline{\Theta}^m_j\rangle_j + \sum_{j=1}^{N_x}\langle\phi^m_{xx},\Theta^m-\overline{\Theta}^m_j\rangle_j, \tag{6.4.28}$$

where $\overline{\Theta}^m_j = \frac{1}{h}\langle\Theta^m,1\rangle_j$. Using the combination of inequalities of subsection 6.3.2 along with Lemma 6.3.1, yield

$$\begin{aligned}\langle\phi^m_{xx},\overline{\Theta}^m_j\rangle_j &\leq Ch^{9/2}h^{-1}h^{1/2}\|\nu^{(6)}\|_{L^2(\Omega_j)}|\Theta^m|_j\\ &= Ch^4\|\nu^{(6)}\|_{L^2(\Omega_j)}|\Theta^m|_j\\ &\leq Ch^8\|\nu^{(6)}\|^2_{L^2(\Omega_j)} + \frac{1}{4}|\Theta^m|^2_j.\end{aligned} \tag{6.4.29}$$

Using Poincare's inequality, the second term on the right-hand side of (6.4.28) gives

$$\langle\phi^m_{xx},\Theta^m-\overline{\Theta}^m_j\rangle_j \leq Ch^8\|\nu^{(5)}\|^2_{L^2(\Omega_j)} + \frac{1}{4}\|\Theta^m_x\|^2_{L^2(\Omega_j)}. \tag{6.4.30}$$

Substituting (6.4.29) and (6.4.30) in (6.4.28), to obtain

$$\langle\phi^m_{xx},\Theta^m\rangle \leq \frac{1}{4}(\|\Theta^m_x\|^2_{L^2}+|\Theta^m|^2_{\mathcal{D}}) + Ch^8(\|\nu^{(6)}\|^2_{L^2(\Omega)}+\|\nu^{(5)}\|^2_{L^2(\Omega)}). \tag{6.4.31}$$

Now, using the notation

$$d_t\Theta^n \equiv \frac{1}{2k}(\Theta^n - \Theta^{n-2}) = \frac{1}{2}(\overline{\partial_t}\Theta^n + \overline{\partial_t}\Theta^{n-1}), \quad n = 4, 5, \ldots, N_t,$$

we obtain

$$k\sum_{n=4}^{m}\left\langle \phi_{xx}^{n-\frac{1}{2}}, \overline{\partial_t}\Theta^n\right\rangle = \langle \phi_{xx}^m, \Theta^m\rangle - k\sum_{n=4}^{m-1}\left\langle d_t\phi_{xx}^n, \Theta^n\right\rangle. \tag{6.4.32}$$

Using the argument discussed in (6.4.28)-(6.4.31), we obtain

$$\begin{aligned} k\sum_{n=4}^{m}\left\langle d_t\phi_{xx}^n, \Theta^n\right\rangle &= k\sum_{n=4}^{m}\left\langle \overline{\partial_t}\phi_{xx}^n, \Theta^n\right\rangle - k\sum_{n=4}^{m}\left\langle \overline{\partial_t}\phi_{xx}^{n-1}, \Theta^n\right\rangle \\ &\leq \frac{1}{4}k\sum_{n=4}^{m}(\|\Theta_x^n\|_{L^2}^2 + |\Theta^n|_{\mathcal{D}}^2) + Ch^8\int_0^{t_m}(\|\nu_t^{(5)}\|^2 + \|\nu_t^{(6)}\|^2)\,d\tau. \end{aligned} \tag{6.4.33}$$

On combining (6.4.31)-(6.4.33), we obtain

$$\begin{aligned} k\sum_{n=4}^{m}\left\langle \phi_{xx}^{n-\frac{1}{2}}, \overline{\partial_t}\Theta^n\right\rangle &\leq \frac{1}{4}(\|\Theta_x^m\|_{L^2}^2 + |\Theta^m|_{\mathcal{D}}^2) + Ch^8(\|\nu^{(5)}\|_{L^\infty(L^2)}^2 + \|\nu^{(6)}\|_{L^\infty(L^2)}^2) \\ &+ \frac{1}{4}k\sum_{n=4}^{m}(\|\Theta_x^n\|_{L^2}^2 + |\Theta^n|_{\mathcal{D}}^2) + Ch^8\int_0^{t_m}(\|\nu_t^{(5)}\|_{L^2}^2 + \|\nu_t^{(6)}\|_{L^2}^2)\,d\tau. \end{aligned} \tag{6.4.34}$$

To estimate $\phi^{n-\frac{1}{2}}$, use of Taylor's theorem provides

$$k\sum_{n=4}^{m}|\phi_1^{n-\frac{1}{2}}|_{\mathcal{D}}^2 \leq Ck^4\|\nu_{ttt}\|_{L^\infty(L^\infty)}^2, \quad k\sum_{n=4}^{m}|\phi_2^{n-\frac{1}{2}}|_{\mathcal{D}}^2 \leq Ck^4\|\nu_{tt}^{(2)}\|_{L^\infty(L^\infty)}^2.$$

Hence

$$k\sum_{n=4}^{m}|\phi^{n-\frac{1}{2}}|_{\mathcal{D}}^2 \leq Ck^4. \tag{6.4.35}$$

Substituting (6.4.34) and (6.4.35) in (6.4.26), the use of discrete form of the Gronwall's inequality yields

$$k\sum_{n=4}^{m}|\overline{\partial_t}\Theta^n|_{\mathcal{D}}^2 + \max_{0\leq m\leq N_t}\|\Theta^m\|_{H^1}^2 \leq C[h^8(\|\nu^{(4)}\|_{L^2(L^2)}^2 + \|\nu^{(5)}\|_{L^\infty(L^2)}^2 + \|\nu^{(6)}\|_{L^\infty(L^2)}^2$$

$$+ \|\nu_t^{(4)}\|^2_{L^2(L^2)} + \|\nu_t^{(5)}\|^2_{L^2(L^2)} + \|\nu_t^{(6)}\|^2_{L^2(L^2)}) + k^4].$$

Now, by following the equivalent approach to that of Theorem 6.4.1, we get the required results. □

6.5 Numerical simulations and discussion

In this section, we numerically validate the theoretical work for the problems with non-smooth terminal condition by solving two different American option pricing problems. Through the experiments it is shown that the proposed algorithm based on the orthogonal spline and Rannacher time-marching scheme is effortless and efficient in attaining high accuracy. It can also be concluded from this section that the present scheme is equally efficient for problems like moving boundary problems, linear complementarity problems, and the problems with non-smooth underlying data arising in different fields. In order to avoid the mess, the selective figures and tables are presented effectively which are in themself sufficient to prove the robustness of the scheme. In both the examples, we consider $\alpha_1 = -1$ and $\alpha_2 = 1$, as the end points of the spatial domain. Also, it is significant to note that in numerical simulations, when OSC scheme is applied we obtain almost block diagonal (ABD) linear system [134] at each time step. To solve the ABD system (at the cost of $O(N)$ operations) COLROW package [135] has been used.

6.5.1 Computational error analysis

The validity of a novel or conjunctive scheme can be checked through error analysis. Since the problems considered in this work do not have the exact solution, we are using the double mesh principle to compute the errors in different norms. The maximum absolute error $E_1^{N_\mathcal{S},N_\tau}$ in $L^\infty-$norm is estimated by using the following formula

$$E_1^{N_\mathcal{S},N_\tau} = \max_j \left(\max_i |\mathcal{P}^{2N_\mathcal{S},2N_\tau}(\mathcal{S}_{2i},\tau_{2j}) - \mathcal{P}^{N_\mathcal{S},N_\tau}(\mathcal{S}_i,\tau_j)| \right),$$

and the error $E_2^{N_\mathcal{S},N_\tau}$ in the L^2-norm is computed by

$$E_2^{N_\mathcal{S},N_\tau} = \sqrt{\sum_j \sum_i h(\mathcal{P}^{2N_\mathcal{S},2N_\tau}(\mathcal{S}_{2i},\tau_{2j}) - \mathcal{P}^{N_\mathcal{S},N_\tau}(\mathcal{S}_i,\tau_j))^2}.$$

Moreover, the error $E_3^{N_\mathcal{S},N_\tau}$ in H^1-norm is computed by

$$E_3^{N_\mathcal{S},N_\tau} = \sqrt{E_2^{N_\mathcal{S},N_\tau} + \sum_j \sum_i h(\mathcal{P}_\mathcal{S}^{2N_\mathcal{S},2N_\tau}(\mathcal{S}_{2i},\tau_{2j}) - \mathcal{P}_\mathcal{S}^{N_\mathcal{S},N_\tau}(\mathcal{S}_i,\tau_j))^2}.$$

The expression $\frac{\log(\text{error}^{N_\mathcal{S},N_\tau})-\log(\text{error}^{2N_\mathcal{S},2N_\tau})}{\log 2}$ is used to compute the numerical order of convergence. Typically the error depends on the underlying data of the problem and its complexity. Thus even though with the A-stable schemes such as CN scheme, it is tough to deal with the discretization error. It leads to decay in the convergence rate as shown in Tables 6.1 and 6.4 for Example 6.5.1 and 6.5.2, respectively. It can also be observed that the scheme is still convergent but the decay in the error is no longer quadratic. On the other hand, one can examine that the BE scheme is strongly A-stable but it converges slowly to the exact solution and exhibits linear order of convergence. Hence, a new scheme known as Rannacher time-stepping scheme is implemented. Table 6.1 and 6.4, also depicted the effectiveness of the Rannacher scheme over the BE and CN schemes. The error decay for different schemes with the increase in number of grid points has been shown in Figures 6.2 and 6.5. We observe that the error for the Rannacher time-marching scheme decay rapidly as compared to BE and CN schemes. In spatial context, note that Tables 6.2 and 6.5 confirm the better accuracy of the present scheme as compared to the non-spline and spline based methods (refer to the articles [136, 137]). Hence, the fourth order accuracy in space and after smoothness quadratic rate of convergence in time makes the method more valuable.

Example 6.5.1. *Consider the Black-Scholes Equation (6.2.1) for the American call option with fixed rate of interest* $r = 0.08$*, volatility* $\sigma = 0.3$*, dividend yield* $\delta = 0.06$*, the exercise time* $\mathbb{T} = 1$ *year and strike price* $\mathbb{K} = 100$*.*

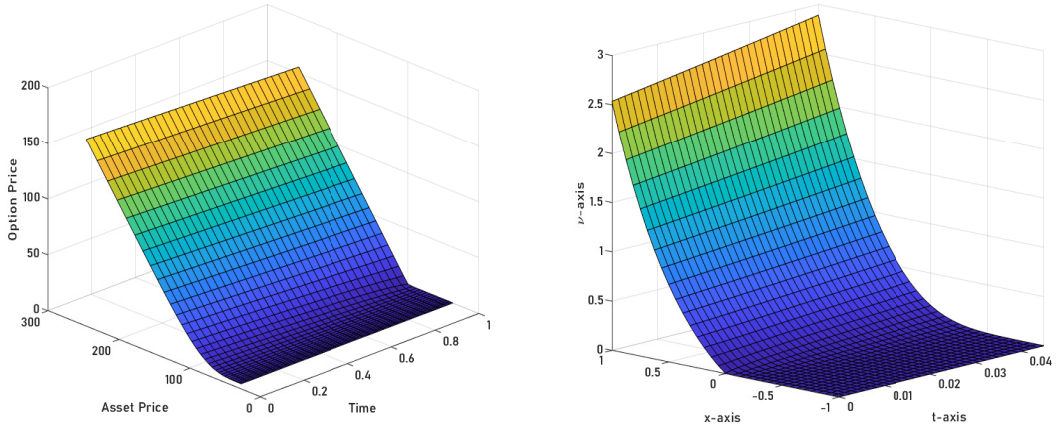

(a) The price of American call option (b) The solution of the transformed equation

Figure 6.1: Computational results for Example 6.5.1.

Table 6.1: $E_1^{N_S,N_\tau}$ for the American call option price given in Example 6.5.1

	Number of collocation points				
	16	32	64	128	256
BE	$7.08e-04$	$3.33e-04$	$1.64e-04$	$8.14e-05$	$4.06e-05$
	1.0882	1.0218	1.0106	1.0035	
CN	$9.03e-03$	$4.51e-03$	$2.26e-03$	$1.13e-03$	$5.64e-04$
	1.0016	0.9968	1.0000	1.0026	
Rannacher	$3.99e-04$	$8.84e-05$	$2.13e-05$	$5.26e-06$	$1.31e-06$
	2.1743	2.0532	2.0177	2.0055	

Example 6.5.2. *Consider the following parameters set in the Black-Scholes Equation (6.2.1) for the American put option: rate of interest* $r = 0.25$*, volatility* $\sigma = 0.6$*, dividend yield* $\delta = 0.2$*, the exercise time* $\mathbb{T} = 1$ *year and strike price* $\mathbb{K} = 10$*.*

6.5.2 Analysis of oscillation reduction

In this section, we numerically investigate the oscillation eliminating property of the Rannacher scheme. The non-smoothness of the terminal condition of problem (6.2.1) causes computational noises since the second derivative of the option price $\mathcal{P}$ does not belong to L^2. Figures 6.3 and 6.6 reveal that the CN time-stepping scheme is prone to spurious oscillations. Although no-oscillation is realized by the BE scheme, it converges

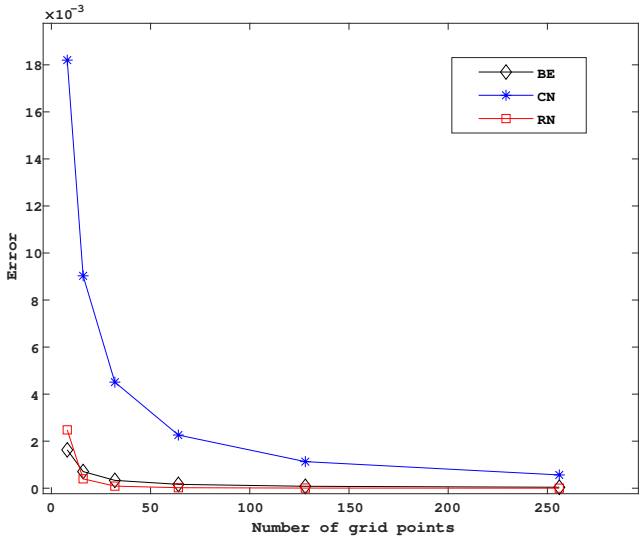

Figure 6.2: Error behavior in L^2-norm for different schemes constructed for Example 6.5.1

Table 6.2: Spatial errors in different norms occur while determining the American call option price for Example 6.5.1 at $t = 0.25$

	Number of collocation points				
	16	32	64	128	256
$E_1^{N_S,N_\tau}$	$1.68e-05$	$8.89e-07$	$5.38e-08$	$3.34e-09$	$2.08e-10$
	4.2401	4.0465	4.0097	4.0052	
$E_2^{N_S,N_\tau}$	$3.62e-06$	$1.97e-07$	$1.10e-08$	$6.41e-10$	$3.8535e-11$
	4.1997	4.1626	4.1010	4.0561	
$E_3^{N_S,N_\tau}$	$7.97e-05$	$6.64e-06$	$5.79e-07$	$5.09e-08$	$4.49e-09$
	3.5853	3.5195	3.5078	3.5029	

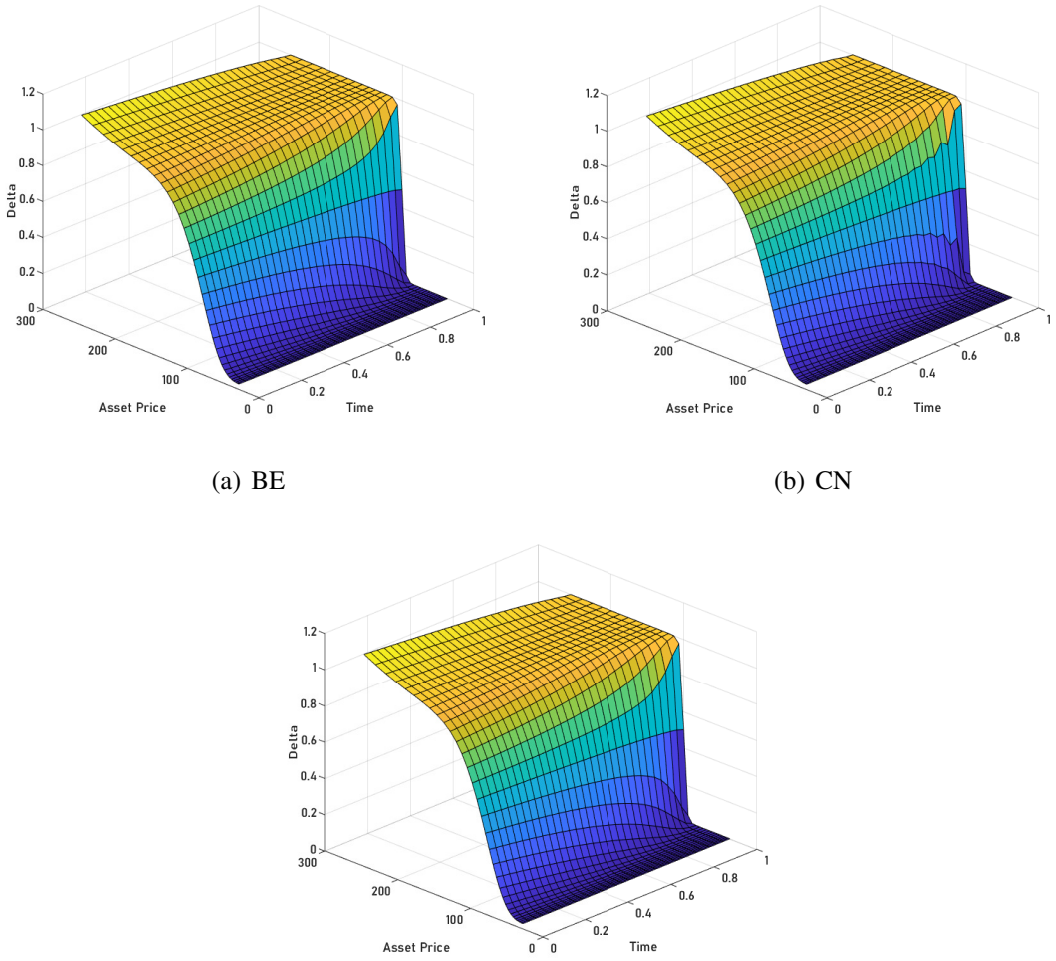

(a) BE

(b) CN

(c) Rannacher

Figure 6.3: Values of delta computed using different time-marching schemes for Example 6.5.1.

Table 6.3: Numerical results for American call option with parameters as in Example 6.5.1 and $T = 1$ year at various asset prices.

		$\mathcal{S} = 60$		$\mathcal{S} = 100$		$\mathcal{S} = 165$	
N_τ	$N_\mathcal{S}$	Option price	Delta	Option price	Delta	Option price	Delta
8	4	0.4036	0.054	11.8808	0.580	68.3689	0.986
16	8	0.4541	0.065	12.3849	0.583	68.6258	0.985
32	16	0.4917	0.069	12.6093	0.584	68.7546	0.984
64	32	0.5123	0.071	12.7162	0.585	68.8190	0.984
256	64	0.5227	0.072	12.7693	0.585	68.8513	0.984

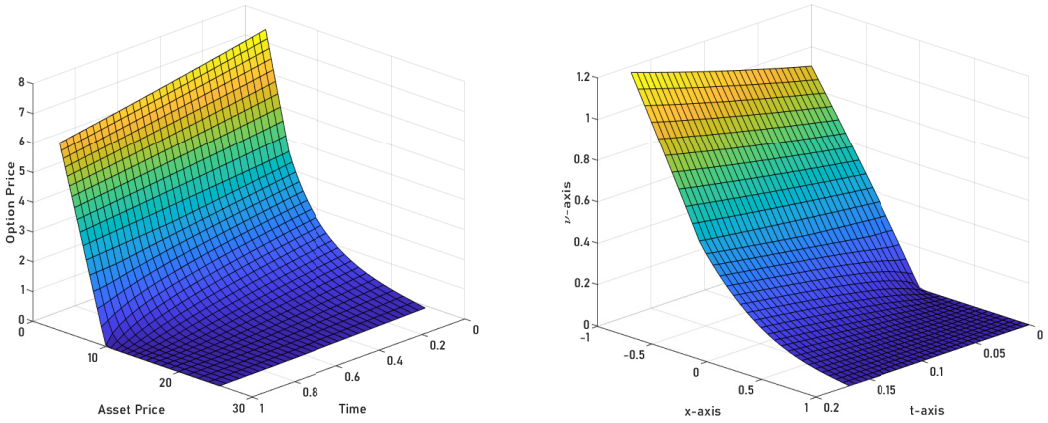

(a) The price of American put option

(b) The solution of the transformed equation

Figure 6.4: Computational results for Example 6.5.2.

slowly. On the other hand, the Rannacher time-marching scheme smoothen the solution function, dampes the oscillations, and provides the expected rate of convergence at the same computational cost.

6.5.3 Application to option pricing

So far in this section, we have discussed the performance and robustness of the scheme numerically and validated the computed results by comparing with the theoretical findings. Now, we explain the application of the present scheme in option pricing and validate the

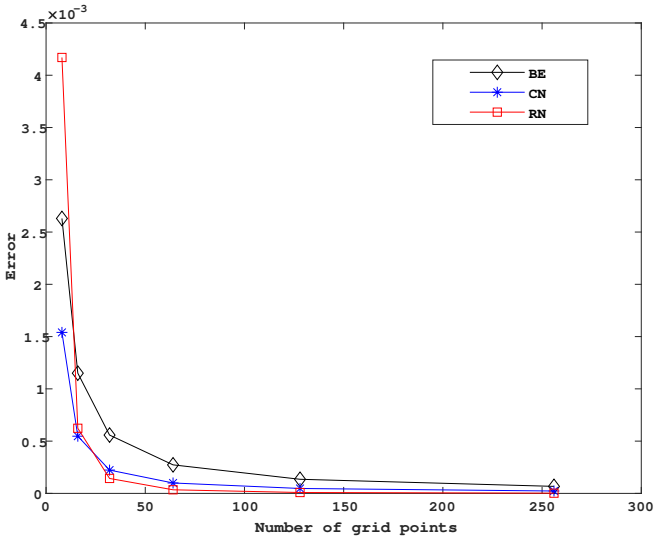

Figure 6.5: Error behavior in L^2-norm for different schemes constructed for Example 6.5.2

Table 6.4: $E_1^{N_S,N_\tau}$ for the value of American put option given in Example 6.5.2

	Number of collocation points				
	16	32	64	128	256
BE	$1.15e-03$	$5.58e-04$	$2.73e-04$	$1.35e-04$	$6.71e-05$
	1.0433	1.0314	1.0159	1.0086	
CN	$5.47e-04$	$2.23e-04$	$9.96e-05$	$4.70e-05$	$2.28e-05$
	1.2945	1.1628	1.0835	1.0436	
Rannacher	$6.23e-04$	$1.43e-04$	$3.44e-05$	$8.47e-06$	$2.10e-06$
	2.1232	2.0555	2.0220	2.0120	

Table 6.5: Spatial error in different norms occur while determining the American put option price for Example 6.5.2 at $t = 0.25$

	Number of collocation points				
	16	32	64	128	256
$E_1^{N_S,N_\tau}$	$1.10e-05$	$7.17e-07$	$4.53e-08$	$2.84e-09$	$1.77e-10$
	3.9394	3.9844	3.9955	4.0041	
$E_2^{N_S,N_\tau}$	$2.59e-06$	$1.57e-07$	$9.20e-09$	$5.46e-10$	$3.29e-11$
	4.0441	4.0930	4.0747	4.0527	
$E_3^{N_S,N_\tau}$	$1.48e-03$	$1.16e-04$	$9.55e-06$	$8.10e-07$	$7.01e-08$
	3.6734	3.6025	3.5595	3.5304	

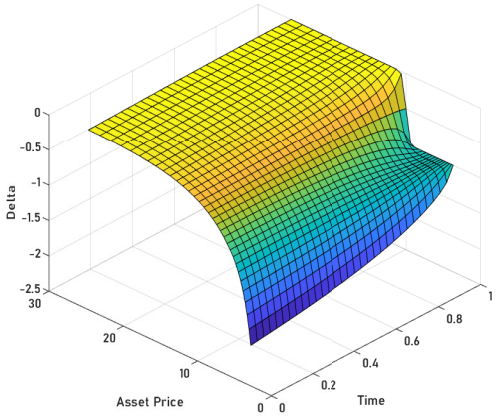

(a) BE

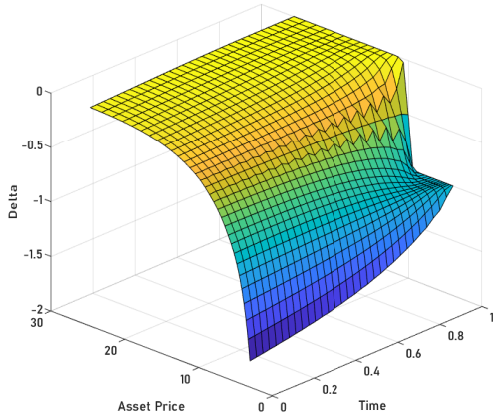

(b) CN

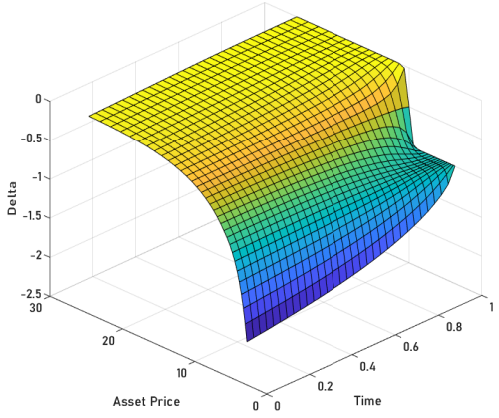

(c) Rannacher

Figure 6.6: Values of delta computed using different time-marching schemes for Example 6.5.2.

Table 6.6: Numerical results for American put option with parameters as in Example 6.5.2 and $T = 1$ year at various asset prices.

		$\mathcal{S} = 6$		$\mathcal{S} = 10$		$\mathcal{S} = 16$	
N_τ	$N_\mathcal{S}$	Option price	Delta	Option price	Delta	Option price	Delta
8	4	4.6362	−0.875	1.9793	−0.377	0.5973	−0.108
16	8	4.6909	−0.878	2.0461	−0.376	0.6481	−0.112
32	16	4.7184	−0.880	2.0784	−0.376	0.6729	−0.114
64	32	4.7323	−0.880	2.0945	−0.376	0.6851	−0.115
256	64	4.7392	−0.881	2.1025	−0.376	0.6912	−0.116

computations which are comparable with the results provided in [7, 14]. Figure 6.1(a) illustrates the price of the American call option. It discloses that when $\mathcal{S} \leq \mathbb{K}$, the call option price is nearly 0 *i.e.,* the option is no longer viable. Instead for $\mathcal{S} > \mathbb{K}$, it is rich in cash with a strong likelihood of the option being exercised. For the convenience of readers, American call option price and the values of delta Greek at various asset prices are provided in Figure 6.3. This figure depicts the temporal effect and impact of moneyness on the delta Greek. A remarkable fact is that all the values of delta are occupied in the interval $[0, 1]$. Furthermore, the option's delta reaches the limits of its spectrum for exceptionally high and low underlying asset values, *i.e.,* since the option's intrinsic value is extremely high as $\mathcal{S}$ approaches its limits, the value of call option's delta reaches 1. While, for $\mathcal{S}$ tending to 0, the option becomes worthless, and hence the delta Greek approaches zero.

Figure 6.4(a) unveils that the function of price of the American put option behaves non-linearly. One can unwound from the graphical result that the put option holder faces loss for $\mathcal{S} \geq \mathbb{K}$. Although for $\mathcal{S} < \mathbb{K}$, it is deep in money, in such a situation, it is feasible to exercise the option. To make it preferable for readers, American put option price and the values of delta Greek at various asset prices are supplied in Figure 6.6. Computational values of delta are depicted in Figure 6.6 for American put option. The figure unwounds that for $\mathcal{S} \geq \mathbb{K}$, the value option delta becomes negligible if we are sufficiently close to the expiry. Additionally to manage a portfolio, delta neutrality can be maintained by analyzing the behavior of the delta Greek. The algorithm can be used to compute all other

Greeks at no additional cost. Moreover, it can be effortlessly applied to all other models and payoff profiles. Empirically Figures 6.1, 6.3, 6.4, and 6.6, confirm the robustness of the present orthogonal collocation spline based scheme. Moreover, from these figures, one can observe the performance gained by the present method due to the use of Rannacher scheme over the well known CN and BE finite difference schemes. Hence, the experiments confirm that the present scheme can be used to explore various option pricing problems.

6.6 Concluding observations and future scope

In this chapter, we present the formulation, analysis, and implementation of a fourth-order accurate orthogonal spline collocation strategy with a second-order time-marching scheme for simulating the hedging parameters of the American option. Solving a problem with irregular initial data using the CN scheme leads to spurious oscillations, hence, a particular attention is paid to a more accurate scheme referred to as Rannacher time-marching scheme. Mainly the present chapter emphasizes on the high accuracy of the present scheme in the given computational cost. Along with solving linear complementarity problems from finance, a practical advantage of the present scheme is that it can be applied to various physical and chemical models with non-smooth data. In addition, it provides high accuracy, and reduces the quantization error near the discontinuity. Moreover, for the linear complementarity American option pricing problem under the Black-Scholes framework, the super convergent behavior of the proposed spline scheme is provided. Also, it has been observed that the proposed method with Rannacher time-marching scheme is second and fourth order convergent in the temporal and spatial directions, respectively. Furthermore, it is significant to conclude that the Rannacher scheme is stable and can be effortlessly used to obtain the second-order convergence even with discontinuities in the initial data. Numerical experiments (in the form of tables and graphs) are carried out for call and put American option pricing problems to validate the performance and accuracy of the present method. Comparative study of the present time-stepping method with different finite difference schemes unveils that the given time-marching scheme is sufficient to

restore the expected behavior. The present work can be used in the trading market to minimize the risk and to manage the portfolios. Also, it is easy to implement and extend the present scheme towards different non-smooth problems for future computational studies.

Chapter 7

A higher order novel numerical scheme for variable order time-fractional option pricing model

---

7.1 Introduction

A major issue in the financial market is the pricing or hedging of financial instruments for investment. Options are amongst the popular financial instruments. The pricing of option contracts has been a hot topic in recent decades because options are one of the most important and widely traded financial products. Thus, in the recent few years, a lot of work has been done to approximate the price of various options based on the Black-Scholes model [138–140]. The standard Black-Scholes model, on the contrary, is based on a set of harsh assumptions [141, 142]. On the other hand, these assumptions are vastly different from the rules that govern the actual financial market. As a result, to obtain perfect pricing outcomes, one must adequately relax the preconceptions of the Black-Scholes model. Even though the Black-Scholes price is quite near to the observed prices, it nevertheless contains well-known flaws such as being dependent on the assumption that with given

constant volatility, the underlying asset moves in a geometric Brownian motion. However, statistical findings illustrate that the distributional assumption of constant volatility does not fit market data well enough [143]. Therefore, in this chapter, we consider the CEV model [144] in which the volatility is determined as a function of the underlying asset's price.

The CEV model permits volatility to change in response to the underlying price, capturing a fundamental regularity in empirical data that is important for option pricing. As a result, when it comes to anticipating option prices, the CEV model beats the Black-Scholes model [145–147]. In financial literature, various approximation methods techniques have been used in pricing an option under the framework of the CEV model, see [148–151]. We can also point out that the traditional Black-Scholes model and its enhancements are based on the notion of constant risk-free interest rates and no dividends. These assumptions often fail to account for real-world issues. As a result, we assume that the interest rate and dividend yield are functions of time.

To this end, it's worth mentioning that we consider the time derivative to be fractional since the integer-order derivative base models would not capture some typical historical features. On the other hand, fractional derivatives are quite flexible for characterizing the behavior of differential equations and adding historical information due to their nonlocal nature [152]. Fractional derivative is defined in a variety of ways. This chapter considers the Atangana-Balenau derivative's definition in Caputo's sense since it has a non-singular and nonlocal kernel. Due to the memory quality of the variable order differential and integral operators, the mathematical systems simulated in engineering, quantum mechanics, pharmacology, and economics are more sensitive and accurate [153, 154]. Thus, we consider the order of the fractional derivative to be variable (space and time-dependent). Refer to [155, 156] for some current numerical techniques for variable-order fractional differential equations.

7.2 Literature survey

In financial literature, recently, various techniques have been used to approximate the value of various options using the fixed-order classical fractional Black-Scholes model since analytical solutions are usually not easy to find. To cite a few, in context to the standard Black-Scholes model, Zhang *et al.* [24] developed an implicit discrete strategy with order $2-\alpha$ temporal precision and second-order spatial accuracy, where α is the order of the fractional derivative. Later, Zhao and Tian [157] investigated the second-order implicit finite difference scheme to solve the space fractional Black-Scholes equation. To explore the higher-dimensional model, Chen and Wang [158] presented a second-order ADI finite difference approach for a 2D fractional Black-Scholes equation deriving European two asset option pricing. For a time-fractional Black-Scholes model, Golbabai and Nikan [159] investigated a computational method based on the moving least-squares approach for pricing double barrier options.

By employing the Jacobi polynomials for the temporal discretization and Fourier-like basis functions for the spatial discretization, An *et al.* [160] proposed a method for the Black-Scholes model with fractional order derivative in time. However, there has been less research into simulating the behavior of fractional CEV model-based option pricing problems. In the last few years, Zhou and Gao [25] utilized the Laplace transform and finite difference method to price American options using the time-fractional Black-Scholes equation under the CEV model. Under the CEV model, Rezaei *et al.* [161] presented numerical pricing based on fractional Black-Scholes equation with time-dependent parameters for barrier options with Caputo's definition of fractional derivative. Most of the work described above is done with the Riemann-Liouville derivative or Caputo's derivative, both of which are quite old in fractional calculus. Thus, other fractional derivative formulations must be investigated.

7.3 Time-fractional constant elasticity of variance model

In this section, we specify the variable order time-fractional CEV model and its derivation. The model assumes that under the risk neutral probability, the underlying asset $\mathcal{S}$ at time $\mathfrak{t}$ evolves according to the following stochastic differential equation introduced by Jumarie [162]

$$d\mathcal{S}(\mathfrak{t}) = (r-D)\mathcal{S}(\mathfrak{t})d\mathfrak{t} + \delta\mathcal{S}^{\gamma+1}(\mathfrak{t})W(\mathfrak{t})(d\mathfrak{t})^{\frac{\alpha(\mathcal{S},\mathfrak{t})}{2}},\ 0<\alpha(\mathcal{S},\mathfrak{t})\leq 1. \tag{7.3.1}$$

The representations of the symbols used in the above model are given below:

$\alpha(\mathcal{S},\mathfrak{t})$	: the fractional order depending upon $\mathcal{S}$ and $\mathfrak{t}$
r	: the rate of interest
D	: the dividend yield
γ	: the elasticity factor
δ	: the scaling parameter
$W(\mathfrak{t})$	: the Gaussian white noise with mathematical expectation 0 and variance 1
$\sigma(\mathcal{S})$	: the local volatility function which for $\gamma<0$ is defined as $\sigma(\mathcal{S})=\delta\mathcal{S}^{\gamma}$

To derive the time-fractional CEV model, let the option price P is sufficiently smooth with respect to both $\mathcal{S}$ and $\mathfrak{t}$. More precisely, it is twice differentiable in $\mathcal{S}$ and the α-order fractional derivative in $\mathfrak{t}$ exists. Therefore, according to [162], using fractional Taylor's expansion for multivariate functions, we get

$$dP = \frac{1}{\Gamma(1+\alpha(\mathcal{S},\mathfrak{t}))}\frac{\partial^{\alpha(\mathcal{S},\mathfrak{t})}P}{\partial\mathfrak{t}^{\alpha(\mathcal{S},\mathfrak{t})}}(d\mathfrak{t})^{\alpha(\mathcal{S},\mathfrak{t})} + \frac{\partial P}{\partial\mathcal{S}}d\mathcal{S} + \frac{1}{2}\frac{\partial^2 P}{\partial\mathcal{S}^2}(d\mathcal{S})^2. \tag{7.3.2}$$

Using the definition of mathematical expectation and following the details in [163], we obtain

$$\begin{aligned}(d\mathcal{S})^2 =&(r-D)^2\mathcal{S}^2(\mathfrak{t})(d\mathfrak{t})^2 + (r-D)\delta\mathcal{S}^{\gamma+2}(\mathfrak{t})W(\mathfrak{t})(d\mathfrak{t})^{1+\frac{\alpha(\mathcal{S},\mathfrak{t})}{2}}\\ &+\delta^2\mathcal{S}^{2\gamma+2}(\mathfrak{t})W^2(\mathfrak{t})(d\mathfrak{t})^{\alpha(\mathcal{S},\mathfrak{t})}\\ =&\delta^2\mathcal{S}^{2\gamma+2}(\mathfrak{t})(d\mathfrak{t})^{\alpha(\mathcal{S},\mathfrak{t})}.\end{aligned} \tag{7.3.3}$$

Replacing Equations (7.3.1) and (7.3.3) in Equation (7.3.2) yields

$$dP = \frac{1}{\Gamma(1+\alpha(\mathcal{S},\mathfrak{t}))}\frac{\partial^{\alpha(\mathcal{S},\mathfrak{t})}P}{\partial \mathfrak{t}^{\alpha(\mathcal{S},\mathfrak{t})}}(d\mathfrak{t})^{\alpha(\mathcal{S},\mathfrak{t})} + (r-D)\mathcal{S}\frac{\partial P}{\partial \mathcal{S}}d\mathfrak{t} + \frac{1}{2}\delta^2\mathcal{S}^{2\gamma+2}\frac{\partial^2 P}{\partial \mathcal{S}^2}(d\mathfrak{t})^{\alpha(\mathcal{S},\mathfrak{t})} + \delta\mathcal{S}^{\gamma+1}W(\mathfrak{t})\frac{\partial P}{\partial \mathcal{S}}(d\mathfrak{t})^{\frac{\alpha(\mathcal{S},\mathfrak{t})}{2}}. \tag{7.3.4}$$

Now on substituting $(d\mathfrak{t})^{\alpha(\mathcal{S},\mathfrak{t})} = \Gamma(1+\alpha(\mathcal{S},\mathfrak{t}))\Gamma(2-\alpha(\mathcal{S},\mathfrak{t}))\mathfrak{t}^{\alpha(\mathcal{S},\mathfrak{t})-1}d\mathfrak{t}$, we get

$$dP = \Bigg(\Gamma(2-\alpha(\mathcal{S},\mathfrak{t}))\mathfrak{t}^{\alpha(\mathcal{S},\mathfrak{t})-1}\frac{\partial^{\alpha(\mathcal{S},\mathfrak{t})}P}{\partial \mathfrak{t}^{\alpha(\mathcal{S},\mathfrak{t})}} + (r-D)\mathcal{S}\frac{\partial P}{\partial \mathcal{S}} + \frac{\Gamma(1+\alpha(\mathcal{S},\mathfrak{t}))\Gamma(2-\alpha(\mathcal{S},\mathfrak{t}))}{2}\delta^2\mathcal{S}^{2\gamma+2}\mathfrak{t}^{\alpha(\mathcal{S},\mathfrak{t})-1}\frac{\partial^2 P}{\partial \mathcal{S}^2}\Bigg)d\mathfrak{t} + \delta\mathcal{S}^{\gamma+1}W(\mathfrak{t})\frac{\partial P}{\partial \mathcal{S}}(d\mathfrak{t})^{\frac{\alpha(\mathcal{S},\mathfrak{t})}{2}}. \tag{7.3.5}$$

Assuming arbitrage free market with a riskfree hedging portfolio and following [161], we get the following fractional differential equation for $\mathcal{S}$ varying from $\mathcal{S}_{\min}$ to $\mathcal{S}_{\max}$ and $\mathfrak{t}$ lying in $[0,T)$ with T being the expiry time

$$\frac{\partial^{\alpha(\mathcal{S},\mathfrak{t})}P}{\partial \mathfrak{t}^{\alpha(\mathcal{S},\mathfrak{t})}} + \delta^2\mathcal{S}^{2\gamma+2}\frac{\Gamma(1+\alpha(\mathcal{S},\mathfrak{t}))}{2}\frac{\partial^2 P}{\partial \mathcal{S}^2} + (r(\mathfrak{t})-D(\mathfrak{t}))\mathcal{S}\frac{\mathfrak{t}^{1-\alpha(\mathcal{S},\mathfrak{t})}}{\Gamma(2-\alpha(\mathcal{S},\mathfrak{t}))}\frac{\partial P}{\partial \mathcal{S}} - r(\mathfrak{t})\frac{\mathfrak{t}^{1-\alpha(\mathcal{S},\mathfrak{t})}}{\Gamma(2-\alpha(\mathcal{S},\mathfrak{t}))}P = \tilde{f}(\mathcal{S},\mathfrak{t}), \tag{7.3.6a}$$

where we consider the interest rate and dividend to be time-dependent, since the characteristics of an asset price are time-dependent. In addition, the equation which implicitly defines the optimal exercise boundary is as follows

$$P(\mathcal{S},T) = \phi(\mathcal{S}),\ \mathcal{S}_{\min} \le \mathcal{S} \le \mathcal{S}_{\max}, \tag{7.3.6b}$$

and the option's behavior at the boundaries of $\mathcal{S}$ is defined as

$$P(\mathcal{S}_{\min},\mathfrak{t}) = \nu(\mathfrak{t}),\ 0 \le \mathfrak{t} \le T, \tag{7.3.6c}$$

$$P(\mathcal{S}_{\max},\mathfrak{t}) = \mu(\mathfrak{t}),\ 0 \le \mathfrak{t} \le T. \tag{7.3.6d}$$

To describe the negative relation between the asset price and its return volatility, a similar model was also derived in [161] using Jumarie's fractional model of 2008. The numerical algorithm is implemented by converting the final value problem to an initial value problem using the transformation $t = T - \mathfrak{t}$. As a result, the problem (7.3.6) is transformed into

$$\frac{\partial^{\alpha(\mathcal{S},t)}P}{\partial t^{\alpha(\mathcal{S},t)}} = \delta^2\mathcal{S}^{2\gamma+2}\frac{\Gamma(1+\alpha(\mathcal{S},t))}{2}\frac{\partial^2 P}{\partial \mathcal{S}^2} + (r(t)-D(t))\mathcal{S}\frac{t^{1-\alpha(\mathcal{S},t)}}{\Gamma(2-\alpha(\mathcal{S},t))}\frac{\partial P}{\partial \mathcal{S}}$$
$$- r(t)\frac{t^{1-\alpha(\mathcal{S},t)}}{\Gamma(2-\alpha(\mathcal{S},t))}P + f(\mathcal{S},t). \tag{7.3.7a}$$

The terminal condition is now converted into initial condition written as

$$P(\mathcal{S},0) = \phi(\mathcal{S}),\ \mathcal{S}_{\min} \leq \mathcal{S} \leq \mathcal{S}_{\max}, \tag{7.3.7b}$$

and the option's behavior at the boundaries of $\mathcal{S}$ is reformulated as

$$P(\mathcal{S}_{\min},t) = \nu(t),\ 0 \leq t \leq T, \tag{7.3.7c}$$

$$P(\mathcal{S}_{\max},t) = \mu(t),\ 0 \leq t \leq T. \tag{7.3.7d}$$

7.4 Fractional operators

This section contains some fundamental definitions of variable-order fractional calculus. Further material on the subject can be found in [23, 164].

Definition 7.4.1. *The variable order Reimann-Liouville fractional derivative with order $\alpha(\mathcal{S},t) \in R$ of a function g is defined as*

$${}_0D_t^{\alpha(\mathcal{S},t)}g(t) = \frac{1}{\Gamma(r-\alpha(\mathcal{S},t))}\frac{d^r}{dt^r}\int_0^t (t-s)^{r-\alpha(\mathcal{S},t)-1}g(s)\,ds,\ t>0, \tag{7.4.1}$$

where r is a positive integer and $r-1 < \alpha(\mathcal{S},t) < r$.

The Riemann-Liouville derivative has some drawbacks when using fractional differential equations to simulate real-world processes [23]. These drawbacks limit the scope of

the Riemann-Liouville fractional derivative's application.

Definition 7.4.2. *Caputo variable order derivative operator with order $\alpha(\mathcal{S},t) \in R$ is defined as*

$$ {}_0^C D_t^{\alpha(\mathcal{S},t)} g(t) = \frac{1}{\Gamma(r-\alpha(\mathcal{S},t))} \int_0^t (t-s)^{r-\alpha(\mathcal{S},t)-1} g^{(r)}(s)\, ds,\ t>0, \tag{7.4.2} $$

where r is a positive integer and $r-1 < \alpha(\mathcal{S},t) < r$.

One of the critical features of the Caputo fractional derivative is that it permits for the inclusion of classical initial and boundary conditions in the problem formulation. This operator, however, has some restrictions due to its singular kernel. It is taken into account in Atangana and Baleanu's definition given below.

Definition 7.4.3. *Atangana-Baleanu Caputo variable order derivative operator with order $\alpha(\mathcal{S},t) \in [0,1]$ of a function $g \in H^1(0,1)$ is defined as*

$$ {}_0^{ABC} D_t^{\alpha(\mathcal{S},t)} g(t) = \frac{\mathcal{N}(\alpha(\mathcal{S},t))}{1-\alpha(\mathcal{S},t)} \int_0^t g'(s) E_{\alpha(\mathcal{S},t),1}\left[\frac{-\alpha(\mathcal{S},t)}{1-\alpha(\mathcal{S},t)}(t-s)^{\alpha(\mathcal{S},t)}\right] ds, \tag{7.4.3} $$

where $\mathcal{N}(\alpha(\mathcal{S},t))$ is termed as normalization function obeying $\mathcal{N}(0) = \mathcal{N}(1) = 1$, and

$$ E_{\alpha(\mathcal{S},t),\beta}(z) = \sum_{r=0}^{\infty} \frac{z^r}{\Gamma(\alpha(\mathcal{S},t)r+\beta)}, \tag{7.4.4} $$

is the Mittag-Leffler function.

7.5 Discretization techniques

To derive the discretized form of the problem (7.3.7), assume that h and τ are the mesh sizes in the spatial and temporal directions, respectively. Let $\mathcal{S}_{\min} = \mathcal{S}_0 < \mathcal{S}_1 < \mathcal{S}_2 < \ldots < \mathcal{S}_{N_\mathcal{S}} = \mathcal{S}_{\max}$, $\mathcal{S}_i = ih$, $i = 0,1,2,\ldots,N_\mathcal{S}$, where $h = \frac{\mathcal{S}_{\max}-\mathcal{S}_{\min}}{N_\mathcal{S}}$ and $0 = t_0 < t_1 < t_2 < \ldots < t_{N_t} = T$, $t_n = n\tau$, $n = 0,1,2,\ldots,N_t$, where $\tau = T/N_t$. We describe the numerical approximation of ABC derivative by two different methods.

7.5.1 Time discretization

We use Taylor's expansion of the derivative of a function $g(t)$ in this method to attain the higher level of convergence. Expand $g'(t)$ using the Taylor's expansion around t_q for $t \in (t_q, t_{q+1})$ to get

$$g'(t) = g'(t_q) + (t - t_q)g''(t_q) + (t - t_q)^2 \frac{g^{(3)}(t_q)}{2!} + O(\,(t - t_q)^3). \tag{7.5.1}$$

Now using

$$\begin{aligned} g'(t_q) &= \frac{g(t_{q+1}) - g(t_{q-1})}{2\tau} - \frac{g^{(3)}(t_q)}{3!}\tau^2 + O(\tau^4), \\ g''(t_q) &= \frac{g(t_{q+1}) - 2g(t_q) + g(t_{q-1})}{\tau^2} - \frac{g^{(4)}(t_q)}{12}\tau^2 + O(\tau^4), \end{aligned}$$

in the Equation (7.5.1), we get

$$\begin{aligned} g'(t) = \frac{g(t_{q+1}) - g(t_{q-1})}{2\tau} + (t - t_q)\frac{g(t_{q+1}) - 2g(t_q) + g(t_{q-1})}{\tau^2} - \frac{g^{(3)}(t_q)}{3!}\tau^2 - \frac{g^{(4)}(t_q)}{12}\tau^2 \\ + (t - t_q)^2 \frac{g^{(3)}(t_q)}{2!} + O((t - t_q)^3), \quad t \in (t_q, t_{q+1}). \end{aligned}$$

Therefore,

$$\begin{aligned} &{}^{ABC}_{0}D^{\alpha}_{t} g(t)|_{t=t_n} = \frac{\mathcal{N}(\alpha)}{1-\alpha}\int_0^{t_n} g'(s) E_{\alpha,1}\left[\frac{-\alpha}{1-\alpha}(t_n - s)^{\alpha}\right] ds \\ &= \frac{\mathcal{N}(\alpha)}{1-\alpha}\sum_{q=0}^{n-1}\int_{t_q}^{t_{q+1}} g'(s) E_{\alpha,1}\left[\frac{-\alpha}{1-\alpha}(t_n - s)^{\alpha}\right] ds \\ &= \frac{\mathcal{N}(\alpha)}{1-\alpha}\sum_{q=0}^{n-1}\int_{t_q}^{t_{q+1}} \left\{\frac{g(t_{q+1}) - g(t_{q-1})}{2\tau} + \frac{g(t_{q+1}) - 2g(t_q) + g(t_{q-1})}{\tau^2}(s - t_q)\right\} \\ &E_{\alpha,1}\left[\frac{-\alpha}{1-\alpha}(t_n - s)^{\alpha}\right] ds + R_n \\ &= \frac{\mathcal{N}(\alpha)}{1-\alpha}\sum_{q=0}^{n-1}\left\{ \left(\frac{g(t_{q+1}) - g(t_{q-1})}{2\tau}\right)\left[- (t_n - s)E_{\alpha,2}\left[\frac{-\alpha}{1-\alpha}(t_n - s)^{\alpha}\right]\right]_{t_q}^{t_{q+1}} \end{aligned}$$

$$
\begin{aligned}
&+\left(\frac{g(t_{q+1})-2g(t_q)+g(t_{q-1})}{\tau^2}\right)\Bigg[\left\{-(s-t_q)(t_n-s)E_{\alpha,2}\left[\frac{-\alpha}{1-\alpha}(t_n-s)^{\alpha}\right]\right\}_{t_q}^{t_{q+1}}\\
&+\int_{t_q}^{t_{q+1}}(t_n-s)E_{\alpha,2}\left[\frac{-\alpha}{1-\alpha}(t_n-s)^{\alpha}\right]ds\Bigg]\Bigg\}+R_n\\
&=\frac{\mathcal{N}(\alpha)}{1-\alpha}\sum_{q=0}^{n-1}\Bigg\{\left(\frac{g(t_{q+1})-g(t_{q-1})}{2}\right)\Big[(n-q)\,{}_1E_q^n-(n-q-1)\,{}_1E_{q+1}^n\Big]\\
&+\Big(g(t_{q+1})-2g(t_q)+g(t_{q-1})\Big)\Big[-(n-q-1)\,{}_1E_{q+1}^n-(n-q-1)^2\,{}_2E_{q+1}^n\\
&+(n-q)^2\,{}_2E_q^n\Big]\Bigg\}+R_n\\
&=\sum_{q=0}^{n-1}\left[\Big(g(t_{q+1})-g(t_{q-1})\Big)A_q^n+\Big(g(t_{q+1})-2g(t_q)+g(t_{q-1})\Big)B_q^n\right]+R_n.
\end{aligned}
$$

On simplifying, finally we have

$$
{}_0^{ABC}D_t^{\alpha}g(t)|_{t=t_n}=\sum_{q=0}^{n-1}\Big[g(t_{q-1})a_q^n+g(t_q)b_q^n+g(t_{q+1})c_q^n\Big]+R_n, \tag{7.5.2}
$$

where ${}_{i-1}E_q^n$ is used for $E_{\alpha,i}\big[\frac{-\alpha}{1-\alpha}(t_n-t_q)^{\alpha}\big]$, $i=2,3,\ldots$, and

$$
\begin{aligned}
A_q^n&=\frac{1}{2}\frac{\mathcal{N}(\alpha)}{1-\alpha}[(n-q)\,{}_1E_q^n-(n-q-1)\,{}_1E_{q+1}^n],\\
B_q^n&=\frac{\mathcal{N}(\alpha)}{1-\alpha}[-(n-q-1)\,{}_1E_{q+1}^n-(n-q-1)^2\,{}_2E_{q+1}^n+(n-q)^2\,{}_2E_q^n],\\
a_q^n&=-A_q^n+B_q^n,\ b_q^n=-2B_q^n,\ c_q^n=A_q^n+B_q^n.
\end{aligned}
$$

Furthermore, the error R_n in this approximation is given as follows:

$$
\begin{aligned}
R_n&=\frac{\mathcal{N}(\alpha)}{1-\alpha}\sum_{q=0}^{n-1}\int_{t_q}^{t_{q+1}}\left(-\frac{g^{(3)}(t_q)}{3!}\tau^2+\frac{g^{(3)}(t_q)}{2!}(s-t_q)^2-\frac{g^{(4)}(t_q)}{12}\tau^2\right)\\
&\quad\times E_{\alpha,1}\left[\frac{-\alpha}{1-\alpha}(t_n-s)^{\alpha}\right]ds\\
&=\frac{\mathcal{N}(\alpha)}{1-\alpha}\sum_{q=0}^{n-1}\left[-\frac{g^{(3)}(t_q)}{3!}\tau^2\int_{t_q}^{t_{q+1}}E_{\alpha,1}\left[\frac{-\alpha}{1-\alpha}(t_n-s)^{\alpha}\right]ds+\frac{g^{(3)}(t_q)}{2!}\int_{t_q}^{t_{q+1}}(s-t_q)^2\right.
\end{aligned}
$$

$$
\begin{aligned}
&\times E_{\alpha,1}\left[\frac{-\alpha}{1-\alpha}(t_n-s)^{\alpha}\right]ds-\frac{g^{(4)}(t_q)}{12}\tau^2\int_{t_q}^{t_{q+1}}E_{\alpha,1}\left[\frac{-\alpha}{1-\alpha}(t_n-s)^{\alpha}\right]ds\Bigg]\\
&=\frac{\mathcal{N}(\alpha)}{1-\alpha}\sum_{q=0}^{n-1}\Bigg[\frac{g^{(3)}(t_q)}{3!}\tau^2\Bigg\{(t_n-s)E_{\alpha,2}\left[\frac{-\alpha}{1-\alpha}(t_n-s)^{\alpha}\right]\Bigg\}_{t_q}^{t_{q+1}}\\
&-\frac{g^{(3)}(t_q)}{2!}\Bigg\{(s-t_q)^2(t_n-s)E_{\alpha,2}\left[\frac{-\alpha}{1-\alpha}(t_n-s)^{\alpha}\right]\Bigg\}_{t_q}^{t_{q+1}}\\
&+\frac{g^{(3)}(t_q)}{2!}\Bigg\{-2(s-t_q)(t_n-s)^2E_{\alpha,3}\left[\frac{-\alpha}{1-\alpha}(t_n-s)^{\alpha}\right]\Bigg\}_{t_q}^{t_{q+1}}\\
&-\frac{g^{(3)}(t_q)}{2!}\Bigg\{2(t_n-s)^3E_{\alpha,4}\left[\frac{-\alpha}{1-\alpha}(t_n-s)^{\alpha}\right]\Bigg\}_{t_q}^{t_{q+1}}\\
&-\frac{g^{(4)}(t_q)}{12}\tau^2\Bigg\{-(t_n-s)E_{\alpha,2}\left[\frac{-\alpha}{1-\alpha}(t_n-s)^{\alpha}\right]\Bigg\}_{t_q}^{t_{q+1}}\Bigg]\\
&=\frac{\mathcal{N}(\alpha)}{1-\alpha}\sum_{q=0}^{n-1}\Bigg[\frac{g^{(3)}(t_q)}{3!}\tau^2\Big\{(t_n-t_{q+1})\,{}_1E_{q+1}^n-(t_n-t_q)\,{}_1E_q^n\Big\}\\
&-\frac{g^{(3)}(t_q)}{2!}\tau^2\Big\{(t_n-t_{q+1})\,{}_1E_{q+1}^n\Big\}\\
&-\frac{g^{(3)}(t_q)}{2!}2\tau(t_n-t_{q+1})^2\,{}_2E_{q+1}^n-\frac{g^{(3)}(t_q)}{2!}\Big\{2(t_n-t_{q+1})^3\,{}_3E_{q+1}^n\Big\}\\
&+\frac{g^{(3)}(t_q)}{2!}\Big\{2(t_n-t_q)^3\,{}_3E_q^n\Big\}\\
&+\frac{g^{(4)}(t_q)}{12}\tau^2\Big\{(t_n-t_{q+1})\,{}_1E_{q+1}^n-(t_n-t_q)\,{}_1E_q^n\Big\}\Bigg].
\end{aligned}
$$

Let $M_1=\max\limits_{0\le t\le t_{n-1}}|g^{(3)}(t)|$, $M_2=\max\limits_{0\le t\le t_{n-1}}|g^{(4)}(t)|$, and $\mathcal{M}=\max\{M_1,M_2\}$. Then

$$|R_n|\le\frac{\mathcal{N}(\alpha)}{1-\alpha}\tau^3\mathcal{M}C_2, \tag{7.5.3}$$

for some constant C_2.

7.5.2 Spatial discretization

Now, the space derivatives of first and second order are approximated as

$$\frac{\partial P}{\partial\mathcal{S}}=\frac{P_{i+1}^n-P_{i-1}^n}{2h}+O(h^2), \tag{7.5.4}$$

$$\frac{\partial^2 P}{\partial \mathcal{S}^2} = \frac{P_{i-1}^n - 2P_i^n + P_{i+1}^n}{h^2} + O(h^2), \tag{7.5.5}$$

where $P_i^n = P(\mathcal{S}_i, t_n)$, for $1 \leq i \leq N_{\mathcal{S}} - 1$ and $1 \leq n \leq N_t$.

7.5.3 Fully discrete scheme

For the deriving the fully discrete scheme for problem (7.3.7), let

$$\begin{aligned}
K_1(\mathcal{S}_i, t_n) &= \delta^2 (\mathcal{S}_i)^{2\gamma+2} \frac{\Gamma(1 + \alpha(\mathcal{S}_i, t_n))}{2}, \\
K_2(\mathcal{S}_i, t_n) &= (r(t_n) - D(t_n))\mathcal{S}_i \frac{(t_n)^{1-\alpha(\mathcal{S}_i, t_n)}}{\Gamma(2 - \alpha(\mathcal{S}_i, t_n))}, \\
K_3(\mathcal{S}_i, t_n) &= r(t_n) \frac{(t_n)^{1-\alpha(\mathcal{S}_i, t_n)}}{\Gamma(2 - \alpha(\mathcal{S}_i, t_n))},
\end{aligned}$$

and substitute the values obtained from Equations (7.5.2), (7.5.4), and (7.5.5) in Equation (7.3.7), the following difference scheme is obtained for the given fractional partial differential equation which yields accuracy of order $O(\tau^3 + h^2)$

$$\begin{aligned}
\sum_{q=0}^{n-1} \left[a_q^n P_i^{q-1} + b_q^n P_i^q + c_q^n P_i^{q+1} \right] &= K_1(\mathcal{S}_i, t_n) \left(\frac{P_{i-1}^n - 2P_i^n + P_{i+1}^n}{h^2} \right) \\
&+ K_2(\mathcal{S}_i, t_n) \left(\frac{P_{i+1}^n - P_{i-1}^n}{2h} \right) - K_3(\mathcal{S}_i, t_n) P_i^n + f(\mathcal{S}_i, t_n),
\end{aligned}$$

where $1 \leq i \leq N_{\mathcal{S}} - 1,\ 1 \leq n \leq N_t$, and the terminal and boundary conditions are discretized as

$$\begin{aligned}
P(\mathcal{S}_i, 0) &= \phi(\mathcal{S}_i), \quad 1 \leq i \leq N_{\mathcal{S}} - 1, \\
P(\mathcal{S}_{\min}, t_n) &= \nu(t_n), \quad 0 \leq n \leq N_t, \\
P(\mathcal{S}_{\max}, t_n) &= \mu(t_n), \quad 0 \leq n \leq N_t.
\end{aligned}$$

On rearranging the above system, for $1 \leq i \leq N_{\mathcal{S}} - 1,\ 1 \leq n \leq N_t$, we obtain

$$\left(- \frac{K_1(\mathcal{S}_i, t_n)}{h^2} + \frac{K_2(\mathcal{S}_i, t_n)}{2h} \right) P_{i-1}^n + \left(\frac{2K_1(\mathcal{S}_i, t_n)}{h^2} + K_3(\mathcal{S}_i, t_n) \right) P_i^n$$

$$+\left(-\frac{K_1(\mathcal{S}_i,t_n)}{h^2}-\frac{K_2(\mathcal{S}_i,t_n)}{2h}\right)P_{i+1}^n+\sum_{q=0}^{n-1}\left[a_q^nP_i^{q-1}+b_q^nP_i^q+c_q^nP_i^{q+1}\right]=f(\mathcal{S}_i,t_n),$$

(7.5.6a)

with

$$P(\mathcal{S}_i,0)=\phi(\mathcal{S}_i),\quad 1\le i\le N_{\mathcal{S}}-1, \tag{7.5.6b}$$

$$P(\mathcal{S}_{\min},t_n)=\nu(t_n),\quad 0\le n\le N_t, \tag{7.5.6c}$$

$$P(\mathcal{S}_{\max},t_n)=\mu(t_n),\quad 0\le n\le N_t. \tag{7.5.6d}$$

For $n=1$, it gives

$$\left(-\frac{K_1(\mathcal{S}_i,t_1)}{h^2}+\frac{K_2(\mathcal{S}_i,t_1)}{2h}\right)P_{i-1}^1+\left(\frac{2K_1(\mathcal{S}_i,t_1)}{h^2}+K_3(\mathcal{S}_i,t_1)+c_0^1\right)P_i^1$$
$$+\left(-\frac{K_1(\mathcal{S}_i,t_1)}{h^2}-\frac{K_2(\mathcal{S}_i,t_1)}{2h}\right)P_{i+1}^1=-(a_0^1+b_0^1)P_i^0+f(\mathcal{S}_i,t_1),$$

For $n=2$, it gives

$$\left(-\frac{K_1(\mathcal{S}_i,t_2)}{h^2}+\frac{K_2(\mathcal{S}_i,t_2)}{2h}\right)P_{i-1}^2+\left(\frac{2K_1(\mathcal{S}_i,t_2)}{h^2}+K_3(\mathcal{S}_i,t_2)+c_1^2\right)P_i^2$$
$$+\left(-\frac{K_1(\mathcal{S}_i,t_2)}{h^2}-\frac{K_2(\mathcal{S}_i,t_2)}{2h}\right)P_{i+1}^2=-(a_0^2+b_0^2+a_1^2)P_i^0-(c_0^2+b_1^2)P_i^1+f(\mathcal{S}_i,t_2),$$

while for $3\le n\le N_t$, we get

$$\left(-\frac{K_1(\mathcal{S}_i,t_n)}{h^2}+\frac{K_2(\mathcal{S}_i,t_n)}{2h}\right)P_{i-1}^n+\left(\frac{2K_1(\mathcal{S}_i,t_n)}{h^2}+K_3(\mathcal{S}_i,t_n)+c_{n-1}^n\right)P_i^n$$
$$+\left(-\frac{K_1(\mathcal{S}_i,t_n)}{h^2}-\frac{K_2(\mathcal{S}_i,t_n)}{2h}\right)P_{i+1}^n=-\sum_{q=1}^{n-2}\left[a_q^nP_i^{q-1}+b_q^nP_i^q+c_q^nP_i^{q+1}\right]-a_{n-1}^nP_i^{n-2}$$
$$-b_{n-1}^nP_i^{n-1}-(a_0^n+b_0^n)P_i^0-c_0^nP_i^1+f(\mathcal{S}_i,t_n). \tag{7.5.7}$$

Assuming

$$\begin{aligned}\tilde{a}_{i,n} &= -\frac{K_1(\mathcal{S}_i,t_n)}{h^2}+\frac{K_2(\mathcal{S}_i,t_n)}{2h},\\ \tilde{b}_{i,n} &= \frac{2K_1(\mathcal{S}_i,t_n)}{h^2}+K_3(\mathcal{S}_i,t_n)+c^n_{n-1},\\ \tilde{c}_{i,n} &= -\frac{K_1(\mathcal{S}_i,t_n)}{h^2}-\frac{K_2(\mathcal{S}_i,t_n)}{2h},\end{aligned}$$

the matrix form of the above system of equations can be written as

$$L^nP^n = H^n + G^n + F^n,$$

where

$$L^n = \begin{bmatrix} \tilde{b}_{1,n} & \tilde{c}_{1,n} & 0 & \dots & 0 \\ \tilde{a}_{2,n} & \tilde{b}_{2,n} & \tilde{c}_{2,n} & \dots & 0 \\ \vdots & \vdots & \ddots & \vdots & \vdots \\ 0 & 0 & \dots & \tilde{a}_{N_{\mathcal{S}}-1,n} & \tilde{b}_{N_{\mathcal{S}}-1,n} \end{bmatrix}_{(N_{\mathcal{S}}-1)\times(N_{\mathcal{S}}-1)},$$

$$P^n = [P^n_1, P^n_2, P^n_3, \dots, P^n_{N_{\mathcal{S}}-1}]^T,$$

$$G^n = [\tilde{a}_{1,n}P^n_0, 0, \dots, 0, \tilde{c}_{N_{\mathcal{S}}-1,n}P^n_{N_{\mathcal{S}}}]^T,$$

$$F^n = [f^n_1, f^n_2, f^n_3, \dots, f^n_{N_{\mathcal{S}}-1}]^T,$$

$$H^n = \begin{cases} -(a^1_0+b^1_0)P^0, \quad n=1, \\ -(a^2_0+b^2_0+a^2_1)P^0_i-(c^2_0+b^2_1)P^1_i, \quad n=2, \\ -\sum_{q=1}^{n-2}\left[a^n_qP^{q-1}+b^n_qP^q+c^n_qP^{q+1}\right] \\ -a^n_{n-1}P^{n-2}-b^n_{n-1}P^{n-1}-(a^n_0+b^n_0)P^0-c^n_0P^1, \quad 3\le n\le N_t. \end{cases}$$

7.6 Stability analysis

In this section, we will prove that the proposed scheme is unconditionally stable. For that purpose, it is enough to prove the stability of the scheme (7.5.6) without the source term

$f(\mathcal{S},t)$. Moreover, in the stability theorem, we use the following notations:

$$(P_i^n)_{\mathcal{S}} = \frac{P_{i+1}^n - P_{i-1}^n}{2h},$$
$$(P_i^n)_{\mathcal{SS}} = \frac{P_{i-1}^n - 2P_i^n + P_{i+1}^n}{h^2}.$$

Theorem 7.6.1. *Let $P^0 \in H_0^2[\mathcal{S}_{\min}, \mathcal{S}_{\max}]$, then there exist a positive constant C such that the solution of the finite difference scheme (7.5.6) satisfies $\|P^n\| \leq C,\ n = 1, 2, \ldots, N_t$.*

Proof. Consider the numerical scheme

$$\sum_{q=0}^{n-1} \left[a_q^n P_i^{q-1} + b_q^n P_i^q + c_q^n P_i^{q+1}\right] = K_1(\mathcal{S}_i, t_n)(P_i^n)_{\mathcal{SS}} + K_2(\mathcal{S}_i, t_n)(P_i^n)_{\mathcal{S}} - K_3(\mathcal{S}_i, t_n)P_i^n, \tag{7.6.1}$$

where $1 \leq i \leq N_{\mathcal{S}} - 1,\ 1 \leq n \leq N_t$, with $P(\mathcal{S}_{\min}, t_n) = \nu(t_n)$ and $P(\mathcal{S}_{\max}, t_n) = \mu(t_n)$.

Rewrite Equation (7.6.1) as

$$a_0^n P_i^{-1} + b_0^n P_i^0 + c_0^n P_i^1 + \sum_{q=1}^{n-1} \left[a_q^n P_i^{q-1} + b_q^n P_i^q + c_q^n P_i^{q+1}\right] = K_1(\mathcal{S}_i, t_n)(P_i^n)_{\mathcal{SS}}$$
$$+ K_2(\mathcal{S}_i, t_n)(P_i^n)_{\mathcal{S}} - K_3(\mathcal{S}_i, t_n)P_i^n.$$

Now considering $P_i^{-1} = P_i^0$, the above equation can be written as

$$(a_0^n + b_0^n)P_i^0 + c_0^n P_i^1 + \sum_{q=1}^{n-1} \left[a_q^n P_i^{q-1} + b_q^n P_i^q + c_q^n P_i^{q+1}\right]$$
$$- K_2(\mathcal{S}_i, t_n)(P_i^n)_{\mathcal{S}} + K_3(\mathcal{S}_i, t_n)P_i^n = K_1(\mathcal{S}_i, t_n)(P_i^n)_{\mathcal{SS}}. \tag{7.6.2}$$

Multiplying (7.6.2) by hP_i^n and summing up for i from 1 to $N_{\mathcal{S}} - 1$, we get

$$(a_0^n + b_0^n)(P_i^0, P_i^n) + c_0^n(P_i^1, P_i^n) + \sum_{q=1}^{n-1} \left[a_q^n(P_i^{q-1}, P_i^n) + b_q^n(P_i^q, P_i^n) + c_q^n(P_i^{q+1}, P_i^n)\right]$$

$$- hK_2(\mathcal{S}_i, t_n) \sum_{i=1}^{N_{\mathcal{S}}-1} \frac{P_{i+1}^n - P_{i-1}^n}{2h} P_i^n + K_3(\mathcal{S}_i, t_n)\|P_i^n\|^2$$
$$= K_1(\mathcal{S}_i, t_n)((P_i^n)_{\mathcal{SS}}, P_i^n), \tag{7.6.3}$$

where $(P_i^q, P_i^n) = h\sum_{i=1}^{N_{\mathcal{S}}-1} P_i^q P_i^n$ and $\|P_i^n\|^2 = (P_i^n, P_i^n)$. Now using the expression

$$-hK_2(\mathcal{S}_i, t_n) \sum_{i=1}^{N_{\mathcal{S}}-1} \frac{P_{i+1}^n - P_{i-1}^n}{2h} P_i^n = \frac{-K_2(\mathcal{S}_i, t_n)}{2} \sum_{i=1}^{N_{\mathcal{S}}-1} (P_{i+1}^n - P_{i-1}^n) P_i^n$$
$$= \frac{-K_2}{2}(P_2^n P_1^n - P_1^n P_0^n + P_3^n P_2^n - P_2^n P_1^n + \ldots + P_{N_{\mathcal{S}-1}}^n P_{N_{\mathcal{S}-2}}^n$$
$$- P_{N_{\mathcal{S}-2}}^n P_{N_{\mathcal{S}-3}}^n + P_{N_{\mathcal{S}}}^n P_{N_{\mathcal{S}-1}}^n - P_{N_{\mathcal{S}-2}}^n P_{N_{\mathcal{S}-1}}^n),$$

the Equation (7.6.3) can be written as

$$(a_0^n + b_0^n)(P_i^0, P_i^n) + c_0^n(P_i^1, P_i^n) + \sum_{q=1}^{n-1} \left[a_q^n(P_i^{q-1}, P_i^n) + b_q^n(P_i^q, P_i^n) + c_q^n(P_i^{q+1}, P_i^n)\right]$$
$$+ \frac{K_2}{2}(P_1^n P_0^n - P_{N_{\mathcal{S}}}^n P_{N_{\mathcal{S}-1}}^n) + K_3(\mathcal{S}_i, t_n)\|P_i^n\|^2 = K_1(\mathcal{S}_i, t_n)((P_i^n)_{\mathcal{SS}}, P_i^n). \tag{7.6.4}$$

Note that $((P_i^n)_{\mathcal{SS}}, P_i^n) = -((P_i^n)_{\mathcal{S}}, (P_i^n)_{\mathcal{S}}) = -\|(P_i^n)_{\mathcal{S}}\|^2$. Thus, we have from (7.6.4)

$$(a_0^n + b_0^n)(P_i^0, P_i^n) + c_0^n(P_i^1, P_i^n) + \sum_{q=1}^{n-1} \left[a_q^n(P_i^{q-1}, P_i^n) + b_q^n(P_i^q, P_i^n) + c_q^n(P_i^{q+1}, P_i^n)\right]$$
$$+ \frac{K_2}{2}(P_1^n P_0^n - P_{N_{\mathcal{S}}}^n P_{N_{\mathcal{S}-1}}^n) + K_3(\mathcal{S}_i, t_n)\|P_i^n\|^2 = -K_1(\mathcal{S}_i, t_n)\|(P_i^n)_{\mathcal{S}}\|^2.$$

Rearranging the terms in the above expression, provides

$$c_{n-1}^n\|P_i^n\|^2 + K_1(\mathcal{S}_i, t_n)\|(P_i^n)_{\mathcal{S}}\|^2 + K_3(\mathcal{S}_i, t_n)\|P_i^n\|^2 = -\sum_{q=1}^{n-2} \left[a_q^n(P_i^{q-1}, P_i^n)\right.$$
$$\left. + b_q^n(P_i^q, P_i^n) + c_q^n(P_i^{q+1}, P_i^n)\right] - (a_0^n + b_0^n)(P_i^0, P_i^n) - c_0^n(P_i^1, P_i^n) - a_{n-1}^n(P_i^{n-2}, P_i^n)$$
$$- b_{n-1}^n(P_i^{n-1}, P_i^n) - \frac{K_2}{2}(P_1^n P_0^n - P_{N_{\mathcal{S}}}^n P_{N_{\mathcal{S}-1}}^n).$$

Now, by using the Young's inequality for inner product, we obtain

$$c_{n-1}^n\|P_i^n\|^2 + K_1(\mathcal{S}_i,t_n)\|(P_i^n)_{\mathcal{S}}\|^2 + K_3(\mathcal{S}_i,t_n)\|P_i^n\|^2 \leq \frac{1}{2}\Bigg\{ -\sum_{q=1}^{n-2}\big[a_q^n(\|P_i^{q-1}\|^2+\|P_i^n\|^2) + b_q^n(\|P_i^q\|^2+\|P_i^n\|^2) + c_q^n(\|P_i^{q+1}\|^2+\|P_i^n\|^2)\big] - (a_0^n+b_0^n)(\|P_i^0\|^2+\|P_i^n\|^2) - c_0^n(\|P_i^1\|^2+\|P_i^n\|^2) - a_{n-1}^n(\|P_i^{n-2}\|^2+\|P_i^n\|^2) - b_{n-1}^n(\|P_i^{n-1}\|^2+\|P_i^n\|^2)\Bigg\} - \frac{K_2}{2}(\|P_1^n\|^2+\|P_0^n\|^2) + \frac{K_2}{2}(\|P_{N_{\mathcal{S}}}^n+\|^2\|P_{N_{\mathcal{S}-1}}^n\|^2).$$

Using the results $a_q^n + b_q^n + c_q^n = 0$ and $a_{n-1}^n + b_{n-1}^n = -c_{n-1}^n$, the above inequality gives

$$\frac{1}{2}c_{n-1}^n\|P_i^n\|^2 + K_1(\mathcal{S}_i,t_n)\|(P_i^n)_{\mathcal{S}}\|^2 + K_3(\mathcal{S}_i,t_n)\|P_i^n\|^2 \leq \frac{1}{2}\Bigg\{ -\sum_{q=1}^{n-2}\big[a_q^n\|P_i^{q-1}\|^2 + b_q^n\|P_i^q\|^2 + c_q^n\|P_i^{q+1}\|^2\big] - a_{n-1}^n\|P_i^{n-2}\|^2 - b_{n-1}^n\|P_i^{n-1}\|^2 - \frac{K_2}{2}(\|P_1^n\|^2+\|P_0^n\|^2) + \frac{K_2}{2}(\|P_{N_{\mathcal{S}}}^n\|^2+\|P_{N_{\mathcal{S}-1}}^n\|^2)\Bigg\}.$$

Since $\|P_i^1\|^2 \leq \|P_i^0\|^2$, so let $\|P_i^q\|^2 \leq \|P_i^0\|^2$ holds for $q < n$, then the above inequality on using the boundary conditions yields

$$\frac{1}{2}c_{n-1}^n\|P_i^n\|^2 + K_1(\mathcal{S}_i,t_n)\|(P_i^n)_{\mathcal{S}}\|^2 + K_3(\mathcal{S}_i,t_n)\|P_i^n\|^2 \leq -\frac{1}{2}\sum_{q=1}^{n-1}\big[a_q^n+b_q^n+c_q^n\big]\|P_i^0\|^2 - \frac{1}{2}(a_{n-1}^n+b_{n-1}^n)\|P_i^0\|^2.$$

Again using $a_q^n + b_q^n + c_q^n = 0$ and $a_{n-1}^n + b_{n-1}^n = -c_{n-1}^n$, we get

$$\frac{1}{2}c_{n-1}^n\|P_i^n\|^2 + K_1(\mathcal{S}_i,t_n)\|(P_i^n)_{\mathcal{S}}\|^2 + K_3(\mathcal{S}_i,t_n)\|P_i^n\|^2 \leq \frac{1}{2}c_{n-1}^n\|P_i^0\|^2,$$

or

$$c_{n-1}^n\|P_i^n\|^2 \leq c_{n-1}^n\|P_i^0\|^2, \text{ as } K_1, K_3 \geq 0.$$

Hence,

$$\|P_i^n\|^2 \leq \|P_i^0\|^2, \text{ as } c_{n-1}^n > 0.$$

Thus, by mathematical induction, we say $\|P_i^q\|^2 \leq \|P_i^0\|^2$ for all $q = 1, 2, 3, \ldots, n$. Therefore, there exists a constant C such that

$$\|P^n\| \leq C, \ n = 1, 2, \ldots, N_t.$$

□

Using the above theorem and the definition of stability given below, we have shown that the present scheme is unconditionally stable.

Definition 7.6.1. *Let P^n and $\tilde{P}^n$ be two distinct approximate solutions for (7.3.7), and $P_0(\mathcal{S})$ and $\tilde{P}_0(\mathcal{S})$ are the corresponding initial conditions, then there exist a constant λ such that the numerical scheme is stable* i.e.,

$$\|P^n - \tilde{P}^n\| \leq \lambda \|P_0 - \tilde{P}_0\|.$$

7.7 Examples and applications

In this section, the proposed scheme is demonstrated on two test problems with varying parameters present in the CEV model. Through, the numerically computed results presented in the form of tables and graphs, we prove that the present scheme is proficient and robust to compute the numerical solution of various time-fractional partial differential equations, in particular for option pricing problems. Furthermore, the theoretically established findings are validated by these computationally extracted results, effectively proving the accuracy of the scheme developed in this study. For error analysis, the formula used to evaluate the difference between the exact and approximate solutions is expressed

as

$$Error^{N_{\mathcal{S}},N_{\mathfrak{t}}} = \|\text{exact} - \text{approx}\| = \max_{0\leq n\leq N_{\mathfrak{t}}} \sqrt{\sum_{i=0}^{N_{\mathcal{S}}} |\text{exact}(\mathcal{S}_i,\mathfrak{t}_n) - \text{approx}(\mathcal{S}_i,\mathfrak{t}_n)|^2},$$

and to show the high precision achieved by the numerical scheme we compute its order of convergence using the formula

$$\frac{\ln(Error^{N_{\mathcal{S}},N_{\mathfrak{t}}}/Error^{2N_{\mathcal{S}},2N_{\mathfrak{t}}})}{\ln 2},$$

where "exact" denotes the exact solution and "approx" represents the approximate solution to the problem (7.3.6). In both examples, the Atangana-Baleanu Caputo derivative variable orders are chosen arbitrarily. The spatial and temporal errors occur while computing the solution of Example 7.7.1 are listed in Tables 7.1 and 7.2 at different values of $\alpha(\mathcal{S},\mathfrak{t})$. Based on these tables, we observe that the numerical order of convergence for the present scheme is two and three in the spatial and temporal directions, respectively. In Table 7.1, we have also computed the CPU-time taken to evaluate the solution function for different values of $\alpha(\mathcal{S},\mathfrak{t})$. The lesser values of CPU-time are sufficient to prove that the method is fast and computationally efficient since the present scheme is explicit. Using the surface plot and the line plot in Figures 7.1 and 7.2 respectively, we can investigate the behavior of the numerical solution of Example 7.7.1. Through Figure 7.3 we examine the accuracy of the present method by plotting the exact and numerical solution together. The overlapping of the approximation points on the exact solution line shows that both the solutions are almost identical.

Example 7.7.1. *Consider the Equation (7.3.6) for* $r(\mathfrak{t}) = 0.1 + 0.05e^{-\mathfrak{t}}$, $D(\mathfrak{t}) = 0.03 + 0.001e^{0.01\mathfrak{t}}$, $\mathcal{S}_{\min} = 0$, $\mathcal{S}_{\max} = 1$, $T = 1$, $\delta = 1$ *and* $\gamma = -0.1$ *subject to the terminal condition* $P(\mathcal{S},T) = \mathcal{S}(\mathcal{S}-1)e^{\mathcal{S}}$ *and the boundary conditions given by* $P(\mathcal{S}_{\min},\mathfrak{t}) = P(\mathcal{S}_{\max},\mathfrak{t}) = 0$.

Example 7.7.2. *Consider the Equation (7.3.6) for* $r(\mathfrak{t}) = 0.2 + 0.3\mathfrak{t}^2$, $D(\mathfrak{t}) = 0.01 + 0.3\mathfrak{t}$,

Table 7.1: Errors, orders of convergence, and CPU time (in seconds) for Example 7.7.1 with $N_{\mathcal{S}} = N_{\mathfrak{t}}$

	$N_{\mathcal{S}}$				
	8	16	32	64	128
$\alpha = \frac{2+\cos(\mathcal{S})\mathfrak{t}}{4}$	$1.95e-02$	$4.34e-03$	$1.14e-03$	$3.24e-04$	$8.94e-05$
	2.1677	1.9287	1.8150	1.8576	
CPU-time	$0.1071s$	$0.1287s$	$0.1909s$	$0.6757s$	$1.2638s$
$\alpha = \frac{1+\sin(\mathcal{S})\mathfrak{t}}{2}$	$1.86e-02$	$4.56e-03$	$9.05e-04$	$2.07e-04$	$5.56e-05$
	2.0282	2.3330	2.1283	1.8965	
CPU-time	$0.1081s$	$0.1280s$	$0.2001s$	$0.6817s$	$1.1563s$

Table 7.2: Errors and orders of convergence for Example 7.7.1 with $N_{\mathcal{S}} = 1000$

		$N_{\mathfrak{t}}$				
	$\mathcal{S}$	8	16	32	64	128
	0.25	$1.28e-03$	$1.79e-04$	$2.36e-05$	$3.03e-06$	$3.93e-07$
		2.8381	2.9231	2.9614	2.9467	
$\alpha = \frac{2+\cos(\mathcal{S})\mathfrak{t}}{4}$	0.5	$2.07e-03$	$2.91e-04$	$3.84e-05$	$4.96e-06$	$6.33e-07$
		2.8305	2.9218	2.9527	2.9701	
	0.75	$1.93e-03$	$2.72e-04$	$3.61e-05$	$4.72e-06$	$6.11e-07$
		2.8269	2.9135	2.9351	2.9495	
	0.25	$7.74e-04$	$1.09e-04$	$1.45e-05$	$1.89e-06$	$2.42e-07$
		2.8280	2.9102	2.9396	2.9653	
$\alpha = \frac{1+\sin(\mathcal{S})\mathfrak{t}}{2}$	0.5	$1.98e-03$	$2.77e-04$	$3.65e-05$	$4.72e-06$	$6.01e-07$
		2.8375	2.9239	2.9510	2.9733	
	0.75	$3.07e-03$	$4.26e-04$	$5.58e-05$	$7.19e-06$	$9.18e-07$
		2.8493	2.9325	2.9562	2.9694	

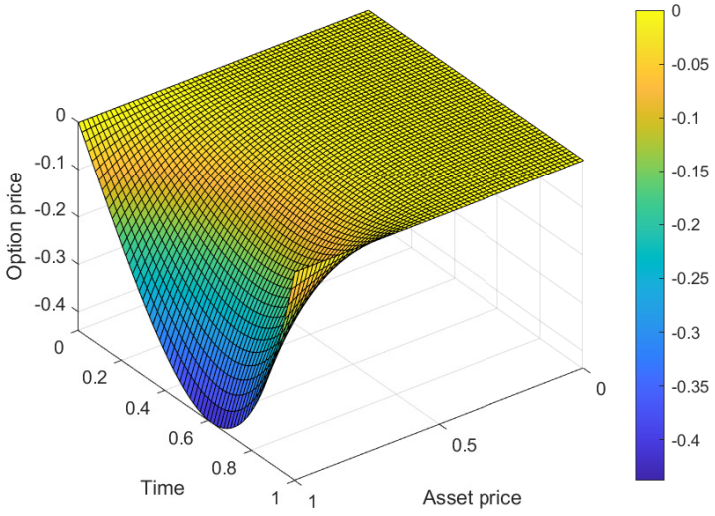

Figure 7.1: Numerical approximation of option price for Example 7.7.1

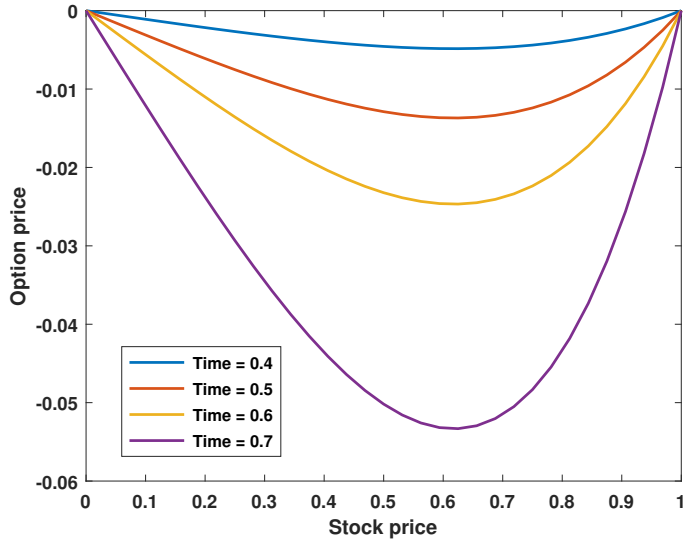

Figure 7.2: Numerical solution at different values of t for Example 7.7.1

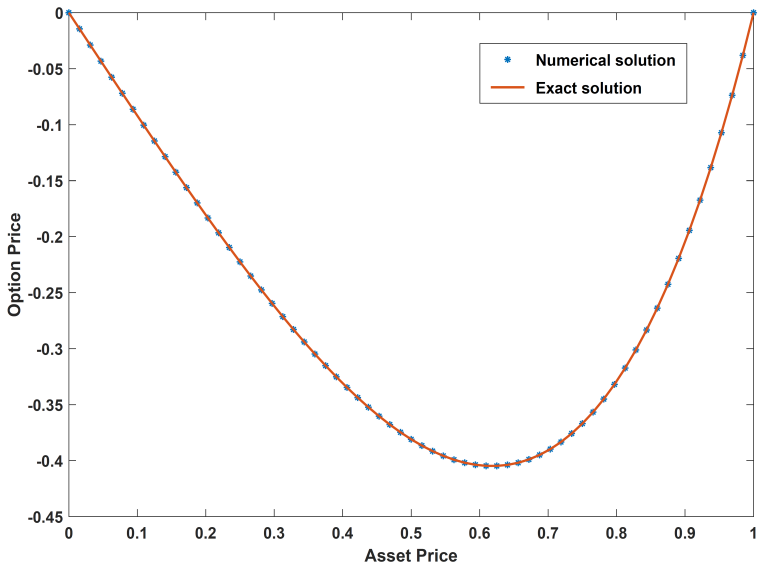

Figure 7.3: Comparing the exact and numerical solution of Example 7.7.1 at $\mathfrak{t} = 0.5$

$\mathcal{S}_{\min} = 0$, $\mathcal{S}_{\max} = 1$, $T = 1$, $\delta = 1$ *and* $\gamma = -0.2$ *subject to the terminal condition* $P(\mathcal{S}, T) = \sin(\pi\mathcal{S})$ *and the boundary conditions given by* $P(\mathcal{S}_{\min}, \mathfrak{t}) = P(\mathcal{S}_{\max}, \mathfrak{t}) = 0$.

Tables 7.3 and 7.4 contain the error occur while computing the solution of Example 7.7.2. From Table 7.3, one can observe that the order of convergence for the proposed method is two in the spatial direction, as the magnitude of the error decreases by one-fourth with the increasing number of collocation points by double. Similar to the previous example, the CPU time is shortened here, strengthening the claim that the current approach is easy to implement with less complexity. From the results presented in Table 7.4, we claim that the present scheme is accurate of $O(\tau^3)$ which is better than several existing methods having $O(\tau^2)$ as their order of convergence. Figure 7.4 represents the price of the option with the changing stock prices and time to maturity. In Figure 7.5, the price of an option at different time levels is presented. Using Figure 7.6, a significant observation is that the numerical solution is in good agreement with the exact solution. To draw all figures, we have used $N_{\mathcal{S}} = N_{\mathfrak{t}} = 64$.

Table 7.3: Errors, orders of convergence, and CPU time (in seconds) for Example 7.7.2 with $N_{\mathcal{S}} = N_{\mathrm{t}}$

	$N_{\mathcal{S}}$				
	8	16	32	64	128
$\alpha = \frac{2+\cos(\mathcal{S})\mathrm{t}}{4}$	$1.06e-02$	$2.98e-03$	$9.09e-04$	$2.72e-04$	$7.18e-05$
	1.8307	1.7130	1.7407	1.9216	
CPU-time	$0.1252s$	$0.2148s$	$0.6766s$	$0.9667s$	$2.3478s$
$\alpha = \frac{1+\sin(\mathcal{S})\mathrm{t}}{2}$	$6.60e-03$	$1.72e-03$	$4.45e-04$	$1.15e-04$	$3.21e-05$
	1.9401	1.9505	1.9522	1.8410	
CPU-time	$0.1407s$	$0.1903s$	$0.6730s$	$1.5159s$	$2.7575s$

Table 7.4: Errors and orders of convergence for Example 7.7.2 with $N_{\mathcal{S}} = 1000$

		N_{t}				
	$\mathcal{S}$	8	16	32	64	128
	0.25	$4.51e-03$	$6.31e-04$	$8.32e-05$	$1.08e-05$	$1.30e-06$
		2.8374	2.9230	2.9456	3.0544	
$\alpha = \frac{2+\cos(\mathcal{S})\mathrm{t}}{4}$	0.5	$6.50e-03$	$9.10e-04$	$1.20e-04$	$1.55e-05$	$2.01e-06$
		2.8365	2.9228	2.9527	2.9470	
	0.75	$5.03e-03$	$7.08e-04$	$9.34e-05$	$1.19e-05$	$1.49e-06$
		2.8287	2.9223	2.9725	2.9976	
	0.25	$2.80e-03$	$3.96e-04$	$5.29e-05$	$6.98e-06$	$9.01e-07$
		2.8219	2.9042	2.9220	2.9536	
$\alpha = \frac{1+\sin(\mathcal{S})\mathrm{t}}{2}$	0.5	$5.86e-03$	$8.20e-04$	$1.08e-04$	$1.40e-05$	$1.79e-06$
		2.8372	2.9246	2.9475	2.9674	
	0.75	$6.86e-03$	$9.52e-04$	$1.25e-04$	$1.58e-05$	$2.00e-06$
		2.8492	2.9290	2.9839	2.9819	

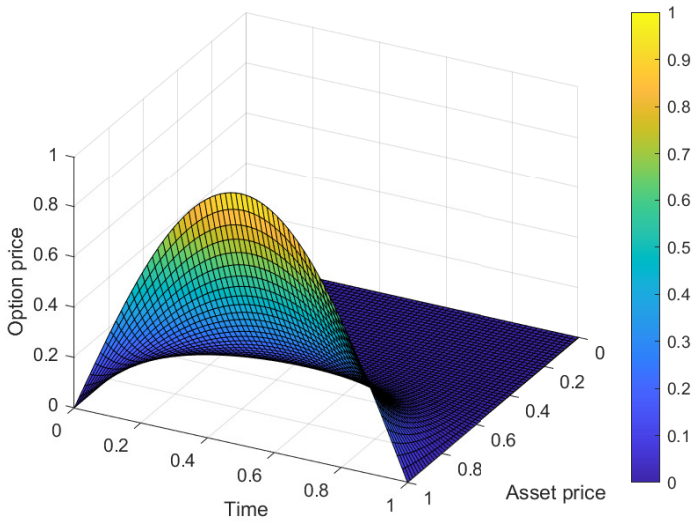

Figure 7.4: Numerical approximation of option price for Example 7.7.2

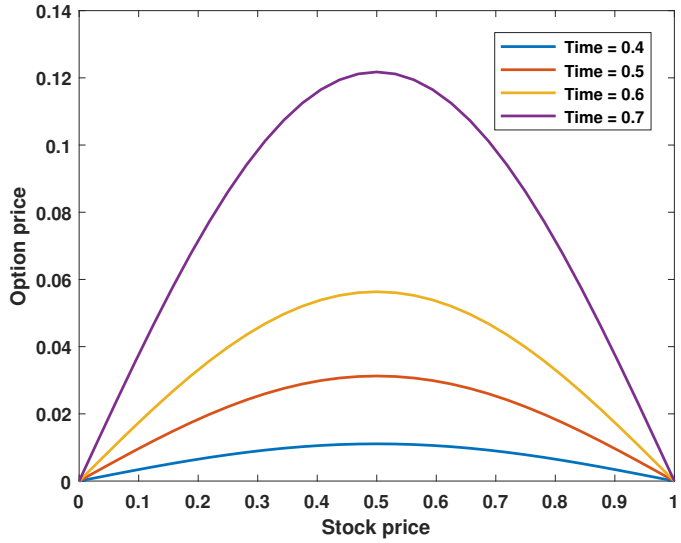

Figure 7.5: Numerical solution at different values of t for Example 7.7.2

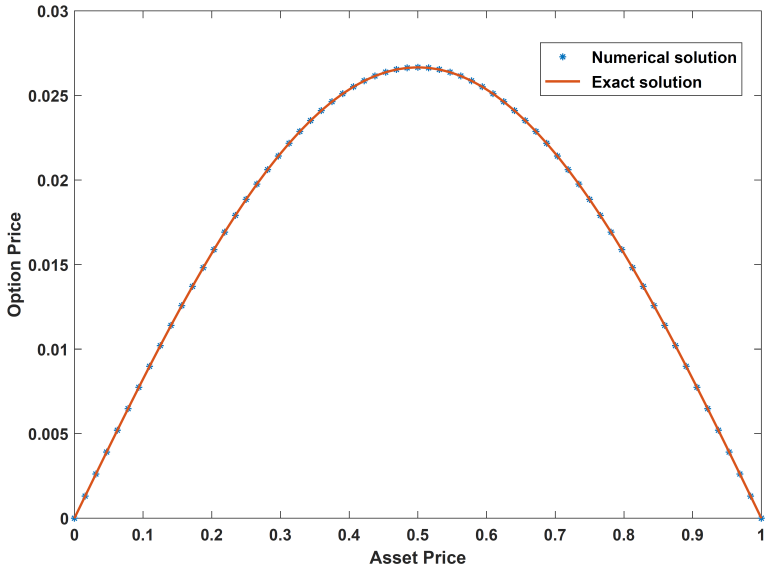

Figure 7.6: Comparing the exact and numerical solution of Example 7.7.2 at $\mathfrak{t} = 0.5$

7.8 Concluding remarks and future scopes

This chapter presents a novel numerical scheme with faster calculation speed and lower storage for a variable order time-fractional option pricing problem under the CEV model. The proposed method is proven to be third-order convergent in time and second-order in space through rigorous analysis. Also, it has been shown that the numerical method is unconditionally stable. Numerous simulations presented in the previous section have validated the reliability and accuracy of the anticipated method. The proposed method's order of convergence and stability are numerically examined. The numerical results disclosed that the present scheme overcomes classical numerical schemes' low temporal convergence rate with time-fractional derivative. We will use the suggested approach to solve other time-fractional variable-order applications in mathematical finance in future research.

Chapter 8

Conclusions

8.1 Summary

This thesis includes a number of unique and efficient numerical approaches for calculating the price and Greeks of various options. It commences with a description of the conceptual and mathematical background of option pricing problems in Chapter 1. The objective of this thesis is to design robust numerical approaches to overcome the challenges of numerically solving option pricing problems. The majority of these issues are discussed in the first chapter.

In Chapter 2, we have presented the two-dimensional Haar wavelet method to approximate the price and Greeks of European call and put options. To explore these financially relevant problems systematically, we reformulate the final value problem into a less cluttered dimensionless initial value problem. To avoid unacceptable large truncation error the actual infinite domain is trimmed into the finite domain by constructing artificial boundaries. To solve the transformed PDE the detailed description and implementation based on the wavelet approximation has been provided. Through rigorous analysis it has been proved that the present wavelet scheme is convergent in the L^2 norm. It is worthy to note from the numerical simulation and discussion part that the proposed Haar wavelet

approach effectively approximate both the Greeks and the solution even if they are not fully smooth in nature. This numerical technique achieves a good compromise between pricing precision and computational effort.

Later in Chapter 3, we looked at a more difficult problem known as the American style choice, which is more difficult than European style options. Due to the possibility of early exercise, American style option pricing problems are moving boundary value problems. Such options under the Black-Scholes framework result in a linear complementarity problem. The payoff function and the Greeks, like the European option, are non-smooth in nature, thus we employed the Haar functions to approximate the spiking functions for better results because to their discontinuous behaviour. Here also, first we reformulate the final value problem into a less cluttered dimensionless starting value problem to study these financially important concerns in a methodical manner. Through numerical investigation the influence of various parameters on the moneyness of the option has been explained. The suggested Haar wavelet approach is effective and straightforward to implement for assessing the different physical and numerical features of the options' Greeks, and it explicitly gives the numerical approximation of all the derivatives of the solution function.

Moving on to Chapter 4, we come to the more complex options than the European and American vanilla options known as the exotic options. Many of the misunderstandings and misuses of exotic derivatives were brought to light during the current financial crisis. Therefore, there is a great need to study the hedging parameters of these option. In this chapter, to study these options numerically we have considered the binary options more precisely, we have considered the cash or nothing, asset or nothing and gap options. To explore these options, we have considered the Haar wavelet method which handles non-smooth reward functions and discontinuous Greeks with ease, thanks to its good approximation technique for estimating spiking functions. The detailed explanation of the method and its implementation have been provided. The stability and consistency of the Haar scheme have been proved. These theoretical implications have been validated through computational results in the end of this chapter. The numerical results presented in the form of graphs and tables reveals the high proficiency of the Haar scheme for solving

the Greeks and solution of the binary option PDE.

The present thesis also contributes the development of the effective numerical approach for the higher dimensional option pricing problems. The options based on a variety of asset plays a significant role in the financial market, therefore in Chapter 5, we have considered a variety of options depending on more than one asset. It results in a multi-dimensional Black-Schole PDE. To solve this, we have considered the higher dimensional Haar wavelet approximation method. The implementation of the proposed scheme has been given in detail. Finally, the proposed method is tested on various test examples based on different types of multi-asset based options. It is worthy to note that irrespective of the problem's geometry, the proposed method is highly accurate and the time taken to get this level of accuracy is significantly less.

We have concentrated on the numerical technique that yields better approximation for spiking functions till chapter 5. (Greeks and payoff in our case). Using it, it's time to shift our focus to the scheme's accuracy, therefore Chapter 6 covers a very accurate orthogonal spline collocation approach with Rannacher time marching. Rannacher time marching is the conjunction of the two classical time stepping scheme BE and CN to reduce the quatization error that occur due to the non-smooth terminal condition present in the Black-Scholes model. Furthermore, with careful examination, second and fourth orders of convergence in the temporal and spatial directions are found for the current method in combination to the Rannacher time stepping scheme. The numerical results for two test problems are supplied in the form of tables and graphs to validate the theory. These findings suggest that the present algorithm is more accurate and capable of restoring predicted behaviour of the solution and the hedging parameters.

In Chapter 7, we extend the present work from the integer order models to fractional order models, since the integer-order derivative base models would miss some important historical details due to their nonlocal nature, fractional derivatives, on the other hand, are highly versatile for defining the behaviour of differential equations and adding historical information. Also, as the standard Black-Scholes model, on the contrary, is based on a set of harsh assumptions. Therefore, in this chapter, we have considered the time-fractional

CEV model in which we have taken the rate of interest and the dividend yield as the function of time. Also, the order of the temporal derivative is considered to be variable in nature since as compare to constant function the variable functions would provide more precise results. We have used the definition given by Atangana and Baleanu in Caputo sense to approximate the time derivative and the finite difference approximation in space. Through meticulous analysis the proposed method is shown to be third order convergent in time and second order convergent in space. The reliability and accuracy of the anticipated procedure have been validated by a number of simulations described in the preceding section. With time-fractional derivative, the new method overcomes the low temporal convergence rate of traditional numerical schemes, according to the numerical results. The methods for assessing option sensitivities given in this thesis can be employed in trading to examine alternative Greek exposures for hedging.

8.2 Future Scopes

Based on the approaches presented in this thesis, we can extend the present work to

1. The system of PDEs arising in finance and engineering, such as the models with variable volatility.

2. The fractional higher order option pricing problems in application of various fractional derivatives.

3. The option pricing jump diffusion models.

4. Various non-financial engineering integer or fractional order models having a huge range of applications in various fields.

Bibliography

[1] Eugene F Brigham and Joel F Houston. *Fundamentals of financial management*. Cengage Learning, 2021.

[2] Prasanna Chandra et al. *Financial management*. Tata McGraw-Hill Education, 2011.

[3] Frank J Fabozzi and Pamela P Peterson. *Financial management and analysis*, volume 132. John Wiley & Sons, 2003.

[4] Ali Hirsa and Salih N Neftci. *An introduction to the mathematics of financial derivatives*. Academic Press, 2013.

[5] Philip Hunt and Joanne Kennedy. *Financial derivatives in theory and practice*, volume 556. John Wiley and Sons, 2004.

[6] Rob Quail and James A Overdahl. *Financial derivatives*, volume 127. John Wiley & Sons, 2002.

[7] Paul Wilmott, Susan Howson, Sam Howison, Jeff Dewynne, et al. *The mathematics of financial derivatives: a student introduction*. Cambridge University Press, 1995.

[8] Alain Bensoussan. On the theory of option pricing. *Acta Applicandae Mathematica*, 2(2):139–158, 1984.

[9] Iain J Clark. *Commodity option pricing: a practitioner's guide*. John Wiley & Sons, 2014.

[10] Rüdiger U Seydel. Pricing of exotic options. In *Tools for Computational Finance*, pages 307–351. Springer, 2017.

[11] Simon Benninga. *Financial modeling*. MIT press, 2014.

[12] David Kelly and Ian Melbourne. Smooth approximation of stochastic differential equations. *The Annals of Probability*, 44(1):479–520, 2016.

[13] Fischer Black and Myron Scholes. The pricing of options and corporate liabilities. In *World Scientific Reference on Contingent Claims Analysis in Corporate Finance: Volume 1: Foundations of CCA and Equity Valuation*, pages 3–21. World Scientific, 2019.

[14] Rüdiger Seydel and Rudiger Seydel. *Tools for computational finance*, volume 3. Springer, 2006.

[15] Carlos Vázquez. An upwind numerical approach for an american and european option pricing model. *Applied Mathematics and Computation*, 97(2-3):273–286, 1998.

[16] Olena Burkovska, Bernard Haasdonk, Julien Salomon, and Barbara Wohlmuth. Reduced basis methods for pricing options with the black–scholes and heston models. *SIAM Journal on Financial Mathematics*, 6(1):685–712, 2015.

[17] Samuli Ikonen and Jari Toivanen. Operator splitting methods for american option pricing. *Applied Mathematics Letters*, 17(7):809–814, 2004.

[18] Jichao Zhao, Matt Davison, and Robert M Corless. Compact finite difference method for american option pricing. *Journal of Computational and Applied Mathematics*, 206(1):306–321, 2007.

[19] Abe Cofnas. *Trading Binary Options: Strategies and Tactics*. John Wiley & Sons, 2016.

[20] Hong-Joong Kim and Kyoung-Sook Moon. Variable time-stepping hybrid finite difference methods for pricing binary options. *Bulletin of the Korean Mathematical Society*, 48(2):413–426, 2011.

[21] Mohan K Kadalbajoo, Lok Pati Tripathi, and Alpesh Kumar. An error analysis of a finite element method with imex-time semidiscretizations for some partial integro-differential inequalities arising in the pricing of american options. *SIAM Journal on Numerical Analysis*, 55(2):869–891, 2017.

[22] Leila Khodayari and Mojtaba Ranjbar. A computationally efficient numerical approach for multi-asset option pricing. *International Journal of Computer Mathematics*, 96(6):1158–1168, 2019.

[23] Igor Podlubny. *Fractional differential equations: an introduction to fractional derivatives, fractional differential equations, to methods of their solution and some of their applications*. Elsevier, 1998.

[24] Hongmei Zhang, Fawang Liu, Ian Turner, and Qianqian Yang. Numerical solution of the time fractional black–scholes model governing european options. *Computers & Mathematics with Applications*, 71(9):1772–1783, 2016.

[25] Zhiqiang Zhou and Xuemei Gao. Numerical methods for pricing american options with time-fractional pde models. *Mathematical Problems in Engineering*, 2016, 2016.

[26] Salvatore Cuomo, Federica Sica, and Gerardo Toraldo. Greeks computation in the option pricing problem by means of rbf-pu methods. *Journal of Computational and Applied Mathematics*, 376:112882, 2020.

[27] Dan Passarelli. *Trading options Greeks: How time, volatility, and other pricing factors drive profits*, volume 159. John Wiley & Sons, 2012.

[28] Pierino Ursone. *How to calculate options prices and their greeks: exploring the black scholes model from delta to vega*. John Wiley & Sons, 2015.

[29] Elyès Jouini, Jakša Cvitanić, and Marek Musiela. *Option pricing, interest rates and risk management*. Cambridge University Press, 2001.

[30] Yves Achdou and Olivier Pironneau. *Computational methods for option pricing*. SIAM, 2005.

[31] Tihomir B Gyulov and Radoslav L Valkov. American option pricing problem transformed on finite interval. *International Journal of Computer Mathematics*, 93 (5):821–836, 2016.

[32] Yves Achdou and Nicoletta Tchou. Variational analysis for the black and scholes equation with stochastic volatility. *ESAIM: Mathematical Modelling and Numerical Analysis*, 36(3):373–395, 2002.

[33] Alexandre Ern, Stéphane Villeneuve, and Antonino Zanette. Adaptive finite element methods for local volatility european option pricing. *International Journal of Theoretical and Applied Finance*, 7(06):659–684, 2004.

[34] Mark Broadie and Jerome B Detemple. Anniversary article: Option pricing: Valuation models and applications. *Management science*, 50(9):1145–1177, 2004.

[35] Ana-Maria Matache, Tobias Von Petersdorff, and Christoph Schwab. Fast deterministic pricing of options on lévy driven assets. *ESAIM: Mathematical Modelling and Numerical Analysis*, 38(1):37–71, 2004.

[36] Luis Ortiz-Gracia and Cornelis W Oosterlee. Robust pricing of european options with wavelets and the characteristic function. *SIAM Journal on Scientific Computing*, 35(5):B1055–B1084, 2013.

[37] Dana Cerná and Václav Finek. Adaptive wavelet method for the black-scholes equation of european options. In *Proceedings of the 34th International Conference on Mathematical Methods in Economics,(A. Kocourek, and M. Vavroušek), Liberec*, pages 120–125, 2016.

[38] Jamal Amani Rad, Kourosh Parand, and Luca Vincenzo Ballestra. Pricing european and american options by radial basis point interpolation. *Applied Mathematics and Computation*, 251:363–377, 2015.

[39] Jamal Amani Rad, Kourosh Parand, and Saeid Abbasbandy. Local weak form meshless techniques based on the radial point interpolation (rpi) method and local boundary integral equation (lbie) method to evaluate european and american options. *Communications in Nonlinear Science and Numerical Simulation*, 22(1-3):1178–1200, 2015.

[40] Jamal Amani Rad, Kourosh Parand, and Saeid Abbasbandy. Pricing european and american options using a very fast and accurate scheme: the meshless local petrov–galerkin method. *Proceedings of the National Academy of Sciences, India Section A: Physical Sciences*, 85(3):337–351, 2015.

[41] Stefanus C Maree, Luis Ortiz-Gracia, and Cornelis W Oosterlee. Pricing early-exercise and discrete barrier options by shannon wavelet expansions. *Numerische Mathematik*, 136(4):1035–1070, 2017.

[42] Fang Fang and Cornelis W Oosterlee. A novel pricing method for european options based on fourier-cosine series expansions. *SIAM Journal on Scientific Computing*, 31(2):826–848, 2009.

[43] Alexander Grossmann and Jean Morlet. Decomposition of hardy functions into square integrable wavelets of constant shape. *SIAM Journal on Mathematical Analysis*, 15(4):723–736, 1984.

[44] Jean Morlet, G Arens, E Fourgeau, and D Glard. Wave propagation and sampling theory—part i: Complex signal and scattering in multilayered media. *Geophysics*, 47(2):203–221, 1982.

[45] N Wichailukkanaa, B Novaprateepa, and C Boonyasiriwatc. A convergence analysis of the numerical solution of boundary-value problems by using two-dimensional

haar wavelets. scienceasia, 42 (5): 346–355, 2016. *Narongpol Wichailukkana Biography/44*, 2016.

[46] Hong-Yi Chen, Cheng-Few Lee, and Weikang Shih. Derivations and applications of greek letters: Review and integration. *Handbook of quantitative finance and risk management*, pages 491–503, 2010.

[47] Cheng F Lee, Alice C Lee, and John C Lee. *Handbook of quantitative finance and risk management*, volume 1. Springer, 2010.

[48] Ravi Myneni. The pricing of the american option. *The Annals of Applied Probability*, pages 1–23, 1992.

[49] Richard W Cottle, Jong-Shi Pang, and Richard E Stone. The linear complementarity problem. academic pr ess. *Inc., Boston, MA*, 5, 1992.

[50] P Wilmott, J Dewynne, and S Howison. Option pricing. mathematical models and computation oxford financial press, 1993.

[51] Michael J Brennan and Eduardo S Schwartz. Finite difference methods and jump processes arising in the pricing of contingent claims: A synthesis. *Journal of Financial and Quantitative Analysis*, 13(3):461–474, 1978.

[52] Lutz Angermann and Song Wang. Convergence of a fitted finite volume method for the penalized black–scholes equation governing european and american option pricing. *Numerische Mathematik*, 106(1):1–40, 2007.

[53] Song Wang, XQ Yang, and Kok Lay Teo. Power penalty method for a linear complementarity problem arising from american option valuation. *Journal of Optimization Theory and Applications*, 129(2):227–254, 2006.

[54] Song Wang, Shuhua Zhang, and Zhiwei Fang. A superconvergent fitted finite volume method for b lack–s choles equations governing e uropean and a merican

option valuation. *Numerical Methods for Partial Differential Equations*, 31(4): 1190–1208, 2015.

[55] Walter Allegretto, Yanping Lin, and Hongtao Yang. A fast and highly accurate numerical method for the evaluation of american options. *Dynamics of Continuous, Discrete and Impulsive Systems Series B: Application and Algorithm*, 8(1):127–138, 2001.

[56] A Andalaft-Chacur, M Montaz Ali, and J González Salazar. Real options pricing by the finite element method. *Computers & Mathematics with Applications*, 61(9): 2863–2873, 2011.

[57] Anthony D Holmes and Hongtao Yang. A front-fixing finite element method for the valuation of american options. *SIAM Journal on Scientific Computing*, 30(4): 2158–2180, 2008.

[58] MM Chawla and David J Evans. Numerical volatility in option valuation from black–scholes equation by finite differences. *International Journal of Computer Mathematics*, 81(8):1039–1041, 2004.

[59] Domingo Tavella and Curt Randall. *Pricing financial instruments: The finite difference method*, volume 13. John Wiley & Sons, 2000.

[60] Houde Han and Xiaonan Wu. A fast numerical method for the black–scholes equation of american options. *SIAM Journal on Numerical Analysis*, 41(6):2081–2095, 2003.

[61] Luca Vincenzo Ballestra and Graziella Pacelli. Pricing european and american options with two stochastic factors: A highly efficient radial basis function approach. *Journal of Economic Dynamics and Control*, 37(6):1142–1167, 2013.

[62] Ahmad Golbabai, Davood Ahmadian, and Mariyan Milev. Radial basis functions with application to finance: American put option under jump diffusion. *Mathematical and Computer Modelling*, 55(3-4):1354–1362, 2012.

[63] Robert Geske and Herb E Johnson. The american put option valued analytically. *The Journal of Finance*, 39(5):1511–1524, 1984.

[64] Song-Ping Zhu. A new analytical approximation formula for the optimal exercise boundary of american put options. *International Journal of Theoretical and Applied Finance*, 9(07):1141–1177, 2006.

[65] Jacqueline Huang and Jong-Shi Pang. Option pricing and linear complementarity. 2003.

[66] Christina Christara and Duy-Minh Dang. Adaptive and high-order methods for valuing american options. *Journal of Computational Finance, Forthcoming*, 2010.

[67] Christoph Reisinger and Jan H Witte. On the use of policy iteration as an easy way of pricing american options. *SIAM Journal on Financial Mathematics*, 3(1): 459–478, 2012.

[68] SAJID Memon. Finite element method for american option pricing: a penalty approach. *International Journal of Numerical Analysis and Modelling, Series B: Computing and Information*, 3(3):345–370, 2012.

[69] Santtu Salmi, Jari Toivanen, and Lina von Sydow. Iterative methods for pricing american options under the bates model. *Procedia Computer Science*, 18:1136–1144, 2013.

[70] Nigel Clarke and Kevin Parrott. Multigrid for american option pricing with stochastic volatility. *Applied Mathematical Finance*, 6(3):177–195, 1999.

[71] Zhe Sun, Zhe Liu, and Xiaoqi Yang. On power penalty methods for linear complementarity problems arising from american option pricing. *Journal of Global Optimization*, 63(1):165–180, 2015.

[72] Peter A Forsyth and Kenneth R Vetzal. Quadratic convergence for valuing american

options using a penalty method. *SIAM Journal on Scientific Computing*, 23(6): 2095–2122, 2002.

[73] Bjørn Fredrik Nielsen, Ola Skavhaug, and Aslak Tveito. Penalty and front-fixing methods for the numerical solution of american option problems. *Journal of Computational Finance*, 5(4):69–98, 2002.

[74] Xian-Jun Shi, Lei Yang, and Zheng-Hai Huang. A fixed point method for the linear complementarity problem arising from american option pricing. *Acta Mathematicae Applicatae Sinica, English Series*, 32(4):921–932, 2016.

[75] Zhongdi Cen and Wenting Chen. A hodie finite difference scheme for pricing american options. *Advances in Difference Equations*, 2019(1):1–17, 2019.

[76] Raul Kangro and Roy Nicolaides. Far field boundary conditions for black–scholes equations. *SIAM Journal on Numerical Analysis*, 38(4):1357–1368, 2000.

[77] Stéphane Mallat. *A wavelet tour of signal processing*. Elsevier, 1999.

[78] Lokenath Debnath and Firdous Ahmad Shah. *Wavelet transforms and their applications*. Springer, 2002.

[79] Stephane G Mallat. Multiresolution approximations and wavelet orthonormal bases of ^{2} (). *Transactions of the American Mathematical Society*, 315(1):69–87, 1989.

[80] William H Press, Saul A Teukolsky, William T Vetterling, and Brian P Flannery. *Numerical Recipes with Source Code CD-ROM 3rd Edition: The Art of Scientific Computing*. Cambridge University Press, 2007.

[81] Peter W Buchen. The pricing of dual-expiry exotics. *Quantitative Finance*, 4(1): 101, 2003.

[82] A Jaworski. Cbot launches binary options. *Securities Industry News*, 18(27):11, 2006.

[83] A Thavaneswaran, SS Appadoo, and Julieta Frank. Binary option pricing using fuzzy numbers. *Applied Mathematics Letters*, 26(1):65–72, 2013.

[84] Bin Peng and Yuqi Han. A study on the binary option model and its pricing. In *Allied Academies International Conference. Academy of Accounting and Financial Studies. Proceedings*, volume 9, page 71. Citeseer, 2004.

[85] Min Gao. The british binary option. *Journal of Mathematical Finance*, 9(4): 747–762, 2019.

[86] Hamish Raw. *Binary options: Fixed odds financial bets*. Harriman House Limited, 2011.

[87] Min Gao and Zhenfeng Wei. The barrier binary options. *Journal of Mathematical Finance*, 10(1):140–156, 2019.

[88] Yuan Guojun and Xiao Qingxian. A new numerical method for pricing binary options in the cev process. In *2011 International Conference on E-Business and E-Government (ICEE)*, pages 1–4. IEEE, 2011.

[89] Guojun Yuan. Pricing binary options based on fuzzy number theory.

[90] Arieh Iserles. *A first course in the numerical analysis of differential equations*. Number 44. Cambridge University Press, 2009.

[91] Rolf Rannacher. Finite element solution of diffusion problems with irregular data. *Numerische Mathematik*, 43(2):309–327, 1984.

[92] Steve Heston and Guofu Zhou. On the rate of convergence of discrete-time contingent claims. *Mathematical Finance*, 10(1):53–75, 2000.

[93] David M Pooley, Kenneth R Vetzal, and Peter A Forsyth. Convergence remedies for non-smooth payoffs in option pricing. *Journal of Computational Finance*, 6(4): 25–40, 2003.

[94] Yin Yang, Fazlollah Soleymani, Mahdiar Barfeie, and Emran Tohidi. A radial basis function—hermite finite difference approach to tackle cash-or-nothing and asset-or-nothing options. *Journal of Computational and Applied Mathematics*, 368: 112523, 2020.

[95] Santanu Saha Ray and Arun Kumar Gupta. *Wavelet methods for solving partial differential equations and fractional differential equations*. CRC Press, 2018.

[96] Gregory Eric Fasshauer, Abdul Qayyum Masud Khaliq, and David Albert Voss. Using meshfree approximation for multi-asset american options. *Journal of the Chinese Institute of Engineers*, 27(4):563–571, 2004.

[97] Pavlo Kovalov, Vadim Linetsky, and Michael Marcozzi. Pricing multi-asset american options: A finite element method-of-lines with smooth penalty. *Journal of Scientific Computing*, 33(3):209–237, 2007.

[98] Jonas Persson and Lina von Persson. Pricing european multi-asset options using a space-time adaptive fd-method. *Computing and Visualization in Science*, 10(4): 173–183, 2007.

[99] Da-Rae Jeong, Jun-Seok Kim, and In-Suk Wee. An accurate and efficient numerical method for black-scholes equations. *Communications of the Korean Mathematical Society*, 24(4):617–628, 2009.

[100] Marjon J Ruijter and Cornelis W Oosterlee. Two-dimensional fourier cosine series expansion method for pricing financial options. *SIAM Journal on Scientific Computing*, 34(5):B642–B671, 2012.

[101] Wenbin Hu and Shenghong Li. The forward-path method for pricing multi-asset american-style options under general diffusion processes. *Journal of Computational and Applied Mathematics*, 263:25–31, 2014.

[102] Muhammad Yousuf, Abdul-Qayyum M Khaliq, and RH Liu. Pricing american options under multi-state regime switching with an efficient l-stable method. *International Journal of Computer Mathematics*, 92(12):2530–2550, 2015.

[103] Mohan K Kadalbajoo, Alpesh Kumar, and Lok Pati Tripathi. Application of the local radial basis function-based finite difference method for pricing american options. *International Journal of Computer Mathematics*, 92(8):1608–1624, 2015.

[104] Victor Shcherbakov and Elisabeth Larsson. Radial basis function partition of unity methods for pricing vanilla basket options. *Computers & Mathematics with Applications*, 71(1):185–200, 2016.

[105] Gemma Colldeforns-Papiol, Luis Ortiz-Gracia, and Cornelis W Oosterlee. Two-dimensional shannon wavelet inverse fourier technique for pricing european options. *Applied Numerical Mathematics*, 117:115–138, 2017.

[106] Slobodan Milovanović and Lina von Sydow. Radial basis function generated finite differences for option pricing problems. *Computers & Mathematics with Applications*, 75(4):1462–1481, 2018.

[107] Fazlollah Soleymani. Pricing multi-asset option problems: A chebyshev pseudo-spectral method. *BIT Numerical Mathematics*, 59(1):243–270, 2019.

[108] Sangkwon Kim, Darae Jeong, Chaeyoung Lee, and Junseok Kim. Finite difference method for the multi-asset black–scholes equations. *Mathematics*, 8(3):391, 2020.

[109] Jing Zhao and Shenghong Li. Efficient pricing of european options on two underlying assets by frame duality. *Journal of Mathematical Analysis and Applications*, 486(1):123873, 2020.

[110] J Lars Kirkby. Efficient option pricing by frame duality with the fast fourier transform. *SIAM Journal on Financial Mathematics*, 6(1):713–747, 2015.

[111] Desmond J Higham. An introduction to financial option valuation: mathematics, stochastics and computation. 2004.

[112] Robert C Merton. Theory of rational option pricing. *The Bell Journal of economics and management science*, pages 141–183, 1973.

[113] Francis A Longstaff and Eduardo S Schwartz. Valuing american options by simulation: a simple least-squares approach. *The Review of Financial Studies*, 14(1): 113–147, 2001.

[114] In Joon Kim. The analytic valuation of american options. *The Review of Financial Studies*, 3(4):547–572, 1990.

[115] Giovanni Barone-Adesi and Robert J Elliott. Approximations for the values of american options. *Stochastic Analysis and Applications*, 9(2):115–131, 1991.

[116] Giovanni Barone-Adesi. The saga of the american put. *Journal of Banking & Finance*, 29(11):2909–2918, 2005.

[117] Zhongdi Cen and Anbo Le. A robust and accurate finite difference method for a generalized black–scholes equation. *Journal of Computational and Applied Mathematics*, 235(13):3728–3733, 2011.

[118] YongHoon Kwon and Younhee Lee. A second-order finite difference method for option pricing under jump-diffusion models. *SIAM Journal on Numerical Analysis*, 49(6):2598–2617, 2011.

[119] Gianluca Fusai, Simona Sanfelici, and Aldo Tagliani. Practical problems in the numerical solution of pde's in finance. *Rendiconti per gli Studi Economici Quantitativi, Università Ca'Foscari Venezia*, 2001:105–132, 2002.

[120] DY Tangman, A Gopaul, and M Bhuruth. Numerical pricing of options using high-order compact finite difference schemes. *Journal of Computational and Applied Mathematics*, 218(2):270–280, 2008.

[121] Hikmet Caglar, Nazan Caglar, and Khaled Elfaituri. B-spline interpolation compared with finite difference, finite element and finite volume methods which applied to two-point boundary value problems. *Applied Mathematics and computation*, 175 (1):72–79, 2006.

[122] Jincai Chang, Qianli Yang, and Long Zhao. Comparison of b-spline method and finite difference method to solve bvp of linear odes. *J. Comput.*, 6(10):2149–2155, 2011.

[123] Mohmed HM Khabir and Kailash C Patidar. Spline approximation method to solve an option pricing problem. *Journal of Difference Equations and Applications*, 18 (11):1801–1816, 2012.

[124] Jalil Rashidinia and Sanaz Jamalzadeh. Collocation method based on modified cubic b-spline for option pricing models. *Mathematical Communications*, 22(1): 89–102, 2017.

[125] Gareth G Haslip and Vladimir K Kaishev. Lookback option pricing using the fourier transform b-spline method. *Quantitative Finance*, 14(5):789–803, 2014.

[126] Christina C Christara and Nat Chun-Ho Leung. Option pricing in jump diffusion models with quadratic spline collocation. *Applied Mathematics and Computation*, 279:28–42, 2016.

[127] Ashish Awasthi and TK Riyasudheen. An accurate solution for the generalized black-scholes equations governing option pricing. *AIMS Mathematics*, 5(3):2226–2243, 2020.

[128] Miloš Zlámal. Finite element methods for parabolic equations. *Mathematics of Computation*, 28(126):393–404, 1974.

[129] Michael Giles and Rebecca Carter. Convergence analysis of crank-nicolson and rannacher time-marching. 2005.

[130] Robert D Richtmyer and Keith W Morton. Difference methods for initial-value problems. *Malabar*, 1994.

[131] Sima Mashayekhi and Jens Hugger. Kα-shifting, rannacher time stepping and mesh grading in crank-nicolson fdm for black-scholes option pricing. *Communications in Mathematical Finance*, 5(1):1–31, 2016.

[132] Reza Mohammadi. Quintic b-spline collocation approach for solving generalized black–scholes equation governing option pricing. *Computers & Mathematics with Applications*, 69(8):777–797, 2015.

[133] Jim Douglas and Todd Dupont. *Collocation methods for parabolic equations in a single space variable*. 1974.

[134] Graeme Fairweather and Ian Gladwell. Algorithms for almost block diagonal linear systems. *SIAM Review*, 46(1):49–58, 2004.

[135] JC Diaz, Graeme Fairweather, and Patrick Keast. Algorithm 603: Colrow and arceco: Fortran packages for solving certain almost block diagonal linear systems by modified alternate row and column elimination. *ACM Transactions on Mathematical Software (TOMS)*, 9(3):376–380, 1983.

[136] Mohan K Kadalbajoo, Lok Pati Tripathi, and Puneet Arora. A robust nonuniform b-spline collocation method for solving the generalized black–scholes equation. *IMA Journal of Numerical Analysis*, 34(1):252–278, 2014.

[137] Reza Doostaki and Mohammad Mehdi Hosseini. Option pricing by the legendre wavelets method. *Computational Economics*, pages 1–25, 2021.

[138] Yinghao Chen, Hanyu Yu, Xiangyu Meng, Xiaoliang Xie, Muzhou Hou, and Julien Chevallier. Numerical solving of the generalized black-scholes differential equation using laguerre neural network. *Digital Signal Processing*, 112:103003, 2021.

[139] S Chandra Sekhara Rao et al. Numerical solution of generalized black–scholes model. *Applied Mathematics and Computation*, 321:401–421, 2018.

[140] Pradip Roul and VMK Prasad Goura. A sixth order numerical method and its convergence for generalized black–scholes pde. *Journal of Computational and Applied Mathematics*, 377:112881, 2020.

[141] LS Jiang, C Xu, X Ren, and S Li. Mathematical modeling and cases analysis of financial derivative pricing. *Hig Beijing*, 2008.

[142] Yue-Kuen Kwok. *Mathematical models of financial derivatives*. Springer, 2008.

[143] Dmitry Davydov and Vadim Linetsky. Pricing and hedging path-dependent options under the cev process. *Management science*, 47(7):949–965, 2001.

[144] John C Cox. The constant elasticity of variance option pricing model. *Journal of Portfolio Management*, page 15, 1996.

[145] Beni Lauterbach and Paul Schultz. Pricing warrants: an empirical study of the black-scholes model and its alternatives. *The Journal of Finance*, 45(4):1181–1209, 1990.

[146] Vipul Kumar Singh and Naseem Ahmad. Forecasting performance of volatility models for pricing s&p cnx nifty index options via black-scholes model. *IUP Journal of Applied Finance*, 17(3):53, 2011.

[147] Alan L Tucker, David R Peterson, and Elton Scott. Tests of the black-scholes and constant elasticity of variance currency call option valuation models. *Journal of Financial Research*, 11(3):201–214, 1988.

[148] Axel A Araneda and Marcelo J Villena. Computing the cev option pricing formula using the semiclassical approximation of path integral. *Journal of Computational and Applied Mathematics*, 388:113244, 2021.

[149] Luca Vincenzo Ballestra and Liliana Cecere. A numerical method to estimate the parameters of the cev model implied by american option prices: Evidence from nyse. *Chaos, Solitons & Fractals*, 88:100–106, 2016.

[150] Jung-Kyung Lee. An efficient numerical method for pricing american put options under the cev model. *Journal of Computational and Applied Mathematics*, 389: 113311, 2021.

[151] Aricson Cruz and José Carlos Dias. Valuing american-style options under the cev model: an integral representation based method. *Review of Derivatives Research*, 23(1):63–83, 2020.

[152] JA Tenreiro Machado and Virginia Kiryakova. Recent history of the fractional calculus: Data and statistics. In *Volume 1 Basic Theory*, pages 1–22. De Gruyter, 2019.

[153] Fidel Santamaria, Stefan Wils, Erik De Schutter, and George J Augustine. Anomalous diffusion in purkinje cell dendrites caused by spines. *Neuron*, 52(4):635–648, 2006.

[154] HG Sun, W Chen, H Wei, and YQ Chen. A comparative study of constant-order and variable-order fractional models in characterizing memory property of systems. *The European Physical Journal Special Topics*, 193(1):185–192, 2011.

[155] Mohammad Hossein Heydari, Zakieh Avazzadeh, and Yin Yang. A computational method for solving variable-order fractional nonlinear diffusion-wave equation. *Applied Mathematics and Computation*, 352:235–248, 2019.

[156] Xiuying Li and Boying Wu. A numerical technique for variable fractional functional boundary value problems. *Applied Mathematics Letters*, 43:108–113, 2015.

[157] Hui Zhao and Hongjiong Tian. Finite difference methods of the spatial fractional black–schloes equation for a european call option. *IMA Journal of Applied Mathematics*, 82(4):836–848, 2017.

[158] Wen Chen and Song Wang. A 2nd-order adi finite difference method for a 2d fractional black–scholes equation governing european two asset option pricing. *Mathematics and Computers in Simulation*, 171:279–293, 2020.

[159] Ahmad Golbabai and Omid Nikan. A computational method based on the moving least-squares approach for pricing double barrier options in a time-fractional black–scholes model. *Computational Economics*, 55(1):119–141, 2020.

[160] Xingyu An, Fawang Liu, Minling Zheng, Vo V Anh, and Ian W Turner. A space-time spectral method for time-fractional black-scholes equation. *Applied Numerical Mathematics*, 165:152–166, 2021.

[161] M Rezaei, AR Yazdanian, A Ashrafi, and SM Mahmoudi. Numerical pricing based on fractional black–scholes equation with time-dependent parameters under the cev model: Double barrier options. *Computers & Mathematics with Applications*, 90: 104–111, 2021.

[162] Guy Jumarie. Stock exchange fractional dynamics defined as fractional exponential growth driven by (usual) gaussian white noise. application to fractional black–scholes equations. *Insurance: Mathematics and Economics*, 42(1):271–287, 2008.

[163] Qing Li, Yanli Zhou, Xinquan Zhao, and Xiangyu Ge. Fractional order stochastic differential equation with application in european option pricing. *Discrete Dynamics in Nature and Society*, 2014, 2014.

[164] Anatoliĭ Kilbas. *Theory and applications of fractional differential equations*.

List of research publications

Journal Publications

1. K. Deswal, D. Kumar, Rannacher time-marching with orthogonal spline collocation method for retrieving the discontinuous behavior of hedging parameters, Appl. Math. Comput., 427 (2022), 127168.

2. D. Kumar, K. Deswal, A wavelet-based novel approximation to investigate the sensitivities of various path-independent binary options, Math. Methods Appl. Sci., (2022).

3. D. Kumar, K. Deswal, Haar-wavelet based approximation for pricing American options under linear complementarity formulations, Numer. Methods Partial Differ. Equations, 37 (2021), 1091–1111.

4. D. Kumar, K. Deswal, Two-dimensional Haar wavelet based approximation technique to study the sensitivities of the price of an option, Numer. Methods Partial Differ. Equations, (2020).

5. K. Deswal, D. Kumar, A wavelet-based numerical scheme to explore the sensitivities of multi-asset option pricing problems. **(Communicated)**

6. K. Deswal, D. Kumar, Higher-order novel numerical approach for variable order time-fractional CEV model using Atangana-Baleanu Caputo operator. **(Communicated)**

Conferences /Workshops attended

Conferences

1. International conference on computational sciences- modelling,computing and soft computing held at Manipal institute of technology, Manipal in 2022. **(Presented)**

2. International conference on advances in mechanics, modelling, computing and statistics held at BITS Pilani, Pilani Campus in 2022. **(Presented)**

3. International Conference on Computational Applied Sciences and Its Applications organized by department of Applied Sciences, University of Engineering Management Jaipur, 2022. **(Presented)**

4. International conference on and 22^{nd} annual convention of vijana parisad of India on advances in operational research, statistics and mathematics held at BITS Pilani, Pilani Campus, 2019.

5. Indo-french research workshop on theory and simulation of hyperbolic PDEs arising mathematical biology and fluid flow held at BITS Pilani, Pilani Campus, 2019.

Workshops

1. TEQIP-III sponsored two days Faculty Development Programme, Research Methodology and Latex held at Rajasthan technical university, Kota, 2018.

2. A seven days workshop on academic writting organised by the department of humanities and social sciences of BITS Pilani held at BITS Pilani, Pilani Campus in 2019.

3. Five days workshop on parallel finite element computing using parmoon held at Indian Institute of Science, Bangalore in 2019.

4. ATAL FDP in financial mathematics and machine learning held at International Institute of Information Technology, Naya Raipur in 2021.

Biography of the Candidate

Ms. Komal Deswal received her B.Sc. (Honours) and M.Sc. degree in Mathematics from Delhi University, Delhi India. In 2018, she joined as a full-time Ph.D. scholar in the Department of Mathematics at Birla Institute of Technology and Science (BITS) Pilani, India under the supervision of Dr. Devendra Kumar. Her research interests include numerical approaches for linear, non-linear, fractional-order, and free boundary PDEs in mathematical finance. She's also working on singular perturbation PDEs. She has served as a teaching assistant for the various courses of mathematics at BITS Pilani, Pilani Campus. More about her research contributions can be found at `scholar.google.com`. Contact her at `p20180027@pilani.bits-pilani.ac.in`.

Biography of the Supervisor

Dr. Devendra Kumar is the current head and an associate professor in the Department of Mathematics at Birla Institute of Technology and Science Pilani, Pilani campus. He has earned his Ph.D. degree from the Department of Mathematics of Indian Institute of Technology Kanpur. His research interests include the development of numerical methods for initial/boundary value problems for ordinary differential equations, partial differential equations, delay/advanced differential equations, singularly perturbed problems, fractional-Order differential equations, etc. More on his research contributions can be found at `https://www.bits-pilani.ac.in/pilani/dkumar/Profile`. Contact him at `dkumar@pilani.bits-pilani.ac.in`.